REACTOR AND FUEL-PROCESSING TECHNOLOGY

A Quarterly Technical Progress Review

Prepared for DIVISION OF TECHNICAL INFORMATION, U. S. ATOMIC ENERGY COMMISSION

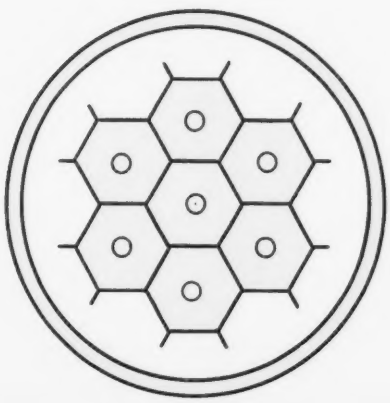

Model of a Clad Fuel Element—
see page 127

Spring 1969

● VOLUME 12

● NUMBER 2

TECHNICAL PROGRESS REVIEWS

The United States Atomic Energy Commission publishes the Technical Progress Reviews to meet the needs of industry and government for concise summaries of current nuclear developments. Each journal digests and evaluates the latest findings in a specific area of nuclear technology and science. *Nuclear Safety* is a bimonthly journal; the other three are quarterly journals.

Isotopes and Radiation Technology
P. S. Baker, A. F. Rupp, and associates
Isotopes Information Center, Oak Ridge National Laboratory

Nuclear Safety
Wm. B. Cottrell, W. H. Jordan, J. P. Blakely, and associates
Nuclear Safety Information Center, Oak Ridge National Laboratory

Reactor and Fuel-Processing Technology

Reactor Materials
E. M. Simons and associates
Battelle Memorial Institute, Columbus Laboratories

All are available from the U. S. Government Printing Office. See the back cover for ordering instructions.

Availability of Reports Cited in This Review

United States Atomic Energy Commission (USAEC) reports are available at USAEC depository libraries and are sold by the Clearinghouse for Federal Scientific and Technical Information (CFSTI), National Bureau of Standards, U. S. Department of Commerce, Springfield, Va. 22151. All reports sold by CFSTI are $3.00 for printed copy and $0.65 for microfiche. Each separately bound part of a report is priced as a separate report. Some reports may not be available because of their preliminary nature; however, the information contained in them will generally be found in later progress or topical reports on the subject.

Other U. S. Government agency reports identified in this journal generally are available from CFSTI.

Private-organization reports should be requested from the originator.

United Kingdom Atomic Energy Authority (UKAEA) and Atomic Energy of Canada Limited (AECL) reports are available at USAEC depository libraries. UKAEA reports are sold by Her Majesty's Stationery Office, London; AECL reports are sold by the Scientific Document Distribution Office, Atomic Energy of Canada Limited, Chalk River, Ontario, Canada. UKAEA and AECL reports issued after March 1, 1967, are sold by CFSTI to purchasers in the United States and its territories.

REACTOR AND FUEL-PROCESSING TECHNOLOGY

Vol. 12, No. 2 Spring 1969

Contents

Superintendent of Documents, U. S. Government Printing Office, Washington, D. C. 20402, $2.50 per year.

Reactor and Fuel-Processing Technology

is a quarterly review of developments in reactor and reactor fuel technology. As such, this journal reports and interprets progress in the reactor field in terms of its significance to the reactor designer, operator, and fuel-cycle specialist. Articles either summarize and critically evaluate recently reported developments or review the "state of the art" of a particular topic. Both types of articles reference reports and publications that merit study; readers are urged to consult the references for additional information and the judgments of the original authors.

The scope of the journal encompasses:

CONCEPTS and APPLICATIONS: Progress in evaluating the applicability and economics of various reactor types and systems (including unconventional approaches), as well as of fuel resources and cycles, for utility central-station generation of electricity, auxiliary power, process radiation and heat, desalting, and propulsion—and for terrestrial, undersea, aerospace, and other advanced uses.

ANALYSIS and EXPERIMENTATION: Advancements in the techniques of reactor physics, fluid and thermal technology, energy conversion, fuel elements, materials, mechanics, and control and dynamics.

SYSTEMS and COMPONENTS: Experience as reflected in design and construction practice, components, systems technology, and operating performance of various specific types of reactors—including pressurized- and boiling-water reactors, molten-salt, organic-, gas-, and liquid-metal-cooled reactors, as well as generally applicable aspects of research and test reactors.

FUEL PROCESSING: Recent research and development on fuel aqueous processing, nonaqueous processing, waste disposal, and processing safety.

Articles for this issue of *Reactor and Fuel-Processing Technology* have been assembled from several sources by the Division of Technical Information, USAEC, pending a decision on the future status of the journal. Contributors include NUS Corporation, Rockville, Md.; Nuclear Safety Associates, Rockville, Md.; Hittman Associates, Inc., Columbia, Md.; Southern Nuclear Engineering, Inc., Dunedin, Fla.; Nuclear Associates International Corporation, Rockville, Md.; Battelle Memorial Institute, Columbus, Ohio; Oak Ridge National Laboratory, Oak Ridge, Tenn.; and Franklin Institute Research Laboratories, Philadelphia, Pa.

We welcome comments on this issue.

U. S. Atomic Energy Commission
Division of Technical Information
Washington, D. C. 20545

Issued quarterly by the U. S. Atomic Energy Commission. Use of funds for printing this publication approved by the Director of the Bureau of the Budget on May 12, 1969.

Research and Development on Coatings for Retaining Fission-Product Iodine

By H. S. Rosenberg, J. M. Genco, D. A. Berry, G. E. Cremeans, and D. L. Morrison*

The increasing number of power reactors currently being sited has required the development of many types of safety features to protect the general public in the event of a serious nuclear accident. One of the major biological problems arising from such an accident would be the release to the environment of ^{131}I vapors and certain compounds such as alkyl iodides (predominantly methyl iodide) and hydrogen iodide containing this isotope. If the released iodine were irreversibly sorbed on the surfaces within the containment vessel under conditions prevalent during an accident, the probability for release to the environment due to leakage would be reduced. Many of the surfaces within the containment shell are mild steel or concrete, which are normally painted for protective purposes. Laboratory experiments[1] have shown that iodine will deposit on most commercial painted surfaces, but the rate of deposition is low and often of little consequence in irreversibly immobilizing the iodine. In addition, the deposition process is reversible, and under some conditions the chemical form of the desorbed iodine is difficult to remove even if active safety systems are operable.

In principle, it should be possible to develop a surface coating that would react rapidly and irreversibly with the chemical forms of iodine anticipated to be released under reactor accident conditions. What is required is a chemical compound or group of compounds that can be used either as a vehicle or as a pigment and will react, when in the form of a surface coating, with vapor forms of iodine. Coatings of this type would be capable of retaining irreversibly copious quantities of fission-product iodine as elemental iodine, CH_3I, and HI, and would thus be supplemental to active systems (e.g., sprays and filters) for limiting the potential hazards of a reactor accident. Such a coating would be applied to surfaces within the containment vessel in addition to or in place of protective coatings now used.

*Battelle Memorial Institute, Columbus Laboratories, Columbus, Ohio.

Basic Chemistry of Coatings Used as Iodine Scavengers

Organic Chemistry

Most coatings systems are composed of three basic components: (1) the binder or film-forming constituent, (2) the pigment or filler, and (3) the solvent or, in the case of emulsion paints, an aqueous suspension medium. Invariably, small amounts of ancillary materials are also added.[2] The primary function of the binder is, of course, to form a film or polymeric barrier over the substrate and to hold the pigments or fillers in place. Although the binder is not usually considered a reactive material, there is no a priori reason that one cannot be chosen that contains reactive groups in its molecular structure to allow rapid chemical reaction with elemental iodine and CH_3I.

On a theoretical basis the binders that appear most capable of allowing irreversible reactions to occur are polymers that contain tertiary amine groups as part of their basic structure. Amine-containing polymers that have shown extremely good promise as iodine scavengers are DMAM [poly(dimethylaminoethylmethacrylate)], and TBAM [poly(*t*-butylaminoethylmethacrylate)]. The repeating units of these polymers are shown below as I and II, respectively.

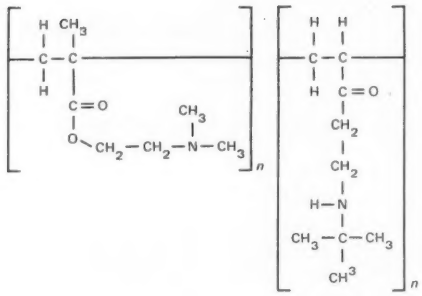

I II

There are two reasons for choosing binders of this type. First, they should react with elemental iodine by formation of so-called charge-transfer complexes. A typical reaction between a tertiary amine and iodine leading to the formation of a charge-transfer complex may be represented by the general reaction

$$R_3N + I_2 \rightarrow [R_3NI]^+ I^-$$

This type of reaction results from the interaction of an electron donor, in this case the tertiary nitrogen atom, and an acceptor, the elemental iodine. The donor has filled electronic orbitals of relatively high energy, and the acceptor has empty electronic orbitals of relatively low energy. The main interaction is therefore between the filled orbitals of the donor and the empty orbitals of the acceptor. Second, polymers containing tertiary amine groups are capable of reacting with methyl iodide through well-known quaternarization reactions. Such reactions result in the formation of the quaternary ammonium salts and may be represented by the reaction

$$R_3N + CH_3I \rightarrow [R_3NCH_3]^+ I^-$$

With HI, similar reactions lead to the amine salts

$$HI + R_3N \rightarrow [R_3NH]^+ I^-$$

Only tertiary amines react with alkyl halides directly to yield the corresponding halide salts. With CH_3I, primary and secondary amines react first to form hydrogen iodide and a substituted amine that is a stronger base than its precursor. The hydrogen iodide that is formed can and probably will react with the new base that is formed and thus prevent further reaction with methyl iodide by making the amine a relatively poor nucleophile. All the methylation reactions are *p*H sensitive, but only the primary and secondary amines have built-in retarders in their reaction mechanisms. Normally, all amines should have a capacity of 1 mole of methyl iodide per mole or reactant. However, if a strong base is used in conjunction with the amine to react with the by-product hydrogen iodide, the molar capacity of primary and secondary amines for methyl iodide can be increased to 3 and 2 moles of CH_3I per mole of amine, respectively.

Another example of an extremely effective polymeric system that scavenges iodine is a two-component epoxy–polyamide formulation composed of Genamid 2000 and Epon 828. These two components, when mixed, will react at ambient temperatures to form a highly cross-linked structure. The epoxy portion (Epon 828) is usually formed by reacting epichlorohydrin with *bis*(2,2-hydroxyphenyl) propane. The simplest possible structure for this type of resin intermediate is shown below.

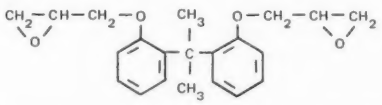

The polyamide portion results from reacting dimerized monobasic fatty acids with a molar excess of a diamine. This results in a polymer which contains a plurality of amine linkages but which is terminated with primary amine groups. For Genamid 2000 the structure would approximate

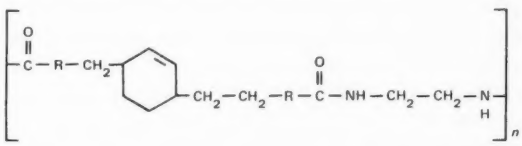

The entire system is cross-linked through the reaction of the epoxide radicals with the amine group. Tertiary amines catalyze this reaction and are often used for this purpose. In the Genamid 2000–Epon 828 binder, 1,10-phenanthroline can be incorporated as a reactive filler and makes a very attractive film-forming iodine scavenger. In this system both the binder and the filler react with fission-product iodine. The structure of 1,10-phenanthroline is a fused aromatic ring system containing two tertiary amine groups as shown below. The molecule is planar, and as a result the two amine groups are fixed in space in such a way as to reinforce the nucleophilic character. However, steric factors prevent the formation of diquaternary salts.

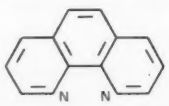

Physical Chemistry

The basic physical chemistry of a coating scavenger system and its relation to iodine deposition may best be explained in terms of a simultaneous solid-phase diffusion with chemical-reaction process. The equations governing fission-product-iodine deposition from either the homogeneous vapor or aqueous phases may be expressed using a modified form of Fick's second law[1]

$$\frac{\partial C}{\partial t} = D\frac{\partial^2 C}{\partial x^2} - \psi_R \qquad (1)$$

where ψ_R refers to the rate of chemical reaction occurring within the coating, D is the iodine diffusivity, and C is the local iodine concentration in the condensed phase. Since the rate of reaction depends on the chemical composition or chemical nature of the coating, the function ψ_R depends upon the local iodine concentration (C) and the number of active sites (N) within the coating capable of reaction. For many commercial coatings and iodine scavengers in particular, the reaction rate ψ_R can be adequately represented by irreversible second-order kinetics in the form

$$\psi_R = v_0 kCN \qquad (2)$$

where v_0 is an arbitrary proportionality constant and k is the second-order rate coefficient for the reaction.[1] The total number of molecules, both sorbed and reacted per unit area, M, at any time t is given by the integral equation

$$M_t = \int_0^L C\,dx + \int_0^L v_0\,(N_0 - N)\,dx \qquad (3)$$

where L is the coating thickness and N_0 is the total concentration of active sites within the coating.

This analytical model may be used to visualize the manner in which a reactive coating traps fission-product iodine. As the fission product comes into contact with the paint, it penetrates the pores of the binder and reacts with the reactive constituents (amine groups) of either the binder or the filler, or both. The reactions between the amine groups and the iodine are for the most part irreversible and lead to either charge-transfer complexes or salts. In this manner the iodine is immobilized and unavailable for desorption back into the containment vessel.

Criteria for Reactive Coatings

The criteria for a coating to function as a passive safety system may be stated as follows:

1. Irreversible reactions with fission-product iodine from ambient temperature to 175°C.
2. A minimum required coating capacity for iodine and CH_3I of 0.66 and 0.08 mg/cm^2 of geometric area, respectively.
3. High deposition rates for fission-product iodine, i.e., wall coefficients or deposition velocities (k_w) of approximately 1 cm/sec.
4. Functionality in steam and under condensing-steam conditions.
5. Thermal and radiation stability.
6. Compatibility with active safety systems such as containment spray solutions.
7. Minimum flammability requirements as yet to be determined by the AEC Committee on Standards for Protective Coatings.

The minimum required coating capacities for elemental iodine and CH_3I were obtained for a typical 1000-Mw(e) boiling-water reactor (BWR) containment shell having a volume of 1.6×10^5 cu ft. The containment shell was assumed to be a sphere with no internal compartmenting, i.e., no additional surface area due to painting of internal surfaces, and the total iodine inventory[3] was taken as 16 kg; 50% of this value was assumed to be released instantaneously during an accident,[4] and 20% of the released iodine was assumed to be in the form of CH_3I. It was further assumed that the released iodine would be uniformly distributed on the containment-shell coating. For a typical 1000-Mw(e) pressurized-water reactor (PWR), the minimum required coating capacities on these bases alone are somewhat lower because a PWR containment shell has a larger volume (2.6×10^6 cu ft) and hence a larger surface area than a BWR containment shell. The method of calculation described above is extremely conservative since considerable internal surface area arises owing to the compartmentation of nuclear reactor containment vessels. Hence the minimum required coating capacities for elemental iodine and CH_3I could be considerably lower than those quoted in criterion 2.

Although the parameters D, k, and N_0 in Eqs. 1 to 3 can be used to describe adequately the iodine-deposition process on painted surfaces, they prove to be impractical for use as a standard by which to judge the relative merits of candidate iodine scavengers. Rather, one must resort to semiempirical techniques to obtain a quantitative measure of the effectiveness of candidate materials. For simplicity in criterion 3, the wall factor or deposition-velocity concept (k_w) has been introduced.[5] The seven criteria listed above do not include

all conditions that a containment-vessel coating must meet, and additional requirements have been listed elsewhere.[6]

Experimental Techniques

Chemical reactions between candidate coatings and elemental iodine and CH_3I were studied both in the vapor state and under condensing-steam conditions, and deposition rates [deposition velocities or wall factors (k_w)], capacities, and degrees of irreversibility were noted. Radiation- and thermal-stability measurements were taken, and resistance to pressurized steam and containment spray solutions was determined.

The apparatus designed to determine the iodine-deposition rates and capacities for candidate coating materials under noncondensing conditions is described in detail in Ref. 7. A steam–air–iodine mixture (tagged with ^{131}I) having a constant iodine concentration was generated in a flow train and passed over a small glass test specimen coated with the material of interest. The mass of iodine sorbed and reacted (deposited) by the coating specimen was monitored continuously by a scintillation probe. This same apparatus was also used to measure CH_3I deposition rates by simply replacing the tagged elemental iodine with ^{131}I-tagged CH_3I. A second apparatus was used for screening a large number of candidates simultaneously.[8] The small test panels employed in this system were removed periodically and radioassayed to determine the amount of iodine deposited.[4]

So that the deposition process could be studied under condensing-steam conditions, test specimens were attached to the walls of a cylindrical chamber.[5] A steam–air–iodine mixture at approximately 115°C was fed into the chamber, and condensation on the specimens was allowed to occur by cooling the chamber walls. The deposition of iodine on one of the specimens was monitored continuously with a scintillation probe. This specimen and the others were radioassayed, following the experiment, to determine the amount of deposition.

Results and Discussion

Screening of Polymer Candidates

Numerous candidates were evaluated at 115 and 170°C to determine their iodine capacities, degrees of sorption irreversibility, and iodine affinities relative to a typical commercial coating (Phenoline 302). All experiments were performed in approximately 50 vol.% steam–50 vol.% air atmospheres containing about 175 mg/m^3 of either elemental iodine or CH_3I. The results of these studies are presented in detail in Refs. 1 and 7. A partial list of polymers studied and their sorption and desorption characteristics for elemental iodine and CH_3I at 115°C are given in Table 1. The mass of elemental iodine or CH_3I sorbed (M_t) is presented after 1 hr of exposure, together with the percentage of iodine sorbed irreversibly by each material. Also included is the ratio of the mass of iodine sorbed after 20 hr by the candidate coating to that by the standard. This table reveals that several of the materials are promising as iodine scavengers. Many candidates have capacities for iodine many times greater than the minimum capacity of 0.66 mg/cm^2, and the reactions produced are quite stable. After 20 hr of exposure using 2-mil-thick specimens, none of the experimental scavengers had reached saturation.

Relative to iodine sorption the candidates invariably did not perform as well with CH_3I. In an effort to increase the capacity for CH_3I sorption, nonfilm-forming reactants suspected of having high affinities for CH_3I were impregnated into asbestos mat for evaluation in the screening apparatus under the same conditions used in evaluating the films. The two most promising reactants appeared to be Genamid 2000 and 1,10-phenanthroline. The CH_3I sorption results for these two reactants impregnated into asbestos mat are listed at the end of Table 1 and are significantly higher than those obtained for the films. Part of the increase in CH_3I sorption is undoubtedly due to the increase in reactive surface area provided by the asbestos mat.

From the standpoint of practicality and ease of application, it would be much more desirable to have a film former as a scavenger rather than an asbestos impregnate. Accordingly, attempts were made to incorporate the most promising reactants into film-forming systems, either as part of the binder or as a reactive filler. Initially, the most promising coatings obtained using this technique were an epoxy–polyamine copolymer of 50 wt.% Genamid 2000 and 50 wt.% Epon 828 and a three-component system of 30 wt.% 1,10-phenanthroline, 35 wt.% Genamid 2000, and 35 wt.% Epon 828. In addition, DMAM coatings appeared to be promising scavengers for fission-product iodine.

Effect of Steam Condensation

Wall factors were obtained in the presence of condensing steam to evaluate the ability of the four most promising coatings to sorb iodine under nuclear

Table 1 The Sorption of Elemental Iodine[a] and Methyl Iodide[b] by Various Coatings[c] at 115°C in 50 Vol.% Air–50 Vol.% Steam at 1 atm

Coating	Mass of elemental iodine sorbed after 1 hr, mg/cm^2	Ratio of 20-hr elemental iodine sorption in candidate coating to that in Phenoline 302	Percent elemental iodine irreversibly retained	Mass of CH_3I after 1 hr, mg/cm^2	Ratio of 20-hr CH_3I sorption in candidate coating to that in Phenoline 302	Percent CH_3I irreversibly retained
Phenoline 302 (standard)	0.063	1[d]	77	0.00075	1[e]	85
Poly(aminopropylmethylsilane)	0.0067	1	82	0.019	9	83
Versamid 125 bubble	0.14	2	56	0.010	7	97
Versamid 125–30 wt.% Epon 828	0.16	7	67	0.014	24	100
Polyvinyl alcohol–60 wt.% dipiperidylpropane	0.034	2	93	0.0023	1	92
Epon 1001–20 wt.% dipiperidylpropane	0.21	7	80	0.0036	8	98
Gentac	0.11	8	72	0.0027	2	69
TBAM-50 wt.% nickel[f]	0.077	6	88	0.0056	8	97
TBAM[f]	0.095	6	94	0.0061	11	99
DMAM[g]	0.17	10	94	0.016	12	100
Genamid 2000 on asbestos mat[h]				0.036	75	100
1,10-phenanthroline on asbestos mat[h]				0.10	190	93

[a]Elemental iodine concentration was 203 mg/m^3.
[b]The CH_3I concentration was 174 mg/m^3.
[c]Coatings were 2 mils thick except where noted.
[d]Mass of elemental iodine sorbed in Phenoline 302 after 20 hr of exposure was 0.304 mg/cm^2.
[e]Mass of CH_3I sorbed in Phenoline 302 after 20 hr of exposure was 0.00642 mg/cm^2.
[f]TBAM is poly(*t*-butylaminoethylmethacrylate).
[g]DMAM is poly(dimethylaminoethylmethacrylate).
[h]Asbestos mats were about 28 mils thick and composites contained about 25 wt.% reactant.

reactor accident conditions. In these experiments the condensation rate over the specimens was maintained constant at 5×10^{-6} g H_2O/(cm^2)(sec). Again, the inlet elemental iodine or CH_3I concentration was approximately 175 mg/m^3 in a 50 vol.% steam–50 vol.% air mixture. The steam–air–iodine mixture entered the chamber at 115°C, and the steam was made to condense by maintaining the walls of the chamber below 100°C. The deposition velocities or wall factors (k_w) were calculated from the experimentally determined mass sorbed (M_t), gas-phase iodine concentration (C_g), and exposure time (θ) by the equation

$$k_w = (M_t/C_g\theta) \quad (4)$$

The deposition velocities for the 37°C (wall temperature) experiments for the four coatings are listed in Table 2 as well as with those for 1,10-phenanthroline impregnated on asbestos and Phenoline 302 coating for comparison purposes. The 37°C experiments should represent the lower limit of deposition for these materials because additional experiments at elevated condensation temperatures, namely, 60 and 90°C, indicated significantly higher deposition rates and capacities.[10] The results listed in Table 2 indicated that it was possible to design film-forming systems having iodine affinities equivalent to those exhibited by the best asbestos composites. Relative to commercial coatings under condensing-steam conditions, these materials represented a significant improvement.

Reducing the Coatings to Practice

Hybrid coatings that could serve as functional paints were developed and were based on the four initially most promising polymers. These coatings had high capacities for elemental iodine and relatively high capacities for CH_3I in steam–air environments over the temperature range 37 to 170°C. The coatings were

Table 2 Deposition Velocities at 37°C Under Condensing-Steam Conditions for Most Promising Candidate Materials*

Candidate coating	Deposition velocity, cm/sec	
	Elemental iodine	CH_3I
1,10-phenanthroline impregnated on asbestos†	0.816	0.0413
30 wt.% 1,10-phenanthroline, 35 wt.% Genamid 2000, 35 wt.% Epon 828‡	0.842	0.0357
50 wt.% Genamid 2000, 50 wt.% Epon 828‡		0.0282
TBAM‡	0.550	0.0197
DMAM‡		0.0796
Phenoline 302§	0.020	¶

*Inlet elemental iodine or CH_3I concentration was about 175 mg/m^3 in 50 vol.% steam.

†25 wt.% phenanthroline on 28-mil-thick asbestos.

‡2-mil-thick coating.

§Control.

¶No detectable CH_3I deposition.

modified by pigmentation, and the formulations were adjusted to obtain adequate resistance to steam at pressures up to 60 psig. The pigmentation studies involved adding various pigments to the most promising coating candidates and determining the effect of pigmentation on CH_3I sorption. The steam-resistance studies involved the application of coating candidates to sandblasted 1- by 1-in. mild-steel coupons, both unprimed and primed with various primers, and the exposure of the coupons to saturated steam at 150°C for 20 hr in an autoclave. The pigmentation and steam-resistance studies are reported in detail elsewhere.[11]

On the basis of previous deposition experiments with elemental iodine and CH_3I, exposure to saturated steam at 150°C, and pigmentation studies, eight coating candidates were subjected to an evaluation program that included both environmental testing and deposition studies. The coating systems selected are given in Table 3 in terms of the weight percentages of each constituent comprising the coatings. The pigment concentrations used in the above formulations, namely, 25 vol.% (based on the dry film) for the TiO_2 (50 wt.% total) and 10 wt.% for the Nuchar, represent normal pigment loadings used in industrial paint applications. All the above materials were applied to one side of 1- by 1- by $\frac{1}{16}$-in. sandblasted iron oxide-primed carbon-steel panels, except in the case of coatings 2*a* and 2*b* where the panels were unprimed. In all cases the reverse side and edges of the panels were coated with iron oxide primer, and the specimens were cured at 50°C for 2 days.

Loss-of-Coolant Accident Environmental Testing

The panels described above were subjected to a comprehensive evaluation program that included the following tests, defined in part by the USAEC Committee on Standards for Protective Coatings.[12]

I. Fission-product-iodine deposition tests
  A. Expose coatings to elemental iodine and CH_3I at 175 mg/m^3
    1. Condensing conditions [5 × 10^{-6} g H_2O/(cm^2)(sec)]
      a. 37, 60, and 90°C for 4 hr
    2. Noncondensing conditions (50 vol.% steam)
      a. 115, 140, and 170°C for 4 hr
  B. Determine irreversibility of deposition process
    1. Use specimens containing sorbed I_2 and CH_3I
      a. Heat at 170°C in flowing helium for 24 hr
  C. Determine effect of gamma radiation on deposition process
    1. Expose specimen to 10^8 rads at 7 × 10^5 rads /hr
    2. Perform deposition experiments with elemental iodine at 90°C under condensing conditions
II. Exposure to saturated steam in an autoclave
  A. A pressure decay from 60 psig down to 5 psig in 24 hr; hold at 5 psig for 12 days, followed by 2 psig for 14 days
III. Exposure to containment spray solutions
  A. One month at 90°C using the following spray solutions:
    1. 1.7 wt.% H_3BO_3
    2. 1.7 wt.% H_3BO_3, 1.6 wt.% $Na_2S_2O_3 \cdot 5H_2O$, 0.6 wt.% NaOH
    3. 1.7 wt.% H_3BO_3, 6.0 wt.% NaOH
IV. Simultaneous exposure to gamma radiation and steam
  A. 10^9 rads at 7 × 10^5 rads/hr in steam at 105°C

The results of the fission-product-iodine deposition tests are summarized in Table 4 for elemental iodine and CH_3I in terms of coating capacities after 4 hr of deposition. The elemental-iodine capacities of all these coatings exceeded the minimum required capacity of 0.66 mg/cm^2 over the entire temperature range 37 to 170°C. A typical curve for iodine deposition vs. time is shown in Fig. 1. The deposition process is seen to approximate first-order kinetics. However, the CH_3I capacities for some of the coatings at the lower temperatures did not approach the minimum required capacity of 0.08 mg/cm^2 e.g., Genamid–Epon at 37°C. The TBAM–DMAM coating systems came close to attaining the required CH_3I capacity after 4 hr of deposition; for longer deposition time the minimum required capacity for CH_3I would be exceeded.

Table 3 Composition of Scavenger Coatings (wt.%)

Coating designation	Genamid 2000	Epon 828	DMAM	TBAM	1,6-dibromo-hexane*	1,10-phenan-throline	TiO_2 pigment	Nuchar pigment†
1*a*	25.0	25.0					50.0	
1*b*	45.0	45.0						10.0
2*a*	15.8	15.8	15.8		2.6		50.0	
2*b*	28.4	28.4	28.4		4.8			10.0
3*a*			23.0	23.0	4.0		50.0	
3*b*			41.5	41.5	7.0			10.0
4*a*			19.5	19.5	3.5	7.5	50.0	
4*b*			35.0	35.0	6.3	13.7		10.0

*Cross-linking agent.
†Trade name for charcoal.

Table 4 Coating Capacities for Elemental Iodine and CH_3I After 4 hr of Deposition*

Coating designation†	Deposition, mg/cm^2, at indicated temperature			
	37°C	90°C	140°C	170°C
	Elemental iodine			
1*a*	1.13	1.75	1.44	1.35
1*b*	1.22	2.06	1.80	1.93
2*a*	2.11	2.09	2.28	2.33
2*b*	2.01	2.30	2.77	2.46
3*a*	2.89	2.42	1.58	2.22
3*b*	2.61	2.51	1.53	2.16
4*a*	1.94	2.32	1.90	1.73
4*b*	2.05	2.04	2.18	2.00
	CH_3I deposition			
1*a*	0.0022	0.015	0.016	0.015
1*b*	0.0020	0.016	0.014	0.015
2*a*	0.0062	0.026	0.026	0.034
2*b*	0.0076	0.032	0.040	0.047
3*a*	0.019	0.045	0.033	0.017
3*b*	0.013	0.041	0.030	0.017
4*a*	0.015	0.049	0.037	0.016
4*b*	0.017	0.049	0.031	0.018

*Run conditions described in the text under test IA.
†For explanation of coating designation, see Table 3.

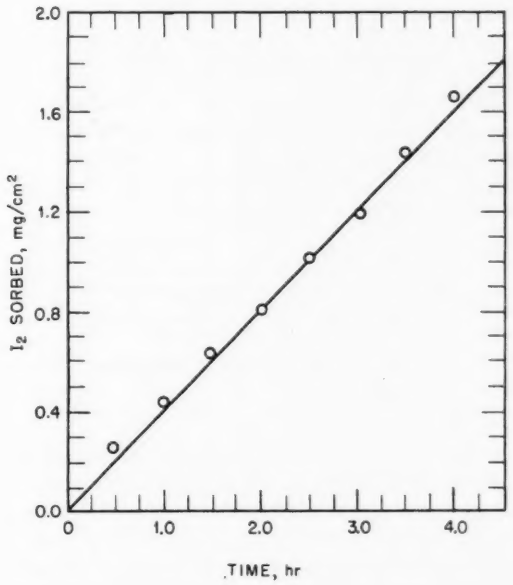

Fig. 1 Deposition of I_2 on Genamid 2000–Epon 828 (white). Temperature, 90°C; I_2 concentration, 166 mg/m^3; flow rate, 4520 cm^3/min; steam, 73.2 vol.%; condensation rate, 4.80 × 10^{-6} g/(cm^2)(sec).

All the specimens from the deposition experiments were desorbed in flowing helium at 170°C for 24 hr. The loss of iodine was about 10%, and the loss of CH_3I was about 5% for all the second-generation coatings, irrespective of the deposition temperature. Desorption at 170°C is a very stringent test, and at lower temperatures the loss of fission-product iodine from the coatings by desorption should be considerably less. In a loss-of-coolant (LOC) accident, the temperature sequence experienced by the paint would be just the opposite of that subjected to the coating candidates in this program, i.e., a fairly high temperature initially (perhaps 150°C), then gradually diminishing to ambient conditions over several days. However, it was decided to check the irreversibility of the deposition process using the reverse-temperature sequence since this is a much more stringent condition.

The effect of gamma radiation on the deposition process was determined by exposing the coatings to 1 × 10^8 rads in a 5000-curie ^{60}Co source at a dose rate of 7 × 10^5 rads/hr. The coatings were then evaluated

for iodine deposition at 90°C under condensing-steam conditions and compared with unirradiated coatings evaluated for iodine deposition under the same conditions. The results of this study, which are summarized in Table 5, indicated that the gamma radiation had no discernible effect on the iodine-deposition process. The effect of gamma radiation on the CH_3I-deposition process remains to be determined.

Table 5 The Effect of Gamma Radiation on Coating Capacities for Iodine After 4 hr of Deposition at 90°C*

Coating designation†	Coating capacity, mg I_2/cm^2	
	Unirradiated	Irradiated
1*a*	1.75	1.78
1*b*	2.06	2.00
2*a*	2.09	2.67
2*b*	2.30	2.77
3*a*	2.42	2.71
3*b*	2.51	2.89
4*a*	2.32	2.25
4*b*	2.04	2.39

*Run conditions described in the text under tests IA and IC.

†For explanation of coating designation, see Table 3.

The results of the LOC-accident environmental tests (tests II to IV) on the coatings are reported in Table 6. The Genamid 2000–Epon 828 coating system (designated 2*a* and 2*b*) passed both the gamma-radiation tests in steam and the spray exposures in basic solutions and performed marginally (slight blistering) in the autoclave test but had unsatisfactory resistance to the acidic spray solution. For the most part the TBAM–DMAM systems (designated 3*a*, 3*b*, 4*a*, and 4*b*), which had the highest affinities for CH_3I, were unsatisfactory in the LOC-accident environmental tests.

Coating Modifications

The failure of the TBAM–DMAM coatings in pressurized steam and/or spray solutions is caused by degradation of the cross-linking between the monomers used to prepare the coatings. Therefore the TBAM–DMAM systems were modified with Epon 828 to increase the extent of cross-linking that occurs in these coatings to permit maintenance of physical integrity

Table 6 LOC-Accident Environmental-Test Results for Coatings

Coating designation*	Test II,† autoclave	Test III, spray solution‡			Test IV, gamma radiation and steam
		1	2	3	
1*a*	S	M	S	S	S
1*b*	S	M	S	S	S
2*a*	M	U	S	S	S
2*b*	M	U	S	S	S
3*a*	U	U	U	U	M
3*b*	U	U	U	U	M
4*a*	U	M	U	U	U
4*b*	M	M	U	U	M

Note: S = satisfactory performance; M = marginal performance; U = unsatisfactory performance.

*For explanation of coating designation, see Table 3.

†Test conditions described in the text.

‡Solution compositions are given in the text under test III:

Solution	*p*H
1	4.9
2	9.2
3	13.2

during the LOC-accident environmental tests. The modified formulations are:

90 wt.% DMAM/10 wt.% Epon 828
45 wt.% DMAM/45 wt.% TBAM/10 wt.% Epon 828
80 wt.% DMAM/20 wt.% Epon 828
40 wt.% DMAM/40 wt.% TBAM/20 wt.% Epon 828

All the above formulations contain 25 vol.% (based on dry film) TiO_2 pigment. These formulations were applied to carbon-steel panels over an iron oxide primer using the procedures described previously.

Preliminary fission-product-iodine deposition experiments with modified coatings have indicated elemental iodine capacities greater than 0.66 mg/cm² and CH_3I capacities as high as 0.05 mg/cm² after 4 hr of deposition at 37°C, with higher CH_3I capacities expected at increased deposition temperatures. Thus the increased extent of cross-linking in these coatings has not been detrimental to iodine deposition. In addition, preliminary results have shown that the modified coatings are able to withstand LOC-accident environmental conditions; they have been placed in boiling water for several hours with no ill effects. These modified coatings are now being subjected to the comprehensive testing program.

At the present time there is no hesitation in recommending the white Genamid 2000–Epon 828

coating as a reactive paint for use as a passive safety system for nuclear power reactors. Furthermore, there is every reason to believe that one of the modified coatings, which sorbs CH_3I at a more rapid rate, can be recommended when the evaluation program for these coatings is completed.

Application to Reactor Accidents

The use of a reactive coating as a passive safety system should decrease materially the half-life of airborne iodine under natural-effects conditions. Quantitatively this may be estimated by considering iodine deposition occurring within the containment vessel to be described by a well-mixed deposition model:

$$\frac{dC_g}{dt} = -\frac{k_w A C_g}{V} \tag{5}$$

where C_g = airborne iodine concentration
A = painted surface area available for deposition
V = volume of the containment vessel
t = time
k_w = deposition velocity or wall factor defined in Eq. 4

In this model the deposition process was assumed to be controlled by the surface reaction rate that was expressed in terms of the deposition velocity (k_w). For the case of a puff release of iodine, the airborne half-life ($t_{½}$) would be given by the expression

$$t_{½} = 0.693 \left(\frac{V}{A}\right)\left(\frac{1}{k_w}\right) \tag{6}$$

Figures 2 and 3 show the airborne iodine half-life ($t_{½}$) for elemental iodine and CH_3I, respectively, plotted against the deposition velocity (k_w), according to Eq. 6, for typical 1000-Mw(e) PWR and BWR reactors. In this calculation the ratio of containment volume to surface area for the PWR was taken to be 8.5×10^2 cm, and that for the BWR was 3.5×10^2 cm. Using experimental iodine-deposition data (M_t) to approximate values for the deposition velocities or wall factors (k_w), according to Eq. 4, one can estimate the airborne-iodine half-lives expected under LOC-accident conditions from Figs. 2 and 3. For the deposition data of Table 4, this estimate is shown as the shaded area in these figures and indicates half-lives of the order of 3 to 20 min for elemental iodine and 5 to 40 hr for CH_3I. Relative to most commercial paints now being used as protective coatings for nuclear reactor containment vessels, the coatings discussed in this paper would represent a significant improvement. This is especially true for CH_3I where airborne half-lives are so long as to be immeasurable, i.e., essentially infinity, in engineering experiments under simulated accident conditions.[13] The half-lives for removal of elemental iodine and CH_3I would be expected to be shorter than those shown in the figures if the total surface area for deposition were considered. If the V/A value for a PWR containment reported by Hilliard[14] were used, the half-lives would be reduced by more than a factor of five.

More complicated iodine-deposition models, considering gas-phase mass-transfer and steam-condensation processes, have been treated elsewhere by the authors.[5] However, for CH_3I deposition the simple model described here should be adequate to permit estimation of airborne half-lives since CH_3I deposition is controlled by the surface reaction rate (k_w). Conversely, for elemental iodine, the deposition rate would, in all probability, be controlled by the gas-phase mass-transfer process and not by the surface reaction rate. Hence the half-lives for elemental iodine estimated here should represent minimum values.

Other advantages inherent in the use of a reactive coating designed to function as a passive safety system during a nuclear reactor accident have been discussed in detail by the authors.[4] These additional advantages may be succinctly summarized as follows:

1. The use of a reactive coating should negate any detrimental iodine desorption effects even in the event that an active safety system is operating; that is, once iodine is sorbed on the coating, it would be immobilized and unavailable for desorption back into the containment-vessel atmosphere. For most commercial paints the deposition process is largely reversible, and significant desorption of iodine is possible.

2. A highly reactive coating will decrease the wall resistance to deposition such that higher gas-phase mass-transfer coefficients can be obtained without having the deposition process become significantly wall-resistance limited. The use of an active safety system (recirculating-air systems, sprays, etc.) should promote high gas-phase mass-transfer coefficients.

3. Compartmented regions within a containment vessel could be sites for high local iodine concentrations and gas velocities. Deposition in such regions would be enhanced if these regions were painted with a coating having an extremely high deposition velocity or wall factor (k_w).

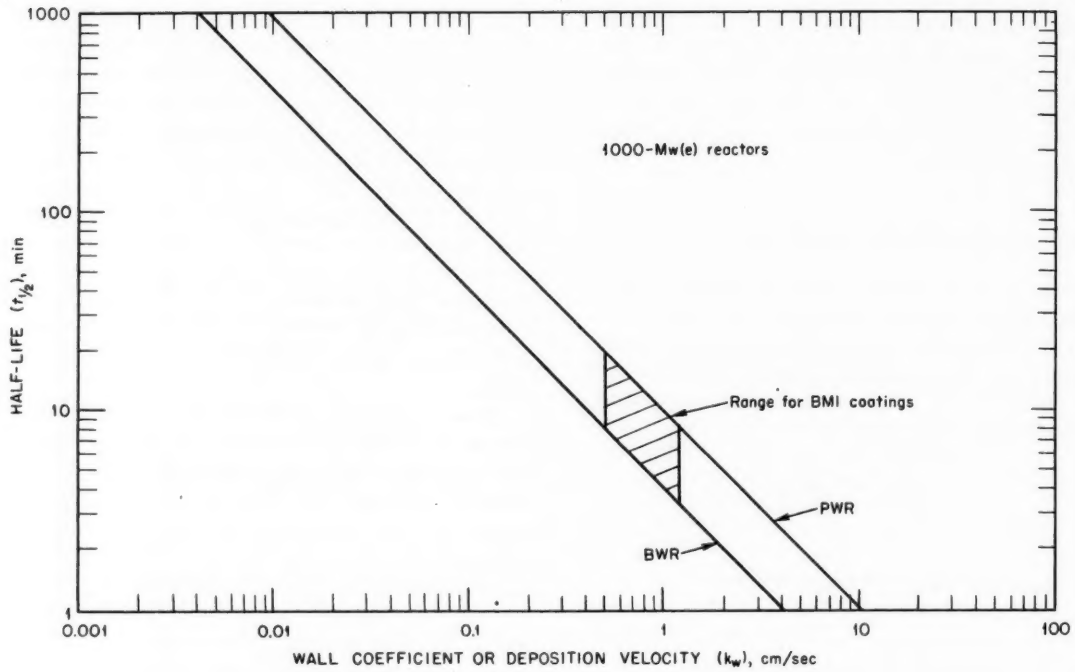

Fig. 2 The I_2 half-life ($t_{1/2}$) vs. wall coefficient (k_w).

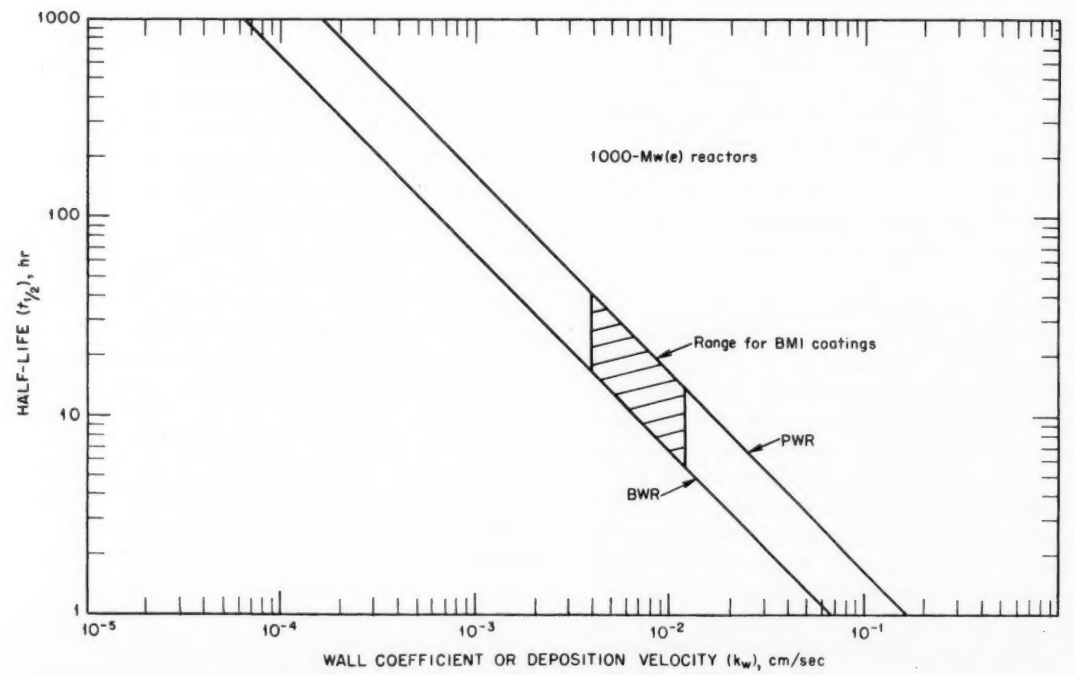

Fig. 3 The CH_3I half-life ($t_{1/2}$) vs. wall coefficient (k_w).

Summary and Conclusions

Experiments have shown that it is possible to form charge-transfer complexes and ammonium salts between amine-containing polymers and elemental iodine and methyl iodide, respectively, under the conditions postulated for serious water-cooled-reactor accidents. Amine-containing polymers have been shown to be amenable for fabrication into film-forming pigmented coatings that are resistant to pressurized steam, gamma radiation, and reactor containment spray solutions. On the basis of geometric areas available for coating coverage, several candidates possess sufficient iodine-retention capacity to react with all the fission-product iodine anticipated to be released during an accident. The two coating systems that can be reduced to practice as a nuclear reactor containment-vessel paint are the copolymer systems of Genamid 2000–Epon 828 and DMAM–Epon 828, both pigmented with TiO_2, applied to carbon steel over an iron oxide primer or applied to unprimed concrete surfaces. By utilizing paints of this type, one would expect significant reductions in the airborne half-life of accident-released iodine under natural-effects conditions relative to half-lives observed with most commercial paints now in use as protective coatings for nuclear reactors.

References

1. J. M. Genco, H. S. Rosenberg, D. A. Berry, G. E. Cremeans, W. E. Berry, and D. L. Morrison, Fission-Product Deposition and Its Enhancement Under Reactor Accident Conditions, Quarterly Progress Report, July–September 1967, USAEC Report BMI-X-10213, Battelle–Columbus, Oct. 1, 1967.
2. R. N. Shreve, *The Chemical Process Industries,* p. 498, McGraw-Hill Book Company, Inc., New York, 1956.
3. R. L. Ritzman, Battelle–Columbus, personal communication.
4. J. J. DiNunno, F. D. Anderson, R. E. Baker, and R. L. Waterfield, Calculation of Distance Factors for Power and Test Reactor Sites, USAEC Report TID-14844, Mar. 23, 1962.
5. J. M. Genco, H. S. Rosenberg, D. A. Berry, G. E. Cremeans, W. E. Berry, and D. L. Morrison, Fission-Product Deposition and Its Enhancement Under Reactor Accident Conditions, Quarterly Progress Report, April–June 1968, USAEC Report BMI-X-10237, Battelle–Columbus, July 1, 1968.
6. J. M. Genco, H. S. Rosenberg, D. A. Berry, G. E. Cremeans, W. E. Berry, and D. L. Morrison, Fission-Product Deposition and Its Enhancement Under Reactor Accident Conditions, Quarterly Progress Report, January–March 1968, USAEC Report BMI-X-10229, Battelle–Columbus, Apr. 1, 1968.
7. D. L. Morrison, D. A. Berry, W. E. Berry, and J. M. Genco, Fission-Product Deposition and Its Enhancement Under Reactor Accident Conditions, Quarterly Progress Report, April–June 1966, USAEC Report BMI-X-10173, Battelle–Columbus, July 1, 1966.
8. J. M. Genco, H. S. Rosenberg, D. A. Berry, G. E. Cremeans, W. E. Berry, and D. L. Morrison, Fission-Product Deposition and Its Enhancement Under Reactor Accident Conditions, Quarterly Progress Report, January–March 1967, USAEC Report BMI-X-10193, Battelle–Columbus, Apr. 1, 1967.
9. J. M. Genco, H. S. Rosenberg, D. A. Berry, G. E. Cremeans, W. E. Berry, and D. L. Morrison, Fission-Product Deposition and Its Enhancement Under Reactor Accident Conditions, Quarterly Progress Report, April–June 1967, USAEC Report BMI-X-10202, Battelle–Columbus, July 1, 1967.
10. J. M. Genco, H. S. Rosenberg, D. A. Berry, G. E. Cremeans, W. E. Berry, and D. L. Morrison, Research and Development on Coatings for Retaining Fission-Product Iodine, IAEA Symposium on Operating and Developmental Experience in the Treatment of Airborne Radioactive Wastes, New York, August 26–30, 1968 (to be published).
11. J. M. Genco, H. S. Rosenberg, D. A. Berry, G. E. Cremeans, W. E. Berry, and D. L. Morrison, Fission-Product Deposition and Its Enhancement Under Reactor Accident Conditions, Quarterly Progress Report, July–September 1968, USAEC Report BMI-X-10244, Battelle–Columbus, Oct. 1, 1968.
12. B. J. Newby, Interim Report—Tests for Protective Coatings for Nuclear Reactor Containments, USAEC Committee on Standards for Protective Coatings (letter to members of the committee), Aug. 9, 1968.
13. R. K. Hilliard, L. F. Coleman, and J. D. McCormack, Comparisons of the Containment Behavior of a Simulant with Fission Products Released from Irradiated UO_2, USAEC Report BNWL-581, Battelle–Northwest, March 1968.
14. R. K. Hilliard and J. G. Knudsen, A Natural Convection Model for Predicting Elemental Iodine Transport in Containment Vessels, *Trans. Amer. Nucl. Soc.,* **11**(2): 668 (November 1968).

Mechanical Analysis of Fission-Gas Swelling of Clad Cylindrical Fuel Elements

By J. A. Walowit, W. F. Adler, and W. Chubb*

Abstract: *A mathematical model is presented in an attempt to describe the radial, fission-gas swelling of high-temperature, clad cylindrical fuel elements. The creep resistances of both the fuel and the cladding are taken to provide the principal modes of restraint. The fuels considered are UC and UN at a temperature of 1700°C.*

Assumptions in the model are that a uniform distribution of a large number of pores exists within the fuel and that temperatures and fission rates are independent of position. The effects of gas release are considered by means of various gas-release vs. porosity relations as input. Creep is treated in terms of the usual power law relation between stress and strain rate.

A number of parametric studies are presented to show the effects of different cladding thicknesses, initial porosities, creep strengths, and gas-release relations on predicted swelling. Comparisons between theoretical predictions and experimental data are given.

Good qualitative agreement between theory and experiment is obtained. Quantitative agreement can be obtained if the fuel creep strengths used are somewhat lower than those measured out of pile. These results support the hypothesis that the fission process weakens the mechanical restraint provided by the fuel.

During the irradiation of nuclear fuels, the fission process results in the formation of a number of gas atoms that tend to form gaseous pores which cause the fuel element to swell. Approximately one gas atom forms for every four fissions, largely in the form of krypton and xenon atoms. At high temperatures the yield of gas atoms can even be higher as a result of cesium and rubidium atoms becoming gaseous.

This article deals with a relatively simple mechanical model that has been used to predict the swelling of clad cylindrical fuel elements.

A mathematical model for the problem for the fission-gas swelling of clad cylindrical fuel elements was developed. The analysis is based on the nonlinear viscoplastic behavior of the fuel material containing a prescribed initial porosity and the cladding material. A uniform pressure builds up within each pore and causes the fuel to expand; however, the cladding provides an external constraint on the overall swelling of the fuel element.

There are a number of theories based on a variety of microscopic mechanisms[1-5] for predicting the irradiation growth of fissile materials. Usually, terms representing the surface tension of the fuel, the strength of the fuel, and the externally applied pressure are included in these analyses to equilibrate the gas pressure within the spherical pore. The majority of these theories ignore the influence of specific external constraints and the strength of the fuel. If these effects are included, some value is assumed for insertion into the governing equations; however, the theories completely neglect the manner in which the external constraint arises or the application of their results to a particular fuel-element configuration. These theories are more concerned with the formation, motion, and coalescence of gas bubbles within the fuel matrix. On the other hand, the analysis to be presented here is not capable of specifying the microstructural aspects of the swelling process but simply assumes that an initial distribution of identical pores is present in the fuel.

*Battelle Memorial Institute, Columbus Laboratories, Columbus, Ohio.

The present approach emphasizes the material-behavior aspects of the swelling phenomenon. Difficulties arise because approximations are required (1) for treating the interaction of the internal stress fields due to expansion of the pores and (2) for solving the boundary-value problem for cylindrical fuel elements. We will discuss the assumptions used to surmount these difficulties and then present some of the results obtained with the use of the model.

Assumptions

The problem of the interaction between pores cannot be treated in an exact manner even when the material behavior is assumed to be perfectly elastic;[6] therefore we will use an approximation introduced by Foreman.[7] We assume that all the pores are equal in size and contain equal pressures. We further assume that the pores are uniformly distributed throughout the material in a hexagonal array and that a polyhedral cell of material is associated with each pore as shown in Fig. 1. A pressure is generated within each pore and causes the fuel to expand. In the absence of cladding, there are no pressures normal to the faces of the dodecahedron. When a cladding is present, however, normal pressures P_0 exist which are the result of the restraint imposed by the cladding (Fig. 2). To a first approximation the cells can be replaced by equivalent spheres of radius b; a uniform pressure P_0 acts on the spherical surface $r = b$. By invoking the above simplifications, we can treat the cells as thick-walled spherical shells subject to uniform external and internal pressures that will depend on time and swelling rate. Thick-walled spherical-shell theory is thus used for treating the fuel, and cylindrical-shell theory is used for treating the cladding. It should be noted that in the absence of a cladding the geometric assumptions used here are identical with those used by Foreman.[7]

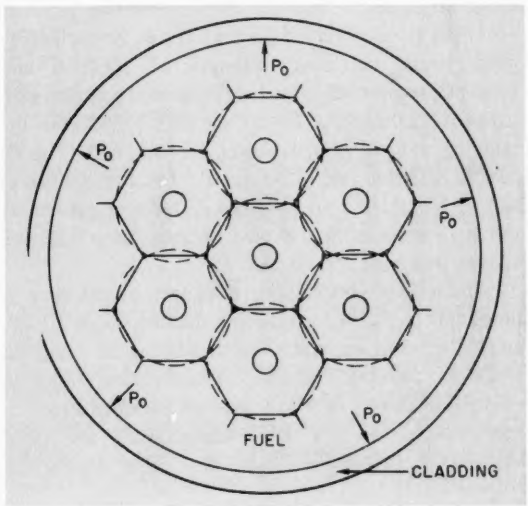

Fig. 1 Model of clad fuel element.

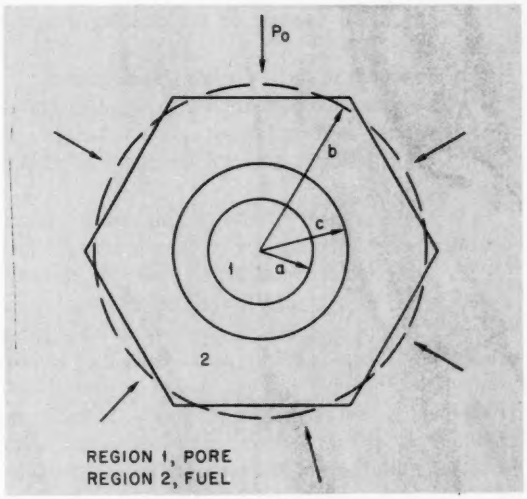

Fig. 2 The role of each cell within the model.

The assumptions used in developing the swelling model are given below:

1. All cells are of equal size and contain pores having equal pressures.

2. As shown in Fig. 2, all polyhedral cells are replaced by spheres of equivalent volume.

3. Each cell is treated as a thick-walled spherical shell subject to the time-dependent internal and external pressures.

4. The internal stress distribution at the cladding is represented by a uniform pressure P_0 which is the same as the normal stress acting on the exterior of each cell.

5. The fuel and the cladding obey nonlinear creep laws which will reduce in the case of uniaxial loading to the form

$$\dot{\epsilon} = \frac{1}{B}\sigma^n \qquad (1)$$

The Von Mises function is used for obtaining effective stresses and strain rate for generalizing uniaxial data to cylindrical and spherical systems.

6. The model assumes an isothermal and incompressible fuel material and cladding. (Incompressibility is applied to the fuel material surrounding the pores.)

7. Only radial swelling of the cladding is considered.

8. The effects of surface tension are neglected.

9. The model has been applied to high-temperature fuels where the swelling is large in comparison to solid swelling and effects of solid swelling have been neglected.

10. The treatment of the system reduces to the consideration of three types of behavior for the fuel: (*a*) The fuel can creep in accordance with the creep law stated in Eq. 1. (*b*) A plastic zone can develop around the pore (radius c in Fig. 2) surrounded by a region which only creeps. (This type of behavior has been studied by Enderby[8] for the case of an unclad fuel.) (*c*) The entire fuel can behave plastically. Likewise, the cladding can deform with the same mechanical behavior as given for the fuel, the net result being three types of behavior for the fuel, three for the cladding, and nine modes of behavior, therefore, to consider.

Appendix A presents the form of the equation for a clad element behaving in a creep mode only. In the case of an unclad highly dense fuel undergoing a relatively small degree of swelling, the relations reduce to those of Foreman.[7]

Parametric Studies Performed with the Swelling Model

The model may be employed to predict the behavior of cermet-dispersion fuels or to describe the behavior of homogeneous alloy fuels. In the analysis of swelling of cermets, the fuel particles are assumed to have no strength, to only occupy space (i.e., the fuel strength is considered negligible in comparison with the matrix material), and to act as sources of gas that exerts pressure on the matrix. Therefore the restraining members of the system are the matrix and the cladding. In the analyses for homogeneous fuels, however, pressure is assumed to build up in bubbles within the fuel; then the restraining members are the fuel and the cladding. The parametric studies discussed here are performed for homogeneous fuels such as UN and UC at 1700°C. The isothermal approximations used in the analysis limit the use of the model to fuels of relatively high conductivity; hence the model in its present form is inapplicable to the swelling of homogeneous systems of oxide fuels.

The parametric studies have been performed by varying parameters about a central case. This central case corresponds to the swelling of a 0.2-in.-OD fuel pellet surrounded by a 20-mil cladding at a constant temperature of 1700°C. The fuel is 99% dense and has a yield stress of 5000 psi and a creep strength* of 70 psi. This creep strength was chosen because it best fits the experimental swelling data for UC. As shown in Fig. 3, the creep strength, chosen so that the central

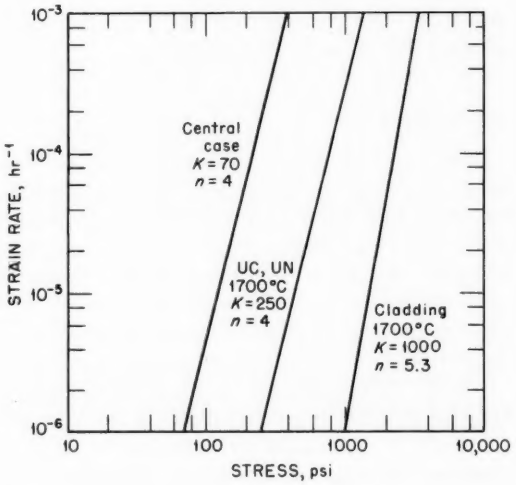

Fig. 3 Stress vs. strain rate for fuel and cladding (K = creep strength).

case will approximate the swelling behavior of UC at 1700°C, is about one-third that of the out-of-pile creep strength of UC. The required reduction in the creep strength of UC is probably the result of in-pile fission effects on creep.

Other parameters for the central case are a cladding yield stress and creep strength of 5000 psi and 1000 psi, respectively. The variation of strain rate with stress is assumed to be to the 5.3 power for the cladding and to the 4 power for the fuel (Fig. 3). Finally, a fission rate of 1.3×10^{13} fissions/(cm^3)(sec) and no gas release are assumed. Effects of gas release will be considered and shown in comparison with the above-mentioned central case.

The effect of cladding thickness on swelling is presented in Fig. 4 for cladding thicknesses of 10, 20, and 40 mils. As expected, the thicker the cladding, the lower the swelling. The effect of a cladding failure on swelling is shown in Fig. 5. For an assumed break in the cladding at 5×10^{19} fissions/cm^3, the rapid increase in swelling indicates that it is mainly the

*Creep strength is defined as the stress to produce a steady-state strain rate of 10^{-6}/hr.

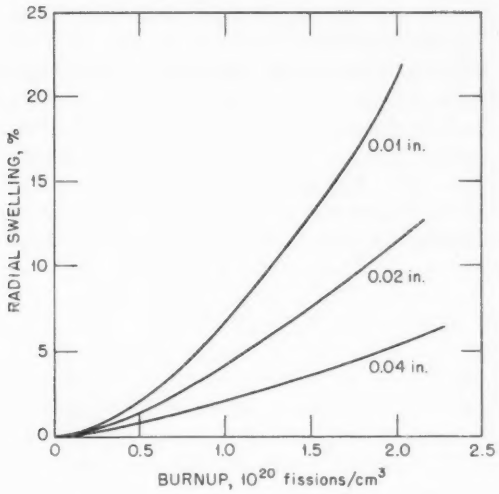

Fig. 4 Effect of cladding thickness on swelling.

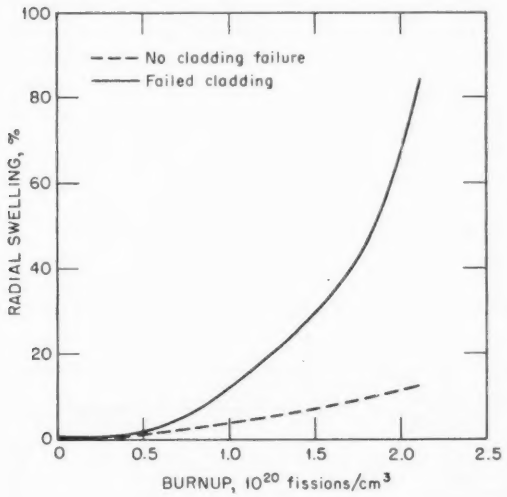

Fig. 5 Effect of cladding failure on swelling (failure at 5×10^{19} fissions/cm^3).

cladding which has a strong effect in restraining the swelling for the central case under consideration.

Figure 6 contains swelling curves for 90, 99, and 99.9% dense fuels. As the fuel density increases, the swelling increases since the less dense the material, the more pores it has and, therefore, the more gas it can retain at low pressure. An increase in density from 90 to 99% corresponds to a reduction in pore volume of the order of 9%; thus pressures are generated more

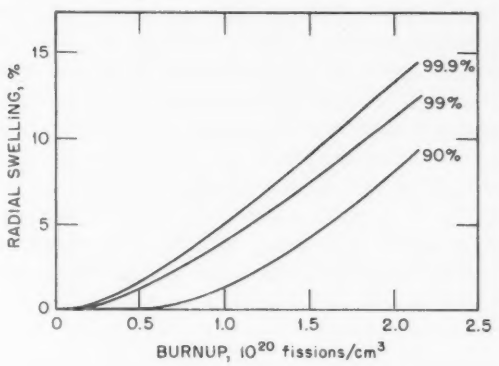

Fig. 6 Effect of fuel density on swelling.

rapidly within the pores, and higher swelling rates are the result. The increasing flat portions of the predicted swelling curves at lower density correspond to increasing times required to develop sufficient pressures within the pores to produce significant swelling.

Figure 7 relates swelling to the creep strength of the fuel for a constant creep strength of the cladding. As expected, the stronger the fuel, the lower the swelling. The curve corresponding to the 70-psi creep strength is the central case under consideration and provides a reasonably good fit to observed swelling data. The lower curve appearing in Fig. 7 (250-psi creep strength) corresponds approximately to the swelling predicted for UC if the fuel were to maintain its out-of-pile creep strength. It should be noted that, even with the reduced creep strength used in this study, the fuel still acts to restrain swelling, as can be seen by the predicted increase in swelling when the creep strength of the fuel is lowered from 70 to 35 psi.

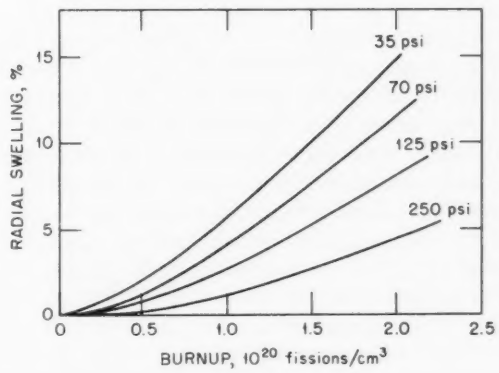

Fig. 7 Effect of fuel creep strength on swelling.

The effect of varying the creep strengtn of the cladding is shown in Fig. 8. Comparisons are made between the predicted swelling of an unclad fuel element, the central case and a fuel element having a cladding that is 10 times stronger than that shown in the central case. The results indicate that strengthening the cladding as well as thickening the cladding (see Fig. 7) can produce a marked decrease in swelling. Experiments performed with thicker claddings (40 mils) have indeed indicated a significant reduction in swelling when thicker claddings are employed.

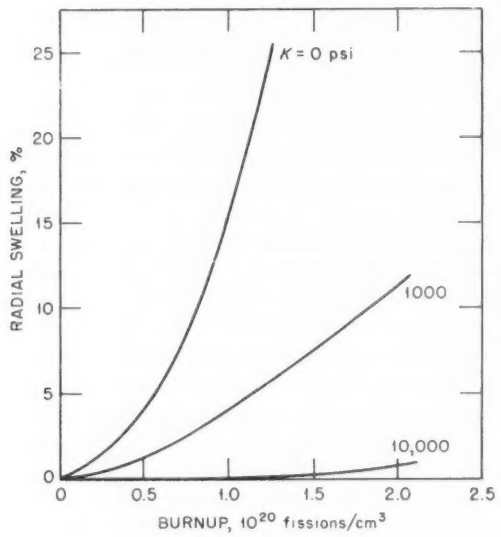

Fig. 8 Effect of cladding creep strength on swelling.

Gas-release data, meager as they are, indicate that the fractional amount of gas released is a direct function of swelling or total porosity and hence depends only indirectly on burnup. Furthermore, if gas release results from a partial cracking of the fuel, it would be reasonable to assume that it would be accompanied by a loss in effective strength of the fuel. The model can account for a continuous dependence of both gas release and strength on swelling. This is done by assuming that both phenomena are functions of the porosity, X, defined as the ratio of the pore volume to the initial fuel volume, which in the case of a 99 to 100% dense material is essentially given by the volumetric swelling. Thus, for an initially dense fuel,

$$X = \frac{\Delta V}{V} \tag{2}$$

where ΔV is the change in fuel volume and V is the initial fuel volume.

Adequate quantitative information concerning gas release is lacking; however, it is reasonable to assume that gas release is a function of the increased porosity created by swelling of the fuel. Therefore the adopted relation governing gas release contains a sufficient number of parameters that may be varied to describe the qualitative gas-release behavior believed to be occurring in a fuel element. The relation is

$$f_g = 1 - e^{-(C_1 X)^m} \tag{3}$$

Here f_g is the fraction of generated gas atoms released. The constant C_1 would probably depend on both material properties and geometry, and m is a factor that permits adjusting the abruptness with which gas release can occur.

Figure 9 shows the variation of gas release for different values of C_1 (Eq. 3) and a constant value of m ($m = 4$). A value of $C_1 = 0$ corresponds to no gas release. As C_1 is increased, the gas is released at lower porosities, and case 4 corresponds to fuels such as UN that release gas at relatively low stages of burnup.

In the same manner, the effective creep strength of the fuel is assumed to decrease in accordance with the relation

$$K = \frac{K_0}{1 + C_2 X} \tag{4}$$

where K is the effective creep strength at porosity X, K_0 is the initial creep strength, and C_2 is a factor

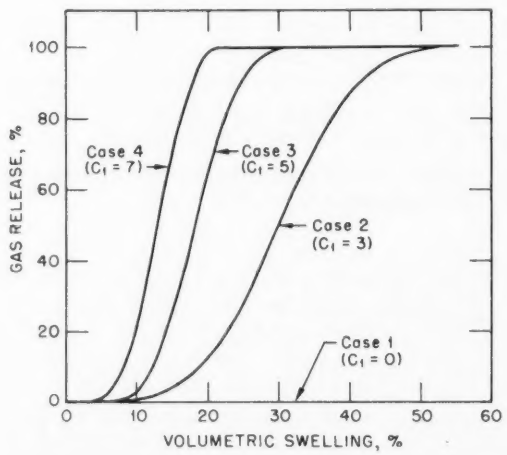

Fig. 9 Gas release as influenced by the volumetric swelling.

that depends upon material properties and geometry. The weakening of the fuel in accordance with Eq. 4 is shown in Fig. 10 for four cases ranging from no loss in strength (case A) to considerable loss in strength (case D). The decrease in creep strength of the fuel with increasing porosity assumed here is a first attempt to compensate for partial cracking of the fuel.

The effect of gas release on swelling is shown in Fig. 11. The four cases shown in Fig. 11 were obtained with the use of the correspondingly numbered gas-release curves appearing in Fig. 9. Cracking of the fuel was treated by assuming that the creep strength decreased with porosity in accordance with case C shown in Fig. 10. It can readily be seen that the degree of swelling and the occurrence of saturation swelling are predicted to be strongly affected by the degree of gas release.

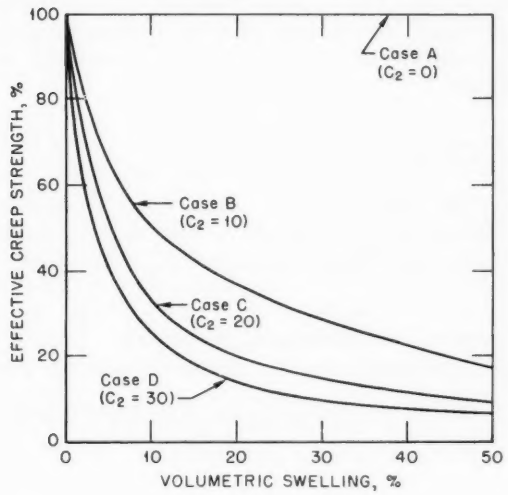

Fig. 10 Loss of strength of fuel as influenced by the volumetric swelling.

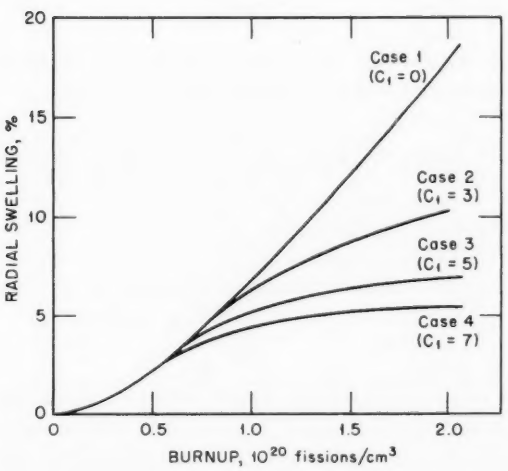

Fig. 11 Effect of gas release on swelling when $m = 4$ and $C_2 = 20$.

The effect of different rates of loss of strength of the fuel in combination with a relatively rapid and abrupt rate of gas release is shown in Fig. 12. Gas release corresponding to case 2 from Fig. 9 is included here ($C_1 = 3$, $m = 4$, $C_2 = 0$ to 30). As can be seen by comparing Figs. 11 and 12, the degree of gas release affects swelling considerably more than weakening of the fuel, and therefore the loss of strength of the fuel with increasing porosity in the presence of a strong cladding has little effect on swelling.

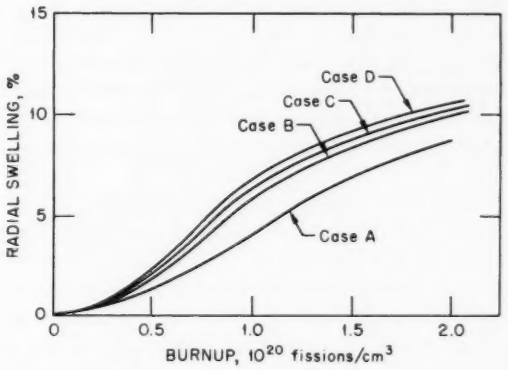

Fig. 12 Effect of loss of strength of the fuel on swelling when $C_1 = 3$ and $m = 4$.

Experimental data for the swelling of clad UC, UN, and UO_2 at high temperatures are given in Fig. 13 in the form of volumetric swelling as functions of burnup. The radial swelling will be more than a factor of 2 lower than the volumetric swelling. The UC curve is very nearly linear and is characteristic of the observations of relatively low gas release occurring in the range of burnup for which data have been obtained. Qualitative consistency of the data with the model is apparent from inspection of Fig. 11. If there were no gas release, the model would predict a swelling curve that was concave upward, such as that appearing as case 1 of Fig. 11. The actual gas-release behavior for UC probably lies somewhere between cases 1 and 2 and can

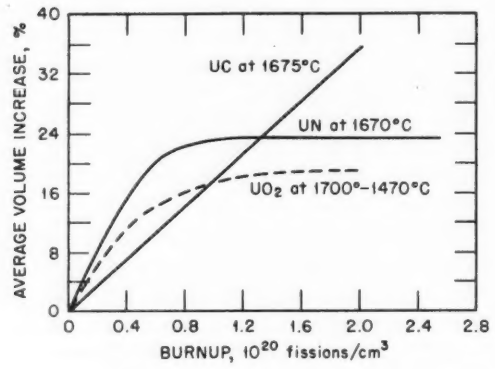

Fig. 13 Swelling of UC, UN, and UO_2 at high temperatures.

account, at least roughly, for the observed linear swelling behavior.

The observed gas-release behavior for UN is more characteristic of cases 3 and 4 and accounts for the saturation swelling at a burnup of 10^{20} fissions/cm^3. Although the isothermal model under consideration is not amenable to the analysis of UO_2, it should be noted that the observed saturation swelling is qualitatively consistent with gas-release characteristics of UO_2.

None of the swelling data can be predicted quantitatively with the use of measured out-of-pile creep properties for UN and UC at 1700°C. Quantitative agreement can be obtained, however, with the use of a reduced creep strength of 70 psi (as was used for the central case in the parametric studies) as opposed to the measured out-of-pile creep strength of 250 psi. The above observations indicate a possible weakening of the fuel as a result of the fission process. The model indicates that even greater weakening effects occur for UC at a temperature of 1300°C when the effects of cladding restraint and gas release are small; thus more credibility is possibly added to the hypothesis of fission-enhanced creep of the fuel.

Conclusions

The swelling model presented here is an extension of the mechanical analyses performed by Foreman[7] and Enderby[8] to predict fission-gas swelling. The extension includes consideration of effects of cladding, arbitrary gas-release relations, and effects of loss of strength with increasing porosity. The model has considerable flexibility and is relatively easy to use in predicting the effects of many of the controlling parameters on fuel-element swelling. Although the model lacks the rigor and sophistication of more elaborate models such as that given in Ref. 9, it does provide rapid results that are in reasonable agreement with the data.

Comparisons of predicted swelling and measured swelling data indicate the possibility of fission-enhanced creep occurring at temperatures as high as 1700°C. The indications of creep enhancement at 1700°C and the greater degree of creep enhancement predicted at 1300°C appear to be considerably beyond the fairly large margins of error resulting from the assumptions employed in the development of the model.

Acknowledgment

The authors wish to acknowledge the valuable assistance of S. M. Bucaram in many of the computations of swelling predictions appearing in this article.

Appendix A: Differential Equation for Swelling Under Pure Creep

If the strain rate under uniaxial loading is related to stress by

$$\dot{\epsilon} = \frac{1}{B}\sigma^n \qquad \text{(A-1)}$$

for the fuel and

$$\dot{\epsilon} = \frac{1}{B^*}\sigma^{n^*} \qquad \text{(A-2)}$$

for the cladding, then, under conditions of pure creep, the swelling equations assume the form

$$p - P_0 = \frac{2n}{3}\left(2B\frac{1}{a}\frac{da}{dt}\right)^{1/n} \cdot \left[1 - \left(\frac{a}{b}\right)^{3/n}\right] \qquad \text{(A-3)}$$

where p = pore pressure
a = pore radius
b = radius interaction zone (see Fig. 2)
P_0 = pressure exerted by fuel on cladding
t = time

If the fuel were unclad, then P_0 would equal zero and Eq. A-3 would reduce to Eq. 10 of Ref. 7. If the fuel is clad, then P_0 is given by the differential equation

$$P_0 = \frac{n^*}{3}\left(\frac{2B^*}{3}\frac{da^*}{dt}\right)^{1/n^*} \left[1 - \left(\frac{a^*}{b^*}\right)^{2/n^*}\right] \qquad \text{(A-4)}$$

where a^* and b^* denote the inner and outer radii of the cladding, respectively. The variations in b and b^* may be related to those in a and a^* by the incompressibility relations

$$a^3 - a_0^3 = b^3 - b_0^3$$

$$a^{*2} - a_0^{*2} = b^{*2} - b_0^{*2}$$

The cladding radius a^* is related to a by the above equations together with the relation

$$\frac{a^{*2}}{a_0^{*2}} = \frac{b^3}{b_0^3}$$

which equates the swelling rate of the fuel to that of the cladding assuming no axial swelling.

The pore pressure p is related to the gas generation rate, the instantaneous pore radius, the temperature, and the degree of gas released. The ideal gas law has been used as the equation of state of the gas; hence p can be replaced by the above-mentioned parameters in a relatively straightforward manner. The numerical method used in solving the swelling equations consists of solving for the derivatives appearing in the above equations by a nesting procedure and integrates the equations by the conventional fourth-order Runge–Kutta method.

References

1. S. F. Pugh, Swelling in Alpha Uranium Due to Irradiation, *J. Nucl. Mater.*, **4**: 177-199 (1961).
2. G. W. Greenwood, A. J. E. Foreman, and D. E. Rimmer, The Role of Vacancies and Dislocations in the Nucleation and Growth of Gas Bubbles in Irradiated Fissile Material, *J. Nucl. Mater.*, **1**: 305-324 (1959).
3. R. S. Barnes, A Theory of Swelling and Gas Release for Reactor Materials, *J. Nucl. Mater.*, **11**: 135-148 (1964).
4. R. S. Barnes and R. S. Nelson, Theories of Swelling and Gas Retention in Reactor Materials, British Report AERE-R-4952, June 1965.
5. F. A. Nichols, Behavior of Gaseous Fission Products in Oxide Fuel Elements, USAEC Report WAPD-TM-570, Bettis Atomic Power Laboratory, October 1966.
6. J. D. Eshelby, Elastic Inclusions and Inhomogeneities, in *Progress in Solid Mechanics*, Vol. 1, I. V. Sneddon and R. Hill (Eds.), Interscience Publishers, a division of John Wiley & Sons, Inc., New York, 1961.
7. A. J. E. Foreman, Calculations on the Rate of Swelling of Gas Bubbles in Uranium, British Report AERE-T/M-134, March 1956.
8. J. A. Enderby, Plastic Flow and the Swelling of Gas Bubbles in Uranium, British Report IGR-R/R-198, November 1956.
9. C. M. Friedrich and W. H. Guilinger, CYGRO-2: A Fortran-IV Computer Program for Stress Analysis of the Growth of Cylindrical Fuel Elements with Fission Gas Bubbles, USAEC Report WAPD-TM-547, Bettis Atomic Power Laboratory, November 1966.

Postoperative Studies of PM-1 and PM-3A Fuel Tubes

By John B. Brown, Jr., and V. W. Storhok*

Abstract: *The Portable Medium Power Plant 3A (PM-3A) type 1, serial 2 core was discharged at 53% of the core's design lifetime primarily because of increasing fission-product accumulation in the primary coolant system, presumably resulting from a fuel leak of undetermined origin. The Portable Medium Power Plant 1 (PM-1) type 1, serial 3 core also experienced an increasing fission-product accumulation in the primary coolant but was permitted to operate to 100% of the core's design lifetime. Coolant fission-product activity buildup was believed to be associated with defects in the 347 stainless-steel cladding on the tubular-type fuel; the fuel consisted of 28 vol.% UO_2 dispersed in 304L stainless steel. Both PM cores were examined in the Battelle–Columbus hot cells to locate and establish the nature of the fuel-tube defects and to determine the cause or causes of such defects.*

Results of the core examinations showed that fuel-tube failures were similar in both PM reactors. Fission products leaked through numerous intergranular cracks in the outer cladding of fuel tubes located in the high-performance region of the cores, where burnups exceeded 13 to 14 x 10^{20} fissions/cm^3. The cracks started on the outer surface of the cladding and generally terminated at UO_2 particles near the fuel dispersion–cladding interface. All cracks in the outer cladding were longitudinal and were associated with hoop strains greater than about 0.3%. No cracks were observed in the tubes' inner cladding or fuel matrix. On the basis of mechanical-property data of irradiated stainless steel, it is possible to attribute the failures solely to fuel swelling and effective cladding ductility losses associated with neutron exposure, low-strain-rate biaxial loading, and thermally induced cyclic loading. However, the similarity of the PM cladding failures to stress-corrosion cladding failures observed in boiling-water reactors suggests the possibility that the PM failures are related to the same type of stress-corrosion cracking as the boiling-water-reactor cladding. Whether strictly mechanical or chemical–mechanical, the failures were strain related, and the solution then is probably the same for either failure mechanism. That is, design the fuel tubes to minimize cladding strain. This may be accomplished by providing more voidage to accommodate swelling internally or by employing a stronger cladding.

*Battelle Memorial Institute, Columbus Laboratories, Columbus, Ohio.

The PM-3A (McMurdo Station, Antarctica) type 1, serial 2 reactor core was discharged November 1964, after an accumulated lifetime of about 7000 effective full-power hours (EFPH) of operation. This represented 53% of the design lifetime energy output of the core (14.7 Mw-years). The Navy's decision to change the core was prompted by an increasing fission-product accumulation in the primary coolant system, presumably resulting from a fuel leak of undetermined origin. The PM-1 (Sundance, Wyoming) type 1, serial 3 core also experienced an increasing fission-product accumulation in the primary coolant system but was permitted to operate to 100% of the core's design lifetime. Both PM cores developed fission-product leaks after approximately 4000 EFPH of operation.

The fission-product buildup was believed to be associated with defects in the 347 stainless-steel cladding on the tubular-type fuel; the fuel consisted of 28 vol.% UO_2 dispersed in 304L stainless steel. The PM-3A core was shipped to the Battelle–Columbus hot cells for examination in an attempt to locate the cladding defects and to determine the cause or causes of such defects. The full-term PM-1 core was later examined in the Battelle–Columbus hot cells to determine full-term operation effects on type 1 PM fuel tubes. Details and results of PM-1 and PM-3A core examinations are presented here.

Work performed in the examinations of both PM cores was sponsored by the Department of the Navy, Naval Facilities Engineering Command. Core operation

data were supplied by both the U. S. Naval Nuclear Power Unit, Fort Belvoir, Va., and the U. S. Air Force.

History

PM Fuel Cores

Core Specifications. The identical type 1 PM-1 and PM-3A cores[1] were cylindrical, heterogeneous, light-water-moderated, highly enriched (93.1%) systems that operated at a pressure of 1300 psia. Type 1 cores (now obsolete) consisted of seven fuel bundles, six peripheral bundles and one center bundle, contained in a core shroud (Fig. 1*a*). The total number of elements in each core was 849, with 139 in each peripheral bundle and 15 in the center bundle. Of this total, 741 were tubular-type fuel elements having a characteristic 0.506-in. outside diameter and 0.417-in. inside diameter. The remaining core elements consisted of burnable poison and dummy rods. The tubular fuel elements were 33 in. long with an active core length of 30 in. The active reactor core diameter was 23 in. The tubular dispersion fuel, clad with 7-mil 347 stainless steel both inside and outside, was 28 mils thick and contained 28 wt.% UO_2 dispersed in 304L stainless steel (Fig. 1*b*). Average operating core coolant temperature was 463°F, average cladding surface temperature was 580°F, and maximum fuel-dispersion temperature was 620°F.

Fuel-Element Construction. Major operations[2] in the fabrication of the type 1 tubular fuel elements for the PM-1 (Sundance) and the PM-3A (McMurdo) cores included the following:

1. UO_2 and stainless-steel powders blended and rolled into a strip.
2. Strip sintered.
3. Strip sheathed in a 2- to 5-mil 347 stainless-steel cladding to protect it from the atmosphere.
4. Sheathed strip hot-rolled to 95 to 97% of theoretical density.
5. Strip cut to length and end cladding welded to strip.
6. Composite strip formed into a tube and fitted between inner and outer cladding tubes.
7. Tube assemblies alternately drawn and annealed to size.

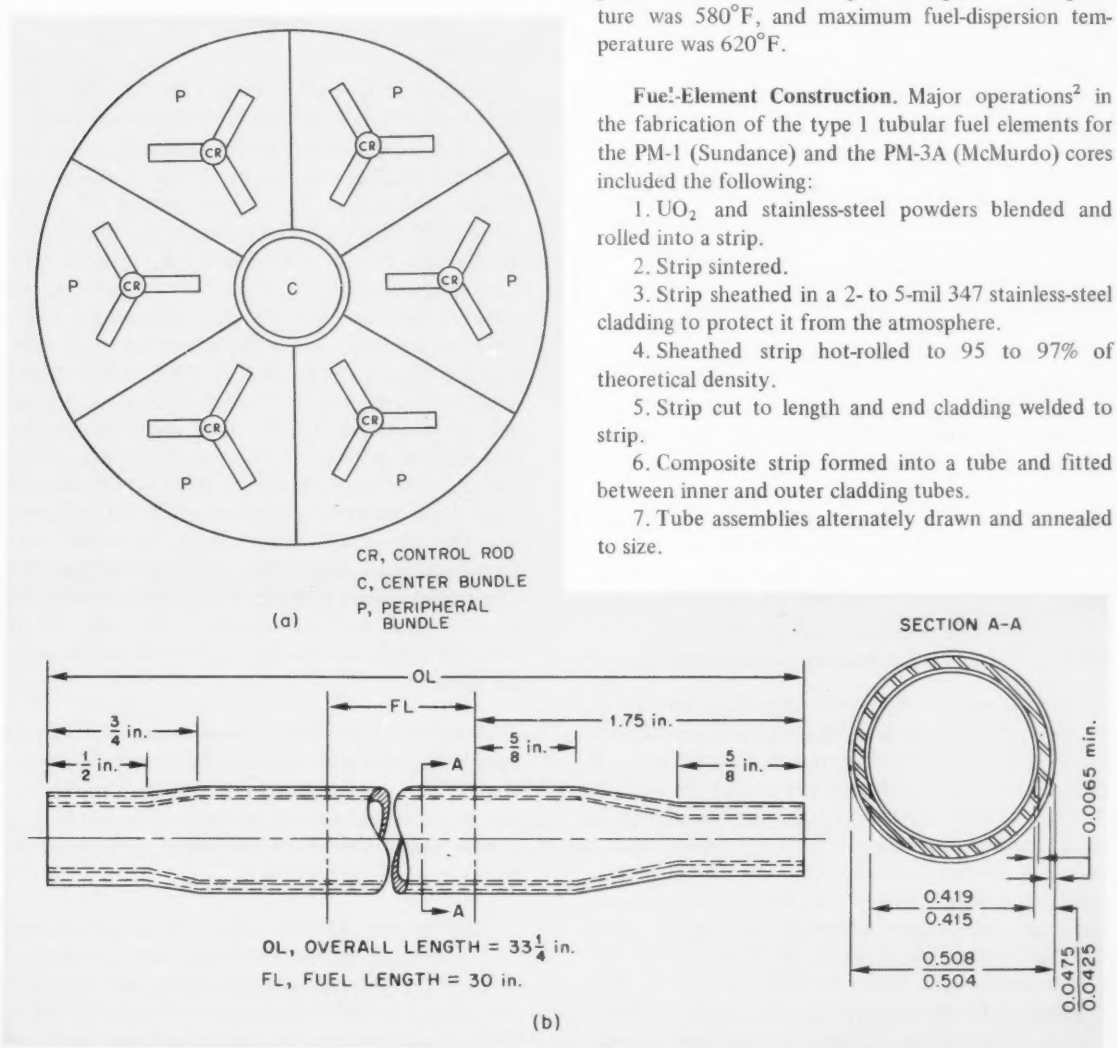

Fig. 1 (a) Top-view sketch of PM type 1 core. (b) Fuel element of PM type 1 core.

8. Tube assemblies isostatically pressed for final densification and bonding.

9. Tubes inspected and assembled into bundles.

Operation and Storage History

Irradiation History. The PM-1 type 1, serial 3 core went critical in February 1962 and was shut down in August 1966. During this period the core accumulated about 15,000 EFPH of operation at a nominal power level of 9.37 Mw(t). The average time-integrated thermal-neutron flux generated by the core was about 5.5×10^{20} neutrons/cm^2. The PM-3A type 1, serial 2 core started power operation in May 1962 and was shut down in November 1964. The PM-3A core accumulated 7165 EFPH of operation at a nominal power level of 9.5 Mw(t). The average fluence generated by the core was about 2.6×10^{20} neutrons/cm^2.

Primary-Water Chemistry. Primary-water chemistry for both the PM-1 and PM-3A cores[3,4] was characterized by low chloride ($\leq$0.1 ppm), high *p*H ($8.5 \leq p\text{H} \leq 10$), and low oxygen (<50 ppb). Ammonia was used for the control of *p*H and dissolved oxygen.

Storage History. After shutdown, both type 1 PM-1 and PM-3A cores were stored in the PM shipping cask, which was submerged in the storage tank located adjacent to the pressure-vessel tank. Following a decay period of about a year, the cores were shipped from their respective locations to Battelle–Columbus for examination. The PM-3A core was examined in summer 1966, and the PM-1 core was examined in fall 1967.

PM Type 1 Core Fission-Product Leaking Histories

Primary-water radioactivity started to increase in all type 1 PM cores after accumulated lifetimes of from 4000 to 6000 EFPH of operation. Figure 2 shows a plot of gross iodine activity in the primary coolant as a function of EFPH of operation for the PM-3A type 1, serial 1 and 2 cores and for the PM-1 type 1, serial 3 core. On the basis of examination of PM-3A type 1, serial 2 fuel tubes (serial 1 core followed serial 2 core operation), the decision to operate the serial 1 core to full-term burnup was made by the Navy without fear of any catastrophic failure occurring in the core. The apparent higher primary-coolant leak rate of the PM-1 system was a contributing factor to the lesser amount of gross iodine activity experienced with the PM-1 type 1, serial 3 core.

Postirradiation Examination

The postirradiation examinations of the PM-1 and PM-3A fuel cores were directed toward locating and establishing the nature of the fuel-tube defects and determining the cause or causes of such defects. A combination of visual macroexamination for defects followed by a microstructural examination of apparent defect areas was utilized in both PM core examinations. These were supplemented with dimensional measurements, fuel-burnup analysis, and gamma scanning. The experimental procedures used in the examination and the results are described in the following sections.

Procedure

Several fuel bundles from both the PM-1 and PM-3A cores were examined in the Battelle–Columbus high-level beta–gamma cell. Fuel-bundle unloading from the shipping cask was performed in a 14-ft-deep storage pool adjacent to the beta–gamma cell. In-cell fuel-bundle handling was performed by utilizing the in-cell crane and a cable-suspended bundle-carrying tray. Macroexaminations of the fuel-tube surfaces were performed at magnifications up to 12 diameters using a remotely operated stereo viewer. Several fuel tubes were cut from the center bundle and from a peripheral bundle of each core to accommodate more detailed macroexaminations. The fuel tubes removed contained the greatest number of outer-cladding-crack indications, as determined during the stereo-viewer examinations. Only results of inspections of the higher burnup center-bundle fuel tubes will be presented here. Outside-diameter measurements, burnup analysis, cladding hardness tests, and metallography were performed to determine the postirradiation condition of the removed fuel tubes. Procedures for these performances are as follows:

Fuel-Tube Diameter Measurements. Fuel-tube outside-diameter measurements were made by using a vernier micrometer accurate to within ±0.0005 in. Several inside-diameter measurements were made using a dial readout inside-diameter-bore micrometer accurate to within ±0.0005 in.

Fuel-Burnup Analysis. Uranium-burnup analyses were performed on two specimens taken from the fuel tubes removed for destructive testing. One specimen was taken from the highest burnup domain of the fuel tube (as determined from gamma-scanning data), and the other specimen was taken from a low-performance domain of the fuel tube. Each specimen was a

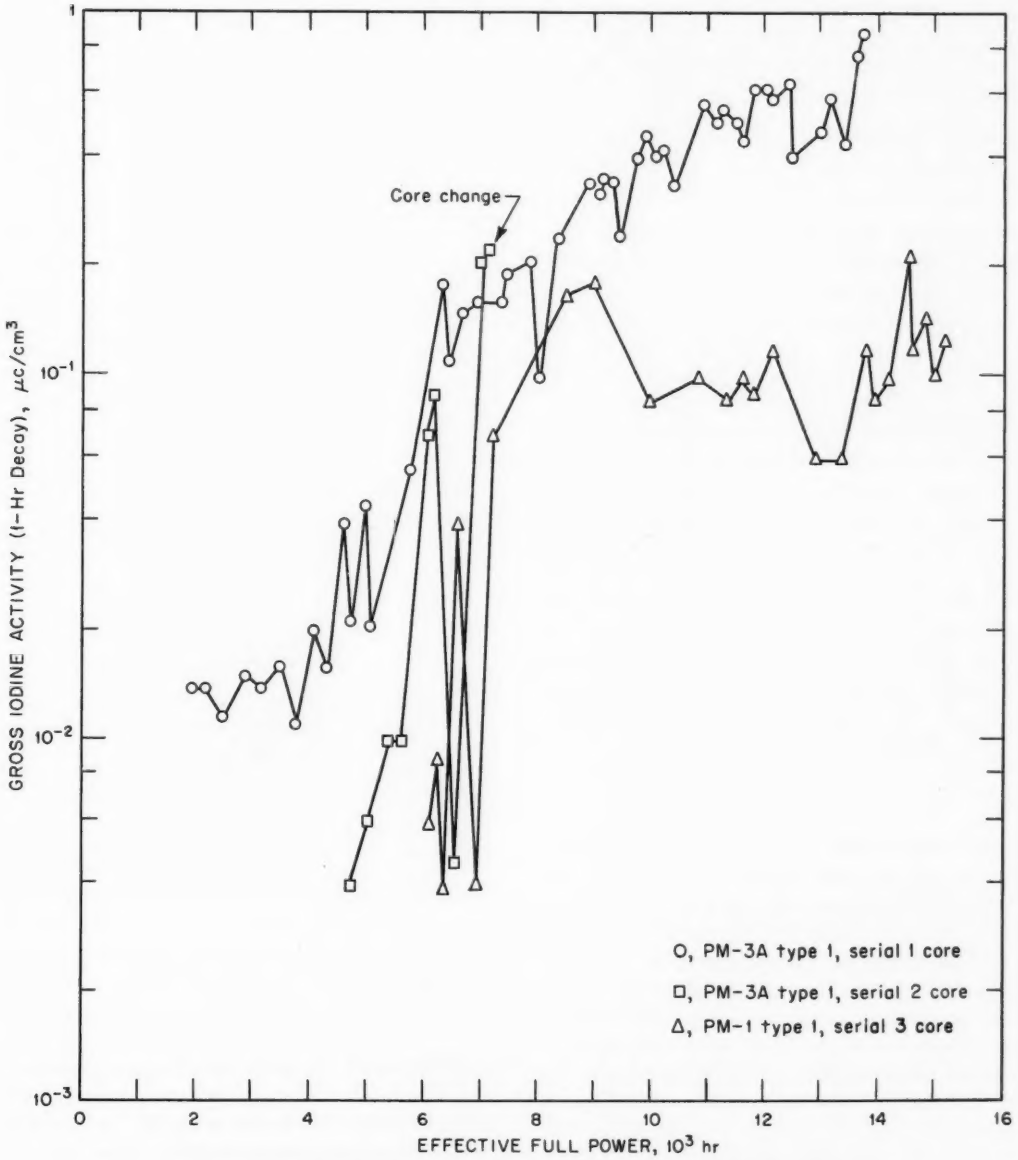

Fig. 2 Gross iodine activity in primary coolant as a function of EFPH of operation for type 1 PM-3A, serial 1 and 2 and PM-1, serial 3 cores.

cylindrical section of the fuel tube about ¼ in. long. The specimens were dissolved, and the aliquots were analyzed by mass-spectrographic techniques. The quantities of ^{234}U, ^{235}U, ^{236}U, and ^{238}U were determined and compared to similar data from an unirradiated control specimen. The burnup was then calculated from the relation:

$$BU = 100\frac{(1+\alpha)E_5^0 - E_5}{E_5^0(1+\alpha-E_5)}$$

where BU is weight percent ^{235}U, E_5^0 is ^{235}U initial enrichment, and α is 0.185.

Removed fuel tubes were gamma scanned to obtain profiles of gamma radiation emitted from high-

performance center-bundle and peripheral-bundle fuel tubes. The burnup profile along the tube length was determined by normalizing the gamma-activity plots to the mass-spectrographic analytical data.

Cladding Hardness Test. Fuel-tube cladding hardness was determined using a remotely operated Knoop hardness tester with a 25-g load.

Metallography. Metallographic specimens were then cut from the removed fuel tubes. Cutting of the fuel tubes was accomplished by using a motor-driven $\frac{1}{16}$-in.-thick abrasive wheel. Selection of the fuel-tube metallographic sections was based on fuel-tube gamma-scanning data. Sections cut from the fuel tubes examined represented highest, average, and lowest burnup regions of the tubes. Cut direction was chosen to permit cuts to intersect the cladding-crack direction at right angles. Since no transverse crack indications were noted, all cuts were transverse to the long dimension of the tube.

Polished specimen surfaces were obtained by (1) grinding through 600-grit silicon carbide paper, (2) rough polishing with Linde A powder mixed with 2% Cr_2O_3 in water, and (3) fine polishing with Linde A and B powders with water as a carrier. The specimens were etched with a reagent containing glycerin, nitric acid, and hydrochloric acid.

Results

General Appearance of Core and Core Bundles. Black scale was observed coating the surfaces of the fuel tubes at the low-performance (low-burnup) and structural surfaces of both the PM-1 and PM-3A type 1 cores. In higher performance regions of the core (i.e., fuel-tube surfaces toward the center of the core where ^{235}U burnups were highest), the thick black scale was absent; the result was a surface color that could be described as a dull metallic luster (for example, Fig. 3).

All circular flow channels (holes in bundle grid plates and fuel-tube inner channels) in both cores appeared to be free from scale or foreign-material buildup. Flow channels were checked by shining a light through the fuel tubes and into grid-plate holes and observing transmissions and reflections visually.

Visual Examination of Fuel Tubes. Examination of the outer cladding of the center-bundle and peripheral-bundle fuel tubes of both cores revealed the presence of numerous longitudinal cracks. All outer-cladding-crack indications were located in the high-performance domain of the fuel tubes, i.e., toward the center of the core. Cracks detected on the outer cladding of high-

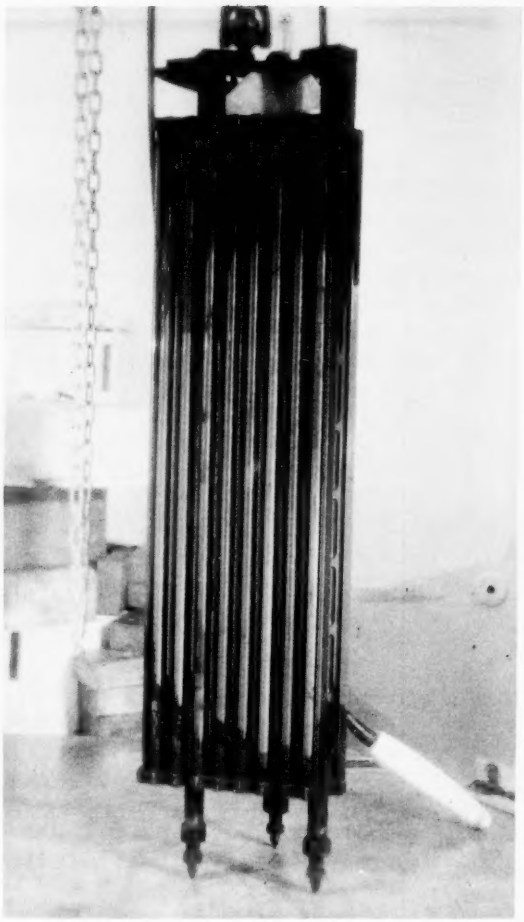

Fig. 3 PM-1 peripheral bundle as viewed through hot-cell window.

performance PM-1 tubes existed in a region extending from about 2 in. from the bottom of the fuel tube to approximately 7 in. from the top. However, apparently because of the premature shutdown of the PM-3A core, outer-cladding-crack indications ranged from 6 to 12 in. above the core's active bottom. The number of cracks per unit area was definitely greater in the higher performance domains (toward the middle of the core) of the fuel tube, and many cracks appeared to have additional material buildup around the periphery of the cracks.

Figure 4 shows a typical crack indication as detected on the outer cladding of a high-performance PM-1 peripheral-bundle fuel tube. For both cores the number of crack indications per unit of outer cladding

Fig. 4 Representative crack indications on high-performance PM-1 type 1, serial 3, peripheral-bundle 2 fuel tube. Magnification, 12 x.

area on the center-bundle fuel tubes was greater than for the high-performance peripheral-bundle fuel tubes. This was not surprising since center-bundle fuel tubes experienced higher burnups than neighboring high-performance peripheral-bundle fuel tubes. Flaking of the thinner gray scale on the tube surface probably accounts for the specks that appear to be on the tube surface (Fig. 4).

Fuel-Tube Diameter Measurements. Outside- and inside-diameter measurements were performed on selected PM-1 and PM-3A fuel tubes in an attempt to determine relative swelling behavior along fuel-tube lengths as a function of burnup.

Outside-diameter measurements were taken at 1-in. intervals along the tube length. Results of these measurements are plotted in Fig. 5 for a half-term PM-3A and a full-term PM-1 center-bundle fuel tube.

Each outside-diameter data point plotted in Fig. 5 is the average value of two outside-diameter measurements (at 90° to each other) per measurement position along the tube length.

Average outside diameters for two full-term PM-1 fuel tubes examined ranged from a nominal 0.507 to a maximum of about 0.512 in. This maximum outside diameter exhibited by high-performance fuel tubes corresponds to an increase of about 1%. Outside-diameter increases observed in the highest performance fuel tubes of the half-term PM-3A type 1, serial 2 core were approximately 0.6%. Fuel-tube outside-diameter increases corresponding to the degree of swelling at which cracking was initiated are estimated at about 1.7 mils above the nominal outside diameter, or 0.3%.

Greatest outside-diameter values for the high-performance PM-1 and PM-3A fuel tubes occurred in the lower half of the fuel tubes. However, maximum outside-diameter values for the PM-1 fuel tubes occurred closer to the midplane of the core than did PM-3A fuel-tube maximum outside-diameter values. This result was expected since maximum thermal-neutron flux, and therefore maximum burnup rates, occurred at higher core elevations in the PM-1 core as a result of greater control-rod-bank withdrawal distances.

Fuel-tube inside-diameter measurements were taken at selected locations for two PM-1 center-bundle fuel tubes and one peripheral-bundle fuel tube. Inside-diameter values ranged from 0.415 to 0.419 in. These inside-diameter values were all within as-built inside-diameter tolerances (ID = 0.415 to 0.419). This result suggests that the inside cladding was not circumferentially strained and that all the fuel-dispersion swelling occurred in an outward direction.

Fuel-Burnup Analysis. Burnups (i.e., percentage depletion of fissile isotope ^{235}U) of fuel specimens taken from high-performance fuel tubes from the PM-1 and PM-3A cores were determined by mass-spectrometric analysis. These point burnup data were used to normalize the fuel-tube gamma-scanning profiles (i.e., relative ^{95}Nb–^{95}Zr concentrations). Results

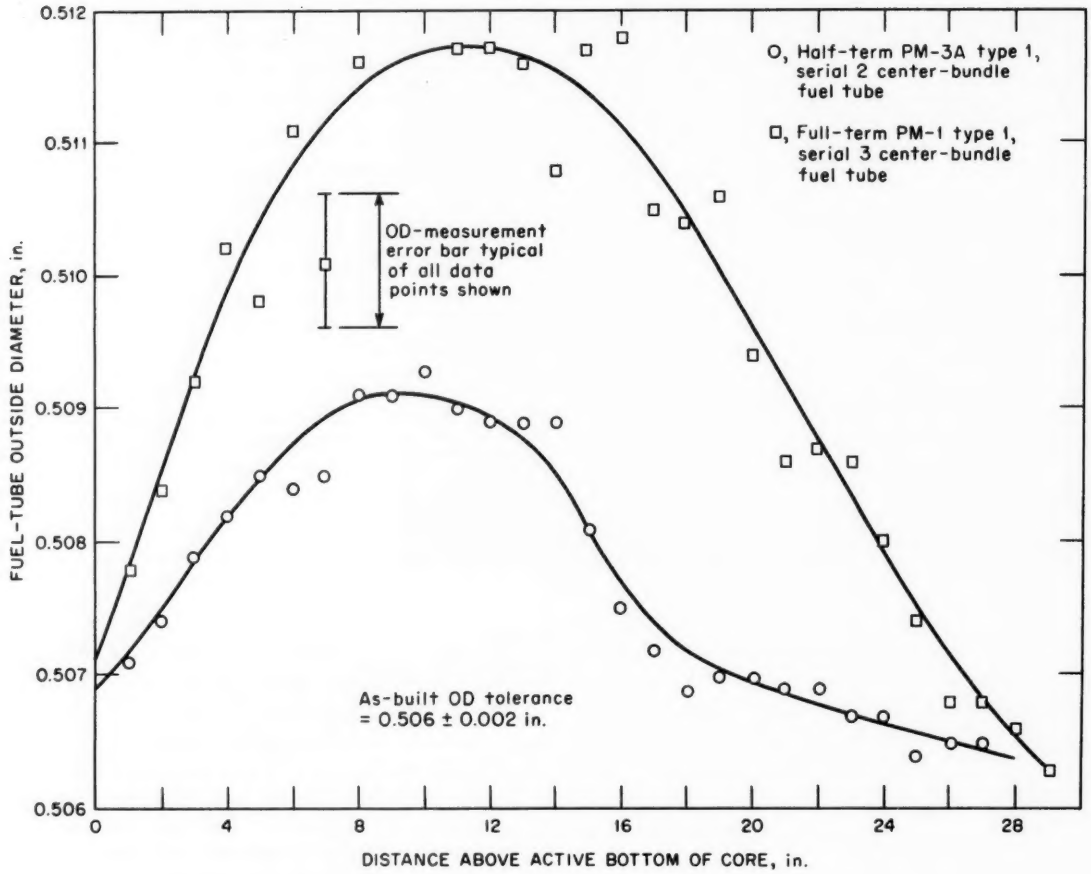

Fig. 5 Average fuel-tube outside diameter as a function of position.

of burnup profiles determined for one PM-1 and one PM-3A center-bundle fuel tube are shown in Fig. 6. Peak burnup in the full-term PM-1 core was 25×10^{20} fissions/cm^3 and occurred 12 to 13 in. above the active bottom of the core. Peak burnup in the half-term PM-3A core was 15×10^{20} fissions/cm^3 and occurred about 9 in. above the active core bottom.

Cladding Hardness Test. Knoop hardness measurements were made to determine the relative hardness of irradiated PM-1 fuel cladding at several performance locations. Table 1 gives the results of the hardness tests with a sketch description of indentation location within the claddings tested. These results showed that the Knoop hardness of the irradiated cladding was significantly higher than the hardness of the unirradiated control cladding. This hardness increase has been explained by Bloom et al.[5] as resulting from fast-neutron displacement damage within the stainless steel. Such damage usually anneals out at temperatures above about 900°F. The fact that damage was not annealed out during operation suggests that operating temperatures were not grossly greater than design temperatures. Also, the essentially constant hardness of the irradiated cladding, even at the lower flux end of the fuel tube, suggests that fast-neutron effects on the cladding reached, or were close to, saturation at the end of core life.

Metallography. The microstructures of specimens cut from the removed PM-1 and PM-3A fuel tubes were studied by metallographic techniques. Although a number of specimens from several peripheral-bundle fuel tubes were examined metallographically, only microstructures of the highest burnup center-bundle fuel tubes will be presented here.

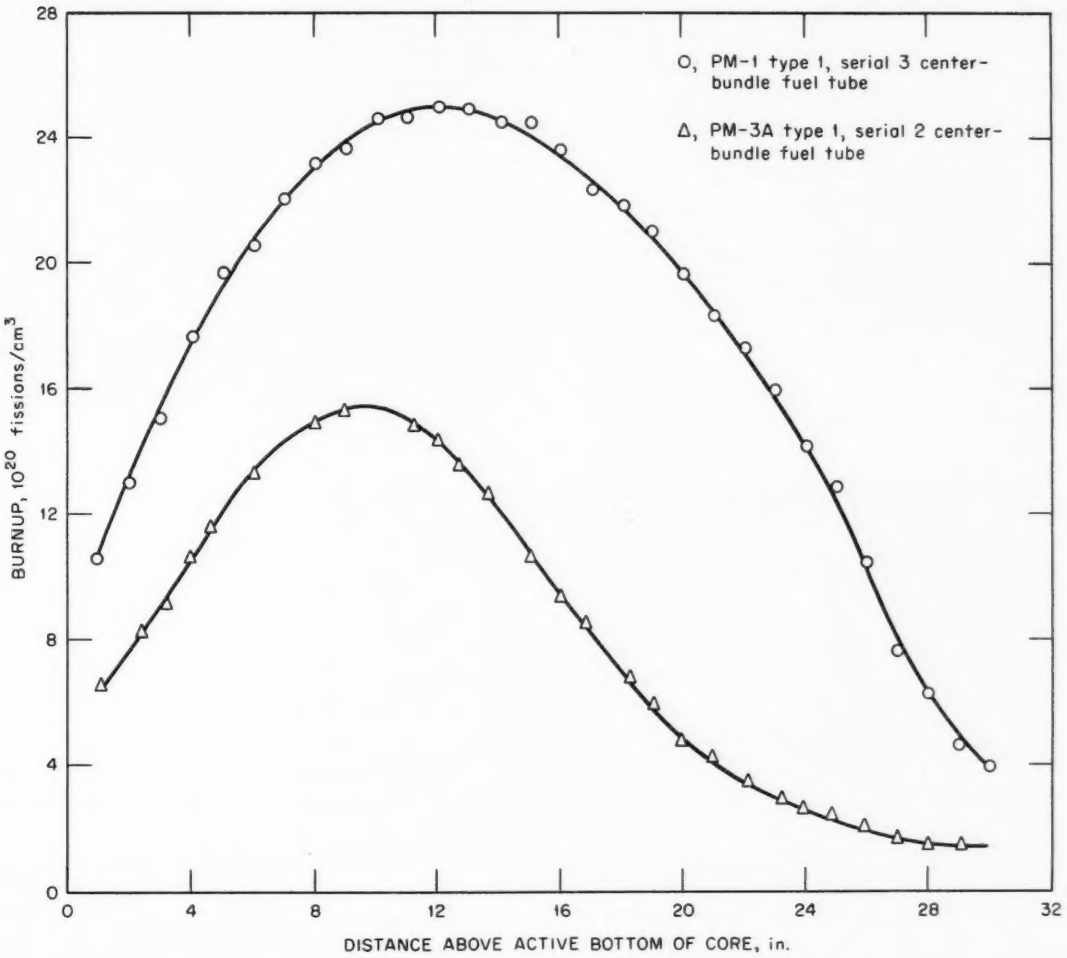

Fig. 6 Fuel-tube burnup as a function of position.

Figures 7 and 8 are comparisons of cladding and fuel-dispersion microstructures for a full-term type 1 PM-1 and a half-term PM-3A center-bundle fuel tube. Figure 9 is composed of a photomicrograph composite of the highest performance specimen removed from the PM-1 center-bundle fuel tube. The specimen was located 13 in. from the lower end of the active core, as shown in Fig. 9. Several comments can be made concerning the micrographs.

1. Primary-coolant fission-product activity experienced during operation of the type 1 PM-1 and PM-3A cores was due to fission products leaking through numerous intergranular cracks in the outer cladding tubes.

2. Outer cladding cracks started at the outer cladding surface and terminated at UO_2 particles close to the cladding–fuel interface.

3. All cracks detected were intergranular in nature and longitudinal in direction.

4. In general, cladding cracks observed on the full-term PM-1 fuel tubes were neither wider nor extended any deeper into the dispersion than cracks observed on the half-term PM-3A fuel tubes (i.e., no matrix cracking).

5. No appreciable grain growth was observed in full-term PM-1 or half-term PM-3A fuel cladding or fuel matrix.

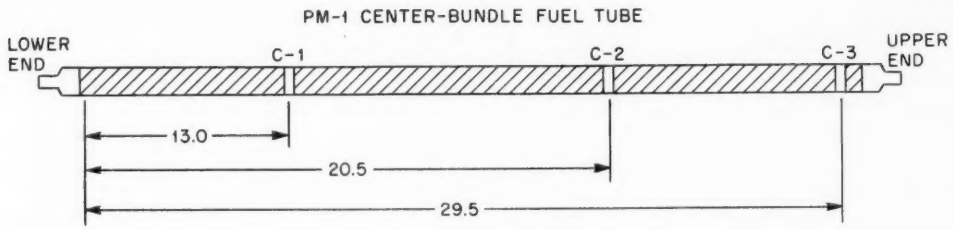

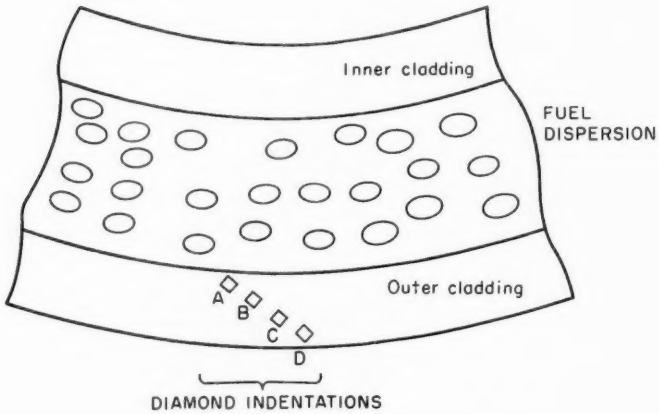

Table 1 Knoop Hardness Numbers for PM-1 Type 1, Serial 3, Center-Bundle Fuel-Tube Claddings with a Sketch Description of Indentation Location Within the Claddings Tested

	Knoop hardness numbers (25-g load) at the indicated indentation position in cladding				
Specimen	A	B	C	D	Average
C-1	168.1	192.4	201.7	192.4	189
C-2	201.65	192.4	211.6	222.3	207
C-3	175.7	201.7	192.4	184.8	189
Control*		92.55	122.0		108

*Unirradiated PM-1 control sample.

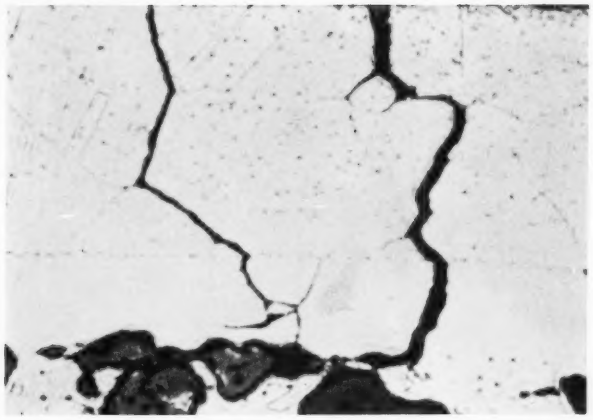

(*a*) Full-term PM-1 type 1, serial 3, center-bundle fuel-tube outer cladding; $BU = 25 \times 10^{20}$ fissions/cm^3.

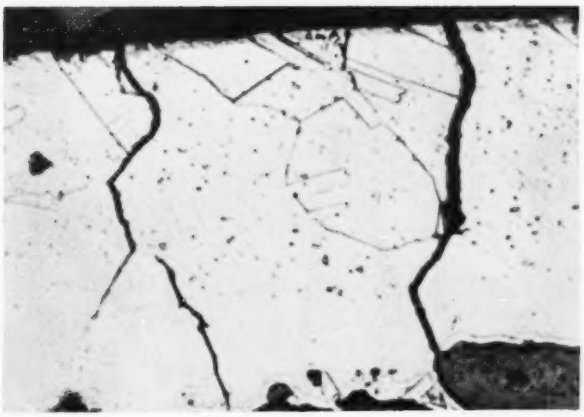

(*b*) Half-term PM-3A type 1, serial 2, center-bundle fuel-tube outer cladding; $BU = 25 \times 10^{20}$ fissions/cm^3.

(*c*) Unirradiated PM-3A fuel-tube outer cladding (fuel tube x3BK-5).

Fig. 7 Comparison of PM-1 and PM-3A fuel-cladding microstructures. Magnification, 250 x. Etched.

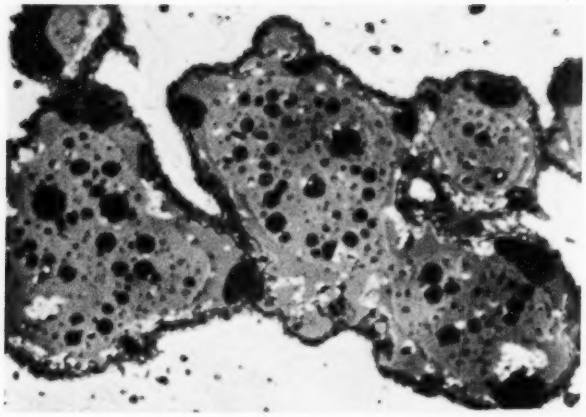

(*a*) Full-term PM-1 type 1, serial 3, center-bundle fuel-tube dispersion; $BU = 25 \times 10^{20}$ fissions/cm^3.

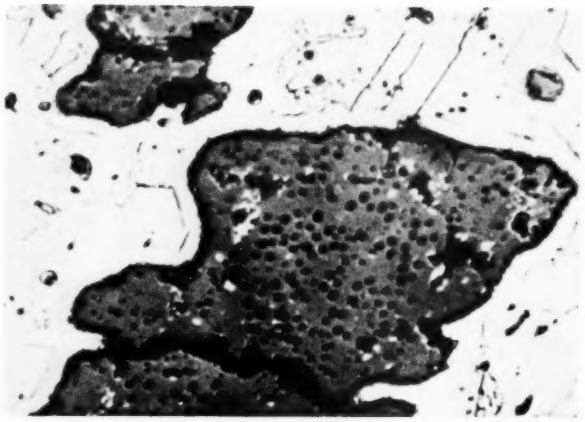

(*b*) Half-term PM-3A type 1, serial 2, center-bundle fuel-tube dispersion; $BU = 15 \times 10^{20}$ fissions/cm^3.

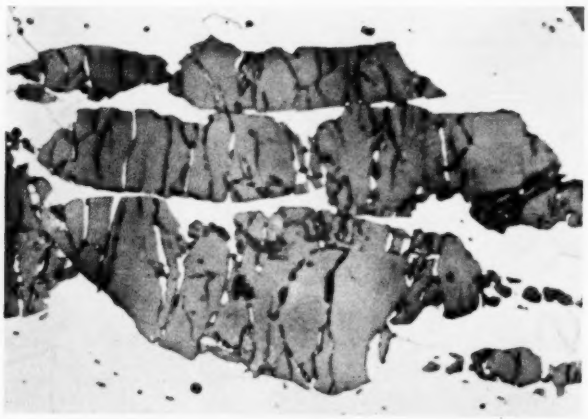

(*c*) Unirradiated PM-3A fuel-tube dispersion (fuel tube x3BK-5).

Fig. 8 Comparison of PM-1 and PM-3A fuel-dispersion microstructures. Magnification, 500 ×. Etched.

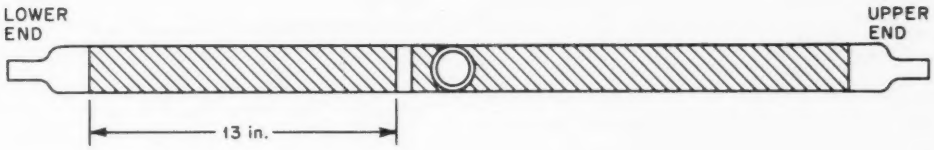

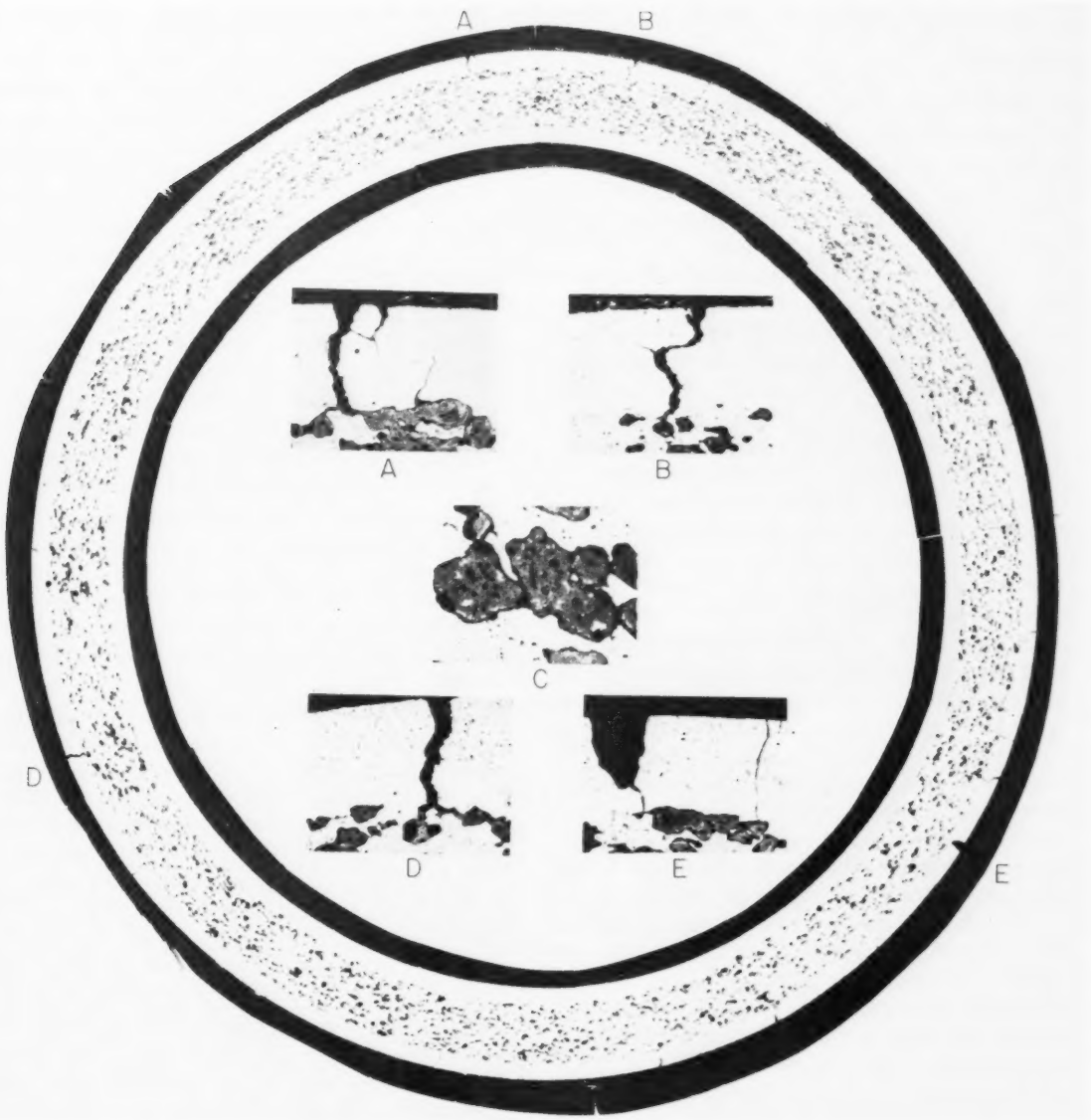

Fig. 9 Micrograph composite of PM-1 type 1, serial 3, center-bundle fuel-tube specimen with selected higher magnification inserts.

6. Fuel-tube cladding–dispersion bonds remained metallurgically sound for half-term and full-term PM-3A and PM-1 reactors.

Although outer cladding cracking occurred over a larger proportion of the high-performance full-term PM-1 fuel tubes, catastrophic fission-product leaking from the fuel tubes did not occur. This demonstrates the slow-leaking characteristics afforded by the dispersion fuels.

Discussion

Examinations of type 1 cores for PM-1 and PM-3A showed that fission products leaked through numerous intergranular cracks in the outer cladding of fuel tubes located in the high-performance regions of both cores (toward the core center). Cracks started on the outer surface of the cladding and generally terminated at UO_2 particles near the fuel dispersion–cladding interface. Cladding grain boundaries were free of precipitates, indicating that the cladding was not sensitized. No cracks in the inner cladding or in the fuel matrix were observed. The retention of matrix structural integrity helped to minimize coolant contamination since only those fuel particles intersected by cladding cracks could release fission products to the coolant. All cracks in the outer cladding were longitudinal and were associated with hoop strains greater than about 0.3%. This fact was illustrated by matching fuel-tube outside-diameter and fuel-burnup data for equal positions along several fuel tubes representing both type 1 PM-1, serial 3 and PM-3A, serial 2 fuel (Fig. 10). The scatter band containing all the data points suggests that early in the operation an incubation period existed where fuel burnup resulted in no fuel-tube swelling. Then, at some threshold burnup (about 8×10^{20} fissions/cm^3), fuel-tube swelling was initiated and continued linearly with increasing burnup. Outer cladding cracking then initiated at a burnup of 13 to 14×10^{20} fissions/cm^3, or at about a 1.7-mil increase in fuel-tube outside diameter (≈0.3% hoop strain). The shaded area of Fig. 10 represents the domain of fuel-tube swelling and burnup where outer claddings failed in both PM-1 and PM-3A fuel tubes. The incubation period for tube swelling is believed to be associated with the ability of UO_2 to accommodate fission products in either porosity or interstitial lattice sites or both.

These results suggest that the failures observed in the PM-1 and PM-3A outer claddings were strain related. However, on the basis of failure predictions of other investigators,[6] the observed strain-related PM failures were premature. Figure 11 shows irradiation performance of plate UO_2–stainless steel dispersions as a function of burnup and temperature. On the basis of the data shown in Fig. 11 and a dispersion temperature of 620°F, the PM-1 and PM-3A type 1 cores clearly operated in the "probably stable region" of the plot at the estimated burnup for crack initiation (13 to 14×10^{20} fissions/cm^3). Perturbations to heat flow introduced by the oxide scale on the PM-1 and PM-3A fuel-tube surfaces may have raised the fuel operating temperature slightly and shifted the operating point toward the stable–nonstable boundary. However, it seems unlikely that the presence of the scale could have raised the temperature sufficiently to bring the operating conditions into the nonstable region of the data shown in Fig. 11.

It should be pointed out that, because of differences in stress states, the use of data for fuel-plate specimens to predict failure of fuel tubes may not be valid. In fuel tubes of the PM type, where fuel and cladding are bonded, swelling of the annular fuel tends to place both the inner and outer cladding in tension. Because of its smaller diameter, the inner cladding is effectively stronger than the equally thick outer cladding in resisting the stresses induced by fuel swelling. This difference in effective strength would tend to force fuel to swell outward to deform the outer cladding. That the PM fuel tubes behaved in this manner is borne out by the observation that no measurable deformation of the inner cladding was detected on any fuel tubes. In plate specimens the swelling should be isotropic since stresses in cladding on both sides of the fuel plate should be essentially equal.

The residual hoop strain of the outer cladding at the estimated threshold for crack initiation was about 0.3%. This hoop strain is lower than would be expected to produce failure in stainless steel, on the basis of tensile specimens irradiated to similar fluence levels and uniaxially tested[7] at intermediate temperatures (600°F) (Fig. 12*a*). However, it is known that ductility under biaxial loads, such as those experienced by the PM claddings, is significantly lower than ductility under uniaxial loads. In burst tests[8] of stainless-steel tubes irradiated to exposures of 0.5 to 1.4×10^{22} neutrons/cm^2, ductility approached zero (Fig. 12*b*). Even though PM-1 and PM-3A fast-neutron fluence levels were a factor of 10 below the lowest levels associated with the tube-burst tests and the PM claddings were about 150°F cooler, the severe loss of ductility experienced by the burst tubes suggests that irradiated stainless-steel tubes strain biaxially to a lesser

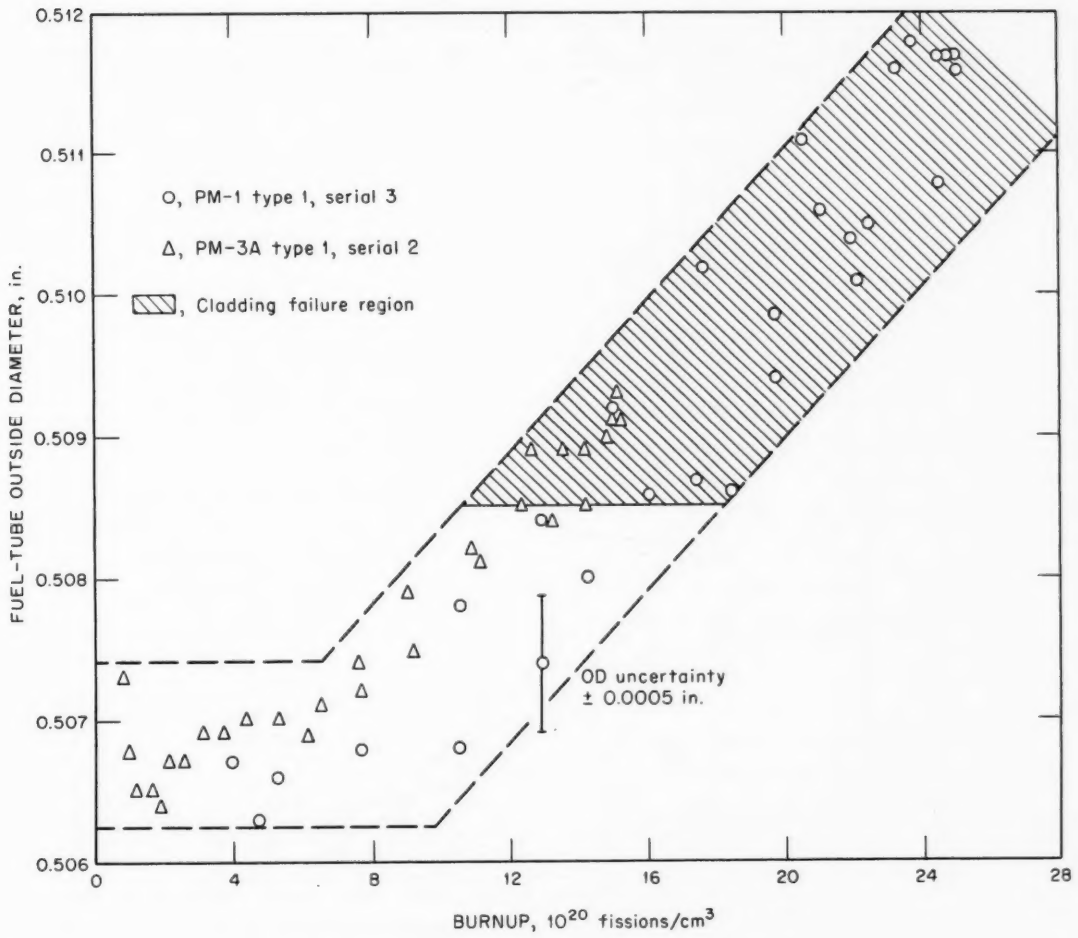

Fig. 10 Fuel-tube outside diameter as a function of burnup.

degree before failing than similarly treated uniaxially tested specimens.

The loss of effective life exhibited by failed PM claddings may also have been accelerated by cyclic fatigue. Cyclic loading of the PM claddings was mostly due to changes in thermal stress that accompanied reactor scrams and power changes. These stress changes were effectively transmitted to the cladding by the metallurgical bond between the fuel and cladding. Cyclic loading can severely reduce the life of a structural member in almost any application. The effect may be even worse with neutron-embrittled materials. Strain fatigue[9] of stainless-steel tubing at high temperatures (1200°F) indicates that irradiation tends to reduce fatigue life. It was not uncommon for fatigue failures to occur in tube specimens totally strained less than 1% and cycled less than 100 times. Because of the specimen temperature (1200°F), these data are not directly applicable for comparison to PM failures. However, the trend for irradiation to reduce fatigue life of stainless steel suggests that cyclic-strain fatigue may have played a role in the PM cladding failures.

On the basis of the above observations, it is possible to attribute the failures solely to fuel swelling and losses of effective cladding ductility associated with neutron exposure, low-strain-rate biaxial loading, and thermally induced cyclic loading. One factor remains, however, that suggests the possibility that failures were not strictly mechanical. Intergranular

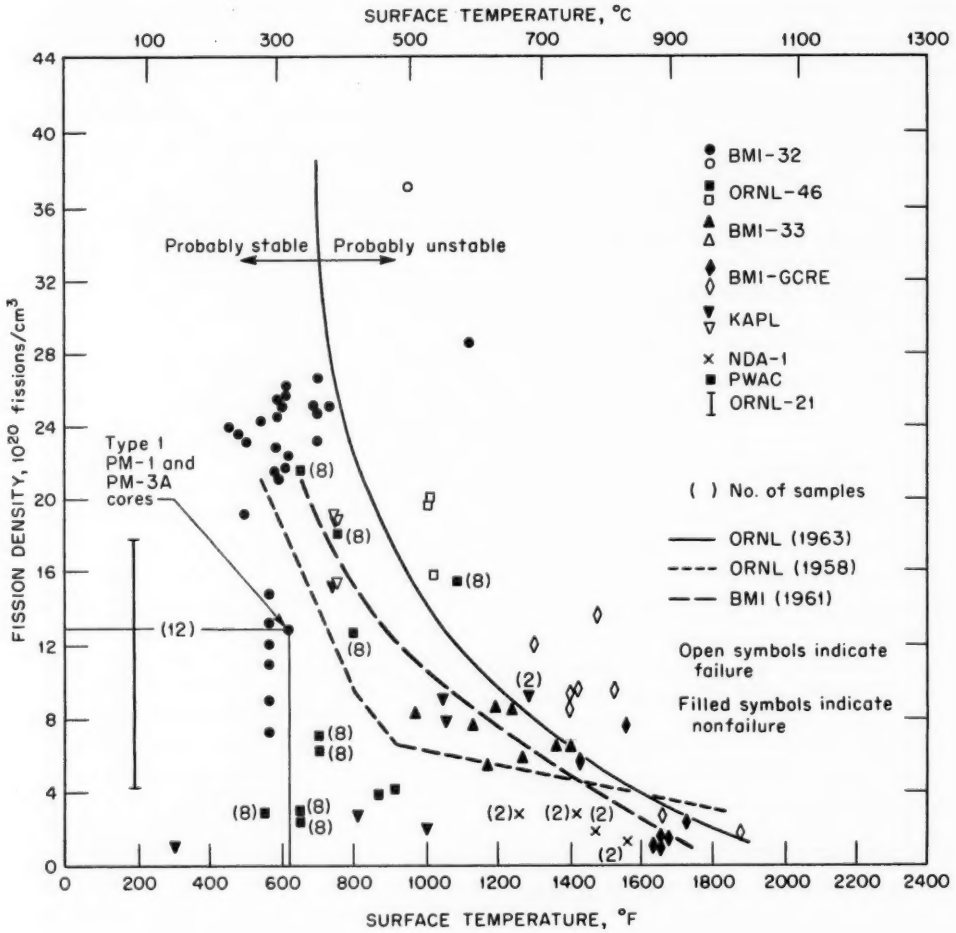

Fig. 11 Irradiation performance of stainless steel–UO_2 dispersions.[6]

failures similar to those found in this examination have been observed in stainless-steel cladding in boiling-water reactors (BWR's). Failures of this type have not been reported for pressurized-water reactors (PWR's) despite the fact that, except for boiling, the operating conditions of BWR's are similar to those of PWR's. Although both PM-1 and PM-3A are nominally PWR's, they are operated under conditions[10] that allow localized boiling, and conditions may have approached those of BWR's. This being the case, it is possible that BWR cladding failures and PM cladding failures are related. Investigators of the BWR failures[11-14] proposed a chemical–mechanical failure mechanism, but the chemical factor was unidentified. If a chemical factor was active in the PM failures, there was nothing obvious in the water chemistry to establish its identity. Concentrations of known stress-corrosion accelerators such as chlorides and caustics were uniformly low.

Conclusions and Recommendations

Conclusions reached as a result of the examination of type 1 PM-1, serial 3 and PM-3A, serial 2 cores are as follows:

Fission-product buildup in the primary reactor coolant resulted from leakage through intergranular cracks in the outer cladding. Cracks were longitudinal in direction and started on the outer surface of the outer cladding and generally terminated at UO_2 particles near fuel dispersion–cladding interfaces. An

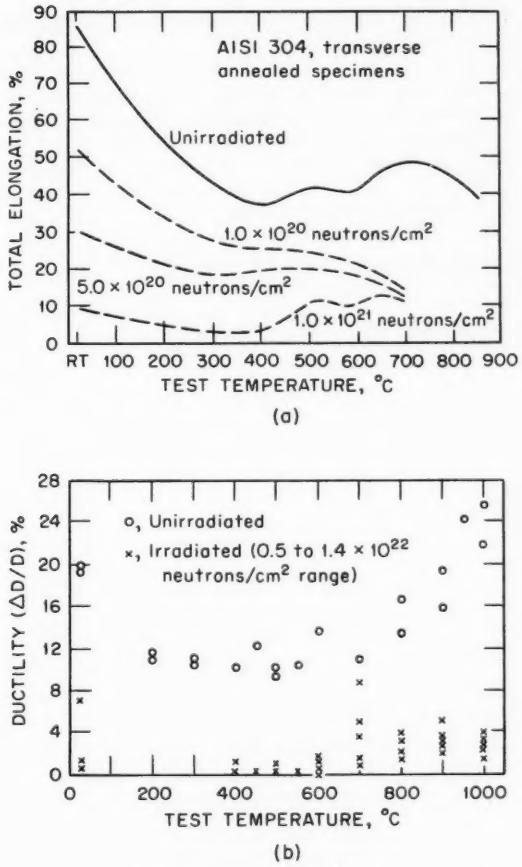

Fig. 12 Mechanical properties of irradiated stainless steel. (*a*) Transverse annealed tensile specimens, (*b*) Thin-walled pressure-tested tubes.

incubation period existed early in the operation where fuel burnup resulted in no fuel-tube swelling. Then, at some threshold burnup (about 8×10^{20} fissions/cm^3), fuel-tube swelling was initiated and continued linearly with burnup to a maximum value of about 25×10^{20} fissions/cm^3 (peak burnup in full-term type 1 PM-1, serial 3 core). Outer cladding cracking was initiated at a burnup of from 13 to 14×10^{20} fissions/cm^3, or at about 0.3% residual hoop strain.

On the basis of mechanical-property data of irradiated stainless steel, it is possible to attribute the failure solely to fuel swelling and effective cladding-ductility losses associated with neutron exposure, low-strain-rate biaxial loading, and thermally induced cyclic loading. However, similarity of the PM cladding failures to stress-corrosion cladding failures in BWR's suggests the possibility that the PM failures may be related to the same type of stress-corrosion cracking as the BWR cladding. Whether strictly mechanical or chemical–mechanical, the failures occurred only where the cladding was strained more than about 0.3%. The solution then is probably the same for either failure mechanism: design the fuel tubes to minimize cladding strain. With the existing fuel-tube design, this might be accomplished by increasing the thickness of the outer cladding sufficiently so that the inner cladding shares the deformation load with the outer cladding. The fuel elements should be redesigned to reduce strain and cyclic loading of the claddings. State-of-the-art methods to accomplish this design change include fuel pellets loosely fitted into a tube cladding. Fuel elements in the PM-3A cores scheduled to operate during the 1970's are of this different design. The results of this study indicate that the pellet-type elements should be designed with sufficiently thick cladding and enough voidage in the UO_2 to accommodate fission-product swelling to preclude cladding strains greater than 0.3% at the end of core life.

References

1. Description of PM-1 (Sundance), Reactor File No. 12, PM-1 on the Line, *Nucleonics*, **20**(9): 37-42 (September 1962).
2. E. E. Goslee, Improving Performance of Stainless Steel UO_2 Cermet Fuels, *Nucleonics*, **21**(7): 48-52 (July 1963).
3. PM-3A Water Chemistry and Radiochemistry Support Team Report for Nuclear Power Field Office, U. S. Army Engineer Reactors Group, Fort Belvoir, Va., Report NUS-228, Nuclear Utility Services, Inc., Washington, D. C., Apr. 1, 1965.
4. Capt. Edwin W. A. Peura and Sgt. Robert Ondike, private communication with PM-1 Project Engineers, December 1967.
5. E. E. Bloom et al., Comparison of Displacement Damage and Strength for Stainless Steel Irradiation at Intermediate Temperature, USAEC Report ORNL-TM-1535, Oak Ridge National Laboratory, June 1966.
6. W. C. Thurber et al., Irradiation Testing of Fuel for Core B of the Enrico Fermi Fast Breeder Reactor, USAEC Report ORNL-3709, Oak Ridge National Laboratory, November 1964.
7. J. E. Irvin and A. L. Bement, The Nature and Engineering Significance of Radiation Damage to Various Stainless Steel Alloys, USAEC Report BNWL-SA-376, Battelle–Northwest, Apr. 1, 1966.
8. W. F. Murphy and H. E. Strohm, Tube-Burst Tests on Irradiated EBR-II Fuel Jackets, USAEC Report ANL-7268, Argonne National Laboratory, October 1966.
9. M. G. Reynolds, Strain-Cycle Phenomena in Thin-Walled Tubing, *Flow and Fracture of Metals and Alloys in Nuclear Environments*, American Society for Testing and Materials, Special Technical Publication No. 380, pp. 323-336, 1965.

10. The Martin Company, PM-1 Nuclear Power Plant Program, Final Periodic Report, Vol. II, Plant Performance Studies, USAEC Report MND-M-2935(Vol. II), April 1963.

11. E. A. Lees, Analysis of Failure of Type 304 Stainless Steel Clad Swaged Powder Fuel Assembly, USAEC Report GEAP-4400, General Electric Company, Vallecitos Atomic Laboratory, Oct. 3, 1963.

12. Progress Report on High Power Density Program, sponsored by the AEC at General Electric under Contract No. AT(04-3)-361.

13. W. H. Arlt and S. R. Vandenberg, Fuel Failure Examinations and Analysis in the High Power Density Program, USAEC Report GEAP-4360, General Electric Company, Vallecitos Atomic Laboratory, Sept. 16, 1963.

14. R. W. Staehle, Investigation of Cracking in Stainless Steel Fuel Elements, USAEC Report COO-1319-30, Ohio State University Research Foundation.

Containment-System Design and Construction Practices in the United States

By William H. Steigelmann and Chen Pang Tan

The What, Why, and How of Containment

The nuclear industry has worked continuously since its inception to devise methods, equipment, and plant features that reduce the possibility and the consequences of an accidental release of radioactivity from nuclear power plants. During their early development stage, nuclear reactors were provided with exclusion areas. Subsequently, however, the principle of exclusion has been complemented and partly replaced by the concept of "containment" of radioactivity, i.e., the restricting of the release of fission products to the environment. In principle, the containment structure is the last of a series of barriers which serve to prevent release of radioactivity from the plant. The containment is designed to be capable of handling any arbitrary failure of the two preceding barriers—fuel cladding and primary-system envelope. Over the years, a multitude of other "engineered safeguards" have been added to nuclear power reactors, many of which are adjuncts to the containment system. Thus, as discussed by Levy[1] of General Electric Company, containment has become only part of a total safety network, and its performance requirements can be established and analyzed only by looking at the overall system.

The containment system for a nuclear reactor can be considered to encompass all structures, systems, mechanisms, and devices that serve to attain with a high degree of reliability some specified control of the radioactivity released to the surrounding environment from the primary system in a reactor accident. Most containment enclosures generally incorporate some radiation shielding to restrict the direct radiation exposure in the event of a major fission-product release. Containment systems are normally referred to as "leaktight" structures, which, in reality, leak a finite amount. Containment systems therefore generally consist of an integrated complex of structures, processes, and subsystems that combine to control the activity release in a prescribed manner with a high degree of reliability.

Containment systems are generally the key part of the plant's engineered-safeguard features, a designation that also includes emergency core-cooling systems, filters, sprays, redundancies of cooling-water sources and power supplies, etc. Engineered safeguards are discussed in the site-criteria guide[2] in the following connotations: "unique or unusual features having a significant bearing on the probability or consequences of accidental release of radioactive material" and "such safety features that are to be engineered into the facility. . . .Where unfavorable physical characteristics of the site exist, the proposed site may nevertheless be found to be acceptable if the design of the facility includes appropriate and adequate compensating engineering safeguards." The definition encompasses features whose function is to prevent the occurrence of an accident, as well as those designed to mitigate the consequences if an accident does occur.

The containment vessel was originally envisioned as a static pressure envelope fabricated of steel which would adequately contain the radioactivity released

from the primary system during any credible accident. From this, containment practice has evolved not only containment structures of composite materials such as steel and concrete, in which a multiplicity of penetrations must be closed at the time of the accident to effect the leaktight enclosure, but also versions that attempt to "suppress" accident pressures or to directly return outleakage to the containment by additional outer barriers and pumping systems.

In general, containment systems can be categorized into three basic groupings: full-pressure containment, pressure suppression, and pressure relief. As explained below and shown in Fig. 1, a number of design options are available within each of these categories. The basic structure may be reinforced concrete, prestressed concrete, plate steel, or a combination of these materials. When a concrete structure is used, the interior surface is lined with ¼- to ½-in. welded steel plate to provide a leaktight membrane. Investigations of various plastic coatings and sealers, including irradiated polymers, are presently under way to avoid the necessity of using metallic liners.

Full-Pressure Containment

The containment vessel used with most pressurized-water-reactor (PWR) systems today is typically a fully continuous concrete and/or steel structure in the shape of a cylinder with a domed roof and a flat foundation slab, as shown in the upper left-hand-corner sketch in Fig. 1*a*. The containment vessel encloses the reactor vessel, steam generators, reactor coolant loops, and portions of the auxiliary and engineered-safeguards systems. The turbine, condensate, and feedwater systems are external to the structure. The containment structure is, in effect, the reactor building and is designed to withstand a postulated accident causing a pressure of ~45 psig with a coincident temperature of ~275°F. The building is designed to safely sustain all external live and dead loading conditions that may be expected to occur during the life of the station.

Following a loss-of-coolant accident the containment pressure rises from its initial level, which is usually normal atmospheric pressure. Although pressure can be reduced rapidly at first, the pressure–time curve is asymptotic to atmospheric pressure, and outleakage of fission products may continue for an extended period of time. Hence, to meet siting criteria for some plants, it has been necessary to incorporate as an engineered safeguard a system of sprays or filters for removing fission products from the containment atmosphere.[3,4]

A refinement of this type of containment is to have a double leakage-control barrier instead of just a single concrete and/or steel vessel. Two variations of this concept have been proposed (the lower pair of sketches in Fig. 1*a*), and the one on the left is being used in three units currently under construction (the two 550-Mw(e) units at the Prairie Island Station of Northern States Power Company and the similar single unit at the Kewaunee Station of the Wisconsin Public Service Corp.). As discussed by Corcoran et al. in a recent ANS paper,[5] and described by Leppke and his associates,[6] the primary containment for these units is a steel shell designed to withstand the maximum pressure resulting in an accident. A cylindrical, reinforced-concrete shield building surrounds the primary containment shell, spaced a few feet from it. The annular space between the containment shell and the shield building is normally at atmospheric pressure, but a negative pressure of ~1 in. of water is created and maintained by the vent exhaust system within 2 min following a postulated primary-system leakage. Inleakage air (<40% of the volume of the annulus per day) mixes with containment-vessel leakage (<1% per day) and is then passed through charcoal filters, reducing the radioactivity to acceptable levels. Following filtration, some air must be exhausted to the atmosphere to prevent containment-pressure buildup. The remainder is recirculated to the annulus and thus provides additional holdup for fission products and additional filtration.

As pictured in the lower right section of Fig. 1*a* and described a few years ago by Malay and Chave,[7] the other double-barrier containment concept makes use of two concentric leaktight chambers (steel shells), with a space between them that is held at all times at a negative pressure. Any leakage from the containment vessel through the inner shell and any outside-air leakage through the outer shell are collected in the annulus, which is filled with a pervious material such as "popcorn" concrete, and pumped into the containment vessel. The containment vessel thus accumulates the air inleakage, with an attendant increase in containment-vessel pressure that eventually must be periodically relieved to the off-gas stack. There is essentially no outleakage from such a containment vessel. Fission products can be removed by filtration and decay, and controlled venting can be deferred for favorable weather.

The outer steel containment vessel is in contact with and surrounded by a thick reinforced-concrete structure that provides shielding from internal radiation sources and resists the pressure forces resulting

from the postulated accidental release of primary coolant. Although the steel vessels contribute to the strength of the structure, they are not designed to withstand the full pressure without the support of the reinforced concrete and are visualized primarily as membranes much more impervious to leakage than is concrete. All penetrations through the containment vessel for piping, electrical leads, ducts, and access hatches are arranged as double-barrier devices and contain negative-pressure zones. These zones are vented to the popcorn annulus to maintain the double-containment and pump-back concepts.

The double-containment concept was originally proposed for the Ravenswood Unit 3 plant in 1964, which would have been the first plant sited within an urban area—directly across the East River from Manhattan in New York City. This project was abandoned before AEC took any official licensing action, however. The concept was also proposed for the Malibu Station of the Los Angeles Department of Water and Power, but this project is currently inactive while awaiting a decision as to the suitability of the site based upon seismicity considerations.

An alternative form of full-pressure containment, termed the low-pressure type, is shown in the upper right-hand sketch of Fig. 1*a*. Here, the entire plant, including the turbine generator and steam, feedwater, and condensate system, is housed with the reactor within the containment shell. This type of containment was used in the BONUS boiling-water-reactor (BWR) plant with integral superheater in Puerto Rico.[8] The advantage of this scheme, particularly with a BWR plant, is that the coolant would be contained regardless of the point of rupture, since the entire plant is enclosed by the containment structure.

Another alternative that can be employed with the full-pressure containment is termed "subatmospheric containment" in a recent ANS paper by Noble.[9] Subatmospheric containment is a concept in which the reactor containment is normally maintained at partial vacuum and, following a loss-of-coolant accident, the pressure within the containment is rapidly reduced to less than atmospheric; thus outleakage is terminated, and a definite time limit is provided for any potential off-site effects of the accident. A subatmospheric operating pressure of 10 psia has been selected for the Surry Units 1 and 2 of Virginia Electric & Power Co. This pressure level was based on the desirability of having access to the containment during operation without a requirement for supplemental breathing apparatus.

Pressure-Suppression Containment

This type of containment system was pioneered by the General Electric Company and used in every BWR plant ordered from them, starting with the Humboldt Bay Unit 3 (Ref. 10). In 1967, Westinghouse Electric Corporation announced a different type of pressure-suppression system that uses ice as the steam-condensing heat sink instead of water as in the General Electric system.

As shown in the right-hand sketch in Fig. 1*b*, the pressure-suppression system developed by General Electric consists of a dry well (which houses the reactor vessel and the coolant recirculation system), a pressure-suppression chamber (which stores a large volume of water), a connecting vent system between the dry well and the water pool, and isolation valves. In the event of a primary-system piping failure within the dry well, the reactor coolant flashes into steam and then flows through the connecting vents into the pool of water in the suppression chamber. The steam condenses in the suppression pool, resulting in a minimum pressure buildup in the dry well. Isolation valves on the various lines that lead from the containment are actuated during this period. Although not shown in Fig. 1, double-barrier concepts are also used with the pressure-suppression containment. The dry well and suppression chamber are located in a reactor building that is designed to be leaktight to the extent required by the site and its environs.

In the Westinghouse ice-condenser reactor containment system (ICRCS),[11] ice is housed in a cold-storage compartment surrounding the nuclear steam supply system (NSSS) and is kept frozen by conventional refrigeration equipment. The containment is divided into an upper chamber and a lower chamber by a concrete deck structure, with the primary system located in the latter (see left-hand sketch in Fig. 1*b*). An increase in pressure in the lower chamber resulting from a loss-of-coolant accident opens access panels located at the bottom of the ice-storage compartment, thus permitting air and steam to flow through the ice bed. The steam is rapidly condensed, and the air passes into the upper chamber via top access panels. This system reduces the size of PWR containment structures, since the design pressure is lower, and likewise eliminates a prolonged elevation of containment pressure with attendant leakage.

The Donald C. Cook Nuclear Plant, to be built at Bridgman, Mich., will be the first plant to utilize ice-condenser reactor containment.[12,13] The owner of this dual 1100-Mw(e) unit plant, the Indiana and

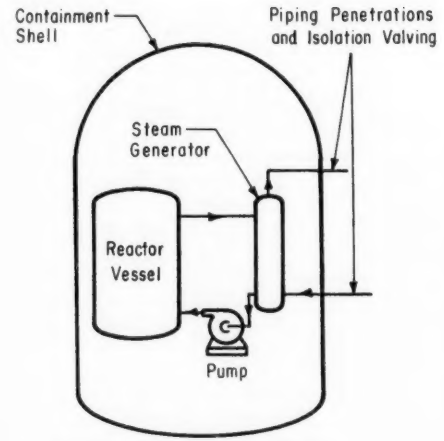

PRESSURE CONTAINMENT
(Shown with PWR, GCR, or LMFBR)

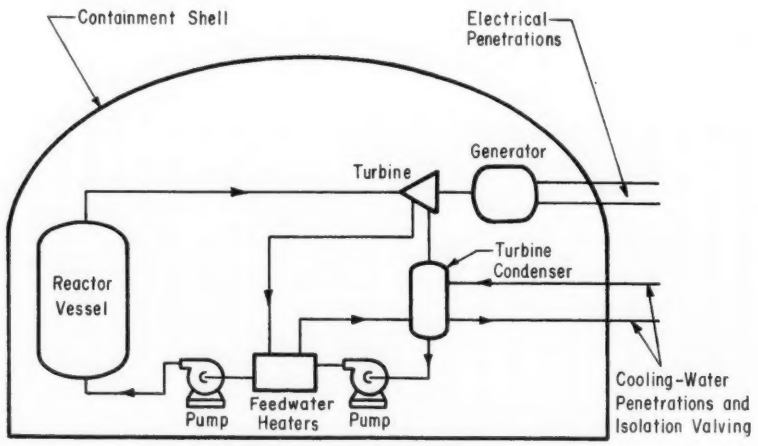

LOW-PRESSURE CONTAINMENT
(Shown with BWR)

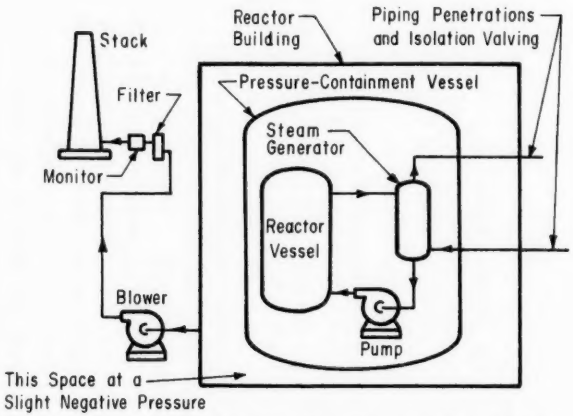

MULTIPLE-BARRIER CONTAINMENT
(Shown with PWR)

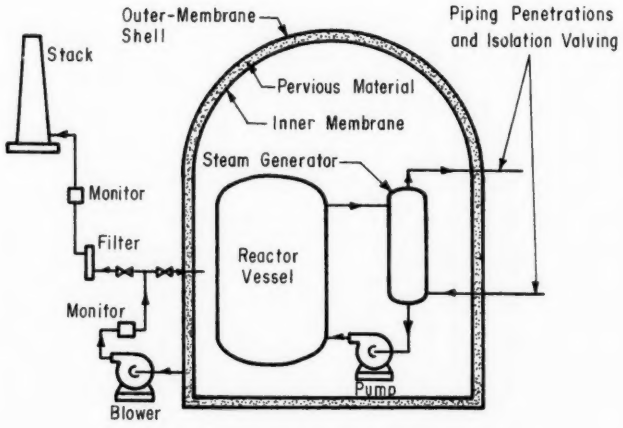

MULTIPLE-BARRIER CONTAINMENT
(Shown with PWR)

(a) PRESSURE-CONTAINMENT TYPES

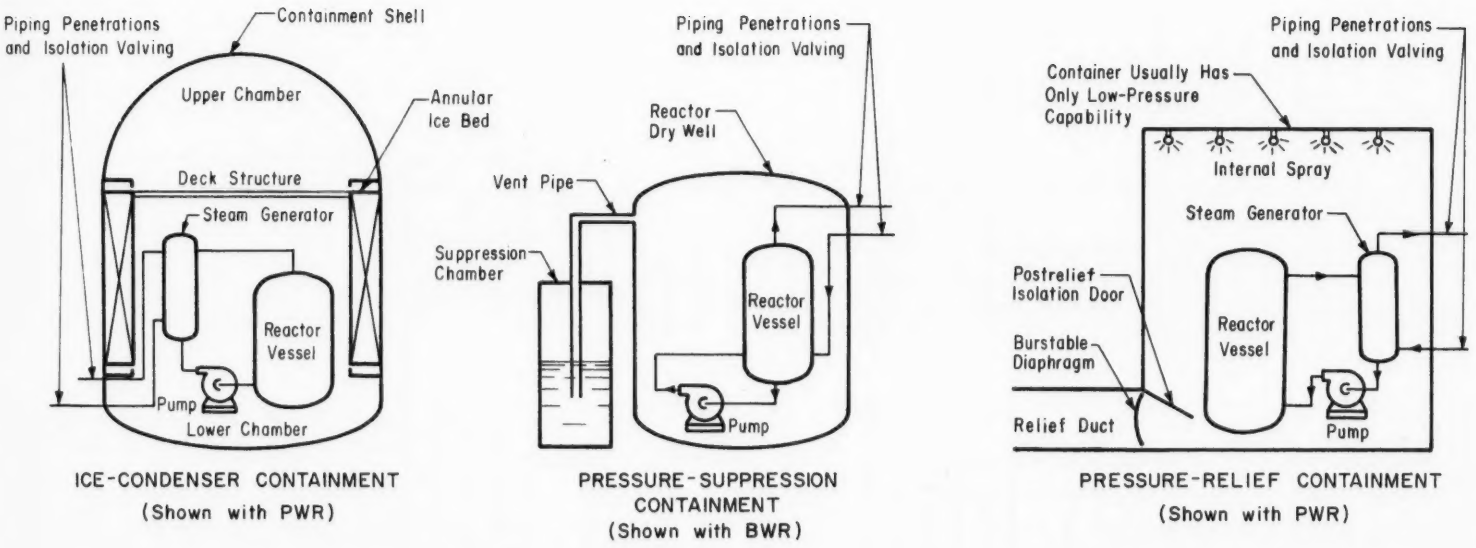

Fig. 1 Schematic diagrams of various containment types.

Michigan Electric Company of the American Electric Power System, received the construction permit in March of this year. The next nuclear power station that will use this type of containment will be the two 1124-Mw(e) units ordered by Tennessee Valley Authority (TVA) for the Sequoyah Generating Station near Chattanooga, Tenn.[14] The preliminary safety analysis report (PSAR) and construction permit application for this plant were filed in October 1968.

Pressure-Relief Containment

This concept is illustrated in Fig. 1*c* and is based on releasing excessive pressure from the building in the event of an accident. This is accomplished by opening valves or by shattering a seal diaphragm in a relief duct, allowing air initially present, some radioactivity, and the initial steam and water released by loss-of-coolant accident to be vented to the atmosphere or to an evacuated receiver building. Steam released later in the accident is condensed by a spray system actuated by the pressure rise. When a burstable diaphragm is used with atmospheric release, it is backed up by a valve that closes immediately after the initial efflux of air to prevent the escape of large quantities of radioactivity. This containment scheme has not been employed in the United States, but the Canadian NPD-2 Reactor plant uses this system for containment of its boiler room, with the release of air initially present to the environment.[15] Since a portion of the radioactivity present in the reactor system is permitted to escape, this variation of the concept will find application only in remote areas.

As reported in a recent ANS paper by Kolev,[16] the four-unit Pickering Nuclear Power Station uses a containment system consisting of four reactor buildings, a vacuum building, and a pressure-relief system of check louvers, ducts, and valves. The reactor buildings and the vacuum building are cylindrical reinforced-concrete structures, with the internal pressure of the vacuum building maintained at 1.0 psia. This structural vessel is 165 ft in diameter and 166 ft high and contains an elevated water-storage tank equipped with a pressure-actuated water spray that discharges to condense the steam atmosphere if the building pressure exceeds 6.2 psia. The peak pressure in any reactor building will be +6.0 psig but will drop below atmospheric within 30 sec from the start of the accident. The outward leakage from the containment volume is thus controlled since, except for this short time interval, the containment volume is at subatmospheric pressure and any leakage will be inward.

Environmental and Service Conditions

Under normal plant operation a containment structure is subjected to environmental and service conditions similar to those prevailing in a conventional industrial building. The various types of loads that may act separately or be superimposed on the containment structures are the dead and live loads, wind- and storm-produced loads (including hurricanes and tornadoes), ground-motion (earthquake) dynamic and static loads, loads produced by steady-state and transient thermal stresses, and prestressing forces (if the structure is prestressed). It is generally assumed that the normal operating internal temperatures are maintained between a minimum of 50°F and a maximum of 135°F. The external ambient temperature depends on the locality of the plant site and the time of year and therefore may conceivably vary between −20°F and +110°F.

Primary-System Failure

As mentioned previously the main purpose of the containment structure is to prevent the release of radioactive materials to the environment should there be a primary-system failure. The containment structures must therefore be designed to withstand the maximum credible accident (MCA), i.e., the credible accident that could cause the most serious consequences to the general public. Typically, the MCA has been assumed to be a clean break in the primary-coolant-system piping that allows the discharge of primary coolant through both ends of the ruptured pipe. This accident would result in a rapid increase of pressure and temperature and, either subsequently or simultaneously, an increase of radioactivity inside the containment vessel. Unless remedial action promptly follows the initial stage of the accident, the pressure and temperature may continue to rise after the initial quasi-equilibrium situation that is reached immediately following the primary-system blowdown. The internal design pressure typically varies from 40 to 60 psi, and the internal temperature ranges from 120 to 135°F under normal conditions to 300°F for the design-basis accident. Figure 2 shows the pressure transients and effectiveness of various combinations of safety features used in a typical BWR plant to limit the consequences[17] of the MCA. The pressure response is related to the number and type of engineered-safeguard systems that are operational following the accident.

In addition to the pressure loading produced by the MCA, there may also be additional dynamic or shock

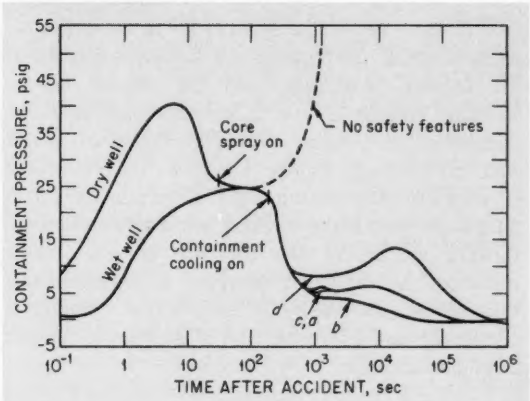

Curve	No. of cooling pumps: Core spray	Containment
a	2	2
b	1	4
c	1	2
d	1	1

Fig. 2 Typical BWR containment-pressure response following a primary-system piping break (from Ref. 17).

loadings resulting from missiles or the blowdown jet impinging upon the containment. There is in addition a new thermal-loading condition since the inner surface of the containment will be suddenly heated. Determination of the final pressure and temperature of the gas–vapor mixture involves consideration of heat transfer to structures within the containment, as well as to the containment structure itself. For concrete containment vessels the high temperatures and temperature gradients give rise to additional thermal-stress problems in the design of the containment components, especially the steel liner.

The peak pressure in an ice-condenser reactor containment following a loss-of-coolant accident may be as low as one-quarter or less of the peak pressure that could occur in the full pressure-containment structure. Since the containment pressure is reduced to a few pounds per square inch within a few minutes after the accident, the probability of significant leakage of radioactive vapor or gases to the environment is decreased. As illustrated in Fig. 3, the containment pressure transients have two distinct pressure peaks. When the blowdown from a pipe break is initiated, steam and hot water enter the lower compartment, pushing air through the ice condenser. The pressure in the lower compartment increases owing to the resistance to air flow through the ice condenser. The steam condenses once it reaches the ice bed, and this condensation terminates the pressure rise at about 10 psig. As the transient progresses the pressure in the lower compartment again increases because of a build-up of back pressure resulting from the remaining small amount of air flow into the upper compartment. Near the end of the blowdown, the pressure is uniform throughout the containment at its final peak value of approximately 10 psig. The pressure then decreases as the remaining steam is condensed; within about 6 min the pressure is usually less than 3 psig.

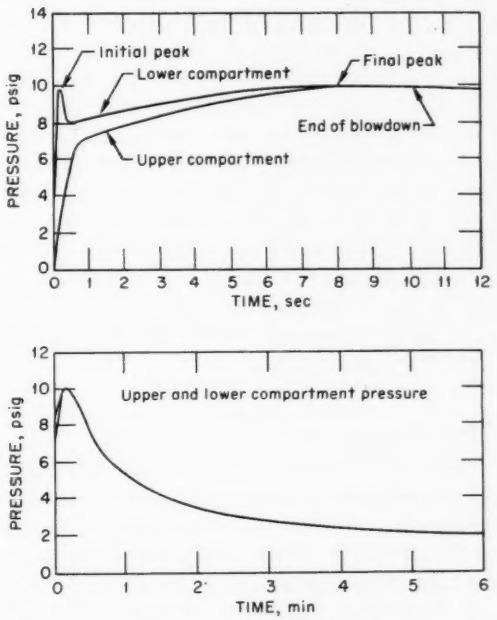

Fig. 3 Pressure transient for maximum hypothetical double-ended pipe rupture in ice-condenser containment (from Ref. 11).

Earthquakes

History of seismic activities all over the world has demonstrated that there are few areas, if any, where the earthquake problem can be completely neglected.[18] Because of this and the high degree of safety required for nuclear structures, designers are faced with highly challenging problems of earthquake-resistant design. Through the use of computers the structural response can be accurately calculated for a specified ground motion—the problem lies in obtaining an

accurate description of an earthquake motion. To predict the total earthquake response, one must know the expected geological-formation response, the expected structural response, and the expected coupling between the ground and the structure. Among these, knowledge of the expected geological-formation response is most difficult. The experience of the Mar. 27, 1964, Alaskan earthquake[19] shows that there was ground motion of the kind customarily associated with earthquakes, and, in addition, there were subsidence, sliding, and gliding of large blocks of earth. Even though it may be possible to predict such landslides from a geological investigation of the area, it is not possible to estimate quantitatively the amount of such displacement. The response of a structure and the response of a site to earthquake impulses are mutually interrelated and combine in a complex manner. Present methods of design are based upon a static approach known as the response-spectrum method. Earthquakes are to a very large extent unpredictable with respect to both their places of occurrence and their magnitudes. Containment structures therefore are required to be designed not only for the maximum intensity that has occurred in the past but also for a higher intensity that could be expected in the future. The former is known as the "design earthquake" and the latter is termed the "maximum credible earthquake."[20]

Tornadoes

From the records of nearly 300 years, it is evident that tornadoes occur frequently throughout much of the United States because the geographical position and the topography of the country favor meteorological conditions that spawn them.[21] Although tornadoes reap terrible tolls, there have as yet been no adequate means of protecting against loss of human life and property. The hazard of the tornado is twofold: (1) it destroys structures and (2) it turns normally harmless objects into dangerous missiles. Structures are demolished by bursting action from the high differential pressure and by the excessive flexing from high lateral loading. The excessively high wind velocities have produced phenomenal penetrations by seemingly fragile objects. Since there are potential missiles from other sources, the tornado-generated missiles will be discussed later with missiles of other kinds.

A tornado may be pictured as a chimney with the air outside rushing in at the bottom to replace hot air being drawn upward, forming a rotating vacuum at ground level. At the same time, the tornado is moving forward. To estimate tornado forces requires knowledge of three values: the speed of the air moving in the circumferential direction of the funnel, the speed of the forward movement, and the amount of the vacuum. Because of the lack of accurate data, the tornado-resistant design of containment vessels is in a state of some uncertainty. Usually, a circumferential velocity of 300 mph and a partial vacuum of 1.5 to 3.0 psi are used without taking into consideration the forward motion of the tornado. In areas where tornadoes are frequent, however, a circumferential velocity of 500 mph is used, a full vacuum is considered, and a forward wind of 50 mph may also be taken into account.

Missiles

Missiles can be classified by source as internal and external. Internal missiles are generated as a result of explosions or equipment failures inside the containment,[22] whereas the latter category covers those which originate from outside the containment from similar causes, those resulting from aircraft accidents, and those generated by tornadoes and windstorms. Gwaltney[23] at Oak Ridge National Laboratory (ORNL) has recently completed a comprehensive survey of the state of current technology of missile generation and protection in relation to the capability of meeting nuclear power-plant-design criteria.

Items such as valve stems, bolts, valve bonnets, and instrument thimbles are the most probable missiles. Less probable but possible missiles are large valve bonnets, turbine rotor pieces, and other rotating masses. The most massive external missiles are the ones resulting from aircraft accidents and wind-propelled objects such as railroad coaches, automobiles, and poles in electric-power and telephone lines. From the investigations of the wreckages of various aircraft accidents by the Civil Aeronautics Board, it has been found that the piston or jet engines usually stay intact during a crash. In view of such findings, aircraft engines have been considered as the basic missiles that can result from airplane crashes. For some plants sited relatively close to airports, principally the Three Mile Island Station of Metropolitan Edison Company, it has been necessary to analyze the probability and consequences of the intact crash of a large aircraft.[24,25] The estimation of the missiles generated by tornadoes is most divergent; various license applicants have considered a utility pole, a compact car, a passenger car, or a 70-ton railroad coach. In most of the containment-vessel designs, a utility pole and a compact car are the external missiles generally taken into consideration.

The basic problem in the design of containment vessels for missile protection is to ascertain what damage can be done by all of the above-mentioned missiles. If the velocity and mass of the missile is known, it becomes possible to estimate the damage. Such estimates generally consist of estimating the penetration and perforation of the containment on the basis of existing formulas that have been derived empirically. The most popular formula is the modified Petry formula,[26] which calculates the depth of penetration into a concrete slab of infinite thickness. The missiles considered were bullets, artillery shells, bombs, etc., which are considerably different from the missiles presumed to be generated in nuclear reactor accidents or as a result of aircraft accidents or by tornadoes. Although the formula may be applicable to missiles of small fragments, large fragments from failed turbines and other heavy equipment and possible missiles from aircraft accidents are outside the limits of this formula. The adequacy of using the modified Petry formula to compute the penetration of the missiles into the concrete containment wall is therefore questionable. Furthermore, the formula is applicable only to reinforced concrete, and there is no formula available specifically for use with prestressed concrete.

Design Features of Containment Structures

The technology of reactor containment is well established, and there is a wealth of information[27] on the subject. Most of the information is, however, related more or less to steel containments, which had until recent years been the most widely used containment structural material. The phenomenal growth of nuclear power stations in both number and unit size during the past few years has led utility companies, their engineering consultants, and the equipment vendors to look for cost advantages and simplified construction methods for containment structures. Because of the need for stress relief of steel plates greater than 1½ in. thick, the construction of steel containment vessels for large PWR plants becomes costly. Reinforced-concrete containment vessels (RCCV) and prestressed-concrete containment vessels (PCCV) are not subject to this limitation in wall thickness. Because the concrete containments resist the internal pressure through a number of reinforcing bars and/or prestressing tendons, the fracture mode of failure that may occur in a steel vessel will not occur in concrete containments. Since concrete is a porous material, a leaktight membrane in the form of a steel liner or nonmetallic coating is needed, however. In addition to offering structural capability, concrete containments simultaneously provide biological shielding and greater missile protection.

With the pressure-suppression type of containment used with BWR plants, steel has been the preferred construction material. Two recent BWR plant designs have utilized a concrete structure, however, and the most recent application of the ICRCS (with the Sequoyah PWR plant) has used steel. It is therefore impossible to make firm statements that one material is preferred over the other for use with a particular plant type.

The containment systems for the prototype-sized [< 100 Mw(e)] organic-, gas-, and sodium-cooled plants constructed in the United States have been the steel-shell full-pressure type. Two reasons for this selection were that (1) virtually all containments were of this type at the time when these plants were designed and (2) because of the relatively small sizes of these plants and the relatively small amount of stored energy in their coolants, steel would probably be the economic choice even if concrete containment technology had then been as established as it is today. With regard to gas-cooled reactors, it should be pointed out that the 330-Mw(e) Fort St. Vrain Nuclear Power Plant,[28] which is the only unit in the United States with a prestressed-concrete reactor vessel (PCRV), does not have a separate leaktight containment structure because a significant loss of primary-system integrity is not considered to be credible with this design in which the reactor, circulators, and steam generators are all enclosed in the PCRV. The plant has a controlled-leakage confinement-type reactor building equipped with ventilation filters for removing particulates and iodine from the building exhaust.

In the following, salient design features of containment structures are discussed in terms of their application to the large nuclear power plants using pressurized- and boiling-water systems that have been recently designed in the United States.

Containment Structures with PWR Units

Steel-Shell Designs. As discussed earlier, the 550-Mw(e) Prairie Island and Kewaunee units utilize a steel-shell containment surrounded by a separate concrete reactor building. The steel cylindrical shell is 1½ in. thick with a ¾-in. hemispherical dome and a 1½-in.-thick ellipsoidal-shaped base. The shell is 105 ft in diameter and 206 ft in overall height. The structure includes two personnel air locks and an equipment

door 21 ft in diameter. A circular crane of 230-ton capacity is mounted on a girder built integral with the vessel wall. The vessel is designed for a maximum internal pressure of 46 psi at a temperature of 268°F.

Since the plate welds are limited to 1½ in. or less, stress relieving of the completed shell in the field is not required. However, some of the heavier penetration insert assemblies are stress relieved prior to welding in place.

The shield building is a cylindrical reinforced-concrete structure with 2½-ft-thick walls and a 2-ft-thick shallow dome roof. A separation of 5 ft between the shield building and the containment vessel provides the necessary construction space as well as the annular volume between structures required for the functioning of the shield-building vent system. The containment vessel and shield building are both supported on a single dished-mat-type foundation. The containment vessel will be erected on temporary columns. After the vessel has been pressure tested and leak-rate tested, the area between the foundation mat and the ellipsoidal head will be grouted in, and the temporary support legs will be removed.

The only other large PWR units that use steel containment are the dual 1124-Mw(e) units at the Sequoyah Generating Station of TVA. The major difference between these two stations and those at Prairie Island and Kewaunee is that the ice-condenser pressure-suppression system is used in these two units. As a result, the maximum internal pressure is only 12 psig, and a steel cylindrical shell and a hemispherical steel dome with nominal wall thickness of ½ in. can be used. The other difference is that Sequoyah 1 and 2 containments will have a flat, concrete slab base similar to current concrete containment designs except that the slab is designed for the reduced pressure of 12 psig. The bottom of the steel shell is reinforced either to bolt to the concrete or to anchor into it with straps or shear rings. The steel liner covering the concrete bottom is welded to the shell to provide a leaktight joint. The shield building will be built of reinforced concrete and will have a shallow dome.

The advantages of the double-barrier steel-shell designs in these three stations are:

1. The design and construction of the steel containment vessel and the concrete shield building are covered by well-established standards, and the licensability of the structures is enhanced by the availability of these standards.

2. An additional safety margin with regard to leakage rate is provided, and the frequency of required prooftesting is decreased.

3. The physical separation of the steel containment from the concrete shielding creates a second barrier for holdup of radioactivity leakage and also facilitates construction and in-service inspectability.

4. The concrete shield building will be designated to take the external loads such as tornadoes and other wind loads and missile loads, eliminating these loadings from the design of the steel vessel.

5. The leakage-rate test is aided, since the steel containment is protected from outside temperature variation.

6. Such a design offers a tight, manageable construction schedule and provides flexibility in the planning of sequence of construction.

Concrete Designs. An examination of the concrete containment designs reveals the following:

1. There are nearly equal numbers of PCCV's and RCCV's.

2. The internal design pressures of PCCV's are about 10 to 20 psi higher than those of the RCCV's of equivalent electrical generating capacity.

3. The wall thicknesses of RCCV's are generally about 6 to 12 in. greater than those of PCCV's of equivalent electrical generating capacity.

There are three types of concrete containments currently used in the United States: reinforced concrete, reinforced concrete with the cylinder axially prestressed, and dome and cylinder fully prestressed. In all the containments, steel liners of thickness varying from ¼ to ½ in. are used on the concrete for leaktightness. The steel liner is anchored to concrete either by studs, channels, or angle sections. All the penetrations are located in the cylindrical portion of the vessel. The diameters of these penetrations vary from a few inches for electrical ducts to 20 ft for the equipment hatch.

Reinforced-Concrete Containment Vessel. Generally, the basic features of this type of containment are:

- Hemispherical dome.
- Wall thickness of 3½ to 4½ ft for the cylinder and 2½ to 3½ ft for the dome.
- Main reinforcement bars placed axially and circumferentially.
- Seismic reinforcement bars placed helically at an angle of 45 deg with the horizontal, in both directions, in the wall of the cylinder.
- Stirrups or diagonal bars provided in the lower portion of the cylinder to resist radial shear.
- Thermal insulation provided on the inside for the bottom 20 ft or so of the cylindrical portion of the containment, so that the stress contribution from

thermal effects is kept to a minimum at the junction of the wall and base slab.

• Studs used to anchor the liner to the concrete wall.

Containments having these typical features are Indian Point Unit 2, Connecticut Yankee, and Surry Nuclear Power Plant. Figure 4 shows the general features of the reinforced-concrete containment of Indian Point Unit 2. For purposes of comparison the elevation through one of the Donald C. Cook Station's two units, which has the ICRCS, is shown in Fig. 5.

Because it is difficult to place the helical seismic-reinforcement bars and diagonal bars, axially and circumferentially placed reinforcing bars may be used instead. In this case the tangential and radial shears will be resisted through dowel action of the axial and circumferential bars. This concept may be adopted in the design of the containments for Main Yankee, Indian Point 3, Salem 1 and 2, and Malibu.

A station that has containment reinforcement features quite different from those mentioned above is Diablo Canyon. These reinforcement features are (1) The main reinforcement bars are placed circumferentially on a helix angle of 60 deg with the horizontal in both directions. The reinforcement bars are placed in continuous loops starting at the base of the cylinder, running up to the spring line and over the top of the dome, and returning to the base of the cylinder. (2) Instead of using bent shear-reinforcing bars placed radially, wide-flange beams are used, spaced on centers 4 ft apart. The beams are attached to the base slab by a hinged connection at their lower ends and are terminated 20 ft above the top of the base slab. (3) The above reinforcing-bar arrangements are accommodated by vessel wall thicknesses of 3 ft 6 in. for the cylinder and 2 ft 6 in. for the dome, which are significant reductions from the corresponding thicknesses of 4 ft 6 in. and 3 ft 6 in. used in the typical RCCV.

Prestressed-Concrete Containment Vessel. The first PCCV was built at Brennilis in Brittany, France, for the Nuclear Power Station EL-4. Another PCCV, which has nearly the same features as those of the EL-4, is located at Hydro-Quebec's Gentilly Nuclear Power Station in the Province of Quebec, Canada.[30] Both the EL-4 and Gentilly PCCV's are truly fully prestressed, i.e., the dome, the cylinder, and the base slab are prestressed in two or more directions. Both are constructed with the slip-form technique and use nonmetallic coatings to maintain leaktightness of the containment. The prestressing tendons in both vessels are bonded.

In the United States there are about 16 PCCV's, either being built or being planned. The basic features of these containments are nearly the same. The wall thicknesses are about 3½ ft for the cylinder and 2½ ft for the shallow dome. All the containments are provided with a steel liner for leaktightness, and the liner is anchored to the concrete by continuous angle or channel anchors. The conventional concrete construction method is used. The prestressing tendons are either bonded or unbonded. The prestressing force in the cylinder is attained by prestressing the tendons in the circumferential and axial directions in all PCCV's except the one at the Fort Calhoun Nuclear Power Station, where the prestressing tendons are placed helically.

Prestressed- and Reinforced-Concrete Containment Vessel. In this type of concrete containment, the concrete in the cylindrical portion is prestressed axially and reinforced circumferentially, whereas the concrete in the hemispherical dome is simply reinforced. Some basic premises of this concept are that axial prestressing will enhance the shear resistance of concrete across a horizontal plane of the cylinder wall and that it may greatly reduce the amount of axial reinforcing steel needed. Because of the reduced reinforcement required, the thicknesses of the vessel wall are reduced to the values used in the containment at Diablo Canyon. In current designs the whole cylinder liner is insulated with PVC foam plastic material covered with a stainless-steel sheet to limit the liner temperature during the worst hypothesized accident and thereby to maintain the liner stresses within design limits. Diagonal reinforcing steel is provided at the bottom portion of the cylinder to resist the radial shear stress resulting from the discontinuity at the base of the wall.

The R. E. Ginna and H. B. Robinson Unit 2 containments have these general features, although there are differences in the detailed design. In the R. E. Ginna design, the cylinder rests on laminated neoprene pads and is assumed to be hinged, whereas in the H. B. Robinson Unit 2 design, the cylinder bears directly on the foundation mat and is considered to be fixed. In the R. E. Ginna design, the BBRV prestressing system is used and the tendons are bonded, and in the H. B. Robinson Unit 2 design, the Stresstell system is used and the bars are also bonded.

Containment Structures with BWR Units

All BWR plants from 1967 until recently have utilized a pressure-suppression containment system which has a steel dry well in the shape of an inverted

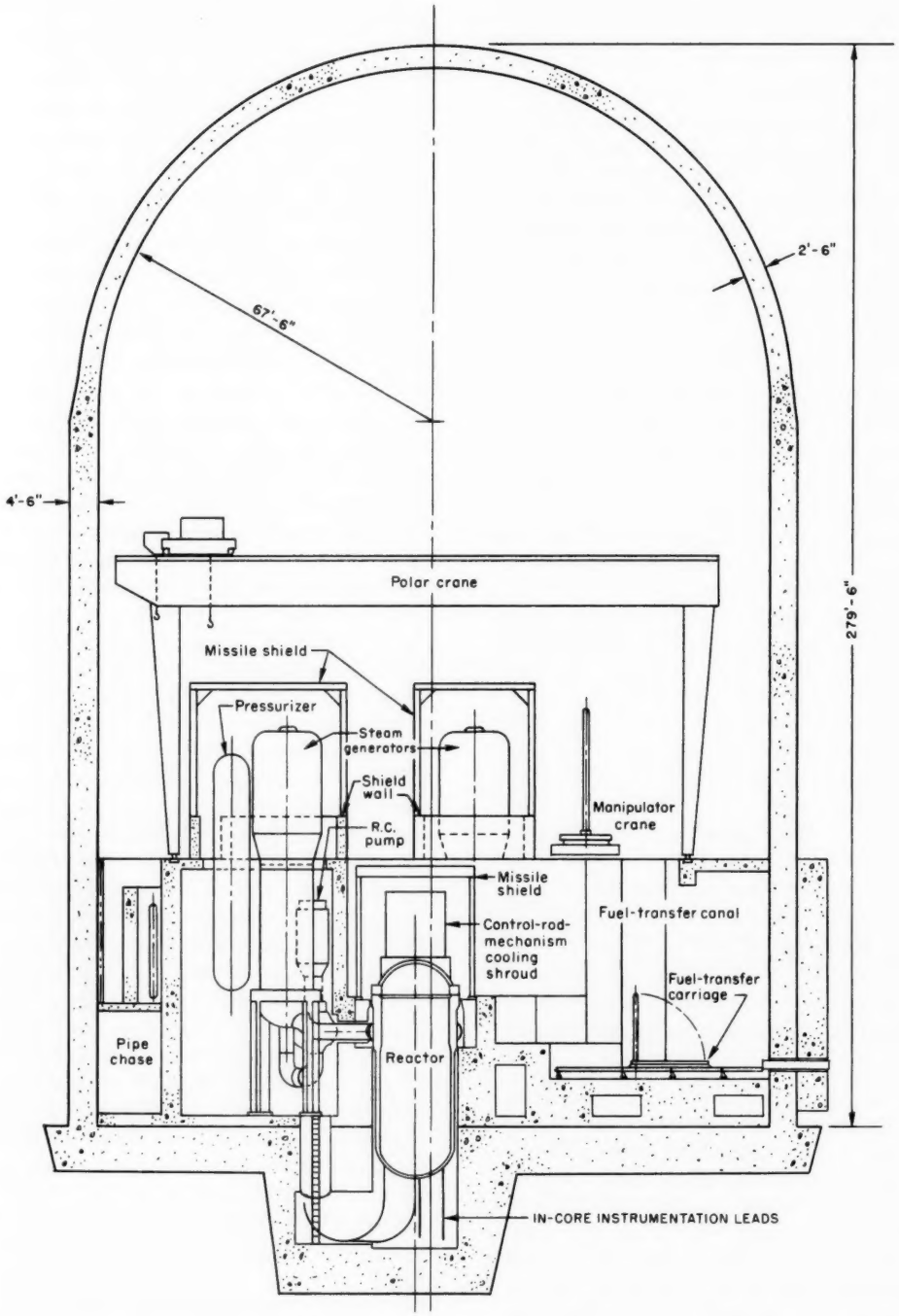

Fig. 4 Containment and reactor arrangement for Indian Point Unit 2 (from Ref. 29).

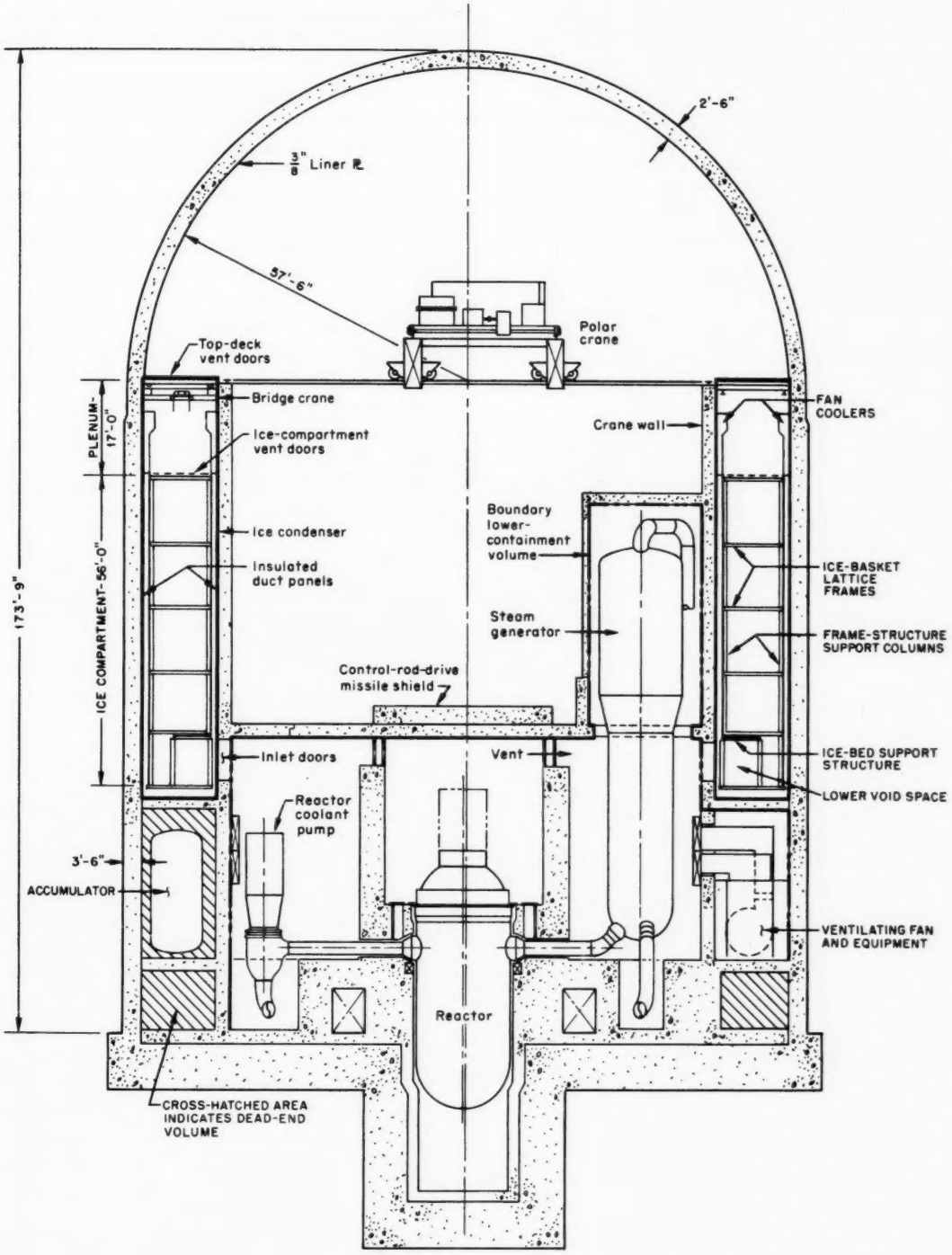

Fig. 5 Containment and reactor arrangement for Donald C. Cook Station, Units 1 and 2 (from Ref. 13).

light bulb surrounded by a toroidal steel pressure-suppression chamber. However, steel-lined reinforced-concrete containment vessels have been proposed for the Bell and Shoreham Nuclear Power Stations. Both the dry well and suppression chambers are enclosed in a relatively low-leakage concrete building held at slightly negative pressure by fans that exhaust through filters to a stack. This is, therefore, a multibarrier system similar to those discussed earlier.

Because of the possible hazard of an explosive mixture of hydrogen and oxygen being present in the containment, with the hydrogen being generated from a reaction between steam and hot Zircaloy cladding during a loss-of-coolant accident, inerting of the containment atmosphere is necessary with the compact BWR containment system. The inerting is accomplished by reducing the oxygen content of the air to the maximum of 4.9% at atmospheric pressure by displacing oxygen with nitrogen. The containment ventilation and cooling system is used in conjunction with a nitrogen supply system to achieve this oxygen content. The primary containment is maintained at a slight positive pressure to ensure maintenance of the reduced oxygen content during plant operation.

Steel-Shell Designs. The pressure-suppression containment system houses the reactor vessel and the reactor-coolant-recirculating loops of the reactor primary system. As shown in Fig. 6 the pressure-suppression system consists of a dry well, a pressure-suppression chamber that stores a large volume of water, a connecting vent system between the dry well and the water pool, and isolation valves. Also present are containment cooling systems and other service equipment.

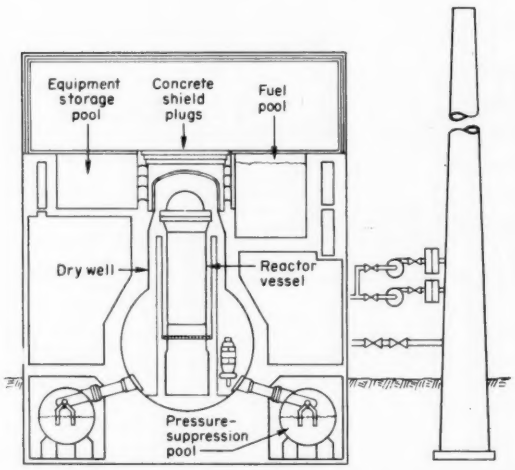

Fig. 6 All-steel containment system for boiling-water reactors.

The steel-plate thickness is about 1¾ in. The top of the dry well is a removable closure head. This head is bolted in place and sealed with gaskets. The dry well is enclosed in a reinforced-concrete shielding structure separated from the reinforced concrete by a gap of approximately 2 in. Radiation shielding at the top of the dry well is normally provided by removable, segmented, reinforced-concrete shield plugs.

The dry well is not normally entered during power operation because of the high radiation levels, but access is normally permissible during a hot standby with the reactor subcritical. Normal environment in the dry well during plant operation is essentially atmospheric pressure with an average ambient temperature of about 135°F. This temperature is maintained by recirculating the atmosphere in the dry well through cooling units that are served by a closed-loop cooling-water system.

The torus-shaped pressure-suppression chamber is located below and encircling the dry well. The suppression chamber is held on supports that transmit vertical and seismic loading to the reinforced-concrete foundation slab of the reactor building. Space is provided outside the chamber for inspection and maintenance. The dry-well vents are normally connected to a vent header that is contained within the air space of the suppression chamber. Projecting downward from the header are the downcomer pipes. The vent header has the same temperature and pressure design requirements as the vent pipes. Baffles are used in the suppression chamber to ensure proper interaction of the vent-pipe discharge with the suppression pool water. Vacuum breakers are used to permit noncondensable gas flow from the suppression chamber back into the dry well so as to prevent a backflow of water from the suppression pool into the vent header system.

The reactor building completely encloses the reactor and its pressure-suppression primary containment. This structure provides secondary containment when the primary containment is in service during power operation. It also serves as the primary containment during reactor refueling and maintenance operations when the pressure-suppression containment is open. The reactor building houses the refueling and reactor servicing equipment, new- and spent-fuel-storage facilities and other reactor auxiliary or service equipment, including the reactor core isolation cooling system, residual heat-removal system, reactor cleanup system,

standby liquid control system, control-rod hydraulic system equipment, and components of electrical equipment.

Figure 7 shows an overview of the Dresden Nuclear Station, with the spherical steel, full-pressure-type containment for Unit 1 at the right and the typical steel dry well–suppression chamber containment vessels for Units 2 and 3 in various stages of construction.

Concrete Designs. Since concrete containments have only recently been considered for BWR plants, the containment configuration has not been standardized to the degree achieved for PWR plants. In the Bell Station the configuration uses bulb-shaped cones and cylinders to approximate the steel dry well.[31] The suppression chamber is a horizontal torus that appears to have the same configuration as in the all-steel design.

In the containment system of the proposed, but canceled, Shoreham Station, the configuration differs appreciably from the all-steel design.[32,33] As shown in Fig. 8, the biological shielding, vapor barrier, and strength member are constructed—and function—as a composite structure. The conical shape, with the suppression chamber beneath the dry well, is considered to be optimum, both for concrete construction and for station arrangement. The wall thickness of the RCCV varies from $4\frac{1}{2}$ to $6\frac{1}{2}$ ft, and the walls are lined with a $\frac{3}{8}$-in. steel plate.

In a recent paper that presents a survey of new designs of steel and composite steel/concrete contain-

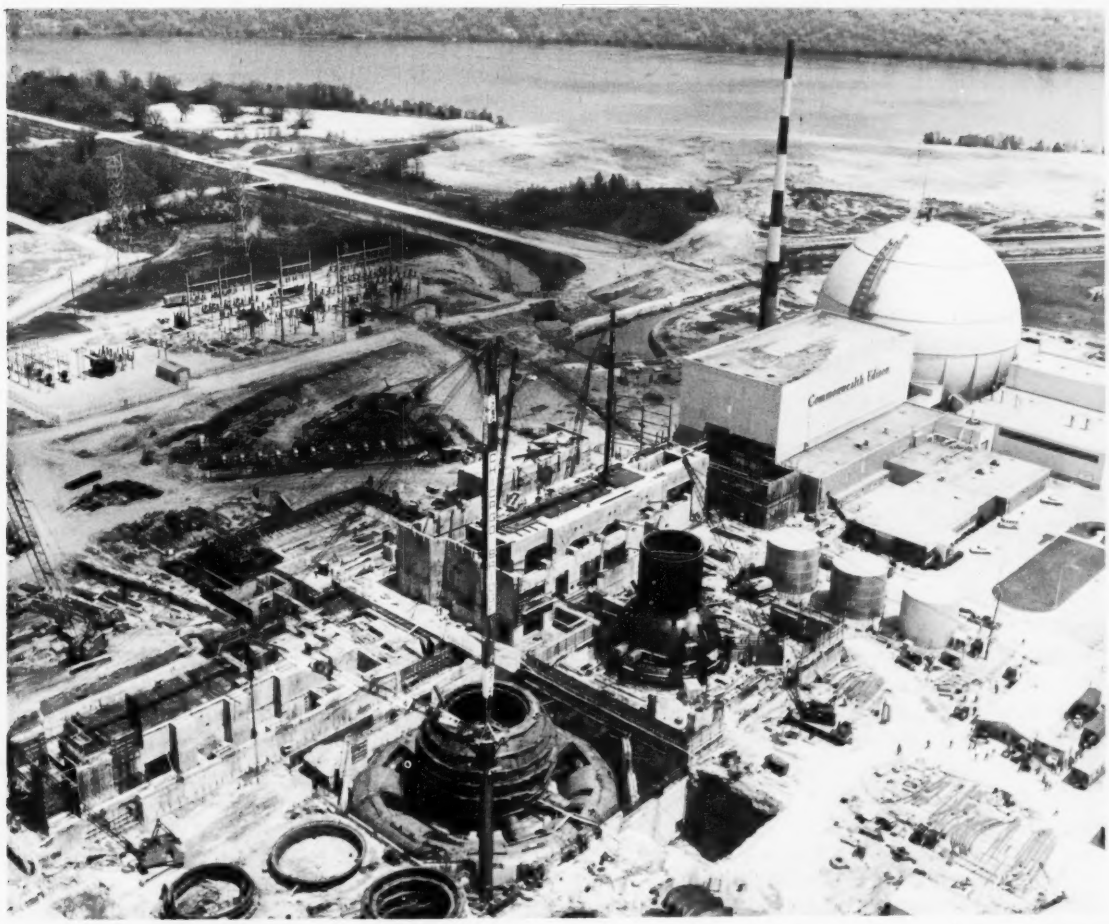

Fig. 7 Aerial view of Dresden Nuclear Power Station showing Units 2 and 3 under construction (photograph courtesy of Chicago Bridge & Iron Co.).

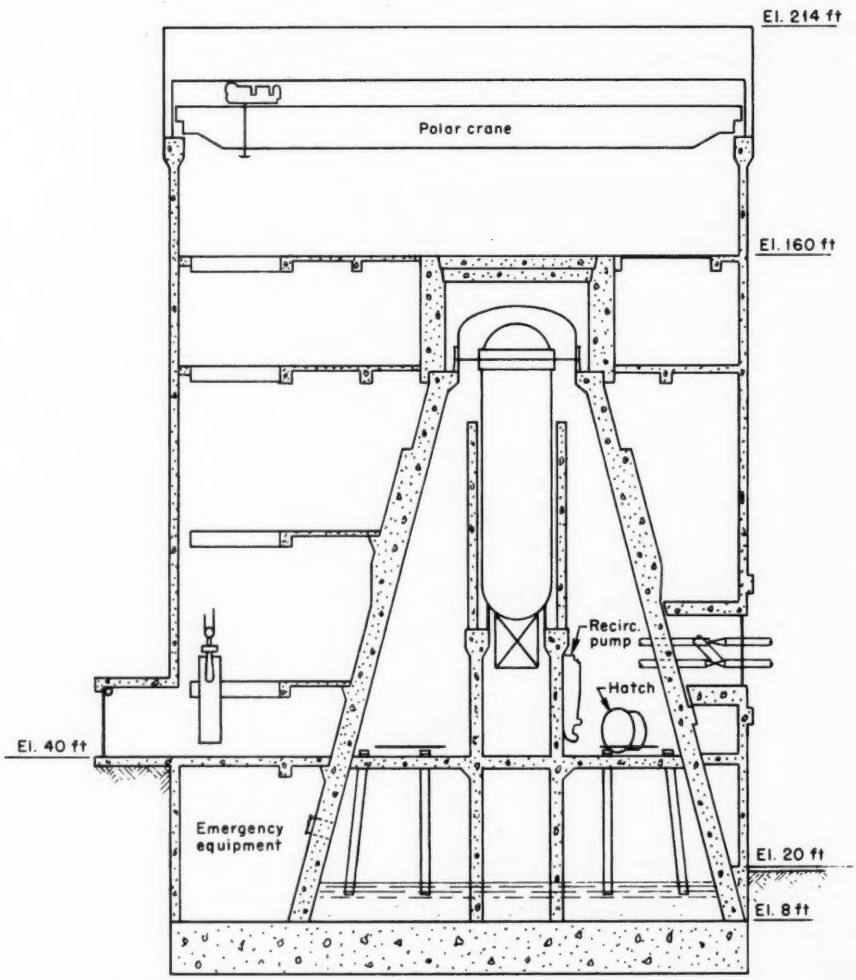

Fig. 8 Containment and reactor building for Shoreham Station (from Ref. 33).

ment vessels, Dunn of CB&I describes an all-steel combined dry well/suppression chamber BWR containment design.[34] In this code-stamped structure, the suppression pool is located immediately beneath the dry well, similar to the configuration in the Shoreham Station.

Foundation Mat

As indicated previously the foundation mats of all concrete containments in the United States, whether the containment is reinforced, prestressed, or a combination of the two, are of reinforced concrete. In addition, some containment designs call for a steel shell for the walls and dome and a reinforced-concrete base mat. The reasons for not using a prestressed-concrete mat in PCCV's are:

1. The resultant membrane forces in a slab are not significant compared to the moments and shears, and prestressing in a slab and a shell is not so efficient as in a beam to counteract the bending moment.

2. The presence of a deep sump for an instrumentation tunnel near the middle of the mat would complicate the prestressing arrangement.

3. Friction between the foundation mat and foundation material, e.g., soil or rock, presents a dilemma, since it is desirable to eliminate the friction to reduce the absorption of prestressing force by the foundation

material, but it would be better to increase the friction to resist the horizontal seismic force.

4. The use of prestressing may also require that the stressing of the tendons be done prior to any significant construction of the walls due to the slab moments created by the added dead load.

5. The cost of a prestressed slab would be higher than the cost of a reinforced-concrete slab.

In spite of the above, the foundation mats of the French and Canadian PCCV's are made of prestressed concrete. One obvious reason for this is that plastic, rather than steel, liners were used; and prestressing is needed to prevent excessive concrete cracking and loss of leaktightness. The foundation slab is preloaded against internal pressure by the external foundation pressure. Because of the preloading effect and the interaction of the slab and the foundation material, a flat slab is usually the most economical solution in nearly all cases, especially if the foundation material is rock. In addition, the high cost of excavation usually eliminates the consideration of an inverted dome in rock. However, there are conditions favoring the considerations of an inverted dome, e.g., (1) the special support requirements for the reactor system, (2) the severity of the seismic criteria, and (3) a more efficient use of prestressing, since the dead load would create mainly membrane compression in the inverted dome.

Penetrations

The various types of penetrations in containment-vessel structures (whether steel types or whether reinforced, prestressed, or hybrid reinforced-and-prestressed concrete types) are basically the same. They consist of:

- Electrical penetrations.
- Piping penetrations.
- Equipment and personnel access hatches.
- Special penetrations such as for fuel-transfer operations.

These penetrations are generally circular, and their sizes vary from a few inches for electrical and piping penetrations to as much as 20 ft for the equipment access hatch. In general, a penetration consists of a sleeve welded to the steel containment structure (plate or liner) and embedded in the concrete wall (if present). The weld to the plate or liner is shrouded by a continuously pressurized channel that is used to demonstrate the integrity of the joint. The pipe, electrical conductor cartridge, duct, or equipment access hatch passes through the embedded sleeve; and the ends of the resulting annulus are closed by welded end plates, bolted flanges, or a combination of these. Provision is made for differential expansion and misalignment between the sleeve and the pipe or cartridge so that no piping loads are imposed on the containment structure.

Isolation valves are installed outside the containment on those pipes which are not inherently sealed off from the containment atmosphere. Each ventilation-system purge duct is isolated by two quick-closing, tight-sealing butterfly valves. One valve is installed inside and the other outside the containment. The valves are closed except during purging of the containment and can be operated either manually or automatically upon a signal of high radiation level in the containment. The space between the valves is pressurized when the valves are closed. The locking mechanisms on each air-lock door are designed so that a tight seal will be maintained when the doors are subjected to either internal or external pressure. The doors are mechanically interlocked so that at least one is closed and locked at all times.

Theories and Methods of Design Analysis for Concrete Vessel Structures

Steel containment vessels are designed in accordance with Sec. III of the *ASME Boiler and Pressure Vessel Code.* In the design of conventional reinforced- or prestressed-concrete structures, either the elastic theory, i.e., the straight-line theory of stress and strain, or the ultimate-load theory is used. In the design of a concrete structure on the basis of elastic theory, the structure should be so proportioned that under service loads the stresses in the structure will be within the allowable as specified in the American Concrete Institute (ACI) code or other applicable codes. For design on the basis of ultimate-load theory, the structure should be so dimensioned that the combination of loads (which would be used in the design based on elastic theory) multiplied by appropriate load factors will result in stresses within the ultimate strength of the structure. In the latter approach, in order to ensure serviceability, consideration is also given to the control of deflection and cracking under service loads.

Two basic criteria should be fulfilled in the design of prestressed- or reinforced-concrete containment vessels: (1) the integrity of the liner plate should be guaranteed under all loading conditions, and (2) the structure should have low-strain elastic response such that its behavior will be predictable under all design loadings. These criteria can be fulfilled by using a design based on elastic theory, i.e., the working-stress

design with due consideration for crack control and for shear and diagonal tension, since the stresses will be within the allowable and the behavior will be elastic with low strain. However, in order to guarantee an adequate margin of strength, there must be an additional criterion. In conventional concrete structures, the ultimate load criterion is used. The ultimate strength assumptions as made in the ACI code for concrete beams in flexure allow the concrete stress to go beyond yield and redistribute at a strain three or four times that which causes yielding. If these same assumptions are used in the design of concrete containments, the strain in the liner will be so great as to impair or to render doubtful its integrity as a leaktight membrane. Even though it may be possible to control cracking through the use of reinforcing steel with stresses larger than the proportional limit, knowledge in this area is still insufficient.

In order to guarantee an adequate margin of safety and at the same time to limit strain both in the concrete and in the liner, the so-called yield-limit design has been used as a basis of design analysis. The essence of the design approach is that the load combinations, with appropriate load factors, will be less than the yield strength of the structure. The yield strength of the structure is defined as the upper limit of elastic behavior of the effective-load-carrying structural materials. For prestressing and reinforcing steel, the limit is the guaranteed minimum yield given in the appropriate ASTM specifications. For concrete it is the ultimate values of shear (as a measure of diagonal tension) and bond per the ACI building code and the 28-day ultimate compressive strength for concrete in flexure.

At present the design of concrete containment vessels is accomplished by using either the working-stress design method or the yield-limit design method. Some use the working-stress method to make the design and the yield-limit method to check its margin of safety. The design criteria as recommended by ACI Committee 349 for concrete containment structures have been more or less followed by most designers of such structures, even though the recommendations have not been officially published.

For working-stress design, ACI Committee 349 recommends the same allowable stresses as specified in the ACI building code (318-63) except in special cases. The ACI building code permits a one-third increase in allowable stresses if wind or earthquake forces are combined with other loads. From the designs of the existing concrete containments, it appears that the use of this increase in allowable stresses is at the discretion of the designers. Obviously, if the yield-limit design method is used, the one-third increase clause is no longer applicable. The basic problem with the present yield-limit design is the lack of a rational and uniform basis for establishing the load combinations and load factors.

Both RCCV's and PCCV's have wall thickness to mean radius, t/r, ratios about 1/15 and can be loosely classified as shells of moderate thickness. There are divergent opinions as to the definitions of thin-shell and thick-shell theories on the basis of this ratio. Some say that thin-shell theory is applicable if this ratio is between 1/1000 to 1/50, whereas others say it may be applicable to a ratio as low as 1/5. Actually, such classification can be only done in a qualitative sense, and it is not possible to formulate precise bounds as criteria. The basic difference between classical thin-shell theory and thick-shell theory is that, in the former, the effects of transverse shear and normal strain are neglected, whereas they are considered in the latter.

Analysis of the Overall Vessel Behavior

It is generally believed that with a t/r ratio around 1/15, there will be no significant difference in the results of analysis based on thin-shell theory. Consequently, some designers of concrete containments are using computer programs written on the basis of thin-shell theory, whereas others use programs based on thick-shell theory. The various methods of analysis and computer programs have been reviewed in a study of prestressed-concrete reactor vessels for ORNL by Tan.[35] Some of the computer programs used in the design analysis of concrete containments are (1) Yale Program, (2) Sor-II Program, (3) FIRL's General Shell Program and Finite Analysis Program (FELAP), and (4) Wilson's Finite Element Program. Some of the designers have developed their own proprietary programs. With the exception of Wilson's program that takes the effects of thick shell into consideration, all other programs are developed on the basis of thin-shell theory.

Analysis of the Area Around Penetrations

Concrete containment vessels generally have numerous penetrations of various sizes. The largest is the equipment hatch that can have a diameter of around 20 ft. The presence of a penetration of such large size compared to the shell diameter presents several problems: (1) stress concentration, (2) reduction of vessel stiffness in its neighborhood, (3) arrangement of pre-

stressing and reinforcing steel around the penetration, and (4) stiffening of the penetration. A basic question is how to make an adequate design analysis of each of these problems.

It is generally agreed that the stresses at points which are removed a sufficient distance from the opening are essentially the same as if there were no opening. On the basis of such an observation, the following analysis procedure is generally followed:

1. The analysis of the containment vessel as a whole is first carried out as an axisymmetrical structure without considering the opening by using a general axisymmetrical-shell program.

2. With the boundary conditions obtained from the above analysis at the top and bottom of the cylinder, half of the cylindrical vessel containing the large openings, such as the equipment hatch and personnel hatch, is analyzed by using a finite-element program.

3. With the boundary conditions of the area around the penetrations obtained from the second analysis, the penetration area is analyzed by using a finite-element program with finer elements.

For stresses around the penetrations, some designers are also using published results on study of penetration in steel plates and shells with the boundary conditions obtained from either axisymmetrical-shell analysis or finite-element analysis.[36]

Steel-Liner Design

In both PCRV and prestressed- (or reinforced) concrete containment vessels, steel liners of thickness varying from ½ to 1¼ in. for PCRV's and of thickness from ¼ to ½ in. for PCCV's or RCCV's are used to meet the specified leaktightness criterion. The steel liner in a PCRV or PCCV experiences much higher compression than that in a RCCV, and obviously its design and construction problems are more critical.

In spite of the difference in the environment and service conditions of the steel liners in PCRV's and PCCV's, the problems in the structure design of these liners are similar. In the design of these vessels, the steel liner is generally not considered to contribute any strength to the overall strength of the vessel. Since the liner is tightly anchored to the vessel, it is restrained from any movement of its own by the vessel, and any deformation in the concrete vessel is transferred to the liner. The liner is a comparatively very thin shell and is under high compression. Under such conditions it is obvious that buckling is a major concern. The problem is more critical in a PCRV because buckling may also impair equipment associated with the liner (e.g., insulation mounted to the inside surface and cooling pipes attached to the outside surface for the purpose of controlling the temperature of the liner and concrete). In a PCCV, performance of the liner as a leaktight membrane is the sole operational requirement to be fulfilled. Hence, in either a PCRV or a PCCV, large buckling deformations must be prevented so that the leaktight integrity as well as the functional requirements of other components may not be jeopardized.

Generally, the thickness of the liner is determined by fabrication considerations and other constructional requirements, such as using the steel liner as the inside-wall form for concreting. Prevention of buckling deformations is attained through the use of anchors, and the design of the liner for elastic and inelastic stability becomes a problem of adjusting the size and spacing of these anchors. Up to now the design of the liner for PCRV's and PCCV's has usually been accomplished through model testing or by using simplified analytical methods.

Besides the general lack of an adequate method of design analysis, there is also a lack of design criteria. The current liner design uses Sec. III of the ASME code as a guide. A steel pressure vessel is usually a tensionally loaded structure, however, whereas a steel liner is compressively loaded. The former behaves independently, whereas the latter must act compositely with the concrete. Basically, a steel liner and a steel pressure vessel are totally different structures. Furthermore, in this composite construction, the compatible stresses in the concrete adjoining the liner must also be studied. The composite behavior of the steel liner and the concrete, especially under a high liner temperature and a temperature gradient, is largely unknown. Calculations based on orthodox theory will often show that stresses in the liner exceed the yield limit of the steel, especially in a prestressed-concrete containment.

Halligan has presented a paper[37] on the basic structural design philosophy and criteria for containments, with emphasis on PCCV's, and includes a discussion of loading conditions. In a related paper, Wahl[38] presents an interesting discussion of typical problems and solutions encountered in the design of prestressed containment structures. His paper covers special design areas such as the foundation slab, tendon configuration, large penetrations, grouped penetrations, and the liner plate.

Construction Methods

From the construction point of view, containment structures are little different from many conventional

structures such as aboveground water-storage tanks, sludge tanks, and silos for grain storage. The only apparent differences are that containments have relatively thicker walls, make more stringent requirements on leaktightness and quality assurance, and have a relatively large number of penetrations.

The construction of a typical steel-plate pressure-suppression type of containment system for a BWR—that at the Oyster Creek plant—has been described by Archer and Brown.[39] Two methods, conventional practice using fixed forms and "slip-forming," have been used in the construction of concrete containments. In the United States, only the former method has been used, whereas prestressed-concrete containments for the cylindrical wall portion of the Gentilly Nuclear Power Station in Canada and of the EL-4 Station in France were built with the slipforming technique. In the United States, with the use of a steel liner on the inside to achieve leaktightness, there is apparently no advantage in using this method. With fixed forms the concreting is accomplished in horizontal rings about 5 ft high for each lift. The basic problem in concreting this portion of the vessel is the congestion of the reinforcing steel and/or of the sheathing for prestressing steel. The situation is worst in the reinforced-concrete type in the region around the equipment hatch where the reinforcing steel bars are diverted. There is little space for the concrete, and special attention is needed, e.g., coarse aggregate of small sizes and large slump may have to be used. This is also true for the region around the equipment hatch in the prestressed-concrete containment. The general practice to ensure proper bond between concrete of different lifts is to sandblast the hardened concrete and cover it with mortar grout immediately before the concreting of the next lift.

In the construction of RCCV's, placing and splicing of large reinforcing bars are extremely time-consuming operations, especially for the longitudinal and the helically placed seismic reinforcing bars. The bars have to be put in place joint by joint. The quality of the splices is controlled and their strength statistically checked by taking some of them out and strength-testing them in the laboratory in accordance with a sliding production schedule. The presence of closely placed bars makes the concreting of the vessel a slow process. The tedious work involved in placing and splicing of the large reinforcing bars is partially eliminated by using the hybrid construction of prestressed concrete in the axial direction and reinforced concrete in the circumferential direction. The placing of concrete is also facilitated, since, by prestressing the vessel in the axial direction, the amount of reinforcing steel for shear is reduced and, by using prestressing tendons, the spacing is increased.

Prestressed-concrete vessels are lightly reinforced compared to RCCV's, so that placing and splicing of the reinforcing bars which are used to distribute the cracks, to resist shear, or to increase ductility, present relatively little problem. If helical prestressing is used, dimension control of the tendon ducts presents some problems at construction; otherwise helical prestressing is probably the ideal method. With helical prestressing, the anchorage ribs for circumferential prestressing are eliminated and tensioning of the prestressing tendons is limited to the top and the bottom of the cylinder without interfering with the construction work of any adjacent structure. A discussion of construction techniques used with prestressed-concrete vessels has been prepared by Gerwick.[40]

Reinforced-concrete foundation mats are usually sectionalized both horizontally and vertically for pouring sequence. Alternating horizontal sections are poured to minimize shrinkage. The steel liner forming the inside face of the sump at the middle of the foundation mat is first erected, and then the concrete is placed behind the erected liner. After a ring section of the concrete slab near the edge of the foundation mat is finished, the steel liner for the bottom portion of the cylinder is erected. The steel liner for the cylinder and the dome is erected in ring courses with the plate joints staggered. The horizontal joints are machine welded. Various inspection techniques consisting of spot radiography, leak checking of joints, and visual inspection are used. The bottom steel liner is attached by welding to the flanges of the sections whose stems are embedded in the top of the foundation-mat concrete.

Steel-shell containment vessels and the steel-liner portion of concrete vessels are erected in rings about 9 to 10 ft high. The rings are joined together circumferentially by automatic welding, but the vertical joints in each ring are usually welded manually. In reinforced-concrete containments the steel liner is anchored by studs, whereas in the fully prestressed- and axially prestressed-concrete containments, the steel liner is anchored to the concrete wall by angle stiffeners spaced at about 15 in. in the horizontal direction and at 60 in. in the vertical direction. The stiffeners are connected to the liner by intermittent welds. Since the steel liner is used as a form on the inside of the vessel wall, care is usually taken so that the deflection will be within the specified tolerance and the liner will not be overstressed. This is accomplished by limiting the

height of each lift of concrete and by using a ring-type truss on the interior to support the liner laterally at the time of concreting, or by using an appropriate spacing of the horizontal and vertical stiffeners.

Performance Tests

The basic reason for requiring performance tests of containment structures is to ensure that in case of a serious accident the containment can fulfill its function of preventing the release of radioactive material in excess of the predetermined safe value for a specific nuclear power station. Generally, the tests consist of a strength test and leakage-rate tests. The leakage-rate test provides assurance that the potential radioactive release through minute holes or cracks at welded joints and penetration connections is tolerable and less than the specified value used as a design criterion. In concrete containment vessels where leaktightness is provided through the use of steel liners, the overall integrity of the steel liner depends on the strength of the concrete containment in case of a serious reactor accident.

A very thorough and comprehensive review of the current status of leak testing of containment systems was recently made by Zapp[41] at ORNL. He recommended that the existing tentative standards and guides[42,43] be subjected to further revision since it is possible within the existing guidelines to obtain widely divergent results. Since his recommendations appear to be apropos for the current concrete containment structures as well as for steel vessels, reference should be made to his document for a detailed appraisal of the state of the art of leak testing.

Most of the reactor containment structures built have been made of steel and designed and tested in accordance with the *ASME Pressure Vessel Code.* Because of the lack of a related code for the design and construction of concrete containment vessels, such structures are presently being structurally tested in accordance with the ASME code for steel pressure vessels (tested at a pressure equal to 115% of design pressure).

The application of prestressed concrete to containment structures is relatively novel. To verify the analytical design of the structure and to study its general behavior during the initial pressure test, various strain and displacement instruments are installed at strategic locations on and within the containment vessel.[44] Since the integrity of the containment vessel depends on the in-service reliability of the prestressing system used in it, a surveillance program is currently required for tendons that are ungrouted and protected with wax or grease. The program generally includes the provisions of the following typical procedures:

1. Lift-off measurements to verify the tendon in one set of hoop shell tendons, three vertical shell tendons, and three dome tendons.
2. Removal of tendon wires (extras intentionally included for this purpose) to check for evidence of corrosion.
3. Testing of removal wires to detect any significant changes in physical properties.
4. Periodic sampling and testing of the tendon protective wax.

A surveillance program may also be required for bonded tendons. Since destructive examination is required for monitoring, the surveillance specimen typically consists of a full-size tendon encased in a concrete block detached from the containment structure but subjected to the same environment.

References

1. S. Levy, A Systems Approach to Containment Design in Nuclear Power Plants (SM-89/51), in *Containment and Siting of Nuclear Power Plants,* Symposium Proceedings, Vienna, 1967, pp. 227-242, International Atomic Energy Agency, Vienna, 1967 (STI/PUB/154).
2. *Code of Federal Regulations,* Title 10, Part 100, Reactor Site Criteria.
3. G. W. Keilholtz and G. C. Battle, Jr., Air Cleaning as an Engineered Safety Feature in Light-Water-Cooled Power Reactors, *Nucl. Safety,* **10**(1): 46-53 (Jan.–Feb. 1969).
4. G. W. Keilholtz, C. E. Guthrie, and G. C. Battle, Jr., Air Cleaning as an Engineered Safety Feature in Light-Water-Cooled Power Reactors, USAEC Report ORNL-NSIC-25, Oak Ridge National Laboratory, September 1968.
5. R. W. Corcoran, A. C. Koehler, and R. J. Jensen, Steel-Shell Containment Vessel with Concrete Shield Building, *Trans. Amer. Nucl. Soc.,* **11**(1): 265-266 (June 1968).
6. D. M. Leppke, R. W. Corcoran, and A. C. Koehler, Steel Containment Advantages, *Power Eng.,* pp. 48-49 (August 1968).
7. F. L. Malay and C. T. Chave, Containment for Nuclear Reactors, *Mech. Eng.,* pp. 30-34 (August 1965).
8. Final Safety Analysis Report, BONUS Nuclear Power Station, Docket 115-4, Puerto Rico Water Resources Authority.
9. J. H. Noble, Subatmospheric Containment, *Trans. Amer. Nucl. Soc.,* **11**(1): 262-263 (June 1968).
10. Final Safety Analysis Report, Humboldt Bay Station Unit 3, Docket 50-133, Pacific Gas & Electric Company.
11. Westinghouse Electric Corporation, PWR Plant Division, *Westinghouse Ice Condenser Reactor Containment System Evaluation Handbook,* 1968.
12. Paul Dragoumis, James W. Cook, Sterling J. Weems, and Walter G. Lyman, Ice Condenser Reactor Containment System, *Trans. Amer. Nucl. Soc.,* **11**(1): 265 (June 1968).
13. Preliminary Safety Analysis Report, Donald C. Cook Nu-

clear Station Units 1 and 2, Dockets 50-315 and -316, Indiana and Michigan Electric Company.
14. Preliminary Safety Analysis Report, Sequoyah Station, Units 1 and 2, Docket 50-327, Tennessee Valley Authority.
15. Atomic Energy of Canada Limited, Nuclear Power Demonstration Reactor, *Nucl. Eng.*, October 1962.
16. K. D. Kolev, Negative Pressure Containment—Pickering Generating Station, *Trans. Amer. Nucl. Soc.*, **11**(1): 263-264 (June 1968).
17. Preliminary Safety Analysis Report, Browns Ferry Nuclear Power Station Unit 1, Docket 50-259, Tennessee Valley Authority.
18. S. K. Ghaswala, "The World Around: The Queer Koyna Earthquake," *Int. Sci. Technol.*, No. 78, p.66 (June 1968).
19. G. V. Berg, and J. L. Stratta, Anchorage and the Alaska Earthquake of March 27, 1964, American Iron and Steel Institute, July 1964.
20. N. M. Newmark, Design Criteria for Nuclear Reactors Subjected to Earthquake Hazards, unpublished, May 25, 1967.
21. J. P. Finley, Tornadoes, *The Insurance Monitor*, New York, 1887.
22. The Study of Missiles Resulting from Accidental Explosions—A Manual for Investigators, USAEC Safety and Fire Protection Bulletin 10.
23. Richard C. Gwaltney, Missile Generation and Protection in Light-Water-Cooled Power Reactor Plants, USAEC Report ORNL-NSIC-22, Oak Ridge National Laboratory, September 1968.
24. Preliminary Safety Analysis Report, Three Mile Island Nuclear Power Station, Docket 50-289, Metropolitan Edison Company.
25. Jorge D. Riera, On the Stress Analysis of Structures Subjected to Aircraft Impact Forces, *Nucl. Eng. Design*, 8(4): 415-426 (1968).
26. A. Amirikian, Design of Protective Structures (A New Concept of Structural Behavior), Report NP-3726, Bureau of Yards and Docks, Department of the Navy, August 1950.
27. Wm. B. Cottrell and A. W. Savolainen (Eds.), U. S. Reactor Containment Technology, USAEC Report ORNL-NSIC-5, Oak Ridge National Laboratory, August 1965.
28. Preliminary Safety Analysis Report, Fort St. Vrain Nuclear Power Plant, Docket 50-267, Public Service Company of Colorado.
29. Preliminary Safety Analysis Report, Indian Point Nuclear Generating Unit 2, Docket 50-247, Consolidated Edison Company of New York.
30. B. Laforte, A. Ziegler, and P. Wong, Gentilly Power Station Prestressed Reactor Containment Building, paper presented at the Canadian Nuclear Association Conference, Montreal, Canada, May 29–31,1967.
31. Preliminary Safety Analysis Report, Bell Station, Docket 50-319, New York State Electric and Gas Company.
32. Preliminary Safety Analysis Report, Shoreham Nuclear Power Station, Docket 50-322, Long Island Lighting Company.
33. W. J. Burns, W. J. L. Kennedy, and Fred Weinzimmer, Shoreham Nuclear Power Station with Concrete Containment, paper presented at the American Power Conference, Chicago, April 1968.
34. J. T. Dunn, Recent Developments in Steel Containment Vessels, paper presented at the 1968 ASCE Annual Meeting and National Meeting on Structural Engineering, Pittsburgh, Oct. 2, 1968.
35. Chen P. Tan, Prestressed Concrete in Nuclear Pressure Vessels: A Critical Review of Current Literature, USAEC Report ORNL-4227, Oak Ridge National Laboratory, May 1968.
36. A. C. Eringen, A. K. Naghdi, and C. C. Thiel, State of Stress in a Circular Cylindrical Shell with a Circular Hole, Welding Research Council, Bulletin No. 102, January 1965.
37. D. W. Halligan, Structural Design Criteria for Secondary Containment Structures, *Nucl. Eng. Design*, 8(4): 427-434 (1968).
38. Howard W. Wahl, Typical Design Problems and Solutions for Prestressed Concrete Containment Structures, *Nucl. Eng. Design*, 8(4): 471-486 (1968).
39. J. C. Archer and T. P. Brown, Design and Construction of the Oyster Creek Containment, *Nucl. Eng. Design*, 9(2): 258-264 (1969).
40. Ben C. Gerwick, Jr., Construction Techniques for Prestressed Concrete Pressure Vessels, *Nucl. Eng. Design*, 8(4): 460-466 (1968).
41. F. C. Zapp, Testing of Containment Systems Used with Light-Water-Cooled Power Reactors, USAEC Report ORNL-NSIC-26, August 1968.
42. USAEC Division of Safety Standards, Safety Standards, Criteria and Guides for the Design, Location, Construction and Operation of Reactors, *The Technical Safety Guide, Reactor Containment Leakage Testing and Surveillance Requirements*, revised draft, Dec. 15, 1966.
43. American Nuclear Society, Proposed Standard for Leakage Testing of Containment Structures, ANS 7.60, June 14, 1967.
44. R. S. Bekowich, Instrumentation in Prestressed Concrete Containment Structures, *Nucl. Eng. Design*, 8(4): 500-512 (1968).

The Removal of Iodine from Reprocessing-Plant Effluents

By Walton A. Rodger and Stanton L. Reese*

Editor's Note: This article reflects the opinions of the authors and not necessarily those of the Atomic Energy Commission.

In the Winter 1968–1969 issue of *Reactor and Fuel-Processing Technology*, the authors presented a discussion of the impact of presently proposed larger reprocessing plants on the fuel cycle.[1] In the article it was pointed out that, under the assumptions usually made in assessing the safety of a plant of this type, the limiting isotope from the standpoint of atmospheric release is ^{131}I. That fact suggests the desirability of delving more deeply into the effect of iodine upon reprocessing-plant design and operation and of reviewing the methods available for the control of iodine emissions.

Iodine Emission as a Function of Plant Size and Cooling Time

For the purpose of this article, it has been assumed that future fuels will reach an average burnup of 40,000 Mwd/metric ton at a specific power of 40 Mw/metric ton. Under these conditions, each metric ton of fuel will contain, at time of discharge, 1.2×10^6 curies of ^{131}I and 0.03 curie of ^{129}I. Because of the very low discharge limits for ^{131}I, it has been the normal practice to cool spent fuel for 100 to 150 days before attempting to carry out fuel reprocessing.

If one assumes a value for X/Q of 5×10^{-8} sec/m^3 as representative of the atmospheric dilution from a reprocessing-plant stack,† the allowable release rate of ^{131}I can be calculated[2] from

$$Q = \frac{C}{(X/Q)_{av.} V_g \tau A} \quad (1)$$

where Q = allowable release rate of ^{131}I, μc/sec

C = FRC (Federal Radiation Council) provisional limit for ^{131}I in milk = 10^{-4} μc/liter

V_g = settling velocity for ^{131}I = 10^{-2} m/sec

τ = effective mean life of ^{131}I on grass = 6×10^5 sec

A = activity in milk resulting from unit deposit on grassland, 0.2 [(μc/liter)/(μc/m^2)]

$(X/Q)_{av.}$ = average dilution factor for entire site, 5×10^{-8} (assumed)

By solving Eq. 1 for the assumed conditions, we obtain an allowable release rate of 1.67 μc/sec for ^{131}I. This is equivalent to an annual allowable release rate of about 50 curies.

The amount of ^{131}I remaining per metric ton of fuel after any desired cooling time is simply determined from

$$I = I_0 \exp(-\lambda t) \quad (2)$$

*Nuclear Safety Associates, Rockville, Md.

†The value of 5×10^{-8} sec/m^3 is approximately that obtained for a 100-m stack located in the center of a relatively flat site of a 1500-m radius with meteorology characteristic of the coastal plain in the southeastern United States, e.g., Savannah River.

where I = activity at time t, curies/metric ton
I_0 = activity at time zero, curies/metric ton
λ = decay constant for ^{131}I = 0.086, day^{-1}
t = cooling time, days

Then it is possible to determine the decontamination factor that must be obtained from the iodine-removal equipment to meet a 50-curie annual discharge limit for ^{131}I:

$$DF = \frac{IP}{50} \tag{3}$$

where DF = required decontamination factor
I = activity at time t, curies/metric ton from Eq. 2
P = total metric tons processed annually

A plot of the required decontamination factor as a function of cooling time for 300 and 1500 metric ton/year plants is shown in Fig. 1.

It can be seen from Fig. 1 that, if the cooling time is less than 100 days, the required decontamination factor is very large; if, for example, the fuel is cooled 30 days, the required decontamination factor is on the order of 10^6, far in excess of the capability of present technology. Probably the only system that would provide such high factors is complete retention of the entire plant atmosphere for a period of months.

The cooling-time range from 100 to 200 days is of more interest. Normally it is expected that fuel will be cooled at least 150 days prior to processing. For a 300 metric ton/year plant processing 150-day-cooled fuel, a decontamination factor of only 20 is required to meet the FRC limit for ^{131}I in milk (under the assumed conditions). This is well within the capability of present technology. For a 1500 metric ton/ year plant, the required decontamination factor is 100, which is also within the present technological capability. This latter degree of iodine removal is equal to that which Allied Chemical has claimed for its plant.[3] It also is within limits that have been deemed acceptable by the Division of Materials Licensing.[4]

In view of the cost of treatment to remove iodine, it is of interest to consider how much additional cooling time would be required to assure that iodine releases could be met without any treatment at all. Reference to Fig. 1 shows that the required cooling times are 184 and 202 days, respectively, for a 300 and a 1500 metric ton/year plant. The cost of additional cooling is simply the cost of money for the additional period of time, since the fuel owner is denied the use of the fuel for that additional period of time. We have assumed that the residual value of a metric ton of spent fuel (uranium plus plutonium, less cost of reprocessing) is about $70,000. If this is charged at 7%, the cost of additional cooling is $4900/365 or $13.50/(metric ton)(day), equivalent to $0.0135/(kg)(day). From this value the following costs are evident:

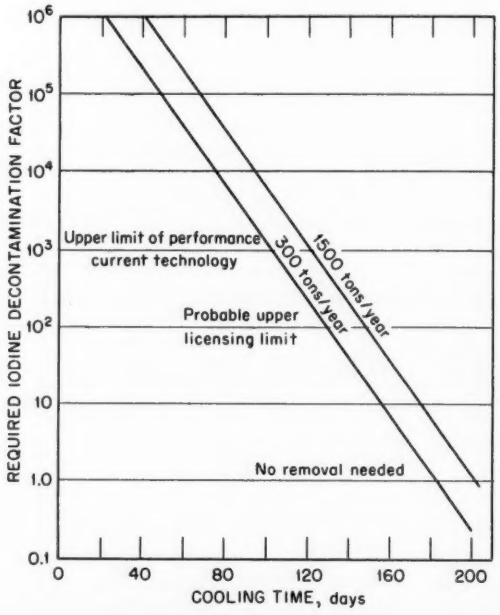

Fig. 1 Required ^{131}I decontamination factor as a function of plant size and cooling time.

	Additional cooling* time required, days	Added cost, $/kg
To make a 1500-metric ton plant equivalent to a 300-metric ton plant	18	0.24
To eliminate need for iodine-removal facilities in a 300-metric ton plant	32	0.43
To eliminate need for iodine-removal facilities in a 1500-metric ton plant	52	0.70

*Cooling beyond 150 days which, it is assumed, is the usual period provided for in reprocessing contracts.

Break-Even Capital Cost

Having determined the above costs, we can then estimate the break-even point on capital expenditures to remove iodine. In the discussion of larger plants presented by the authors in the previous issue of this journal,[1] the annual cost related to a dollar of capital expenditure was taken as:

Item	Annual cost, $/$ of capital
Operating cost	0.084
Cost of money	
70% equity at 16%	0.112
30% debt at 7%	0.021
Depreciation (straight line over 15 years)	0.067
Total	0.284

Then, if the annual cost of a dollar of capital investment is taken as $0.284, the maximum capital investment that can be made and still break even with the alternate of paying the penalty for additional cooling is as follows:

Item	300 metric ton/year plant	1500 metric ton/year plant
Metric tons of fuel processed	300	1500
Cooling penalty, $/kg	0.43	0.70
Annual cost of cooling, $	129,000	1,050,000
Break-even capital cost, $	455,000	3,700,000

This suggests that for a 300 metric ton/year plant it will quite likely be cheaper simply to cool the fuel the additional month, rather than to install iodine-removal facilities at all. For the larger plant, however, it would seem likely that the required facilities could be constructed for sufficiently less than $3,700,000 to permit a worthwhile savings. It does indicate, however, that there is a definite limit to the amount of capital that can be justified for the purpose of removing ^{131}I.

Effect of ^{129}I

Before it is possible to conclude that iodine is best handled, even for a small plant, by cooling alone, it is necessary to determine the effect of the long-lived ^{129}I. Using the same assumptions as before, the expected ^{129}I concentrations in the environs of the two plant sizes being considered are shown in Table 1.

Table 1 ^{129}I Concentration in Plant Environs

Plant size, metric tons/year	^{129}I conc.,* $\mu c/cm^3$	^{129}I MPC, $\mu c/cm^3$	Fraction of MPC
300	1.4×10^{-14}	2×10^{-11}	7×10^{-4}
1500	7×10^{-14}	2×10^{-11}	3.5×10^{-3}

*Assumes no removal of iodine and X/Q of 5×10^{-8} sec/m^3

It has been well established that the maximum permissible concentration (MPC) for ^{131}I should be reduced to allow for reconcentration in the environment through the milk cycle. Normally this effect can be approximated by using a factor of 1.4×10^{-3} applied to MPC. It is not at all established that a similar factor applies to ^{129}I. If it does not and only the limits of 10CFR20 apply, ^{129}I may be neglected. If it does, it can be seen from Table 1 that the ^{129}I release from a 300 metric ton/year plant would not be controlling. For the larger plant the effect of ^{129}I would be about twice that of ^{131}I, if the latter were handled by decay rather than removal. Since economics seem to dictate that iodine-removal facilities be used in the larger plant, the ^{129}I problem will be taken care of by removal in that plant. The conclusion is still valid, however, that, for the smaller plant, simple cooling can be considered for handling iodine.

Iodine-Removal Technology

Shortly after the startup in 1945 of the first chemical reprocessing plant, the Bismuth Phosphate Plant at Hanford, ^{131}I was identified on samples of vegetation collected near the plant site. The initial response to this information was to increase the cooling time of the fuel, even though this action temporarily delayed plutonium production at a crucial time in the war. In addition, meteorological controls were placed upon the dissolving operation.[5]

The discovery of iodine in the plant environs led to the rapid development of a method of iodine removal—the silver reactor. Since that time no reprocessing plant has operated without some means of iodine removal. And, although there have been almost 25 years of operating experience, particularly on silver

reactors, the open literature contains surprisingly little definitive operating information, particularly on the shortcomings of the methods, which are privately admitted to be many. This is in remarkable contrast to the plethora of references over the past 10 years to the removal of iodine from reactor-containment-shell atmospheres. It would seem highly desirable for the operating contractors of Savannah River and Hanford to put out detailed and critical evaluations of their operating experience into the open literature.

Operating Experience

Qualitative information is available on the removal of iodine at Hanford and Savannah River. The systems used at the two sites are basically the same. At the Hanford Purex Plant, the equipment sequence consists of:[6]

1. Downdraft condenser.
2. Ammonia scrubber tower (during declad step).
3. Heater.
4. Silver reactor.
5. Filter.
6. Filter.
7. Two nitric acid scrubbers (16 bubble-cap trays).
8. Steam jet.
9. Stack.

Generally about 80% of the iodine in the dissolver is volatilized into the dissolver off-gas system. However, 80% of the iodine released from the stack has been traced to the vessel off-gas system. It is evident that the silver reactors used in the vessel off-gas system do not work well, if at all. This is believed to be due to the fact that they are operated at too low a temperature.

Older literature[5] suggests that the decontamination factors which can be obtained from silver reactors vary from 100 to 1000. It is understood that these levels are not always obtained in practice.

At the Idaho Chemical Processing Plant, short-cooled fuels have been processed to produce barium. Up to 2.5×10^4 curies of ^{131}I have been present in a dissolving unit. The equipment sequence consisted of:

1. Condenser.
2. $Hg(NO_3)_2$–HNO_3 scrubber.
3. Charcoal bed.
4. Micrometallic filters.

The overall decontamination factor measured at the stack was 3×10^4. The efficiency of the mercury scrubber was not measured, but the charcoal bed and filter showed an overall decontamination factor of about 40. The charcoal bed removed 99.99% of the gaseous iodine but only 88% of the particulate iodine. A caustic scrubber, used initially, removed 90% of the iodine, increasing to about 97% when 0.1*M* thiosulfate was added to the caustic.[7-9]

The technology available for the removal of iodine from process gas streams falls into the following categories:

1. Scrubbing.
2. Silver reactors.
3. Adsorbents.
4. Volatilization suppressants.
5. Combinations of the above.

In following sections the chemistry of iodine in these systems is reviewed, together with the present status of each of the technological systems available.

Iodine Chemistry

As indicated above, most of the literature on iodine removal from gas streams relates to the removal from reactor-containment-shell atmospheres. However, some of this work may be applicable to reprocessing applications. Generally three species of volatile iodine have been identified: an elemental form, a reaction product between iodine and an organic material usually thought to be methane, and a species that appears to be iodine adsorbed on very fine particulate matter.[10] Since in all reprocessing applications the off-gas is filtered through absolute filters before discharge, it can be expected that the species associated with particles will be removed adequately. Therefore the elemental and organic species are of the more interest.

Elemental iodine is formed directly by heating fuels or during dissolution into nitric acid. Nitrous acid converts iodides or iodates into elemental iodine. Iodates form from oxidation of I_2 by nitric acid; iodides are formed by reactions of I_2 with reductants such as uranium metal. Organic iodides form when organic vapors contact iodine; they are also formed from radiolysis of organic materials in the presence of iodine. Methyl iodide has received the most study (again mostly in reactor-containment atmospheres), but many other organic compounds are also formed. In one study[11] fuel-processing-plant off-gas was fractionated by gas chromatography and measured by gamma-ray spectroscopy. A complex mixture of organic iodides with a boiling-point range of 40 to 255°C was found. The lower boiling compounds were identified as methyl, ethyl, *n*-propyl, and *n*-butyl iodides. The methyl and *n*-butyl iodide and the materials in the boiling-point range of pentyl through heptyl iodide

contained approximately 70% of the observed alkyl iodides. The organic components can be derived from impurities in or on the fuel, solvents and solvent degradation products, impurities in the air, etc.

Solubility and vapor-pressure data for elemental iodine in water[12] are given in Table 2. Vapor–liquid distribution coefficients can be determined from these data if the assumption is made that the solution is always saturated. Such an assumption is valid for solubilities as low as these. These data suggest that, at low temperatures and a high mole ratio of scrub solution to gas flow, iodine can be scrubbed into water. If the temperature is raised to 50 to 70°C, the elemental iodine would be easily removed from the scrubbing water.

Table 2 Elemental-Iodine Properties

Temp., °C	Solubility in H_2O, mole fraction	Vapor pressure		Vapor–liquid distribution coefficient, Y/X
		mm Hg	Mole fraction in vapor	
0	1.11×10^{-5}	0.03	4.22×10^{-5}	3.81
20	1.99×10^{-5}	0.20	2.85×10^{-4}	14.3
50	5.35×10^{-5}	2.20	3.10×10^{-3}	58.0
70	8.0×10^{-5}	8.20	1.16×10^{-2}	145
87.8	1.1×10^{-4}	22.60	3.67×10^{-2}	335

Taking methyl and ethyl iodides as representative of organic iodine species, the vapor pressures of these two compounds, compared to that of I_2, are shown[13] in Table 3. It is evident from these data that it should be very difficult to remove methyl or ethyl iodides from an air stream by an aqueous scrubbing–volatility mechanism.

Table 3 Vapor Pressure of Organic Iodides

Temp., °C	Vapor pressure, mm Hg		
	I_2	CH_3I	C_2H_5I
0	0.03	137	42.5
20	0.20	335	110
50	2.20	700	370
70	8.20		710

Scrubbing

Scrubbing is a generally accepted unit operation for removing soluble components from a gas stream; it is a preferred primary treatment in fuel reprocessing where large amounts of nitrogen oxides and iodine must be retained. Eggleton[14] performed a theoretical study of partition coefficients which indicates that high scrubber efficiencies can be obtained by a proper control of variables. The effects of oxidizing and reducing agents are extremely important, particularly in dilute iodine solutions, and this may help explain some of the many anomalous values in the literature.

Caustic has always been a favorite scrubbing solution because of its high potential efficiency for retaining iodine and its suitability as a storage medium. Laboratory studies show that caustic removes I_2 and HI with decontamination factors[7,15] from 100 to 10^4. But caustic scrubbers are probably inefficient for removing organic iodides or small particles. This fact or low inlet iodine concentration may be the explanation for rather poor performance of large scrubbers at Idaho and Hanford.[16]

The use of caustic as a scrubbing solution for gas streams that contain large amounts of nitrogen oxides is limited by the rapid depletion of the caustic by the formation of nitrate salts. These salts also become a burden on the waste-storage system. Consequently the use of weak nitric acid as a scrubbing solution has considerable appeal. The Hanford Purex Plant uses two nitric acid scrubbers in series at the end of its gas-treatment train. A decontamination factor of 100 for the pair of scrubbers has been reported.[6]

Some years ago Stromatt[17] studied in some detail the use of 5 and 10% HNO_3 with and without the addition of $Hg(NO_3)_2$ as scrubbing solutions for iodine. Removal of iodine at concentrations to be expected in the plant was greater than 99.9% with either acid concentration and with or without the mercury addition. At high iodine concentrations there appeared to be some value to the mercury addition so long as the Hg molarity in the solution exceeded that

of the iodine. Greater than 99.9% removal of methyl iodide has also been demonstrated using $Hg(NO_3)_2$–HNO_3 as the scrubbing medium.

Silver Reactors

Silver reactors have been used routinely at Hanford and Savannah River for many years. The usual equipment consists of a heater to raise the gas temperature to about 200°C and a column containing a porous packing material impregnated with silver nitrate. The heated iodine combines chemically with the silver and is retained on the column. The column is sized to give a superficial velocity of about 1 ft/sec at a length-to-diameter ratio of 4. The most suitable packing is unglazed Berl saddles that have been immersed in 18 to 20*M* silver nitrate solution for 1 min, drained, and then baked at 105°C for 4 hr.[5]

The chemistry of the iodine-removal process is complex and not completely understood. The following reactions probably take place:

$$AgNO_3 + \tfrac{1}{2}I_2 = AgI + \tfrac{1}{2}O_2 + NO_2$$

$$AgNO_3 + \tfrac{1}{2}I_2 + O_2 = AgIO_3 + NO_2$$

$$AgIO_3 = AgI + \tfrac{3}{2}O_2$$

The reaction mechanisms have been studied in more detail by Lacksonen et al.,[18] who conclude that the net reaction is probably

$$6AgNO_3 + 3I_2 = 4AgI + 2AgIO_3 + 6NO_2$$

The equilibrium pressure of iodine increases as the square of the NO_2 pressure and directly with the O_2 pressure. High collection efficiency is favored by high temperatures, but the temperature must be kept below 200°C lest the silver nitrate melt and run off the packing. At temperatures below the condensation temperature for nitric acid vapors (110°C), essentially no iodine removal occurs.

It has been reported that such silver reactors have run for about a year with iodine removals of 99.99%, although the more generally expected figure[5] is 99.5%. However, recent qualitative observations suggest that the contribution of the silver reactor to the overall decontamination factor in the dissolver off-gas system may be only about 10, whereas that in the vessel off-gas system may be as low as unity (the silver nitrate is not working at all).[6]

When the efficiency of a unit begins to fall, it can be regenerated. The requirement for regeneration is brought about primarily by the temperature–chemical environment and the total iodine processed. The amount of ^{131}I has a negligible impact on life expectancy. Regeneration is done by cooling the reactor to 65°C and spraying the packing with 0.04 cu ft of 5*M* silver nitrate per cubic foot of packing. The bed is then heated to 105°C and baked for 4 hr. The unit is again cooled, sprayed, and baked for 6 hr at 110°C. A reactor may be regenerated about 10 times. Regeneration produces a liquid waste that must be stored. It is also reasonably expensive—a single regeneration treatment has been estimated to use about $2500 of silver nitrate.[19] The capital cost of a silver reactor has been reported to be about $50,000 (mid-1950's dollars).[20]

Solid Adsorbents

A variety of solid adsorbents can be used for the removal of iodine under some circumstances.

Charcoal and Impregnated Charcoal. The most exhaustively studied adsorbent for iodine is charcoal. The literature is replete with references to such work, nearly all of it directed at the removal of iodine from reactor-containment shells.[21-25] Decontamination factors up to 10^5 are obtainable with either plain or impregnated charcoal for elemental iodine. Water vapor, carbon dioxide, and organic compounds (other than organic iodides) do not markedly reduce the sorption capacity for elemental iodine. The sorption capacity of plain charcoal for organic iodides is poor, however.

Methyl iodide can be removed by factors of 10^3 to 10^4 by charcoals impregnated with KI–I_2 or triethylene amine.[24,26] However, acid vapors, organic vapors, and moisture seriously affect the efficiency of impregnated charcoal.

In either case the use of charcoal in a dissolver off-gas system is severely limited by the presence of nitrogen oxides. In an atmosphere containing more than 6 vol.% nitrogen oxides, charcoal bursts spontaneously into flame. At a concentration of 3 vol.% nitrogen oxides, charcoal heats up but does not burn.[19] Thus, in order to use charcoal as a removal agent in a dissolver system, it would first be necessary to remove the nitrogen oxides to levels well below 3 vol.%. Even if this were done, it would still be necessary to show that the oxide-removal system could not fail, since a failure at this point could lead to ignition of the charcoal bed with concomitant release of the stored iodine. In the opinion of these authors, this possibility probably precludes the use of charcoal for iodine removal, at least for the dissolver system.

Molecular Sieves. Molecular Sieves* (synthetic zeolites) are effective for the removal of iodine either in the elemental or organic state.[19] However, the Sieves also have a strong affinity for nitrogen oxides and even more for water vapor. Thus, in order for a bed of Molecular Sieves to remove iodine from dissolver off-gases, the bed must be large enough to remove the oxides of nitrogen and water vapor as well. This effectively precludes the use of the Sieves directly for iodine removal.

However, Maeck et al.[27] have shown that Molecular Sieves converted to the silver form will strongly adsorb both elemental iodine and organic iodine even from a steam–air mixture. This material can adsorb iodine up to 500°C and retain it to 1000°C. It is nonflammable. Retentions of greater than 99.98% have been measured for elemental iodine and methyl iodide for a variety of conditions varying from dry flows at room temperature and at 500°C to steam–air mixtures. Although this system has not been tested in production, it appears to have great promise for use in a reprocessing plant.

Other Sorbents. Alumina–bismuth metal mixtures and iodized zirconium oxides have been shown to have efficiencies greater than 99.99% for removing elemental iodine but not methyl iodides.[27] These materials may be cheaper than silver–zeolite.

Boron nitride has been tested as an adsorbent for iodine.[28] Generally more than 99% of the iodine can be adsorbed on boron nitride under a variety of conditions. Boron nitride has the advantage of being more specific toward iodine (in relation to rare gases) than charcoal. But its very high cost (500 times the cost of charcoal) makes it an unlikely candidate for use in processing plants.

Suppression of Iodine Volatilization

Another approach to reducing iodine emissions from a processing stack is to suppress the volatilization of the iodine from the process in the first place. In normal Purex processing, radioiodine is evolved during dissolution with HNO_3, clarification, subsequent solvent extraction, and waste evaporation. About 80% of the iodine is evolved from the dissolver and removed in a silver reactor. The remainder flows through into the rest of the process, from which some is evolved into the vessel vent system and discharged through the stack. This latter release can be largely suppressed by adding mercuric nitrate to the dissolver solution.[29] With 0.04*M* Hg^{2+} in the dissolver solution, the total iodine release was reduced 55-fold. A material balance indicated that the Hg–I complex remained in the organic solvent where it was slowly removed by solvent scrubbers and subsequently transferred to a seepage basin.

*Trademark, Linde Division, Union Carbide Corporation.

Conclusions

The following represent the conclusions of these reviewers:

1. For larger (5 metric ton/day) processing plants, it will be economical to install iodine-removal systems to permit processing at about 150 days cooling. For 1 metric ton/day plants, it may well be cheaper to handle the problem simply by cooling an additional month.

2. Processing short-cooled (30 to 60 days) fuel from fast reactors is going to require iodine-removal technology that does not exist today.

3. Several techniques are available today, and they can be expected to give iodine decontamination factors of about 100 in routine operation. This is adequate to permit operation of 5 metric ton/day plants on 150-day-cooled fuel. None is so clearly superior as to be the obvious choice for use in all cases.

4. The accumulated experiences of the processing plants on iodine removal should be recorded and documented for general use.

5. Some of the large amount of effort going into the study of removal of iodine from reactor-containment shells could profitably be redirected toward reprocessing-plant effluents. The latter are likely to introduce far more curies of iodine into the atmosphere than leakage from reactor-containment shells.

References

1. W. A. Rodger and S. L. Reese, The Impact of Large-Scale Plants on Fuel Reprocessing, *Reactor Fuel-Process. Technol.*, **12**(1): 27-40 (Winter 1968–1969).
2. P. M. Bryant, *Health Phys.*, **10**: 249-257 (1964).
3. Preliminary Safety Analysis Report, Barnwell Nuclear Fuel Plant, Allied Chemical Nuclear Products, Incorporated, Docket No. 50-332 (filed Nov. 6, 1968).
4. Safety Evaluation by the Division of Materials Licensing, United States Atomic Energy Commission, in the Matter of General Electric Company Midwest Fuel Recovery Plant, Grundy County, Ill., Docket No. 50-268, Oct. 6, 1967.
5. A. G. Blasewitz and W. C. Schmidt, Treatment of Radioactive Waste Gases, in *Proceedings of the Second United Nations International Conference on the Peaceful Uses of Atomic Energy, Geneva, 1958*, Vol. 18, p. 187, United Nations, New York, 1958.

6. R. Van der Cook, private communication, March 1969.
7. G. K. Cederberg and D. K. MacQueen, Containment of Iodine-131, Released by the RaLa Process, Oct. 30, 1961.
8. G. K. Cederberg and J. R. Bower, Minimizing Gaseous and Particulate Activity in Idaho Chemical Processing Plant Off-Gas, in Sixth AEC Air Cleaning Conference, USAEC Report TID-7593, pp. 9-17, October 1960.
9. D. M. Paige, P. N. Kelly, and E. S. Grimmett, Two Gas Cleaning Problems at the Idaho Chemical Processing Plant Site, in Fifth AEC Air Cleaning Conference, USAEC Report TID-7551, pp. 17-23, April 1958.
10. R. D. Ackley et al., Retention of Methyl Iodide by Charcoal Under Accident Conditions, in Nuclear Safety Program Semiannual Progress Report for the Period Ending December 31, 1965, USAEC Report ORNL-3915, pp. 61-80, 101-111, Oak Ridge National Laboratory, March 1966.
11. W. A. Haller, Organic ^{131}I Compounds Released from a Nuclear Fuel Chemical Processing Plant, in Annual Report for 1965 in the Physical Sciences, USAEC Report BNWL-235, p. 133, Battelle–Northwest, May 1966.
12. J. H. Perry (Ed.), *Chemical Engineers Handbook,* 3rd ed., pp. 151, 196, McGraw-Hill Book Company, Inc., New York, 1950.
13. C. D. Hodgman (Ed.), *Handbook of Chemistry and Physics,* 41st ed., pp. 2364, 2367, The Chemical Rubber Publishing Company, Cleveland, Ohio.
14. A. E. J. Eggleton, A Theoretical Examination of Iodine–Water Partition Coefficients, British Report AERE-R-4887, February 1967.
15. W. E. Browning, Jr., Removal of Radioactive Iodine, *Nucl. Safety.*, **1**(3): 41-45 (March 1960).
16. R. E. Tomlinson, private communication, March 1969.
17. R. W. Stromatt, Removal of Radioiodine from Purex Off-Gases with Nitric Acid and Nitric Acid–Mercuric Nitrate Solutions, USAEC Report HW-55735, Hanford Atomic Products Operation, Apr. 15, 1958.
18. J. W. Lacksonen, W. H. Kirby, and C. E. Dryden, Iodine Vapor–Silver Nitrate Reaction Mechanisms and Phase Equilibria, USAEC Report TID-16914, October 1962.
19. M. E. Weech and M. Ross, unpublished work, May 1967.
20. R. E. Tomlinson, *Release of Gases, Vapors, and Particles to the Atmosphere, Hearings on Radioactive Waste Disposal of the Joint Committee on Atomic Energy, 86th Congress of the United States,* Vol. I, p. 270, U. S. Government Printing Office, January 1959.
21. R. E. Adams and R. D. Ackley, Removal of Radioiodine from Gases, *Nucl. Safety*, 9(5): 373-382 (Sept.–Oct. 1968).
22. R. E. Adams, R. D. Ackley, and Z. Combs, Trapping of Radioactive Iodine and Methyl Iodide by Iodized Charcoals, in Nuclear Safety Program Annual Progress Report for the Period Ending December 31, 1967, USAEC Report ORNL-4228, pp. 99-114, Oak Ridge National Laboratory, April 1968.
23. R. E. Adams and R. D. Ackley, Removal of Elemental Radioiodine from Flowing Humid Air by Iodized Charcoals, USAEC Report ORNL-TM-2040, Oak Ridge National Laboratory, Nov. 2,1967.
24. R. E. Adams, R. D. Ackley, and R. P. Shields, Application of Impregnated Charcoals for Removing Radioiodine from Flowing Air at High Relative Humidity, IAEA Symposium on Operating and Developmental Experience in the Treatment of Airborne Radioactive Waste, Paper SM-110/37, New York, August 1968.
25. R. E. Adams, R. D. Ackley, and R. L. Bennett, Brief Investigation of Radioiodine Behavior in Off-Gas System of the TRU Facility, USAEC Report ORNL-TM-2369, Oak Ridge National Laboratory, Sept. 24, 1968.
26. D. A. Collins, L. R. Taylor, and R. Taylor, Development of Impregnated Charcoals for Trapping Methyl Iodide at High Humidity, British TRG-Report-1300, 1967.
27. W. J. Maeck, D. T. Pence, and J. H. Keller, A Highly Efficient Inorganic Adsorber for Airborne Iodine Species, USAEC Report IN-1224, Idaho Nuclear Corp., October 1968.
28. F. O. Cartan and L. L. Dickerson, Sorption of Krypton, Xenon, and Iodine on Boron Nitride, in Annual Report of Division Analytical Branch for 1965, USAEC Report IDO-14679, p. 37, Phillips Petroleum Co., June 1966.
29. S. R. Smith, Suppression of Radioiodine Releases from a Radiochemical Separations Plant, USAEC Report DP-MS-66-78, Savannah River Laboratory, Mar. 28, 1967.

Fuel Reprocessing–Commercial Experience

By L. A. Abrams*

Commercial reprocessing of spent fuel has been influenced by a number of factors, among them research and development sponsored by the U. S. Atomic Energy Commission (AEC) at national laboratories, the still limited market for commercial reprocessing services, known process dependability, and regulatory and safety considerations. These factors, in conjunction with increasing operating experience, will continue to influence the course of the U. S. reprocessing industry in the near future. Reprocessing technology developed abroad may assume a more significant role in the long term.

At the present time there is only one commercial reprocessing plant in operation in the United States, i.e., the plant at West Valley, N. Y., which is owned and operated by Nuclear Fuel Services, Inc. (NFS).

The process used at West Valley is the chop–leach solvent extraction process that resulted from work performed at Oak Ridge National Laboratory (ORNL). Although the chop–leach step had not been used in the Purex process or proved on a production scale with irradiated fuel, the potential saving in waste volume to be stored which would result from not dissolving the hulls was a sufficiently large incentive to accept the risk. Purex solvent extraction had been developed and was in current use at the AEC plutonium-production plants: Savannah River at Aiken, S. C., and Hanford at Richland, Wash. It is a dependable process backed up by years of experience. When the West Valley plant was designed in 1962 and 1963, the only available alternative to solvent extraction was the fluoride volatility process then under investigation at Argonne National Laboratory (ANL). This process, however, was in so early a stage of development as to exclude it from consideration at that time.

Since the market for commercial reprocessing was expected to be quite small when the plant started up in the spring of 1966, the plant was sized for only 225 metric tons of uranium per year with an ultimate capacity, after certain additions, of about 450 metric tons per year. A much smaller initial capacity would have taken care of the commercial load during the first 5 years of operation, but the cost for fuel reprocessing would have been extremely high since it is very sensitive to economies of scale in construction costs, operating costs, and plant capacity. To receive government approval of its proposed price for reprocessing, NFS adjusted the plant size so that the combination of commercial load plus a 5-year base load from the AEC would bring the cost of reprocessing down to a level acceptable to the AEC and the industry. It is not expected that the plant will be fully loaded until 1972. For this reason the plant was also designed to process both high- and low-enrichment fuels in order to increase plant utilization as much as possible in the early years of operation.

The plant site size of 3000 acres, its remote location, as well as controls over operations and effluent release, were largely determined by regulatory requirements.

The first commercial power-reactor fuel processing in the United States was accomplished in 1967. The history of the processing campaigns† and a description of the more significant problems encountered since

*NUS Corporation, Rockville, Md.

†Campaign—a processing run on a specific fuel including cleanout and turnaround of the plant in preparation for the next campaign.

startup in mid-1966 are presented below. Note that these operations were a pioneering effort in the field of commercial reprocessing of irradiated fuel, which is still in an embryonic stage. Equipment modifications for ease of maintenance, plant-design alterations, and resolution of both process and analytical problems on the basis of experience accumulated so far should serve to improve the NFS plant efficiency, particularly by reducing the required downtime for general repairs and maintenance.

Fuel-Assembly Description

Most feed material for commercial reprocessing plants is and will be in the form of low-enrichment (<5%) UO_2 spent-fuel assemblies from light-water reactors of both boiling-water-reactor (BWR) and pressurized-water-reactor (PWR) designs. The NFS reprocessing plant now in commercial operation, General Electric's projected Midwest Fuel Reprocessing Plant (MFRP), and the other plants now in the planning stage are all designed for low-enrichment UO_2. Although the NFS facility can process high-enrichment fuel, none of the plants are designed for the sodium-bonded, graphite-dispersion, or carbide fuels proposed for advanced converter reactors. For a better understanding of the complex handling, disassembly, and processing steps involved, typical fuels from the two major reactor types are described below.

BWR Fuel

A typical BWR fuel assembly consists of a fuel bundle and the channel that surrounds it. The fuel assemblies are arranged in the reactor core to approximate a right circular cylinder inside the core shroud and are supported by a fuel support piece and the top fuel guide. Each fuel bundle contains 49 fuel rods that are spaced and supported in a square (7 by 7) array by lower and upper tie plates. The lower tie plate has a nosepiece that fits into the fuel support piece and distributes coolant flow from the fuel support piece to the fuel rods. The upper tie plate has a handle for transferring the fuel bundle from one location to another. Both tie plates are fabricated from 304 stainless-steel castings.

Fuel rods consist of fuel pellets stacked in a Zircaloy-2 cladding tube that is evacuated, backfilled with helium, and sealed by welding Zircaloy end plugs in each end. The fuel-rod cladding thickness is adequate to withstand external reactor pressure without collapsing onto the enclosed pellets. Although most fission products are retained within the UO_2, a fraction of the gaseous products is released from the pellet and accumulates in a plenum at the top of the rod. Sufficient plenum volume is provided to prevent excessive internal pressure from these fission gases or other gases liberated over the design life of the fuel. A spring, or retainer, in the plenum space exerts downward pressure on the pellets.

The fuel consists of high-density ceramic uranium dioxide manufactured by compacting and sintering uranium dioxide powder into cylindrical pellets. The average density of the pellets in the core is approximately 95% of the theoretical density of UO_2.

The reusable fuel channel enclosing the fuel bundle is fabricated from Zircaloy-4 and makes a sliding seal fit on the lower tie-plate surface. It is attached to the upper tie plate by the channel fastener assembly. The fuel channel has a smooth surface with no protrusions.

A typical modern 800-Mw(e) BWR plant will have an initial reactor core loading of about 135 tons of UO_2 fuel contained in about 560 fuel assemblies. Approximately one-fifth of the core loading (22 metric tons of uranium) will be discharged each year as fuel for a reprocessing plant.

PWR Fuel

Typical PWR fuel assemblies are square in cross section, nominally 8.4 in. on a side, and have an overall height of 160.1 in.

The fuel rods in a fuel assembly are arranged in a square array with 15 rod locations per side and a nominal centerline-to-centerline pitch of 0.563 in. between rods. Of the total possible 225 rod locations per assembly, 20 are occupied by guide thimbles for the Rod Cluster Control (RCC) assemblies and 1 occupied by in-core instrumentation. The remaining 204 locations contain fuel rods. In addition, a fuel assembly incorporates a top nozzle, a bottom nozzle, and 7 grid assemblies.

The fuel rods consist of uranium dioxide ceramic pellets in Zircaloy-4 tubing that is plugged and seal welded at the ends to encapsulate the fuel. Sufficient void volume and clearances are provided within the rod to accommodate fission gases released from the fuel, differential thermal expansion between the cladding and the fuel, and fuel swelling. Shifting of the fuel within the cladding during handling or shipping prior to core loading is prevented by a helical compression spring that bears on the top of the fuel. About 200 fuel assemblies, placed in an array that can be thought of as a right cylinder, comprise the reactor core. A typical

modern 800-Mw(e) PWR plant will have an initial loading of about 100 tons of UO_2 fuel. Approximately one-third of the core loading (~13.5 metric tons of uranium) will be discharged each year as fuel for a reprocessing plant.

Process Description

Since the vast majority of the commercial power reactors that will be placed in operation during the next decade are expected to be thermal converters of dissolution of the fuel. The AEC plants completely dissolve the fuel and cladding, whereas at NFS the fuel rods are chopped to expose the spent fuel and then leached with nitric acid (chop–leach) to leave a residue of hulls. This modification reduces the quantity of liquid waste and thus waste-storage costs. Variations of the Purex solvent extraction process are planned for Allied Chemical's nuclear fuel plant at Barnwell, S. C., and Atlantic Richfield's reprocessing plant to be near Leeds, S. C. For a step-by-step diagram of the NFS chop–leach process, see Fig. 1. The product nitrate

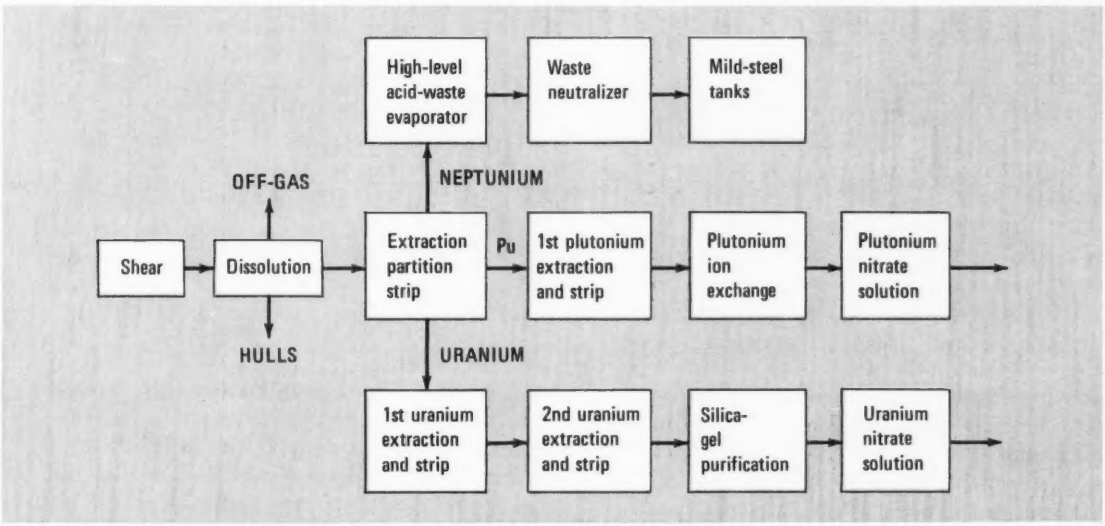

Fig. 1 Nuclear Fuel Services—process description.

either the PWR or BWR type, the fuel-reprocessing technology of interest is one capable of handling and processing fuel bundles or assemblies of fuel pins that are of low-enrichment UO_2 (or a UO_2–PuO_2 mixture) encased in Zircaloy or, in some instances, stainless-steel tubing. There are four processes; one of these is presently used on a commercial scale, and the other three are in various stages of development.

Solvent Extraction

The solvent extraction aqueous process has been used by the AEC for nearly 20 years. The Purex solvent extraction process uses kerosene-diluted tributyl phosphate as the organic solvent and nitric acid in aqueous solution as the salting agent for separation of fission products and partition of the uranium and plutonium ions. The NFS process differs only in the solutions are eventually purified by ion exchange (plutonium) or silica gel (uranium). The proposed Allied Chemical plant will differ from the NFS plant primarily in equipment design such as a larger shear, semicontinuous dissolvers, and criticality control by soluble poison instead of concentration adjustment. Allied Chemical also plans to use the new centrifugal mixer–settlers for extraction and partition instead of pulse columns as used by NFS. Figure 2 shows the proposed Allied Chemical process.

Aquafluor

The Aquafluor process is a proposed combination of the aqueous and fluoride-volatility processing schemes. The General Electric Company patented Aquafluor process, based on aqueous and fluoride-volatility processes developed by AEC, has not yet been

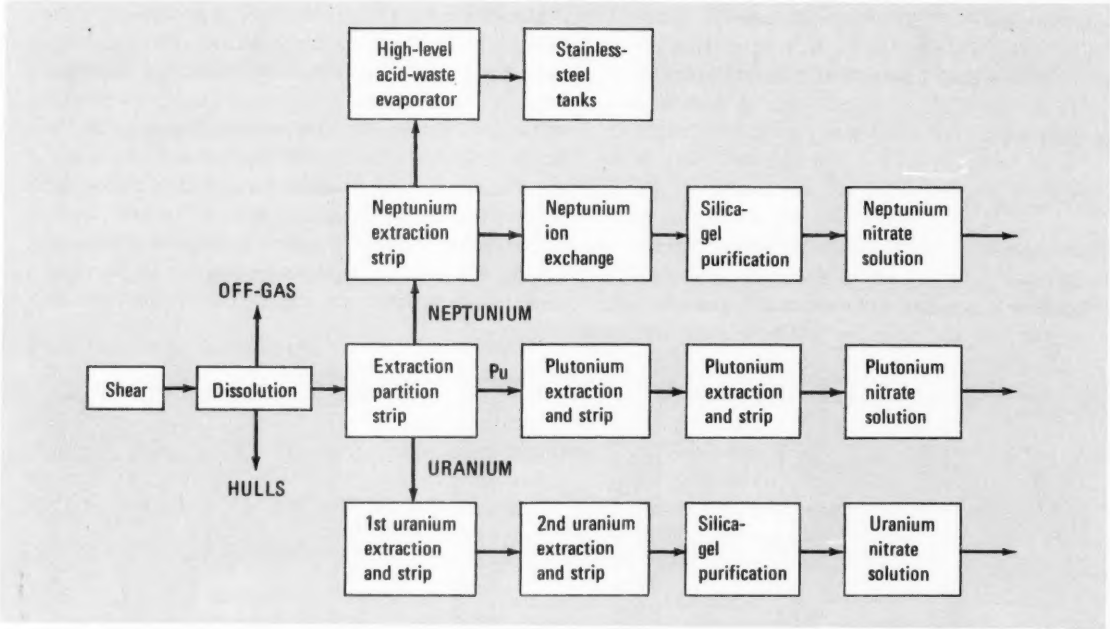

Fig. 2 Allied Chemical Corp.—proposed-process description.

applied commercially, although various steps have been tested. General Electric has announced its intention to use the process at its Midwest Fuel Recovery Plant at Morris, Ill. As now planned, the mechanical chop–leach technique will be followed by semicontinuous dissolution and single-cycle solvent extraction for primary fission-product removal. The uranium and plutonium streams will be concentrated and partitioned in a continuous ion-exchange unit and the resulting U–Np stream separated in a second continuous ion-exchange unit. The uranium product will be calcined and converted to UF_6 for final purification by distillation and absorption. The plutonium and neptunium products will be in the form of nitrate solutions. For a diagram of this process, see Fig. 3.

Fluoride Volatility and Pyrochemical Processes

Fluoride-volatility process development was initiated by ANL as an alternative to the aqueous process. Work on the process was carried out by ANL, ORNL, and the Oak Ridge Gaseous Diffusion Plant. However, because a number of problems could not be completely resolved in time to assure reliability for plants that would reprocess fuels for light-water reactors, work has been curtailed. The process is now under evaluation by ANL on fuels for fast breeder reactors only. The ANL workers have essentially discarded chemical decladding as originally planned and expect to utilize a mechanical head end such as chop–leach. At ANL they are also working on a pyrochemical extraction process, but this, too, is intended for reprocessing of fast reactor fuels.

Commercial Reprocessing Experience

The NFS plant was designed and constructed by Nuclear Fuel Services and its architect–engineer–contractor, Bechtel Corporation, on a site provided by New York State at West Valley, N. Y. Groundbreaking was in June 1963, and the provisional operating license was awarded by the AEC on Apr. 19, 1966. Initial startup of operation with irradiated fuel was on Apr. 20, 1966, and through 1968, 11 campaigns have been completed on fuel from the New Production Reactor (NPR) at Hanford–AEC, Dresden 1, Yankee–Rowe, and Consolidated Edison–Indian Point 1 core A. As of Dec. 31, 1968, a total of approximately 380 metric tons of uranium had been processed with a uranium loss of less than 1%. The quantity of material processed and the measured uranium loss are as follows:

Reactor	Amount processed, MTU*	U loss	
		MTU	%
NPR	279.4	2.73	0.98
Dresden	50.0	0.3	0.6
Yankee	49.8	0.34	0.68
Indian Point A†	0.616	0.003	0.49

*Metric tons of uranium.

†Partial total is 1.097 MTU, completed in 1969.

The processing history presented in Table 1 gives the dates on which each campaign was started and the shipping dates of the final product from each campaign. The total uranium processed from Apr. 20, 1966, to Oct. 13, 1968 (907 operating days) amounts to 379.2 metric tons of uranium. Using the NFS standard 1.333 conversion factor approved in AEC and utility contracts to account for normal maintenance and turnaround of the plant between campaigns, the overall plant operating efficiency is

$$\frac{(379.2 \times 1.333)}{907} \times 100 = 55.7\%$$

A shutdown is defined by NFS as any outage exceeding 24 hr. The plant underwent a total of 66 unplanned shutdowns in addition to scheduled downtime for maintenance. Since the NFS plant was a venture using both proved and new technology, as well as differences in scale and basic equipment design, startup and shakedown problems were to be expected. It is therefore not surprising that premature equipment replacement and extensive maintenance were more frequent and time consuming than had been anticipated. The following description of unplanned shutdowns will indicate the magnitude of the problems encountered in the early operations.

Campaign 2 had one special planned outage to install a cyclone separator in part of the system; however, equipment adjustment and maintenance caused partial shutdowns and slow processing. Campaign 3 was interrupted by 2 unplanned shutdowns. The first, due to an electrical failure, lasted 24 hr; the second took 56 days, beginning with a runaway acid truck rupturing a steam line in the utility room and followed the next day by the boilover of an evaporator that contaminated the acid-recovery system and required extensive repairs and decontamination. Campaign 4 on Dresden fuel was interrupted by 9 shut-

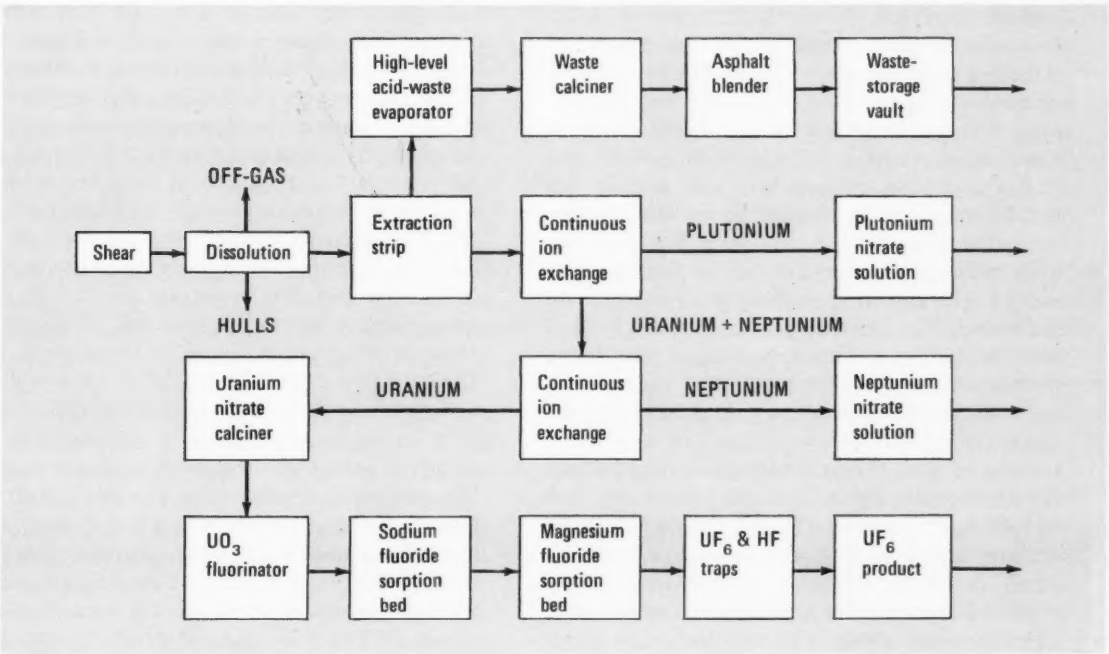

Fig. 3 General Electric's Midwest Fuel Reprocessing Plant—proposed-process description.

Table 1 NFS Processing History,[1] 1966 to 1968

Campaign	Fuel	MTU*	Revenue units	Starting date	Finishing date	Processing time, days†	% on-stream factor	Shut-downs	Days down
1	NPR	19.7	26.3	4/20/66	5/18/66	28	94	0	‡
2	NPR	28.8	38.4	5/18/66	7/6/66	50	77	1	1
3	NPR	46.6	62.1	7/11/66	11/14/66	126	49.3	2	57
4	Dresden	50.0	66.8	11/11/66	6/30/67	217	30.8	9	71
5	Yankee	49.8	66.5	6/6/67	10/16/67	133	50	23	‡
6	NPR	21.7	29.0	10/1/67	12/7/67	67	43.5	8	27
7	NPR	26.0	34.7	11/22/67	1/22/68	61	57	1	15
8	NPR	42.4	56.5	1/3/68	4/7/68	94	60	8	54
9	NPR	39.0	52.0	5/5/68	6/29/68	55	95	4	11
10	NPR	55.2	73.6	6/29/68	10/13/68	117	63	8	29
11	Indian Point A§	0.616		11/8/68					

*Metric tons of uranium.
†Includes overlap of mechanical and chemical processing time.
‡Not available.
§Partial figure.

downs totaling 71 days of downtime, of which 59 days were taken for major plant repairs. The other 12 days of downtime were for miscellaneous reasons such as a leak in a vapor line, pump failure, interference in the shear, and the necessity to rework acid-waste solutions. The Yankee campaign was interrupted by 23 unplanned shutdowns, 9 of which originated in the mechanical processing area and 14 in the chemical processing area. The delays were of short duration and included electrical repairs, equipment malfunctions, plugged lines, leaks, decontamination, and additional rework of recovered acid. The processing of NPR fuel in Campaign 6 was stopped by a new problem, i.e., fires in the general processing cell and the dissolver, due to ignition of the Zircaloy hulls. The fires were easily extinguished without damage to plant or equipment. The shear knife was redesigned to eliminate the fire hazard. The chemical processing area was down owing to lack of feed because of repair work in the mechanical area. On restart of the chemical cell, additional delays resulted from inoperative equipment, plugged lines, and a power failure. The time lost in Campaign 6 was 27 days. Campaign 7, chemical processing, and Campaign 8, mechanical processing, both of NPR fuel, were interrupted for 15 days by an AEC directive in January 1968 after an incident involving a highly publicized trespass of plant property during which samples had been taken of the low-level waste effluent before dilution by the Buttermilk Creek waters. Following investigation of this incident, the plant was restarted. Campaign 8 was in progress at shutdown, and, on resumption of processing, additional delays were caused by failure and subsequent repair of the crane in the mechanical cell and another shear-knife replacement. The chemical processing area was shut down 12 days owing to lack of feed while the shear repairs were in progress. The total time lost in Campaign 8 was 54 days. Campaign 9 encountered only relatively minor problems, such as plugged lines, jet-pump repairs, filter replacement, and malfunction of the acid-recovery system. Campaign 10 progressed reasonably smoothly, with plugged lines and one pump failure costing a total of 8 days, until a filter failure in the main ventilation system in early September released minor contamination to the plant roof. The AEC requested that the plant be shut down pending investigation of the cause and the consequences of the release. The plant was inoperative for 11 days. After resumption of processing, electrical failure of the off-gas blower shut the plant down for another 6 days. The last 4 days of the total of 29 days lost were due to a plugged decanter and loss of column control.

Plant startup on Campaign 11 was delayed by lack of AEC approval of the process for recovery of the high-enrichment uranium and plutonium from the Indian Point core A urania–thoria fuel. Table 1 shows that 616 kg were processed through the NFS plant between Nov. 8 and Dec. 31, 1968. This material was 93.2% ^{235}U prior to irradiation. The remaining 481 kg of the 1097 kg that comprised core A were processed early in 1969. Initial processing was slow, since this was the first highly enriched fuel processed at NFS,

and considerable preparation and checkout of the processing and waste-storage facilities were performed. Two major and several minor malfunctions caused some delay in processing. During the first dissolution a leak was discovered in one of the two dissolvers. The cause and location were determined, and the other dissolver was modified to prevent recurrence. The proposed design for the replacement dissolver is expected to eliminate this problem. The leaking dissolver will be replaced. Subsequently the high-enrichment-uranium evaporator-drain line was found to be partially plugged and required cleanout and modification. The modification of the evaporator drain, repair of a crane failure, and a plugged pump caused 11 days of shutdown during core A processing between Nov. 8 and Dec. 31, 1968. Campaign 11 was completed early in 1969 and was reported to have proceeded without major difficulties.

The Dresden 1 and Yankee fuels reprocessed by NFS were the first commercial power-reactor fuels to be processed in the United States. The records of NFS for these fuel-reprocessing campaigns show that low-exposure fuel (less than 17,000 Mwd/metric ton of uranium) can be reprocessed successfully without major difficulties. The records[2,3] show that performance improved from Dresden to Yankee as indicated by better product accountability and correspondingly smaller losses (see Tables 2 and 3). Although both campaigns ran into problems, it was possible to apply improvements made in the course of the Dresden work to the Yankee campaign.

From November 1966 to October 1967, NFS reprocessed 50 metric tons of uranium of Dresden 1 fuel and 50 metric tons of uranium of Yankee fuel. The Dresden fuel was reprocessed from November 1966 to June 1967, with frequent delays. Processing was completed about mid-May, but final shipment of uranium product took place on June 1, 1967, and of plutonium product on June 30, 1967. The Yankee fuel was reprocessed from June 1967 to the latter part of 1967. Product shipments were not completed until Oct. 16, 1967.

Tables 4 and 5 summarize the daily input and output from the NFS plant during the reprocessing of the Dresden and Yankee fuels. The input number actually represents the amount of uranium measured in the first dissolution steps. Note in the case of the Dresden campaign the extended period between February and April during which no Dresden fuel was reprocessed. These tables also show that the capacity of the fuel-dissolving system at NFS exceeds 2 metric tons of uranium per day for this type of fuel. A typical Dresden bundle contains 110 kg of uranium and a typical Yankee bundle 270 kg of uranium, as compared with current design weights for BWR's and PWR's of roughly 200 and 500 kg of uranium, respectively.

These data indicate that the mechanical and chemical head-end facility at NFS is now capable of handling a throughput of at least 2 metric tons of uranium per day. However, expansion of the chemical processing area of the plant to this capacity is required. This is a point worthy of note.

Tables 2 and 3 summarize the operation of the Dresden and Yankee campaigns showing the material balance, the precision limits for the material balance, the percent recovery, and a batch-by-batch data summary. These tables also show that losses in the Dresden campaign were greater than in the Yankee campaign, probably owing to (1) different analytical measuring techniques and (2) improvements in detailed processing methods carried over from the Dresden experience. For instance, NFS abandoned a technique for measuring uranium concentration during the Dresden campaign for it was giving questionable results.

To account for the quantities of special nuclear material contained in the fuels, NFS made physical and analytical measurements of the dissolved fuel solutions, recovered product solutions, and waste streams as required by its contract with AEC. The AEC verified these measurements by an on-site program of surveillance and independent analytical measurements to ensure equitable financial settlements between the Commission and NFS for the reprocessing service and between AEC and Commonwealth Edison and Yankee for the value of the uranium and plutonium contained in the fuels. The accountability techniques and analytical problems encountered during the Dresden and Yankee campaigns are described in detail in the literature.[2,3]

The estimated precision of the analytical methods at a 95% confidence level was determined on the basis of analysis of standard solutions (see Tables 6 and 7).

A major analytical problem encountered early in the Dresden campaign was the measurement of the plutonium concentration in input samples. The AEC and NFS were not able to obtain good agreement in measurements of supposedly duplicate samples. Repeat analyses likewise did not agree with the original results, and the plutonium : uranium ratios were about 5.20% lower than expected from reactor data calculations. It was found that, apparently, un-ionized plutonium was being formed on dilution of the samples and was not present in the process. Addition of a few drops of hydrofluoric acid to the sample resulted in plutonium

Table 2[2] NFS Campaign on Dresden 1 Fuel

	Uranium, g	Plutonium, g	$^{239}Pu + ^{241}Pu$, g	Value
Material balance				
Beginning inventory	9,081	356	325	
Input (I)	50,017,392	191,016	152,694	$3,940,279
Product (P)	49,567,256	183,089	146,153	3,853,150
Input–product difference	450,137	7,927	6,551	
Measured loss (ML)				
Hulls	56,159	183	153	
Liquid waste	199,717	5,465	4,361	
Total ML	255,876	5,648	4,514	57,509
Ending inventory	9,069	1,805	1,539	
Material unaccounted for (MUF)	194,272	830	813	
MUF = (beginning inventory + input)–(product + measured loss + ending inventory)				

	Uranium, %	Plutonium, %	$^{239}Pu + ^{241}Pu$, %	Value, %
Recovery (R) and loss (L)				
R = 100 P/I	99.1	99.8	95.7	97.8
L = 100 ML/I	0.51	2.96	2.96	1.46

Limits of error

The following are 95% precision limits for the campaign. The figures are plus or minus (±) quantities and represent upper and lower boundaries for the measurement errors.

	Uranium		Plutonium	
	g	%	g	%
Material balance				
Beginning inventory	407	4.49	23	6.46
Input	225,145	0.45	1,034	0.54
Product	159,126	0.32	504	0.28
Measured losses				
Hulls	12,074	21.5	40	21.7
Liquid waste	11,324	5.67	432	7.91
Total ML	16,554	7.44	434	7.52
Ending inventory	514	5.67	143	7.91
Materials unaccounted for	276,853		1,238	

	Uranium, g	^{235}U, g	Plutonium, g	$^{239}Pu + ^{241}Pu$, g
Special input measurements summary				
Batch 1	20,295,526	190,877	67,517	55,699
Batch 2	20,527,321	150,752	92,666	70,715
Batch 3	8,927,693	158,389	30,328	25,863
Batch 4	266,852	3,417	505	417
Total	50,017,392	503,435	191,016	152,694

Table 3[3] NFS Campaign on Yankee Fuel

	Uranium, kg	Plutonium, g	$^{239}Pu + ^{241}Pu$, g	Value
Material balance				
Beginning inventory	9	1,805	1,539	
Input (I)	49,759	285,067	246,498	$12,455,094
Product (P)	49,448	280,323	242,169	12,354,804
Input–product difference	311	4,744	4,329	
Measured loss (ML)				
Hulls	50	285	246	
Liquid waste	316	3,763	3,248	
Total ML	366	4,048	3,494	108,422
Ending inventory	17	164	139	
Material unaccounted for (MUF)	−63	2,335	2,235	
MUF = (beginning inventory + input)−(product + measured loss + ending inventory)				

	Uranium, %	Plutonium, %	$^{239}Pu + ^{241}Pu$, %	Value, %
Recovery (R) and loss (L)				
R = 100 P/I	99.4	98.3	98.2	99.2
L = 100 ML/I	0.74	1.42	1.42	0.87

Limits of error

The following are 95% precision limits for the campaign. The figures are plus or minus (±) quantities and represent upper and lower boundaries for the measurement errors.

	Uranium		Plutonium	
	kg	%	g	%
Material balance				
Beginning inventory	1	5.67	143	7.91
Input	143	0.29	1,339	0.47
Product	163	0.33	1,065	0.38
Measured losses				
Hulls	6	13.0	38	13.0
Liquid waste	17	5.6	268	7.5
Total ML	21	5.9	302	7.8
Ending inventory	2	9.9	22	10.2
Material unaccounted for	217		1,374	

	Uranium, kg	^{235}U, kg	Plutonium, g	$^{239}Pu + ^{241}Pu$, g
Special input measurements summary				
Batch 1	20,074	522.20	91,376	80,481
Batch 2	20,216	481.56	119,721	103,376
Batch 3	9,469	244.91	73,970	62,641
Total	49,759	1,248,67	285,067	246,498

Table 4 Dresden 1 Fuel Reprocessed by NFS

Uranium First-Dissolution Measured Inputs

Batch	Date	Quantity, MTU*	Batch	Date	Quantity, MTU*
1	11/24/66	1.4	24	2/7	1.0
2	12/9	2.0	25	2/10	1.0
3	12/15	1.0	26	4/9	1.9
4	12/16	1.0	27	4/16	2.0
5	12/18	1.0	28	4/20	1.0
6	12/20	2.0	29	4/21	1.0
7	12/24	2.0	30	4/26	2.0
8	12/25	1.0	31	4/28	1.9
9	12/29	1.0	32	4/30	1.0
10	12/30	1.0	33	5/2	1.1
11	1/2/67	2.0	34	5/4	1.0
12	1/11	1.0	35	Dissolver flush	
13	1/15	1.0	36	5/5	0.7
14	1/17	0.4	37	5/6	0.9
15	1/19	1.0	38	5/7	1.0
16	1/20	1.0	39	5/8	0.9
17	1/21	0.5	40	5/9	1.8
18	1/23	0.8	41	5/11	1.8
19	1/24	1.0	42	5/13	0.9
20	1/26	1.0	43	5/14	1.0
21	1/27	0.9	44	Dissolver flush	
22	1/29	1.0	Special	5/28	0.3
23	2/5/67	0.8			

Uranium-Product Shipments

Shipment	Date	Quantity, MTU
1	12/26/66	4.2
2	12/30	4.2
3	1/26/67	4.1
4	1/29	4.1
5	2/1	4.2
6	3/7	3.8
7	3/9	2.4
8	4/26	3.8
9	5/8	4.2
10	5/21	4.2
11	5/25	4.2
12	5/29	4.2
13	6/1	2.0

*Metric tons of uranium.

Table 5 Yankee Fuel Reprocessed by NFS

Uranium First-Dissolution Measured Inputs

Batch	Date	Quantity, MTU*	Batch	Date	Quantity, MTU*
1	6/13/67	2.2	23	7/27/67	1.6
2	6/19	2.2	24	7/29	1.5
3	6/21	1.1	25	7/31	1.7
4	6/23	1.1	26	8/2	1.5
5	6/24	1.1	27	8/3	1.7
6	6/25	1.1	28	8/5	1.6
7	6/27	0.7	29	8/7	1.1
8	7/6	1.2	30	8/9	1.1
9	7/9	1.1	31	8/10	1.1
10	7/10	1.1	32	8/13	1.1
11	7/11	1.1	33	8/14	0.9
12	7/13	1.1	34	8/15	0.9
13	7/14	1.1	35	8/16	0.9
14	7/15	1.7	36	8/17	0.9
15	7/16	1.6	37	8/19	0.9
16	7/18	0.9	38	8/20	0.9
17	7/20	1.6	39	8/20	0.9
18			40	8/23	0.9
19	7/23	1.6	41	8/23	0.9
20			42	8/25	0.9
21	7/24	1.7	43	8/26	0.6
22	7/26	1.5	44	9/7	0.01

Uranium-Product Shipments

Shipment	Date	Quantity, MTU
1	6/29/67	4.4
2	7/6	4.2
3	7/14	2.3
4	7/31	4.2
5	8/2	4.2
6	8/3	4.2
7	8/10	4.2
8	8/17	4.2
9	8/20	4.2
10	8/28	4.0
11	9/7	3.4
12	9/26	3.9
13	9/27	1.9

*Metric tons of uranium.

Table 6 Dresden Campaign

Analysis	Technique	Precision
Uranium concentration	Amperometric titration or isotope dilution–mass spectrograph	1.5%
Uranium isotopic content	Mass spectrograph	0.1% for ^{238}U
Plutonium concentration	Isotope dilution–mass spectrograph	1.0%
Plutonium isotopic content	Mass spectrograph	0.5%

concentrations that were in good agreement with reactor estimates. The addition of hydrofluoric acid was incorporated into the routine sample-preparation procedure.

Early Dresden input samples for uranium concentration that NFS analyzed by amperometric titration gave measurements 4 to 5% lower than AEC results. Acceptable agreement was obtained upon reanalysis by NFS. It was concluded that increased fission-product concentration in Dresden fuel as compared to NPR fuel was causing interferences, and the method was subsequently substituted by the isotope dilution–mass spectrograph technique that was used for later Dresden batches and for Yankee.

The analytical agreement between AEC and NFS measurements on Yankee fuel was good. Initial variations were resolved, and it was concluded by the AEC that both its own and NFS plutonium-concentration values were the best measurements that could be obtained and that the NFS plutonium concentrations, which would be used in official accountability calculations, contained no significant overall bias.

The sampling and analysis method of determining the uranium and plutonium remaining in the cladding (losses) had a major defect. Sample-size limitations in the laboratory made it impossible to obtain representative samples of the hull batches. Individual batch losses showed a wide range of variation from less than 0.1% to greater than 1% of the input. The samples with the larger losses contained a disproportionate number of end pieces with one end closed. The accumulated data on more than 150 batches showed that the uranium and plutonium losses were about 0.1% of the total input. AEC approved the adoption of 0.1% as a standard loss ratio and the elimination of the sampling and analysis of spent hulls. The spent hulls are now inspected and weighed, and the weight is compared with the theoretical weight to prevent gross loss in any individual batch. Variations exceeding the 5% margin allowed for scale accuracy were to be considered uranium. No hull batches during the latter part of the Yankee campaign were discovered to exceed the limit. The liquid-waste losses were also verified by the AEC but in less detail than the input and product measurements. Standard analytical methods were used for waste samples, and these are, by their very nature, not precise for the present purpose. An individual measurement can be as poor as ±100%, depending on the composition and concentration of the sample. The NFS quality-control data indicate a precision of normally about ±30%. The AEC measurements on about 20 typical samples prior to the start of the campaign were in agreement within ±50%, which was considered reasonable.

Table 7 Yankee Campaign

Analysis	Technique	Precision
Uranium concentration	Isotopic dilution–mass spectrograph	0.7%
Uranium isotopic content	Mass spectrograph	0.2% for ^{235}U
Plutonium concentration	Isotopic dilution–mass spectrograph	1.1%
Plutonium isotopic content	Mass spectrograph	0.1% for ^{239}Pu

Although the accountability measurements made at NFS are official for all AEC–NFS accountability and financial settlements, measurements were also made by the receiver at Richland, Wash., to assure the receiver that the previous measurements were reasonable.

Each bottle of plutonium product solution was weighed as received. This provided the receiver with a gross weight of bottle and solution from which the shipper's empty bottle weight was subtracted to obtain the solution weight. Solution weights obtained in this manner for containers of both Dresden and Yankee plutonium were on the average lower than those obtained by the shipper by about 50 g, or 0.4%. This weight loss can probably be attributed to evaporation and radiolytic decomposition of solution through the vent slit in the cap of the plastic bottle.

The contents of at least one bottle from each shipper's tankful of product solution were sampled and analyzed by the receiver. The data indicate that solution weight losses were offset by increases in concentration. However, no detailed bottle-by-bottle accountability comparison is possible because not all bottles are analyzed by the receiver.

The overall product accountability accuracy for both plutonium and uranium is shown in Table 8.

In summary, the experience gained at NFS since startup, and especially during the Dresden and Yankee fuel campaigns, shows that problems can be expected even in a plant that is designed to minimize risk by utilizing existing technology. The pioneering effort in fuel reprocessing has proved to be a technical success. Simplicity both of equipment and process appears to be mandatory to assure accessibility for maintenance and repairs and to minimize downtime for better plant utilization.

Table 8 Product Accountability (95% Confidence Level)

	Precision, %	
	Dresden	Yankee
Uranium concentration	0.2	0.7
Density	0.1	0.1
Plutonium concentration	0.7	0.7
Density	0.2	0.2
Shipping weight	±0.2	±0.2

Estimated Cost Analysis

The actual cost of owning and operating the NFS West Valley plant has not been made public owing to the potential competition in the reprocessing industry in the near future. Cost analysis is made difficult by the scarcity, occasional inconsistency, and relative lateness of the cost data that have been released. The total capitalization of NFS–West Valley of $33 million[4] included the waste-storage facilities built by New York State. Disclosures[5] made in February 1966 give the cost breakdown as follows:

Facility costs		$26,073,000
Construction	$24,011,000	
NFS provided	2,062,000	
Plant site (ASDA)*		500,000
NFS field engineering and interest		1,135,000
Working capital		1,260,000
Preoperating cost (to 3/31/66)		3,401,000
Contingency		131,000
	Total	$32,500,000

*New York State Atomic and Space Development Authority.

The total cost of owning and operating the plant comprises annual fixed charges for capital recovery; fixed operating expenses such as salaries, overhead, insurance, and taxes; and variable operating expenses such as materials, supplies, and utility services.

The following estimate of annual labor costs was taken from a report[6] that dates back to 1962. The present validity of this figure is generally confirmed by the NFS price-escalation terms for labor, which are on the basis of 17.5% of total cost.

Annual labor expenses	
Direct operating	$ 335,000
Maintenance	172,000
Analytical	215,000
Health and safety	81,000
Subtotal	803,000
Labor overhead	390,000
Total	$1,193,000

The approximate capitalization[7] was developed using a capital-recovery period on the bank debt of 10 years at 5½% interest and the annual-lease charge to New York State of $660,000. The amount for annual lease plus debt service and retirement is $2,451,000. The annual return on equity is in addition to this. The total annual fixed expenses of $4,144,000 include taxes, etc., plus salaries. The variable cost of operating has never been revealed. A representative cost can be obtained by using the logic applied to a check on the labor costs. The NFS escalation based on commodities is 20.3% of the per diem charge, i.e., those materials which must be replaced to make up for consumption or destruction. This suggests a value of $4800 per day to which must be added $1400 per day for waste storage and perpetual care. Thus a total variable cost of $6200 per day is considered reasonable in the absence of documented information. Table 9 presents a summary of the costs and the calculated unit costs ($/kg U) of the plant as a function of revenue days. The break-even point is about 175 metric tons of uranium per year (235 days) at the present charge of $31.33 per kilogram, excluding escalation.

From evaluation of available data, it can be concluded that the NFS plant operation will not yield a normal chemical-industry return on equity until such time as the potential load increases to permit expansion of plant capacity to a level approaching 500 metric tons of uranium per year at current unit reprocessing costs.

Table 9 Total Annual Cost Summary

		Annual payment
Capitalization		
New York State lease	$ 8,500,000	$ 660,000
Bank loan @ 5½%	13,500,000	1,791,000
Equity financing	8,500,000	
	$30,500,000	$2,451,000
ESADA grant	2,000,000	
	$32,500,000	
Fixed charges		
Annual payment		$2,451,000
Annual taxes, insurance, miscellaneous		500,000
Annual labor expenses		1,193,000
		$4,144,000

Variable costs = $6200/day

	200 operating days	250 operating days	300 operating days	350 operating days
Revenue, 10^6 $	4.700	5.875	7.050	7.490
Fixed charges, 10^6 $	4.144	4.144	4.144	4.144
Variable charges, 10^6 $	1.240	1.550	1.860	2.170
Total	5.384	5.694	6.004	6.314
Cost, $/kg U	$35.80	$30.29	$26.62	$23.99

References

1. NFS Quarterly Reports, AEC Public Document Room.
2. Savannah River Operations Office, Reprocessing of Dresden Reactor Fuel at Nuclear Fuel Services, Inc., West Valley Facility, USAEC Report SRO-123, Oct. 14, 1968.
3. Savannah River Operations Office, Reprocessing of Yankee Reactor Fuel at Nuclear Fuel Services, Inc., West Valley Facility, USAEC Report SRO-124, Oct. 21, 1968.
4. Remarks by T. C. Runion, President, NFS, during Conference on Nuclear Power Fuel Processing, Augusta, Ga., May 11–12, 1967.
5. NFS License Application to USAEC, Docket No. 50-201.
6. T. C. Runion, NFS Chemical Reprocessing Plant Capability and Cost Basis, May 2, 1962.
7. Hearing Before the Joint Committee on Atomic Energy, Congress of the United States, First Session on Chemical Reprocessing Plant, May 14, 1963.

In-Core Instrumentation for Power Reactors

By L. E. Phillips*

The design evolvement of commercial water-cooled power-generating reactors has been characterized by an increase in core size and power density for improved station economics. The larger core size has increased the complexity of monitoring the neutron-flux distribution and related local thermal-hydraulic conditions under the multitude of possible operating conditions, i.e., under the possible operating combinations of reactor power level, coolant flow rate, control-rod configuration, transient poison inventories and distribution, and fuel isotopic compositions relative to various local burnup conditions and in-core management configurations.

Operation at higher power density tends to reduce the margin between normal operating conditions and the operating limits imposed to protect against fuel damage and possible consequences relative to design accident considerations. Thus the importance of accurate interpretation of core monitor data to ensure that operating limits are not exceeded at any point in the core has increased.

Since it is not practical or even possible to monitor all pertinent operating variables at every point in a reactor core, some combination of measured data and analytical procedures is required to evaluate local conditions throughout the core. The analytical procedures are based on precalculated factors that, when applied to the measured data, will yield the quantity of interest, e.g., maximum heat flux at a particular location and maximum linear heat rate.

As a minimum, in-core measurements are required to permit evaluation and assessment of the predicted core-design parameters to assure that operation is within the technical constraints. In this case the procedure is to define limits on out-of-core measured parameters to assure that the entire core is within operating limits. However, before plant safety functions based on out-of-core measurements can be considered adequate, we must be sure that any unsafe condition which could occur within the core will not go undetected by the safety-system instrumentation. The present trend in large water-cooled-reactor designs is toward greater reliance on in-core instrumentation for plant safety and control functions and/or as an aid in core analysis and in-core fuel management.

The objective of this article is to review the recent developments and experience with in-core instrumentation and to relate the current design practice with respect to in-core instrumentation by the leading water-reactor vendors in the United States.†

Nuclear Instrumentation for Power Reactors

By way of background, it is desirable to review briefly the operation of neutron sensors in reactors. The power level of nuclear reactors can be monitored by radiation detectors. Radiation detectors are electronic devices that respond to neutron radiation or gamma radiation by the passage of current between electrodes. The current is proportional to the intensity of the neutron or gamma flux which, in turn, is proportional to the power generation.

Low levels of neutron flux (source range) are measured by pulse-type instruments known as count-

*Nuclear Associates International Corporation.

†This article updates two previous articles on this subject, the first in Vol. 4, No. 4, and the second in Vol. 9, No. 1, of *Power Reactor Technology*.

ers. Counters detect each radiation particle in a sensing chamber by its ionizing action on the chamber fill gas. This produces a current pulse that is fed into an amplifier and registered on a log level meter. The rate of change of the signal is also computed to monitor the reactor period. The number of counts is proportional to the number of incident neutrons provided the undesired pulses due to gamma photons are biased out. The thermal-neutron-sensing material in counters can be either uranium or boron that will emit charged fission fragments and alpha particles, respectively, when absorbing neutrons. The uranium is usually coated on the electrode, and the boron can be either in the form of boron trifluoride gas or a boron coating on the electrode.

For higher levels of neutron flux (intermediate range and power range), uranium- or boron-coated ionization chambers are used. The ionizing action of a number of particles is either averaged or totaled (integration) and read out of the system as a continuous (d-c) current. In the power range the current due to gamma photons is a small fraction of the total and can be neglected. In the intermediate range a compensated ionization chamber should be used. This instrument has two similar volumes, one sensitive to neutron and gamma flux and the second sensitive to gamma flux only. The output signals are combined so that the current due to gamma flux is canceled out. The lower range of the instrument can be further extended by using a guard-ring construction. Leakage currents through the insulators due to applied voltage will thus be grounded to prevent their contribution to the signal-circuit output. Reactor period is normally monitored in the intermediate power range ($\sim 10^{-5}$ to 10% of full power).

Gamma detectors are similar to neutron ionization chambers and produce a current that is proportional to the gamma dose rate at the detector.

The construction details and principles of operation of neutron detectors are presented by Harrer.[1]

The early reactors designed for commercial power generation are equipped with thermal-neutron detectors located circumferentially around the core and external to the reactor vessel. The thermal-neutron flux at the detector locations is calibrated in terms of total reactor power level. The output signal from these detectors is normally relayed to the reactor safety system, which initiates scram action to render the reactor subcritical in event of abnormal reactor power level or abnormal reactor period.

Since the neutron flux at out-of-core detector locations is sensitive to reactor operating conditions, the detectors must be periodically calibrated by a heat balance to reflect true core power. Sources of the error in the indicated power are the axial variation of power distribution due to changes in control-rod configurations, especially in peripheral elements and the possible variation of moderator density in the annular region between the core and the vessel.

In addition to the difficulties in monitoring total power and assuring that there is adequate margin between the operating parameters and the design limits, the possible error in the detector signal to the safety system could either result in premature scram or would necessitate reduced power density limits, depending on the error direction; these early out-of-core instruments provided no detail information on the local effects within the core.

Boiling-Water Reactors

To avoid the disadvantages cited above, designers of recent boiling-water reactors (BWR's) have incorporated a complete system of in-core monitors that provide continuous signals proportional to the neutron flux within the core for power-level monitoring and safety-system input. However, most of the early BWR's used out-of-core detectors, and a number of these were provided with in-core instrument thimbles that extend through the core at selected radial locations. Flux-monitoring instruments are periodically inserted into the thimbles to map the core power distribution. Information thus obtained is compared with calculated power distributions and used as an aid in in-core fuel management and core monitoring.[2,3]

An early method for flux mapping is based on driving a wire into and out of the core and measuring the induced activity with a scintillation counter. Flexible-cable systems are commercially available with appropriate drive units, cable-storage chambers, control devices, counters, and transfer mechanisms to provide remote positioning control and accurate response times. However, the flux-wire technique is cumbersome, and variations in core power distribution during the accumulation of flux-mapping data can complicate its interpretation.

General Electric Company developed a miniature fission chamber[1] suitable for in-core use in Dresden Unit 1. A mineral-insulated triaxial cable used with the chamber is sufficiently stiff to permit insertion of the chamber into the instrument guide tube. The center conductor is the signal lead, and the outer conductor acts as a guard to limit the leakage current for the cable high-voltage-to-signal lead. A substantial number of

miniature ionization chambers have now been designed, constructed, and tested by in-core service. Some characteristics of typical detectors that have been used as traversing in-core probes in power reactors are given in Table 1.

When the detectors in Table 1 are not in use for flux mapping or calibration of other instruments, they are retracted from the cores and stored in low-neutron-flux environments to prolong their lives. A detector remaining in the core of a typical water-cooled reactor operating at 85% plant factor would accumulate on the order of 10^{21} neutrons/cm^2 exposure in a single year. However, a traversing monitor in a General Electric BWR would receive about 14.5 years of normal use before accumulating an exposure[4] of 10^{19} neutrons/cm^2.

It is emphasized that the data of Table 1 represent detector characteristics as reported by the manufacturer. There appears to be no standardized method of reporting the detector lifetime, and caution should be exercised in comparing the detector models. In some cases, lifetime ratings may represent the limit of test experience. Also, the significance of a small loss in detector sensitivity is not clear. If a detector maintains linearity over its monitoring flux range and if the gamma and noise fraction of the signal output remains

Table 1 Characteristics of Typical Traversing In-Core Ion Chambers

	Model NA13*	Standard model for General Electric BWR's	Model WL-23238	Model RSN-216S-M3
Manufacturer	General Electric	General Electric	Westinghouse	Reuter-Stokes (Cleveland)
Reactor service	La Crosse BWR (Allis-Chalmers)	KRB (Germany) BWR; design model for Oyster Creek et al.	Connecticut Yankee PWR and Zorita (Spain) PWR	Connecticut Yankee PWR and Zorita PWR
Neutron-sensitive coating material	Fully enriched boron	^{235}U	^{235}U (90% enriched)	^{235}U (93% enriched)
Shell material	Commercially pure titanium	Titanium (wear surface of nitrided AISI 304 stainless steel)	AISI 304 stainless steel	AISI 304 stainless steel
Chamber diameter, in.	0.160	0.180	0.188	0.188
Cable diameter, in.			0.062	0.040
Chamber length, in.			2.10 ± 0.12	2.1 max.
Sensitive length, in.	0.5	1.0	1.0	1.0
Connector			Subminax plug, Amphenol 27-7	Amphenol 27-7
Cable-sheath material	AISI 304 stainless steel	Carbon steel	AISI 304 stainless steel	Inconel
Inner-electrode material	Titanium		Stainless steel	Inconel
Detector insulation	Forsterite		Alumina	Forsterite and Alumina
Cable insulation	Quartz and glass		Alumina	Alumina
Fill gas	Helium	Argon	Helium	Helium
Resistance, ohms	~2×10^{10} @ 70°F		5×10^{10} @ 100°F	>5×10^{12} @ 77°F
Rated temp., max.	850°F		650°F	700°F
Thermal-neutron-flux range, neutrons/(cm^2)(sec)	10^{12} to 10^{14}	1.4×10^{12} to 1.4×10^{14}	10^{11} to 10^{14}	10^{8} to 2×10^{14}
Lifetime, neutrons/cm^2	1.4×10^{19}†	>10^{19}‡	2.8×10^{20} §	3×10^{19} ¶
Operating voltage, volts d-c	100	100 to 200	50 to 150	20 to 100
Thermal-neutron sensitivity, amp/[neutrons/(cm^2)(sec)]	3.03×10^{-18} ± 20%	7×10^{-18} ± 20%	1.5×10^{-17}	2×10^{-17}
Gamma sensitivity, amp/(r/hr)	1.18×10^{-15}	2.5×10^{-14} ± 20%	2.0×10^{-14}	3×10^{-14}
Reference	ACNP-65544, pp. 8-35; AEC Docket 115-5	APED-5706, November 1968	Westinghouse Electronic Tube Division correspondence and descriptive literature	Reuter-Stokes correspondence and descriptive literature

*Indicated data are based on Allis-Chalmers specifications and calibration records.
†For accuracy between +0 and −5% of calibrated sensitivity.
‡Based on test data.
§Basis for lifetime rating not given.
¶Before 1% decrease in sensitivity.

within acceptable limits, there is no apparent reason why its use could not continue. The service application of the detector is also a factor in its useful life.

The reliability of a traversing in-core monitoring system is highly dependent on the total system design and the quality of all system components. The flexible-cable systems and positioning control devices, the design of mechanical and electrical junctions, and the electronic-signal conditioning and readout components are important considerations that are not fully reviewed within the scope of this article.

Previous discussion has indicated the disadvantages of out-of-core detectors for power-range monitoring of BWR's. The large downcomer water annuli associated with the present generation of BWR's also present formidable obstacles for source-range neutron detectors. In the smaller power reactors, an in-core source producing 3×10^4 neutrons/(cm^2)(sec) is attenuated to approximately 0.5 to 3.0 neutrons/(cm^2)(sec) at the out-of-core detector. The neutron-source attenuation to the detector has been projected to be about 10^{-9} for large BWR designs.[5] Consequently an extensive development program for an in-core startup system was conducted by General Electric Company under AEC contract. The system consists of high-temperature fission chambers employing the Campbell technique[5,6] for discrimination against gamma and leakage current[7] in the intermediate range [10^8 to 5×10^{13} neutrons/(cm^2)(sec)]. By this method the detector produces a significant number of pulses that overlap and accumulate to form a gross level which is proportional to the neutron flux. The mean square of the variance of the detector signal is used instead of the average values. This technique results in a much larger ratio of the neutron signal output to the gamma photon signal output.

The development program included tests to qualify the in-core counting detector, the in-core Campbelling detector, and the in-core transmission lines and to confirm the feasibility of the integrated system. Tests in General Electric Company's nuclear test reactor, called the General Electric Testing Reactor, and in Consumers Power Company's Big Rock Point Reactor have verified the sensitivity, static, and dynamic response of the Campbelling technique.

The source- and intermediate-range detectors have been tested to a total neutron exposure of 10^{19} neutrons/cm^2 in the Big Rock Point Reactor, and they continued to have satisfactory sensitivity. The source-range detectors have been operating in the KRB Reactor in Germany since its startup in March 1967.

The power-range detectors have been tested to greater than 10^{21} neutrons/cm^2, and they maintained adequate linearity. The chamber burnout with exposure was predictable. Some characteristics of the source-, intermediate-, and power-range detectors are presented[4] in Table 2.

Typical General Electric In-Core System

The typical in-core instrumentation for the General Electric BWR's consists of fixed in-core chambers for monitoring the source range, the intermediate range, and the power range and utilizes traversing-type ion chambers for calibration of the fixed chambers.

The source-range monitoring (SRM) system uses pulse-counting techniques coupled with logarithmic count-rate readout to monitor the neutron flux from the shutdown condition through criticality to a level of about 5×10^8 neutrons/(cm^2)(sec) ($\sim 10^{-3}$% of full power). The intermediate-range monitoring (IRM) subsystem overlaps the SRM system from about 10^8 neutrons/(cm^2)(sec) and extends into the power range to approximately 10^{13} neutrons/(cm^2)(sec) (>15% of full power). The SRM detectors and the IRM detectors are retracted from the core when their range is exceeded and are stored about 2 ft below the active core. The lower flux environment in that region prolongs the calendar life of the detectors. The detector drive system consists of a rack-and-pinion-type assembly that moves the detector axially within the instrument tube over a range from 2 ft below the core to 2 ft above the core center line.

The power range extends from about 10^{12} neutrons/(cm^2)(sec) (1% of full power) to approximately 2×10^{14} (150% of full power). It is monitored by several strings of four fission chambers axially distributed and with the strings distributed radially throughout the core. The output of the local power-range monitoring system (LPRM) is amplified and used in the rod-block monitoring (RBM) system and the average power-range monitoring (APRM) system. The RBM system automatically prevents control-rod withdrawal if the local flux in the region of the selected rod is too great. The output of a selected core-wide number of LPRM's is calibrated proportional to gross reactor power in the APRM and is displayed to the operator. In addition, the output of each LPRM is fed to an on-line computer for use in power distribution and local limit determinations as an operating aid and for longer term in-core fuel-management data logging.

Table 2 Characteristics of Typical In-Core Ion-Chamber Assemblies for General Electric Boiling-Water Reactors

	SRM* detector system	IRM† detector subsystem	LPRM‡ detector system
Reactor service	Big Rock; KRB (Germany) BWR; design model for Oyster Creek et al.	Big Rock	Big Rock; GETR
Electrode coating	U_3O_8 with >90% ^{235}U	U_3O_8 with >90% ^{235}U	U_3O_8 with >90% ^{235}U
Neutron sensitivity	5×10^{-4} to 2.5×10^{-3} cps/[neutrons/(cm^2)(sec)]	7×10^{-18} amp/[neutrons/(cm^2)(sec)] ±20%	2.15×10^{-17} amp/[neutrons/(cm^2)(sec)] ±20%
Gamma sensitivity	2.5×10^{7} r/hr (max. operating)	2.5×10^{-14} amp/(r/hr) ± 20%	2.0×10^{-14} amp/(r/hr) ± 30%
Neutron flux, max. storage	1×10^{10} neutrons/(cm^2)(sec)	1.5×10^{13} neutrons/(cm^2)(sec)	1.8×10^{14} neutrons/(cm^2)(sec)
Temp., max.	600°F	1000°F (detector)	600°F
Fill gas	Argon	Argon	Argon
Sensitive length	1.00 in.	1.00 in.	1.00 in.
Diameter	0.265 in. (max.)		0.23 in.
Case and collector material	Titanium	Titanium	Stainless steel
Collector-to-emitter insulator	Alumina	Alumina	Alumina
End seal	Titanium and Forsterite	Titanium and Forsterite	
Lifetime	10^{19} neutrons/cm^2	10^{19} neutrons/cm^2	3.8×10^{21} neutrons/cm^2

*Source-range monitoring.
†Intermediate-range monitoring.
‡Local power-range monitoring.

The nuclear instrumentation output signals are also used in the reactor safety system to provide period and power-level protection. A description of the arrangement of typical safety-system circuitry can be found in the PSAR for any 500-Mw(e) (or larger) General Electric BWR. The number of detectors employed in the system is determined in part by the safety-system redundancy requirements. Excess redundancy is incorporated to accommodate the bypass capabilities needed for channel test and calibration and to permit a reasonable degree of chamber failures without forcing a plant shutdown to maintain plant safety. A typical 500-Mw(e) plant will contain 4 SRM channels, 8 IRM channels, and about 30 strings of LPRM's.

The traversing in-core probe (TIP) system is used for calibration of the fixed LPRM's.[8] The system consists of fission chambers, cable runs, driving mechanisms to move the chambers, indexing mechanisms to select the position to be traversed, and control and readout equipment. Each TIP machine can service up to 10 instrument thimbles. A TIP guide tube is provided in each instrument tube that contains LPRM assemblies. The characteristics of TIP fission chambers are given in Table 1 (standard for GE BWR's).

Current Systems

All three leading PWR vendors now use out-of-core nuclear instrumentation that spans the length of the active core,[9-11] thereby minimizing any calibration error due to changes in axial flux distribution. Therefore some of the disadvantages previously discussed for the early out-of-core detectors do not apply to PWR's. However, there has been some concern about the ability of out-of-core detectors to respond to flux tilts in the large cores of the present-generation PWR's. Such a capability has taken on new importance since recent studies indicate that the large PWR cores may be prone to axial mode oscillations due to xenon instability.[12-14]

Westinghouse performed studies to evaluate the extent to which out-of-core neutron detectors can depict conditions within the core.[15] On the basis of data from Yankee (Rowe), Indian Point Unit 1 core A, and the CVTR facility, it was concluded that a divided ionization-chamber arrangement spanning the core height could adequately detect flux tilts. Combustion Engineering reached the same conclusion and presents the results of an analytical example to illustrate the capability.[16]

Part-length control rods have been proposed as one means to correct any xenon-induced axial mode oscillations should they occur.[12] In-core monitors will be used either to provide the basic data for this type of control or to supplement information available from the out-of-core detectors.

Pressurized-Water Reactors

The first three in-core instrumentation systems designed by Westinghouse (WAPD) employed flux-wire systems described earlier for in-core neutron monitoring (i.e., Yankee Rowe). For the San Onofre Nuclear Generating Station, the flux-wire method was replaced by an Aeroball flux-monitoring system.[17] The Aeroball system is operated by pneumatically moving a column of $\frac{1}{16}$-in.-diameter steel balls to the core for irradiation and to a scintillation detector for scanning. It is similar to the flux-wire system in that both measure neutron flux by the response of a scintillation detector to the gamma activity from ^{56}Mn, which is the activated product resulting from the core residence of ^{55}Mn. The Aeroball system theoretically offers advantages over flux wires in the speed and accuracy of measurements, since the aeroballs are irradiated simultaneously in all flux channels.

In August 1968, Southern California Edison submitted a license amendment asking permission to install ^{235}U fission chambers in San Onofre.[18] The stated purpose is to test 12 Westinghouse and General Electric models of miniature sealed fission chambers. The objective of the tests is to provide information for development of long-lived and accurate in-core flux monitors. Two models of self-powered detectors,[19,20] one with a cobalt emitter and the other with a rhodium emitter, are being tested at San Onofre.

Self-powered neutron detectors were developed by Atomic Energy of Canada Limited (AECL). AECL has been operating self-powered detectors at Chalk River since 1962 and first reported the data[20] in 1964. The self-powered detector consists of a coaxial cable with a section of the central conductor replaced by a material that emits energetic electrons when exposed to thermal neutrons. A typical detector construction is shown[21] in Fig. 1. The energetic electrons penetrate the solid insulation and come to rest on the collector or its surroundings. The deficiency of electrons in the emitter results in a positive charge on the central conductor of the coaxial cable. The rate of this positive-charge production can be continuously measured by a current meter that connects the central conductor to the outer sheath of the coaxial cable through a resistor. The sensitivity, response time, and burnout rate of the detector depend on the choice of emitter material. Some characteristics of commercially available detectors with various emitter materials are given[21] in Table 3. Since the sensitivity of these detectors is relatively low (compared to fission detectors), care must be exercised in the design of the detector and the signal-transmitting and -conditioning system to prevent unacceptable background levels. Relatively simple design techniques for reducing the background signal have been developed.[20,21]

Typical Westinghouse In-Core System

The typical in-core instrumentation system design for the current generation of Westinghouse PWR's consists of (1) Chromel–Alumel thermocouples that are positioned to measure fuel-assembly coolant-outlet temperature at preselected radial locations and (2) flux thimbles that run the length of selected fuel assem-

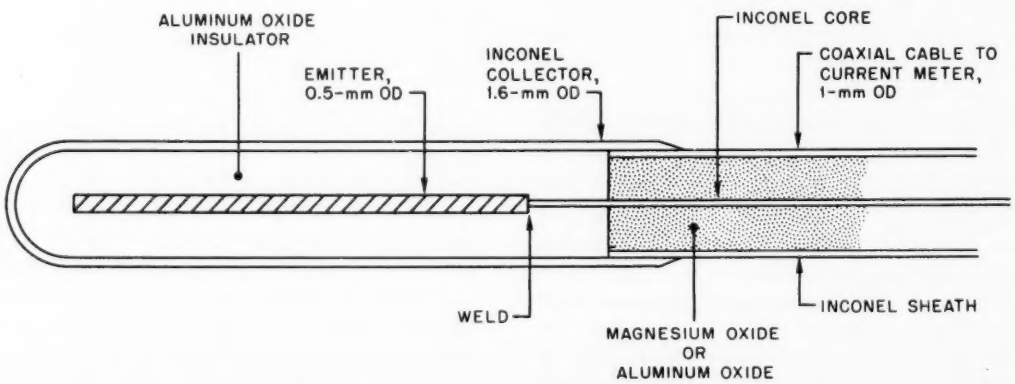

Fig. 1 Typical self-powered neutron-detector construction.

Table 3 Characteristics of Typical Emitter Materials

Material*	Neutron sensitivity, amp/[neutrons/(cm^2)(sec)(cm)]	Detection mechanism	Burnout	Burnout rate, 10^{13} neutrons/(cm^2)(sec)	Comments
^{103}Rh	1.2×10^{-21}	n,β	95 barns†	0.23%/month	Highest sensitivity
^{51}V, 0.040-in. OD	7.7×10^{-23} 4.7×10^{-23}	n,β	5 barns†	0.013%/month	1/v detector
Cadmium	1.6×10^{-22}	n,γ,e	500 barns‡	1.3%/month	480°F¶
^{59}Co	1.7×10^{-23}	n,γ,e	36 barns§	0.094%/month	Long life

*Values are for 0.020-in.-diameter emitter in $\frac{1}{16}$-in.-OD detector unless noted otherwise.
†Experimental results. Hilborn and Morin, to be published.
‡Estimate only. Experimental confirmation under way.
§Self-shielding ignored.
¶Several cadmium detectors with extended temperature range are under development.

blies.[11] For a 550-Mw(e) unit, it is estimated that there will be 39 in-core thermocouples, 4 movable flux monitors, and 36 flux thimbles. The in-core thermocouples in a PWR provide an indication of fuel-channel enthalpy rise that can be used in conjunction with the calculated flow distribution to determine channel power. The reference flux monitors are the Westinghouse model WL-23238 fission chamber described[19] in Table 1.

The stainless-steel-sheathed thermocouples are threaded into guide tubes that penetrate the reactor-vessel head and terminate at the exit-flow end of the fuel assemblies. The lower ends of the guide tubes are open to the coolant to achieve good thermocouple response. The flux thimbles are sealed at the leading end and are retractable from the core to avoid interference during maintenance or refueling.

The stated purpose of the Westinghouse in-core instrumentation system is to provide supplementary data to confirm the reactor-core-design parameters and calculated hot-channel factors. The out-of-core nuclear instrumentation is relied on to detect flux tilts and to provide the required outputs to the plant safety system.

Typical Combustion Engineering In-Core System

The typical in-core instrumentation for the current generation of Combustion Engineering PWR's consists of fixed in-core instrument assemblies that span the length of the active core through the center of fuel assemblies at preselected radial locations.[22] For an 800-Mw(e) plant, there will be 45 radial positions. Each instrument assembly contains one full-core-length vanadium self-powered neutron detector and four shorter rhodium detectors placed at selected axial locations. The vanadium detectors have lower sensitivity per unit length but longer life than the rhodium detectors. They are used to measure total channel flux and as a calibration check of rhodium detector burnout. Their useful life is expected to be about 3 years at full power.

The self-powered detector has been used in the Chalk River high-flux NRX and NRU Reactors and the Douglas Point Reactor at flux levels above and below those required for the design application. It has also been tested successfully in the Savannah River Plant production reactors. Detector reliability depends primarily on the integrity of the insulation in the coaxial cable. Insulation resistance will be checked periodically during operation. The instrument assemblies can be replaced during plant shutdown.

The stated function of the in-core instrumentation is to provide power-distribution data for evaluation of thermal margins and as an aid in in-core fuel management. The instruments have no automatic protective or control function in the plant operation.

Typical Babcock & Wilcox In-Core System

The typical in-core instrumentation for the current generation of Babcock & Wilcox PWR's consists of assemblies of self-powered neutron detectors located at 52 preselected radial positions within the core.[9] Each assembly consists of 6 local flux detectors and 1 background detector (for compensation) and is installed in the central instrumentation tube of its fuel assembly. The local detectors are positioned at 6 axial elevations spanning the core.

The readout for the in-core detectors is performed by the plant data logger/computer system. If the local flux values exceed predetermined limits, an alarm is initiated. The system incorporates on-line diagnostic routines that test the ability of the alarms to function.

The data-handling system generates a burnup correction factor to be applied to each detector signal before it is printed out. In addition, it computes and provides the core power-distribution pattern.

The self-powered neutron detectors used are of the type that have been proven in the NRX and NRU Reactors by AECL. In addition, they have been assembled and irradiated in The Babcock & Wilcox Co. comprehensive development program that was initiated in 1964. Results of test programs at the Babcock & Wilcox test reactor, the Babcock & Wilcox Lynchburg pool reactor, and the Big Rock Point Nuclear Station provided additional evidence that the self-powered detectors are satisfactory for the design application.

The stated purpose of the in-core instrumentation system is to provide power-distribution information and fuel-burnup data as an aid in in-core fuel management. The instruments have no automatic protective or control function in the plant operation. However, 9 of the 52 in-core monitors have been designated for xenon-instability detection.[12] The sensitivity of the detector system is said to be sufficient for relative local flux changes amounting to 2 to 3% of full-power values, which will be adequate for detection of xenon oscillations. If part-length rods are required to control xenon, the out-of-core information will provide the basic control information, and the in-core system will confirm it. However, the Safety Evaluation[12] by AEC's Division of Reactor Licensing (DRL) points out that a redundant readout system for the in-core system is available. Thus the in-core system appears to be approaching a control function even though none is claimed.

PWR In-Core Thermocouples

Although designers at Babcock & Wilcox do not include thermocouples in their standard in-core system, they indicate that their first large PWR will have in-core thermocouples[23] and will be used to measure the temperature difference across the fuel channels to confirm thermal-hydraulic calculations. The thermocouples are inserted at the 52 instrument locations, and the in-core junctions are located approximately 2 in. above the top of the fuel pins.

Similarly, Combustion Engineering has included thermocouples in its Palisades unit,[10] even though later reactors do not include in-core thermocouples. Two Inconel-sheathed Chromel–Alumel thermocouples are contained in each detector assembly. Their junctions are located at the fuel-assembly inlet and outlet.

As previously described, thermocouples are typically included in the Westinghouse in-core system.

The performance of thermocouples in a radiation environment has been the subject of considerable study. The decalibration effect due to gamma heating is small and predictable.[17] However, there are conflicting reports in the literature regarding neutron-radiation-produced decalibration effects. Leonard[24] attributes apparently conflicting experimental results[25-29] to the relative location of flux and temperature gradients as an important factor in experimental results. He concludes that in-pile thermocouple installations should be designed such that temperature gradients along the leads are restricted to locations outside high-flux regions. This will tend to minimize decalibration effects involving radiation-produced and self-annealing scattering centers occurring in the thermoelectric materials in the region of the temperature gradients.

Most practical experience with thermocouples in water-reactor environments has been satisfactory. Chromel–Alumel is the generally accepted couple. Experience with Inconel sheathing is somewhat superior to stainless steel, although either is satisfactory.

Other In-Core Instrument Technology

Initial applications of in-core instrumentation were oriented toward investigation of core operating characteristics in various reactor-development efforts. Heavily instrumented fuel assemblies were inserted into the cores of research reactors to determine limiting fuel and channel characteristics for use in core evaluation and core design. An extensive line of in-core instruments was developed for such an application in the 20-Mw Halden Boiling-Water (D_2O) Reactor (HBWR) at Halden, Norway.

The HBWR is particularly well suited for in-core instruments with the wide lattice spacing that is characteristic of D_2O reactors and with 200 penetrations of the reactor head which can accommodate up to 24 instrument leads from individual 7- or 5-rod-cluster fuel bundles. The in-core instrument experience reported[30,31] for that reactor is illustrative of the existing technology of in-core instruments available to study fuel and channel characteristics. The instrument applications included the following: turbine flowmeters, consisting of a turbine rotor supported in graphite bearings, were used at the channel inlet and outlet to determine flow rate and exit void fraction; tungsten/tungsten–rhenium thermocouples with magnesia insulation and molybdenum sheathing were in-

serted into fuel oxide pellets to evaluate central fuel temperature; Chromel–Alumel thermocouples were peened into a weld bead slot on the fuel-cladding surface for use in determining fuel time constants; an impedance void gauge was used to measure dynamic void fraction; gamma thermometers and self-powered neutron detectors were used to indicate channel power; special low-volume transducers, communicating with the fuel-rod gas space through a 1-mm tube, were used to monitor fission-gas pressure; and four types of burnout detectors were employed to detect critical heat-transfer conditions. The burnout-detector types were: a thermocouple mounted inside the fuel cladding in a special geometry section to detect overheating in that locality; a differential transformer that detects fuel-pin elongation due to fuel-cladding overheating; a resistance detector that measures the change in fuel-cladding resistance due to overheating; and a 0.5-mm coaxial cable mounted inside and along the length of the fuel rod to measure change in resistance of the alumina cable insulation under critical heat-transfer conditions.

Numerous other examples of special in-core instruments developed primarily as investigative tools are reported in the literature. The only instruments, not previously reviewed, of some interest for application to water-cooled power reactors are radiation monitors that maintain a nearly constant sensitivity during exposure. One such instrument is the self-powered gamma detector,[21] which is presently under development. Good results have been obtained using a lead emitter and an aluminum collector; a Zr–Ni combination has also been tested.

Regenerative in-core neutron-flux monitors[32-34] have also received considerable attention and are commercially available. They consist of a fertile–fissile isotope mixture of ^{234}U and ^{235}U. The ^{234}U isotopes transmute by thermal-neutron absorption to replace similar atoms lost due to burnout. Test characteristics[34] of these instruments have been very good, and the instruments are commercially available. However, the only source of ^{234}U is a diffusion plant. This raises some question concerning the continued availability of the isotope and the economic feasibility of the instrument.

Conclusions

The practical application of in-core instrumentation to commercial water-cooled power reactors is limited to in-core radiation detectors and thermocouples. In-core neutron detectors have completely displaced out-of-core detectors for application to large BWR's. They respond better to transient conditions and provide improved reactor protection and in-core fuel-management efficiency by a better knowledge of local power conditions and actual core power distribution.

In-core instrumentation is now used extensively in conjunction with out-of-core nuclear instrumentation for large PWR's. The power-distribution data that are continuously supplied by the in-core monitors are a valuable aid to formulate near-term operating decisions and longer-term fuel-management decisions for the reactor.

The gross quantity of continuous data generated by the in-core monitors of both BWR's and PWR's has made necessary the use of data logger/computers for efficient handling and processing of the data.

The computers used for this function are generally the on-line process-type computer that has the capability for rapid scanning of the data being measured. In the current power-reactor designs, one of the functions of the computer is to perform a check on the data to eliminate spurious signals. The valid data are then averaged over a short time interval and compared to preset operating alarm limits. In addition, on-line performance calculations of ranging degrees of complexity are performed to assist the plant operator with the evaluation of the large amount of data being obtained. The data and information derived from the calculations are printed out on a periodic log but can also be obtained on special request.

There are a variety of in-core radiation detectors now available. Ionization chambers provide better sensitivity and better response (important only for safety-system or plant-control applications) than the self-powered neutron detectors. However, the self-powered detectors offer advantages in simplicity and cost, and development is continuing to achieve detector systems with prompt response and still adequate sensitivity. The relative merits of ionization chambers and self-powered detectors with respect to reliability and lifetime are not clearly established.

The electronic design of the signal-transmission, -conditioning, and -readout equipment and the mechanical design for installation of the in-core system and for its mobility as required are important factors in the performance and lifetime of the in-core system. The integrity of the coaxial-cable insulation is known to be particularly important to detector reliability.

Because of the still limited experience with in-core monitors, it is probable that continued development effort will lead to power-monitoring systems with

improved performance characteristics and better economics. It seems probable that such a trend will lead to greater reliance on in-core instruments, including the assignment of plant control and safety functions in PWR's. Concurrently, it is probable that the data-handling system will be expanded to provide increased automation in the operation and control of nuclear reactor power plants.

References

1. J. M. Harrer, *Nuclear Reactor Control,* p. 179, D. Van Nostrand Company, Inc., Princeton, N. J., 1963.
2. J. R. Fisher, Method for Utilization of In-Core Flux Monitor Data with Application to LACBWR Monitors, *Trans. Amer. Nucl. Soc.,* **11**(2): 631-632 (November 1968).
3. R. J. McWhorter and G. R. Parkos, Nuclear Performance of Boiling-Water Reactors—An Evaluation of Reactor Operating Data and Reactor Calculations, in Nuclear Performance of Power-Reactor Cores, USAEC Report TID-7672, p. 71, September 1963.
4. W. R. Morgan, In-Core Neutron Monitoring System for General Electric Boiling-Water Reactors, Report APED-5706, General Electric Company, Atomic Power Equipment Department, November 1968.
5. R. A. DuBridge et al., Reactor Control Systems Based on Counting and Campbelling Techniques. Full-Range Instrumentation Development Program, USAEC Report GEAP-4900, General Electric Company, Atomic Power Equipment Department, July 1965.
6. N. Campbell, The Study of Discontinuous Phenomena, *Proc. Cambridge Phil. Soc.,* **15**: 117-136 (Oct. 28, 1908–June 6, 1910).
7. R. A. DuBridge, Application of In-Core Detectors to Startup of Large Boiling-Water Reactors, *Trans. Amer. Nucl. Soc.,* 8(1): (June 1965).
8. Philadelphia Electric Company, Preliminary Safety Analysis Report—Peach Bottom, AEC Docket 50-277, 1967.
9. Sacramento Municipal Utility District, Preliminary Safety Analysis Report—Rancho Seco, AEC Docket 50-312, 1967.
10. Consumers Power Company, Final Safety Analysis Report—Palisades, AEC Docket 50-255.
11. Wisconsin Public Service Corporation, Preliminary Safety Analysis Report—Kewaunee, AEC Docket 50-305, 1967.
12. Safety Evaluation by Division of Reactor Licensing, AEC, in the matter of Sacramento Municipal Utilities District, Rancho Seco Nuclear Generating Station, Unit 1, AEC Docket 50-312, pp. 12-14, Aug. 12, 1968.
13. Safety Evaluation by Division of Reactor Licensing, AEC, in the matter of Metropolitan Edison Company Three Mile Island Nuclear Station, Unit 1, AEC Docket 50-289, p. 52, Feb. 5, 1968.
14. P. S. Lacy and E. D. Kendrick, Neutron Transient Calculations in Large Light-Water Reactors, *Reactor Fuel-Process. Technol.,* **12**(1): 10-18 (Winter 1968–1969).
15. Consolidated Edison Company of New York, Inc., Preliminary Safety Analysis Report —Indian Point 2, Question 14 f, Supplement No. 1, AEC Docket 50-247, Apr. 1, 1966.
16. Consumers Power Company, Final Safety Analysis Report—Palisades, AEC Docket 50-255, pp. 3-29.
17. W. D. Leggett III, In-Core Instrumentation for the San Onofre Nuclear Generating Station, USAEC Report WCAP-3269-46, Westinghouse Electric Corp., Atomic Power Division, March 1965.
18. Southern California Edison Company, Final Safety Analysis Report—San Onofre, Amendment No. 16, AEC Docket 50-206, Aug. 30, 1968.
19. Personal communication, letter dated Mar. 13, 1969, and manufacturer's literature from Westinghouse Electronic Tube Division.
20. John W. Hilborn, Self-Powered Neutron Detectors for Flux Monitoring, *Nucleonics,* **22**(2): 69-74 (February 1964).
21. Manufacturer's descriptive brochure, Self-Powered Flux Detectors, Reuter-Stokes Canada Ltd. (Box 45, Preston, Ontario), Reuter-Stokes Electronic Components Inc. (Warrensville Heights, Ohio 44128).
22. Baltimore Gas & Electric Company, Preliminary Safety Analysis Report—Calvert Cliffs, AEC Docket 50-317, 1968.
23. Metropolitan Edison Company, Three Mile Island Nuclear Station, Unit 1, Question 16.1, Supplement No. 3, AEC Docket 50-289, Dec. 8, 1967.
24. J. H. Leonard, Conditions Contributing to Radiation-Induced Thermocouple Decalibration, *Nucl. Appl.,* **6**(3): 202 (March 1969).
25. James H. Leonard, Radiation-Induced Temporary Decalibration of Thermocouples, *Trans. Amer. Nucl. Soc.,* **11**(1): 340-341 (June 1968).
26. J. H. Leonard and D. E. Hunkar, Direct Radiation Effects on Thermocouples, *Nucl. Appl.,* **3**(12): 718 (1967).
27. Gary J. Dau and Ronald R. Bourassa, Results of Thermocouple Calibration in a Pulsed Reactor, *Trans. Amer. Nucl. Soc.,* **11**(1): 341-342 (June 1968).
28. Gary J. Dau, Photon Dependence of Thermocouple Calibration, *Trans. Amer. Nucl. Soc.,* **10**(2): 638-639 (November 1967).
29. Gary J. Dau, R. R. Bourassa, and S. C. Keeton, Nuclear Radiation Dose Rate Influence on Thermocouple Calibration, *Nucl. Appl.,* **5**(5): (November 1968).
30. H. Ager-Hanssen and R. D. Smith, Advanced In-Core Instrumentation from Halden, *Nucleonics,* **22**(4): 49-56 (April 1964).
31. J. A. Firing et al., In-Core Instrumentation, An Important Tool for Achieving High Specific Powers in Heavy-Water Reactors, in *Heavy-Water Power Reactors,* Symposium Proceedings, Vienna, 1967, pp. 865-881, International Atomic Energy Agency, Vienna, 1968 (STI/PUB/163).
32. Charles N. Jackson, Jr., Regenerative In-Core Thermal-Neutron Detector, *Trans. Amer. Nucl. Soc.,* **10**(1): 310-311 (June 1967).
33. W. L. Bunch, Technique of Optimizing the Composition of Regenerating Neutron-Flux Monitors, *Nucl. Appl.,* **1**(3): 259 (June 1965).
34. C. N. Jackson, Jr., Recent Advances in Regenerative In-Core Neutron Flux Monitors, *Trans. Amer. Nucl. Soc.,* **11**(1): 336 (June 1968).

Thermometry for Fast Breeder Reactors*

By R. L. Shepard†

Abstract: *The U. S. Atomic Energy Commission's (AEC) program for development of liquid-metal fast breeder reactors (LMFBR) will require sensors that can measure sodium coolant temperatures from 420 to 1100°C reliably for 1 year in a fast-neutron flux of 10^{16} neutrons/(cm^2)(sec). Mixed-oxide fuel-pin centerline temperatures of 2300 to 2750°C and fuel-pin cladding temperatures to 1100°C must be measured in fuel-development studies. Commercially available, sheathed, type K thermocouples are being evaluated to meet reliability requirements for routine coolant-temperature monitoring in LMFBR plants. High-temperature W–Re thermocouples are being developed for fuel-pin temperature measurement. New techniques and instruments are being studied as alternative means for overcoming some of the basic limitations of thermocouples and thus assuring accurate, safe, reliable, and economical instrumentation for the fast breeder reactor.*

The LMFBR Program

The Division of Reactor Development and Technology of the U. S. Atomic Energy Commission has established the development of a liquid-metal-cooled fast-neutron fuel-breeder reactor (LMFBR) as a national goal of highest priority. Large-scale commercial breeder reactors are expected to be operational by 1985 to provide the utility industry with 1000-Mw(e) stations that will regenerate additional fissile fuel on a 10-year cycle. The LMFBR demonstration plants are scheduled for operation in the late 1970's, and the Fast Flux Test Facility (FFTF) is scheduled for startup in 1974. This program will enable the industry to make maximum use of available ore supplies as raw materials for fabrication into nuclear fuel and, at the same time, to meet this country's projected energy requirements during the next 30 to 50 years. Intensive engineering development will be conducted during the next several years to meet the severe and stringent requirements of this advanced reactor concept and to assure a system that is safe, economical, and reliable.

The Reactor

The "1000-Mw(e) LMFBR Follow-On Study" presentations made at the International Conference on Sodium Technology and Large Fast Reactor Design, Nov. 7–9, 1968, at Argonne National Laboratory[1] describe a range of core designs that can be expected for the first generation of LMFBR plants. Part of the information presented at this conference is summarized in Table 1. On the basis of these studies, a typical LMFBR reactor core might contain 250 fuel subassemblies, each containing 190 individual ¼-in.-diameter stainless-steel-clad fuel pins. The fuel will be a mixture of 20% PuO_2 and 80% UO_2 or, alternatively, mixed UC–PuC. Heat generated in the fuel pins will be conducted through the 0.012-in.-thick cladding at a rate of about 800,000 Btu/(hr)(sq ft) and removed by liquid sodium flowing through the subassemblies at 30 ft/sec. The coolant temperature will rise 170°C, and the coolant will experience a pressure drop of about 75 psi. The hot sodium will yield its heat to intermediate and secondary sodium heat-transfer loops, finally supplying heat to a steam-generating loop.

Core Temperatures

Sodium will enter the core at a temperature of 420°C and leave the core under normal conditions at about 600°C. During transient overpower operation, the outlet temperature may rise to the 760 to 1100°C range; the normal fuel-cladding temperature of 610 to 700°C may rise to 1100°C. During reactor transients the coolant, cladding, and in-core sensors are expected

*Research sponsored by the U. S. Atomic Energy Commission under contract with the Union Carbide Corporation.

†Oak Ridge National Laboratory, Oak Ridge, Tenn.

Table 1 LMFBR Thermometric Design Parameters

	FFTF (proposed)	LMFBR reference	1000-Mw(e) follow-on studies, November 1968				
			Atomics International	Babcock & Wilcox	Combustion Engineering	General Electric	Westinghouse Electric
Core							
Fuel	UO_2-PuO_2	–	UO_2-PuO_2	UO_2-PuO_2	PuC–UC	PuO_2-UO_2	PuC–UC
Fuel assemblies	77	–	274	288	279	*	244
Fuel pins/assembly	217	–	217	*	163	*	168
Fuel pins							
Cladding thickness, in.	0.015 to 0.016	0.010 to 0.020	0.015	0.010	0.011	*	0.012
Fuel-pin outside diameter, in.	0.23	0.25 to 0.28	0.30	0.28	0.40	0.25	0.30
Centerline temperature, max., °C	2650	2210 to 2750	*	2100 to 2150	1120 to 1420	*	1300 to 1430
Cladding temperature, °C	600 to 760	650 to 700	610 to 650	630	605 to 655	700	650 to 700
Heat flux (peak), kw/ft	8.5	15 to 20	16	*	*	*	18.7 to 36.3
Heat flux, 1000 Btu/(hr)(sq ft)	–	–	785	*	*	*	810 to 1570
Primary coolant							
Inlet temperature, °C	260 to 480	427	416	427	426	430	410
Outlet temperature, °C	480 to 650	760	616	593	590	621	540
ΔT (in core), °C	490	333	200	165	165	190	130
Flow velocity, ft/sec	15	10 to 30	33	*	33	*	28 to 29
Pressure drop, psi	30	–	100	34	75	64	56 to 60

*Information not presented.

to be subjected to thermal shocks of about 110°C/sec for a period of 2 to 3 sec. The centerline temperature within the fuel pin will depend on the material used for fuel (oxide or carbide), on whether the fuel pin is sealed or vented, and on the degree of compaction of the fuel. For a sealed, uncompacted oxide fuel, centerline temperatures will range from a normal of 2300°C to a maximum of about 2750°C during transients.

Thermometry Requirements

The severe conditions in these high-performance reactors require extraordinary sensor durability and reliability for successful plant operation, control, and safety. Knowledge of the behavior of components and materials is being advanced into the unexplored regions of higher temperatures and fast-neutron environments. Sophistication and care must be used with conventional instrumentation, and, in some cases, entirely new instruments and methods must be conceived and proved to overcome inherent limitations of existing devices.

A knowledge of the LMFBR requirements must form the basis for the evaluation of existing capabilities of instruments to meet the new requirements and to guide the development of new and advanced techniques. A series of studies contained in the LMFBR program plan[2] has delineated the requirements of this new class of power reactors and has shown that improved temperature sensors will be required to meet the projected needs of the program.

Temperature-Sensor Life

Temperature sensors for the LMFBR must operate reliably at high temperatures and in harsh chemical and intense nuclear environments for long periods of time. Fuel-pin temperatures will be at their highest levels during an initial period of 80 to 100 hr while the fuel consolidates, and the sensors used in fuel-development studies will be exposed to their maximum thermal limits. Compatibility problems between temperature sensors and fuel will likely occur during a period of 1000 to 3000 hr after startup, during which time the sensors will receive a large neutron dose. Coolant sensors are prone to failure after repeated thermal cycling and shock. Unless coolant sensors can be replaced during operation of the reactor, they must serve reliably for the entire core life (about 9000 hr),

and some sensors may be required to last for the projected 30-year life of the reactor itself.

Experience is limited or nonexistent on the reliability of temperature sensors at temperatures above 2000°C for periods longer than a few hundred hours, and such experience must be obtained prior to the use of sensors in fuel-development studies for the LMFBR. Long-term reliability of temperature sensors can be achieved in some cases by increasing the size or mass of the sensors, but this would be at the expense of the time response of the sensors. In addition to long-term reliability, the LMFBR also requires fast time response of the coolant temperature sensors—as short as 100 msec—to provide prompt indication to the reactor control system of transient conditions for corrective action within about 1 sec.

Radiation Environment

In the unmoderated core of the LMFBR, a fast-neutron flux of 10^{16} neutrons/(cm^2)(sec) will subject fuel, cladding, structural components, and in-core sensors to a flux two or three orders of magnitude higher than that of presently existing power reactors and from 2 to 10 times greater than that obtained in present test reactors. For a 1-year fuel cycle, an accumulated dose approaching 10^{23} neutrons/cm^2 (fast) must be sustained by core components. Although the effects of fast-neutron irradiation have not been fully explored, experimental evidence has shown changes in density due to void formation in materials at a fluence of 10^{20} to 10^{21} neutrons/cm^2, significant decalibration of thermocouples at 10^{21} neutrons/cm^2, and physical damage to structural materials at a fluence above 10^{23} neutrons/cm^2. Fast-neutron damage, however, is minimized by a self-annealing process when the material is irradiated at a temperature above approximately 0.6 of its absolute melting point. Hence damage to core components and sensors in high-temperature regions may be minimal even in the presence of high levels of fast-neutron flux.

Thermal-neutron flux in the LMFBR is expected to be at most 5×10^{11} neutrons/(cm^2)(sec) (thermal), or several orders of magnitude *below* that found in most power reactors. Transmutation effects on components and sensors should be well within the limits of previous experience and are susceptible to analysis and prediction well based on theory and experiment.[3,4] Thermal fluences of 10^{17} to 10^{19} neutrons/cm^2 (thermal), however, will produce significant changes in the output of temperature sensors, for which corrections must be made.

The gamma heating of 10^7 to 10^9 r/hr expected for the LMFBR and fuel test reactors is approximately that found in existing research reactors (Oak Ridge Research Reactor and High Flux Isotope Reactor) and could produce appreciable localized overheating in sensor elements not in good thermal contact with the coolant or with core components.

A summary of the temperatures and fluxes anticipated in the LMFBR is shown in Table 2 for four different locations in which the temperature may be measured. With the exception of the fuel centerline

Table 2 LMFBR Thermometry Requirements

Temperature-sensor location	Temperature		Thermal shock, °C/sec	Flux environment			Fluence (1 year)	
	Normal high, °C	Excursion high, °C		Thermal neutron, neutrons/(cm^2)(sec)	Fast neutron, neutrons/(cm^2)(sec)	Gamma, r/hr	Thermal neutron, neutrons/cm^2	Fast neutron, neutrons/cm^2
Coolant, out-of-core in sodium	650	760	10 to 20	$<10^{11}$	10^{14}	10^6 to 10^7	10^8	10^{21}
Coolant, in-core in sodium	650	1100	110	5×10^{11}	10^{16}	10^7 to 10^9	10^{17} to 10^{19}	10^{21} to 10^{23}
Fuel cladding, in-core in sodium	760	1100	*	5×10^{11}	10^{16}	10^7 to 10^9	10^{17} to 10^{19}	10^{21} to 10^{23}
Fuel meat centerline mixed oxide	2300	2750	*	5×10^{11}	10^{16}	$>10^9$	10^{19}	10^{23}

*Not yet specified.

location, temperature excursions over 1000°C, and the effects of prolonged exposure to fast neutrons, these temperature-measuring requirements can be filled by existing sensors.

Sensor Size and Accessibility

In addition to the constraints placed on temperature-sensor selection and design by temperature and radiation, proper application of temperature sensors in the LMFBR fuel-development programs requires that the sensor be small in size and have a sensitive region approximating a point or line and that the sensor provide a temperature indication with a minimum of perturbation of the nuclear or thermal environment. Fuel-pin centerline sensors must be small in diameter compared with the fuel-pin diameter of about 0.25 in., and they probably cannot exceed 0.0625 in. in outside diameter, including any sheath. They should not, of course, contain any nuclear poisons. A sensor for the cladding temperature should offer a minimum disturbance of the heat flow from the fuel to the coolant. Also, the sensor should be able to resolve differences in temperature across the 0.01-in. cladding thickness for heat-flow calculations, or it should be able to resolve differences in temperature between the inner surface of the cladding and the fuel in contact with it or between the outer surface of the cladding and the coolant in contact with it.

Temperature sensors in fuel-development programs and in LMFBR plant operation will be in contact with the hot sodium coolant or must be inserted through sodium to the core positions. Access through core containment and coolant above the core will require corrosion-resistant metal-clad sensor leads 30 to 50 ft long. Fuel-handling and sensor-replacement procedures may require sensor-signal connectors within the pressure vessel; these sensors will be subjected to moderately high temperatures and fluxes and to sodium vapor or liquid. The stringent reliability requirements for core instrumentation apply equally to the sensors and to their signal-transmitting mechanisms and connectors.

Sensor Reliability

Three thermocouples connected in a 2-out-of-3 scram logic will, in many cases, be used to measure the exit temperature of the coolant in each fuel subassembly. Two additional thermocouples for each assembly are being planned in one FFTF plant design for use in information channels. The FFTF will have about 300 thermocouples, whereas the LMFBR plants will have about 850 thermocouples for monitoring coolant exit temperature. To attain a plant factor in excess of 75%, these thermocouples must have a reliability of 95%; i.e., fewer than 5% may fail within the core life period of 1 year. In addition to the coolant thermocouples, other temperature sensors will be used to monitor components in or near the core. They must all operate with similar high standards of reliability to assure economy and safety of operation of the reactor. Temperature sensors may be used to detect blockage of the coolant in the core, core-coolant boiling, or cladding failure—conditions that could result in damage or collapse of the core. To minimize random failure and to eliminate common mode failures, extensive quality-assurance programs will necessarily precede the successful use of temperature sensors in fast breeder reactors.

Contemporary Reactor Thermometry

In present practice, type K (Chromel–Alumel) thermocouple assemblies having stainless-steel sheaths and MgO insulation are used with satisfactory results in reactors for measurement of temperatures to about 1000°C and at thermal-neutron fluences up to about 10^{22} neutrons/cm^2. Tungsten–rhenium thermocouples are used for in-core structural-material measurements and fuel-development measurements to about 2300°C, but they show calibration shifts of 5 to 10% caused by low electrical-insulation resistance at high temperatures and by changes in composition of the thermocouple wires by thermal-neutron transmutation. Platinum resistance thermometers are sometimes used for precise temperature-difference measurements out-of-core to about 600°C. Optical pyrometers are used infrequently for reactor temperature measurement because it is difficult to obtain an optical path to the core. Other methods of measuring temperatures within a reactor have been explored within the last 5 years. These methods are in various stages of development and have not received widespread use.

Thermocouples

Of the base-metal thermocouples, Chromel–Alumel is preferred for nuclear reactor service because it is relatively immune to thermal-neutron transmutation[3] and because extensive experience has been accumulated with its use in service.[5] Its upper useful temperature is about 1100°C for longtime service.

Selected, commercially fabricated ⅛-in.-OD, stainless-steel-sheathed, MgO-insulated, type K thermo-

couples with insulated junctions provide better than 0.5% accuracy for temperature measurement up to 900°C, show less than 1°C drift in over 800 hr of out-of-pile use at 870°C, and have time responses as fast as 0.5 sec for a step change in temperature. The preferred fabrication parameters for type K coolant thermocouples in FFTF application are shown in Table 3 along with some alternative choices.

Stainless-steel or nickel-base alloys are generally used for sheaths for low-temperature thermocouples; Ta, Mo, and W–Re alloys have been used for the high-temperature thermocouples.[6] Tungsten–rhenium appears to have an advantage over tantalum and molybdenum because of its lower permeability to hydrogen and oxygen[7] and its superior compatibility with oxide insulators and fuels.[17]

Table 3 FFTF Coolant Thermocouple Fabrication Parameters

Parameter	Choice	Alternative	Basis for choice
Wire material	Chromel–Alumel	None	Stability in-pile
Wire size, AWG	22	24	Insulation thickness
Junction style	Insulated	Grounded	Breakage vs. response time
Insulator	Magnesia	Alumina	Fabrication properties
Compaction, %	High (>90)	Low (>70)	Drift characteristics and mechanical stability
Sheath size, in. OD	1/8	1/16	Failure probability vs. time response
Sheath material	S.S. 304L	Incoloy 800	Thermal-expansion match and corrosion sensitization
Stock fabrication	Swaged	Drawn	Higher compaction

Precious-metal thermocouples offer higher temperature possibilities, but as a class they are typically susceptible to transmutation-induced changes in calibration owing to their large thermal-neutron cross sections. Of the few possible combinations of refractory metals, only tungsten and its alloys with rhenium offer good, high-temperature stability for possible use up to 2500°C. Characteristics of three combinations of W–Re alloy thermocouples are shown in Fig. 1. Also shown in Fig. 1 are the melting points of refractory metals and insulators for possible use in high-temperature thermocouples and sheaths, as well as the temperatures at which the electrical resistance of high-temperature thermocouple insulators decreases to 10 ohm-ft. Very high purity of material is required of the insulator to maintain high electrical resistance at high temperatures. Magnesia (MgO) is preferred for low-temperature thermocouples because it has favorable fabrication properties, but it may absorb moisture during assembly of the thermocouple. Beryllia (BeO) is preferred in high-temperature thermocouples because it maintains a high electrical resistivity nearly up to its melting point of 2530°C, but reactions have been noted between BeO and Ta sheaths at high temperatures. Thoria (ThO_2) and hafnia (HfO_2) show good promise of being useful to extend the upper temperature limit of the W–Re thermocouples above 2500°C.

There is extensive information in the literature on thermocouples and their use in past and present nuclear reactor programs, including the CANEL,[8] FARET,[9] NERVA,[10–12] Phoebus,[13] GCR,[14] BORAX-V,[15,16] and SEFOR[17,18] programs. This literature indicates that significant problem areas will be encountered in the selection and specification of thermocouples as temperature sensors for the LMFBR program. These include:

1. Acquisition of data on long-term stability of coolant thermocouples in a fast-neutron reactor environment.
2. Effects of thermal cycling and thermal shock on the reliability of thermocouples.
3. Determination of materials compatibility with reactor environment for the thermocouple sheath and its insulator and for the thermocouple elements.
4. Shunting effects in high-temperature thermocouples related to insulator purity and to insulator and element configuration; methods of compensation or correction for shunting effects.
5. Effects of fabrication variables on reliability.
6. Standardization of high-temperature thermocouples.
7. Effects of transmutation and fast-neutron damage on high-temperature thermocouples in fast reactors.

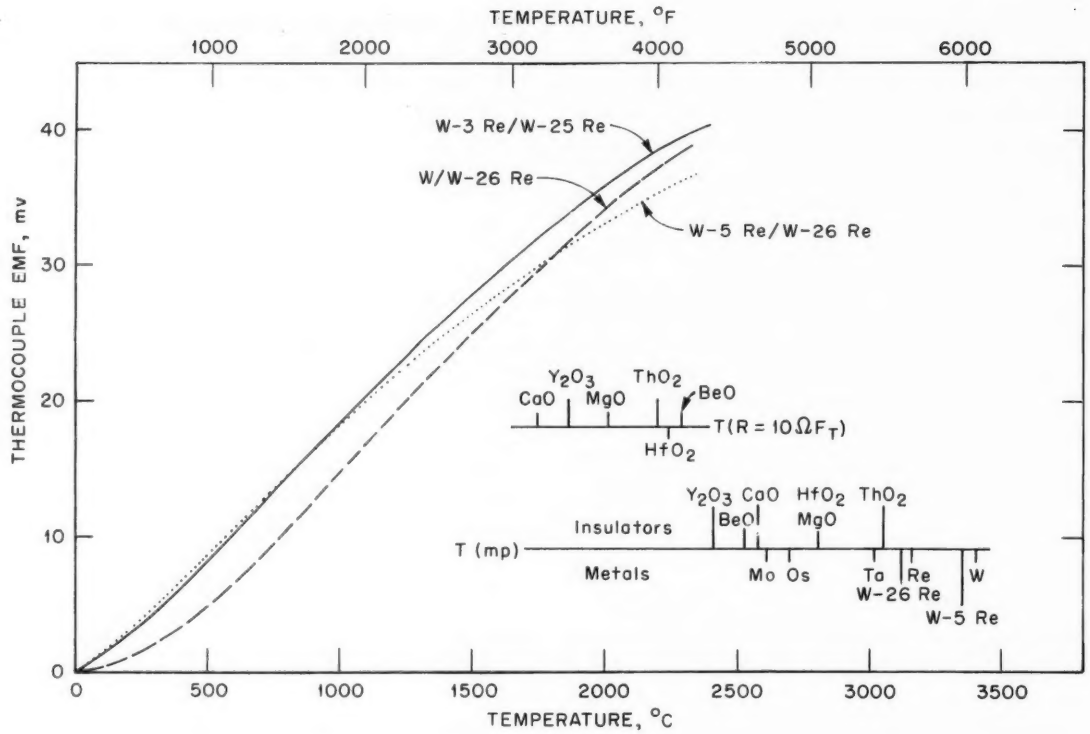

Fig. 1 Characteristics of W–Re thermocouples and high-temperature insulators and metals.

Resistance Thermometers

Resistance thermometers hold some attractiveness as alternative temperature sensors to thermocouples for use in fast reactors. They are being used[19] in the French Rhapsodie fast reactor for precise, coolant-temperature-difference measurements, and, when combined with a measurement of coolant flow, these measurements allow a determination of reactor thermal power to within 1%. Long-term thermal-cycle tests in progress at Oak Ridge National Laboratory (ORNL) to 800°C are now demonstrating drift stability within 1% for commercial, ceramic-insulated, metal-sheathed, platinum resistance thermometers.

Extensive studies of the platinum resistance thermometer as a temperature standard have been performed by Berry of the National Research Council in Canada[20] to 900°C and by Evans and Burns of the National Bureau of Standards.[21] Sias and others at General Electric Company[22-24] have investigated a tungsten resistance thermometer for nuclear marine application to 300°C, with use projected to 1000°C. Chambers, of the Advanced Technology Laboratories of American-Standard, has reported[25] on the development of an iridium resistance thermometer for use to 1600°C, with use projected to 2000°C. Further development along these lines might produce a temperature sensor for use in fast reactors, if problems of nuclear transmutation, high-temperature insulation leakage, sensor size, and slow thermal response can be overcome.

LMFBR Thermometry Program

To meet the projected needs of the LMFBR program, the AEC has established thermometry-development and sensor-testing programs in the national laboratories and at industrial laboratories. These programs were established to determine through extensive testing the performance of commercially available thermocouples, to ascertain existing manufacturing capabilities for thermocouples, and to examine and evaluate improvements and innovations proposed for temperature sensing. Maximum participation of industrial firms in the development and supply of

temperature sensors is a prime object of the program. The Liquid Metal Engineering Center has been designated to collect and evaluate information on temperature sensors of established art. Oak Ridge National Laboratory has been designated to contribute to advancements in the state of the art by coordinating temperature-sensor development programs and evaluating new temperature-measurement concepts.

Thermocouple Development

A program is under way for testing and specifying coolant thermocouples for the FFTF. These studies, undertaken by Pacific Northwest Laboratory of Battelle Memorial Institute and by Oak Ridge National Laboratory, include the determination of effects of fabrication processes and materials on short- and long-term characteristics of the sheathed, type K thermocouples and the effects of irradiation on reliability of the thermocouples. A similar program is being initiated to provide specifications for high-temperature W–Re thermocouples for in-core use in the fast reactor fuel-development program. Current research and development programs on high-temperature W–Re fuel-pin thermocouples are in progress at General Electric[26,27] (Nuclear Systems Programs), Battelle–Columbus,[7] Los Alamos Scientific Laboratory,[4] Argonne National Laboratory,[28] and Oak Ridge National Laboratory. The multiplicity of laboratories engaged in W–Re thermocouple work is the result of the widely varying performance goals set for instrumentation by fuel-development investigators. This is understandable and generally recognized as the only way to meet specific research goals.

New Methods in Reactor Thermometry

None of the five programs mentioned above can, at this time, guarantee unequivocally that a high-temperature thermocouple can be developed measuring fuel-pin centerline temperatures for long periods of time (e.g., 10,000 hr) without unacceptable degradation or shunting errors. The AEC is therefore supporting other investigations aimed at developing new concepts in high-temperature thermometry for application to the LMFBR program requirements. A brief description of these programs is given below.

A study[29] is under way at Panametrics, Inc., for the development of an ultrasonic temperature sensor that utilizes the relation between temperature and velocity of sound in a short length of wire. The system (Fig. 2) measures the time difference between the sonic pulses reflected from each end of a 2-in. length of rhenium wire fixed at the end of a lead-in wire. Temperatures up to the melting point of rhenium (3150°C) have been determined with a resolution of 1%. The sonic pulse-echo method is equally applicable to virtually any sensor material, inherently avoids the high-temperature insulation-resistance problems of thermocouples, and is insensitive to temperature-gradient effects along the lead-in line. In-pile testing of the device was scheduled for spring 1969 in the Oak Ridge Research Reactor.

Gulf General Atomic Incorporated developed, in work supported by the AEC, a high-temperature gas equivalent of the Panametrics ultrasonic sensor. The system was designed for use to 1500°C in the Peach Bottom High-Temperature Gas-Cooled Reactor.[30] The temperature dependence of a gas contained in the reduced-diameter portion of a graphite tube (Fig. 3), corresponding to the rhenium wire in the Panametrics sensor, is measured by the sonic pulse-echo method. The gas can be exchanged continuously and can therefore provide a thermometric substance that is independent of accumulated radiation effects. Since the sonic velocity in a gas is calculable from known gas constants, this device has the potential for use as a primary temperature standard. Changes in the length of the graphite tube with temperature affect the indicated temperature by less than 1%.

Battelle Memorial Institute's Pacific Northwest Laboratory developed and tested a thermometer based on microwave techniques.[31] This system (Fig. 4) measures the change in dimensions of a microwave cavity through measurement of a change in the resonant frequency of the cavity. Since only the thermal expansion of the cavity material affects the temperature determination, the sensor should be relatively free of radiation damage. It has potential application to in-core coolant temperature measurement as high as 1100°C.

A fluidic temperature sensor developed by the Marquardt Corp.[32] uses the change in the resonant frequency of an acoustic resonant-channel oscillator to measure the change in the temperature-dependent velocity of sound of a gas or vapor passing through the fluidic element. This sensor is presently limited to about 1300°C by materials technology, but it has capability for use at higher temperatures. It shares with the General Atomic gas acoustic sensor the advantage that the thermometric substance is constantly exchanged and hence is immune from accumulated radiation damage. In addition to the temperature-sensing device, the other circuit functions shown in Fig. 5 have been realized as fluidic elements, resulting

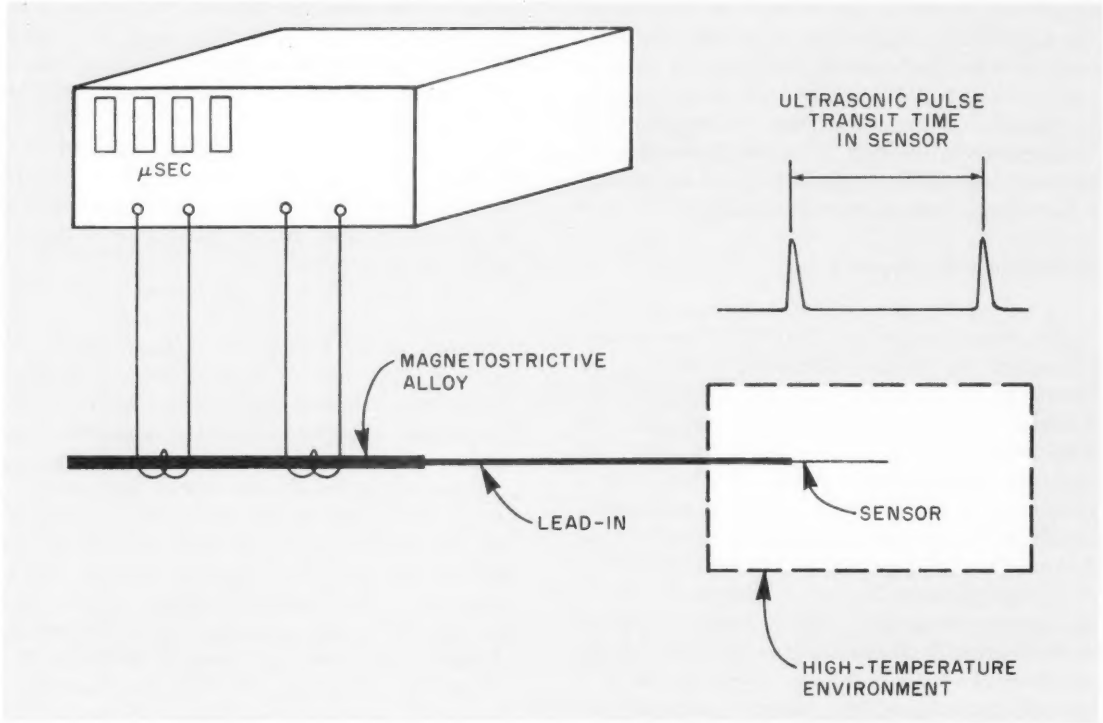

Fig. 2 Ultrasonic temperature sensor. (From Fig. 1 of Ref. 29 and modified slightly.)

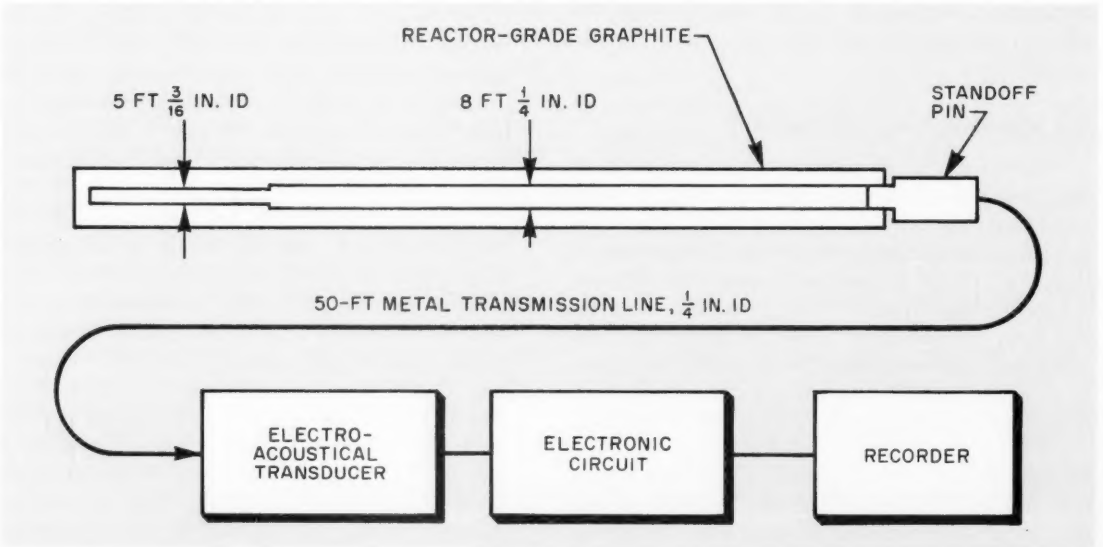

Fig. 3 Basic acoustical (sonic) thermometer. (From a portion of Fig. 2 of Ref. 30.)

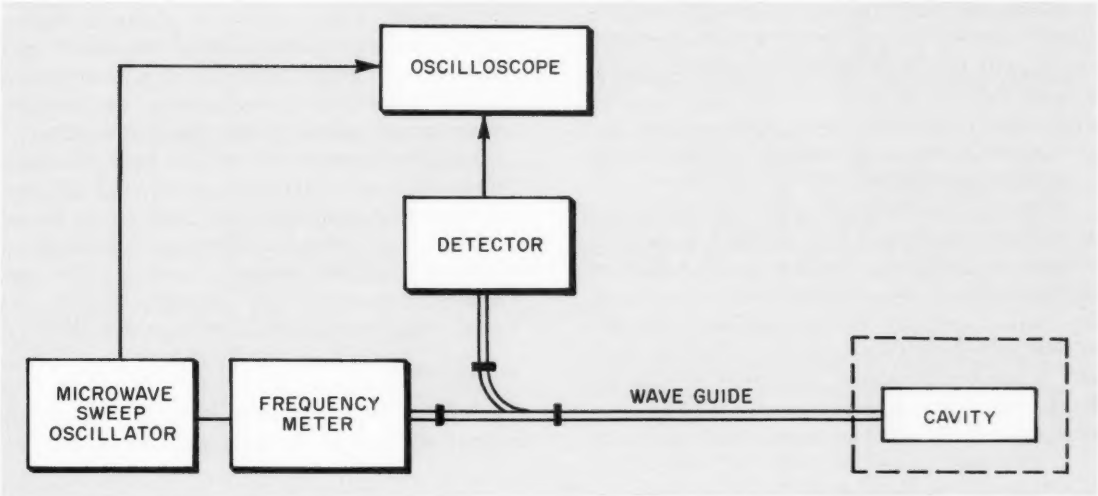

Fig. 4 Microwave temperature monitor. (From Fig. 4 of Ref. 31 and modified for this article.)

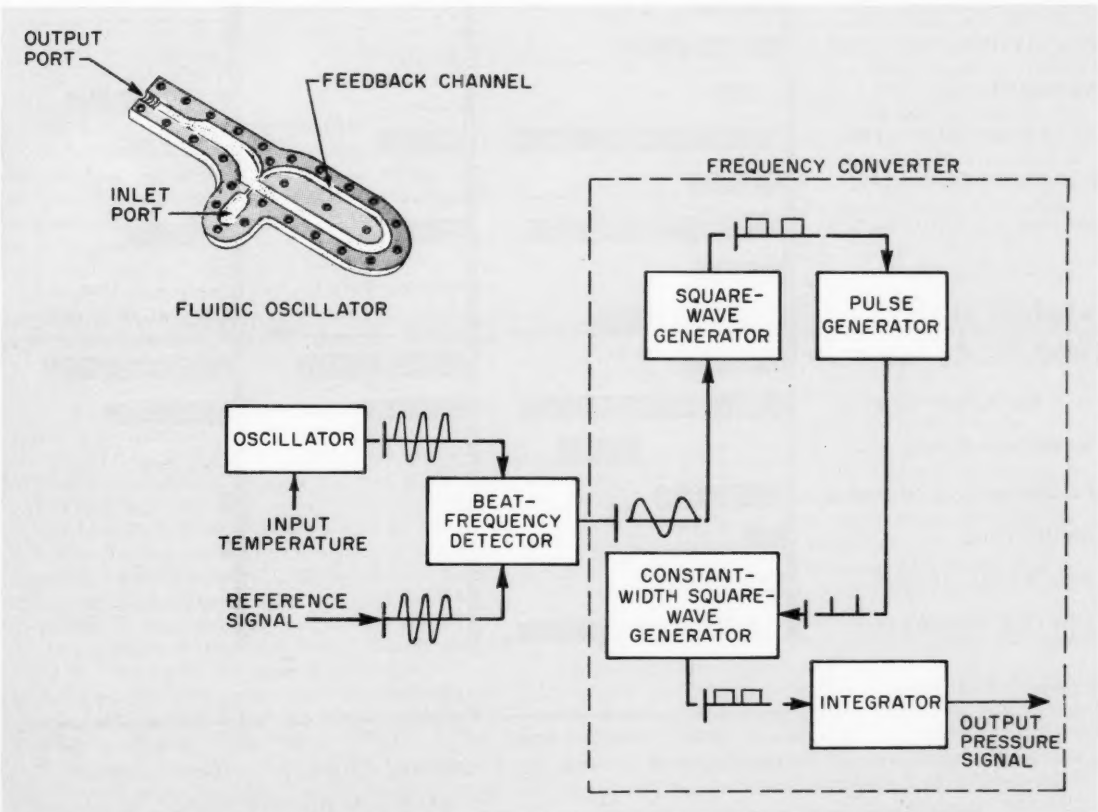

Fig. 5 Fluidic temperature-sensor concept. (Partly from Ref. 32 and partly from SAN-750-1.)

in an integrated fluidic system. This system provides an output pressure proportional to the sensed temperature and suggests that all-fluidic reactor control might be achieved if fluidic temperature sensors were combined with other fluidic flux, flow, level, position, and pressure sensors and with available industrial fluidic control and logic elements.

Other innovational methods for temperature sensing are being sought in a study at ORNL to meet the stringent requirements of LMFBR systems. Nearly any conceivable physical process that has a temperature dependence, preferably but not necessarily reversible or even continuous, has potential use for incorporation into a temperature sensor. A number of schemes, described in a series of review articles on temperature measurement,[33-42] are being evaluated in the light of new materials technology, radiation-damage studies, and the strenuous requirements of the LMFBR program. Figure 6 shows a variety of temperature sensors and their approximate present and projected temperature limitations and neutron-damage characteristics.

Additional consideration is being directed toward methods for circumventing some of the inherent limitations of existing sensors by such means as the use of continuous computer correction of degrading signals, the use of composite sensors, or in situ calibration.

Conclusions

The short-term thermometry needs of the LMFBR program will be met, probably with known types of

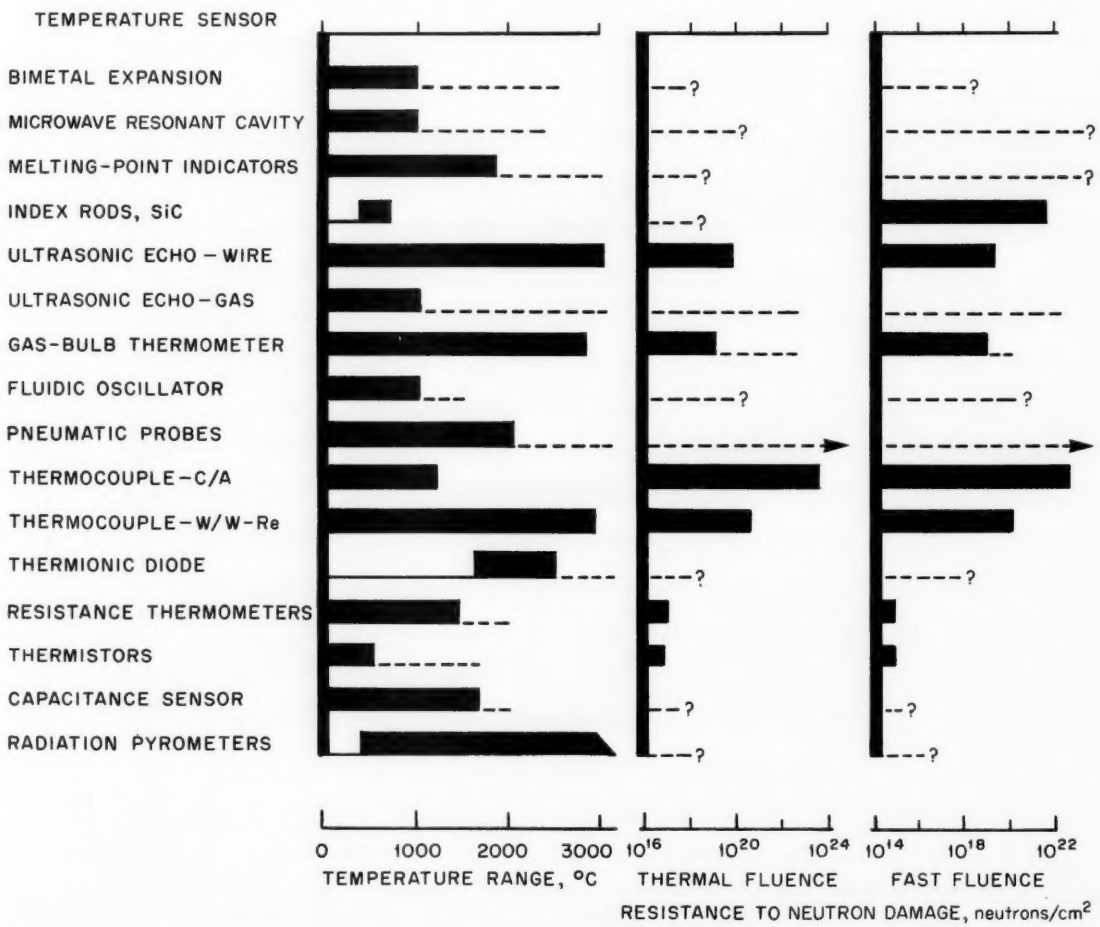

Fig. 6 Temperature sensors for reactor applications.

thermocouples built to stringent specifications and tight manufacturing controls and subjected to extensive, long-term, rigorous in-pile testing. No present information can predict, however, the long-term stability and reliability of thermocouples in a fast reactor. Additional investigation and development are required to establish the reliability of sensors, to overcome their present inherent limitations, and to improve their characteristics. New types of temperature sensors under study now, if successfully developed and proved under reactor conditions, could offer useful alternatives or backup techniques in temperature instrumentation for the fast reactor and could be of special value in fuel-development studies and component testing preceding construction of the LMFBR.

References

These references represent only a portion of an extensive bibliography on reactor thermometry collected at the Nuclear Safety Information Center (NSIC), Oak Ridge National Laboratory, P.O. Box Y, Oak Ridge, Tenn. 37830.

1. R. F. Sweek and A. Amorosi, Liquid Metal Fast Breeder (LMFBR) Program Plan, Vols. 1–10, USAEC Reports WASH-1101 to WASH-1110, Argonne National Laboratory, August 1968.
2. USAEC Report ANL-7520, in preparation.
3. W. E. Browning, Jr., Methods of Measuring Temperature in Nuclear Reactors, in *Progress in Nuclear Energy, Technology and Engineering,* Series IV, Vol. 5, pp. 1-54, Pergamon Press, Inc., New York, 1963.
4. S. R. Skaggs, W. A. Ranken, and A. J. Patrick, Decalibration of a Tungsten–Tungsten 25% Rhenium Thermocouple in a Neutron Flux, USAEC Report LA-3662, Los Alamos Scientific Laboratory, March 1967.
5. J. F. Potts, Jr., and D. L. McElroy, Thermocouple Research to 1000°C—Final Report, USAEC Report ORNL-2773, Oak Ridge National Laboratory, January 1961.
6. G. F. Popper and A. E. Knox, The Materials Selection Problems as Related to Thermocouples Used To Measure Nuclear Reactor Fuel Pin Temperatures up to 2800°C, *IEEE (Inst. Elec. Electron. Eng.), Trans. Nucl. Sci.,* NS-14: 333-41 (February 1967).
7. J. W. Droege, N. E. Miller, M. E. Schimek, V. E. Wood, and J. J. Ward, Refractory-Metal Thermocouples in Nuclear and High-Temperature Applications, USAEC Report BMI-X-10246, Battelle Memorial Institute, November 1968.
8. P. Bliss and S. Fanciullo, High Temperature Thermometry at Pratt & Whitney Aircraft–CANEL, USAEC Report PWAC-462, Pratt & Whitney Aircraft, June 1965.
9. G. F. Popper and A. E. Knox, FARET In-Core Instrument Development, USAEC Report ANL-7161, Argonne National Laboratory, July 1966.
10. G. J. Zellner, Thermoelement and Sheath Evaluations for High Temperature Thermocouples in Nuclear Rocket Engines, paper presented at the High Temperature Symposium of the 71st annual meeting of ASTM, San Francisco, Calif., June 23–28, 1968.
11. G. A. Remley, High-Temperature Thermometry, in Proceedings of the Symposium on Liquid Metal Instrumentation and Control, Idaho Falls, Idaho, March 1–2, 1967, USAEC Report ANL-7380, pp. 52-62, Argonne National Laboratory, 1967.
12. A. W. Hoppe and P. J. Levine, Status of High Temperature Thermometry for the NERVA Reactor, in High Temperature Thermometry, Seminar Proceedings, Washington, D. C., February 24–26, 1965, USAEC Report WASH-1067, pp. 32.1–32.45, March 1966.
13. C. R. Tallman, High Temperature Thermocouples in the Phoebus and Pewee Reactors, paper presented at the 71st annual meeting of ASTM, San Francisco, Calif., June 23–28, 1968.
14. N. H. Briggs, E. L. Long, Jr., and F. R. McQuilkin, Summary of Experience with High-Temperature Thermocouples Used in the ORNL–GCR Program Fuel Irradiation Experiments, in High Temperature Thermometry, Seminar Proceedings, Washington, D. C., February 24–26, 1965, USAEC Report WASH-1067, pp. 1.1-1.22, March 1966.
15. E. J. Brooks and W. C. Kramer, Tungsten–Rhenium Alloy Thermocouples and Their Use in a UO_2-Fueled Reactor, USAEC Report ANL-6981, Argonne National Laboratory, November 1965.
16. E. J. Brooks, Reactor Fuel Temperature and Thermal Time Constant Measurements with Tungsten–Rhenium Thermocouples, *ISA (Instrum. Soc. Amer.) Trans.,* 5(3): 217-222 (July 1966).
17. R. R. Asamoto and P. E. Novak, A Survey for a High-Temperature Sensor for SEFOR, USAEC Report GEAP-4903, General Electric Company, Atomic Power Equipment Department, April 1965.
18. D. P. Hines and K. M. Horst, SEFOR Development Activities, in Proceedings of the Symposium on Liquid Metal Instrumentation and Control, Idaho Falls, Idaho, Mar. 1–2, 1967, USAEC Report ANL-7380, pp. 15-21, Argonne National Laboratory, 1967.
19. G. Gajac, J. L. Ratier, L. Reynes, and M. A. Valantin, Rhapsodie: First Year of Operation, paper presented at the International Conference on Sodium Technology and Large Fast Breeder Reactor Design, November 7–9, 1968, to be published as ANL-7520.
20. R. J. Berry, Platinum Resistance Thermometry in the Range 630–900°C, *Metrologia,* 2(2): 80-90 (April 1966).
21. J. P. Evans and G. W. Burns, A Study of the Stability of High Temperature Platinum Resistance Thermometers, in *Temperature—Its Measurement and Control in Science and Industry,* pp. 313-318, Vol. 3, Part 1, Reinhold Publishing Corporation, New York, 1962.
22. F. R. Sias, Resistance Thermometer for Nuclear Reactor Service, *Nucleonics,* 15(8): 75-82 (August 1957).
23. F. R. Sias, A Resistance-Temperature Detector for Nuclear Reactor Service, *Trans. Amer. Inst. Elec. Engrs.,* 76, Part 1, 363-365 (July 1957).
24. F. R. Sias, J. R. MacIntyre, and A. Hansen, Jr., A Tungsten Resistance Thermometer, *Trans. Amer. Inst. Elec. Engrs.,* 73: Part 1, 66-69 (March 1954).
25. J. T. Chambers, Feasibility Investigation and Development of 2000°C Resistance Temperature Sensor, Report ASD-TDR-62-417 (AD-282358), American-Standard Advanced Technology Laboratories (ATL-D-757), July 31, 1962.
26. E. S. Funston and W. C. Kuhlman, Fast Breeder Reactor

Thermocouple Development, in Seventh Annual Report, AEC Fuels and Materials Development Program, USAEC Report GEMP-1004, pp. 351-360, General Electric Company, Mar. 31, 1968.

27. E. S. Funston and W. C. Kuhlman, Fast Breeder Reactor Thermocouple Development, in AEC Fuels and Materials Development Program, Progress Report No. 74, USAEC Report GEMP-1006, pp. 183-193, General Electric Company, June 28, 1968.
28. A. E. Knox and G. F. Popper, ANL Participation in the FFTF Instrument Development Effort, in Proceedings of the Symposium on Liquid Metal Instrumentation and Control, March 1–2, 1967, Idaho Falls, Idaho, USAEC Report ANL-7380, pp. 9-14, Argonne National Laboratory, 1967.
29. S. S. Fam, L. C. Lynnworth, and E. H. Carnevale, Ultrasonic Thermometry for LMFBR Systems, USAEC Report NYO-3906-4, Panametrics, Inc., September 1968.
30. J. B. Roes and D. L. Peat, The Development of an Acoustical Thermometer for a Graphite Matrix Nuclear Fuel Element, USAEC Report GA-7413, General Atomic Division, General Dynamics Corp., Oct. 8, 1966, and in *IEEE (Inst. Elec. Electron. Eng.) Trans. Nucl. Sci.*, NS-14: 348-359 (February 1967).
31. T. R. Billeter and D. P. Brown, Microwave Measurement of High Temperatures Within Nuclear Reactors, Interim Report, USAEC Report BNWL-399, Battelle–Northwest, Pacific Northwest Laboratory, October 1967.
32. C. R. Halbach, B. A. Otsap, and R. A. Thomas, Fluidic (Pure Fluid) Temperature Sensor, Phase I Final Technical Report, USAEC Report SAN-639-7, ASTRO Division, Marquardt Corp., January 1967.
33. J. S. Hochheiser, Liquid Metal Temperature Measurement (Sodium) State-of-the-Art-Study, USAEC Report LMEC-Memo-68-10, Atomics International, Liquid Metal Engineering Center, May 31, 1968.
34. J. I. Slaughter and J. L. Margrave, Temperature Measurement, in *High Temperature Materials and Technology*, Part V, pp. 717-792, I. E. Campbell and E. M. Sherwood (Eds.), John Wiley & Sons, Inc., 1967.
35. R. F. Walker, High Temperature Measurements and Standards: 1000–3000°C, in *High Temperature Technology*, Proceedings of the Third International Symposium on High Temperature Technology, Sept. 8–11, 1963, Stanford Research Institute, Asilomar, Pacific Grove, Calif., Butterworths, Inc., Washington, 1964.
36. C. R. Barber, Conference on the Measurement of High Temperatures, London, May 1964, *Brit. J. Appl. Phys.*, 15: 1003-1010 (1964).
37. R. P. Benedict, Temperature and Its Measurement, *Electro-Technol.*, 72: 72-86 (July 1963).
38. F. A. Ferguson and R. C. Phillips, High Temperature Technology, in *Advances in Chemical Engineering*, Vol. 3, pp. 61-118, Thomas B. Drew et al. (Eds.), Academic Press Inc., New York, 1962.
39. J. C. Hedge et al., Temperature Measuring Techniques, Report WAAD-Tn-60-487, Vol. 1 (AD-253483), Armour Research Foundation, June 1960.
40. V. D. Sanders, Review of High-Temperature Immersion Thermal Sensing Devices for In-Flight Engine Control, *Rev. Sci. Instr.*, 29(11): 917-928 (November 1958).
41. B. Regent and A. H. Samuel, An Investigation of Temperature Measuring Techniques for Use in High Power Density Nuclear Reactors, USAEC Report UCRL-5305, Broadview Research and Development, 1957.
42. H. W. Maynor, Summary of Investigation to Date of Methods of Measuring Excessively High Temperatures, Report NEPA-746-ISC-7, Iowa State College, August 1948.

The Plutonium Content of Irradiated Fuel from Power Reactors

By Kenneth E. Roach*

The reactor designer should be able to calculate, with confidence, the amount and isotopic composition of plutonium in power-reactor fuel. Economic and safety considerations in current reactors, projected requirements for diffusion-plant operations, and effects on breeder-reactor programs are among the reasons such a capability is important.

Plutonium-content data obtained from the reprocessing of batches of irradiated fuel will be useful; a reactor-physics model that can be used with these data must be a three-dimensional one. Three-dimensional calculations, which are quite complex and expensive, require that the physics of any point in the system under study be known. Thus the importance of having measured point data on the plutonium content of irradiated fuel from reactors of current design should not be underestimated.

The purpose of this article is to present information on the measured point data that are available, to compare results from calculations based on presently accepted design methods with the measured data, and to compare the measured data on pressurized-water-reactor (PWR) fuel with predictions that have been made for water reactors of current design.

Measured Data

Several sets of measurements have been made to determine the plutonium content of irradiated uranium fuel as a function of burnup. One series of measurements has been made for fuel consisting of a mixture of natural uranium and plutonium. The results, and some details, of the measurements are discussed in the following paragraphs.

Yankee

Results of a large program to measure burnup and heavy-isotope content of irradiated fuel from a PWR are given in Ref. 1. This work, performed on fuel from the Yankee (Rowe) reactor, constitutes the most complete program of its kind related to light-water reactors. Fifty-six fuel rods were removed from 14 different fuel assemblies in the first core of Yankee and were subjected to extensive postirradiation examinations. In addition, 7 fuel rods were removed from an assembly that was irradiated in the first core and then recycled in the second core. From the first-core irradiations, 191 pellet-size samples were selected for burnup and heavy-isotope analyses. The samples covered a burnup range of 1300 to 18,000 Mwd per initial metric ton of uranium. From the first-core fuel that was recycled in the second core, 28 pellet-size samples were selected. These samples covered a burnup range of 10,000 to 31,000 Mwd/metric ton of uranium. In addition, results from pellet-size samples taken from a Yankee first-core assembly that was cycled through the second and the fourth cores have been reported.[2] Samples from this assembly increased the burnup range to 46,000 Mwd/metric ton of uranium. Extensive comparisons between the local energy release inferred from the operating history of the Yankee core and the energy release determined from measurements on the samples described above indicate that the procedures used to measure burnup in individual samples were reasonably accurate. Burnup in individual samples was measured several different

*Southern Nuclear Engineering, Inc., Dunedin, Fla.

ways: by analysis of the isotopic composition of the depleted fuel; by counting the ^{137}Cs activity; by counting the ^{90}Sr activity; and, later in the program,[3] by determining the $^{148}Nd/^{238}U$ ratio.

Some of the Yankee samples might be considered to have been irradiated in the near-asymptotic spectrum, i.e., away from control rods and water slots and near the center of the fuel assembly. Other samples were taken from locations where the spectrum was perturbed, i.e., locations near control rods and water slots. Measurements made on samples that had been irradiated in the near-asymptotic spectrum are easier to compare with calculations and, consequently, represent the most useful data. Figures 1 to 4 were taken from Ref. 1. The points on these figures represent the measured specific plutonium content as a function of burnup for the isotopes ^{239}Pu, ^{240}Pu, ^{241}Pu, and ^{242}Pu, respectively. The dashed lines on the figures represent simple freehand fits to the data, and the solid lines are results of calculations, which will be discussed later. Since presently proposed PWR's are designed for average burnups of about 28,000 Mwd/metric ton of uranium, the burnup range indicated on Figs. 1 to 4 should be adequate for checking analytical models. Although the measured plutonium data represent an

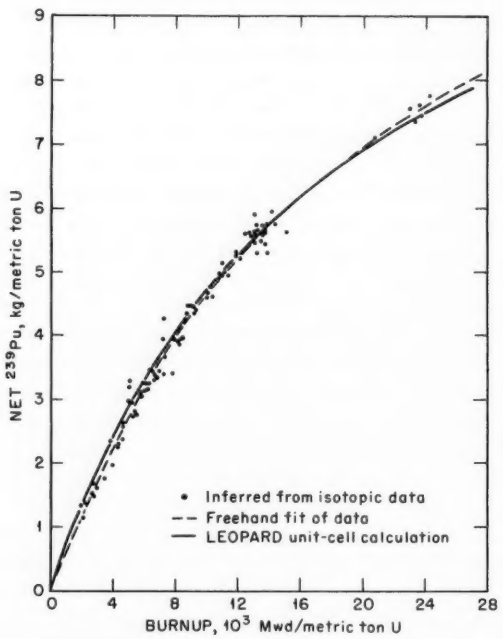

Fig. 1 Specific production of ^{239}Pu vs. burnup in the Yankee asymptotic neutron spectrum.[1]

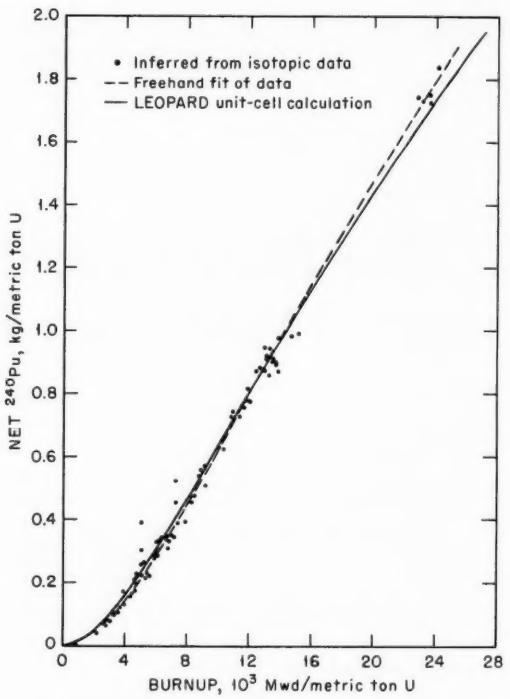

Fig. 2 Specific production of ^{240}Pu vs. burnup in the Yankee asymptotic neutron spectrum.[1]

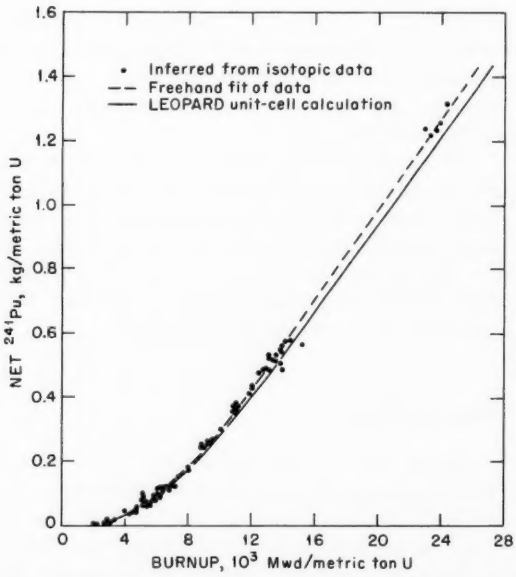

Fig. 3 Specific production of ^{241}Pu vs. burnup in the Yankee asymptotic neutron spectrum.[1]

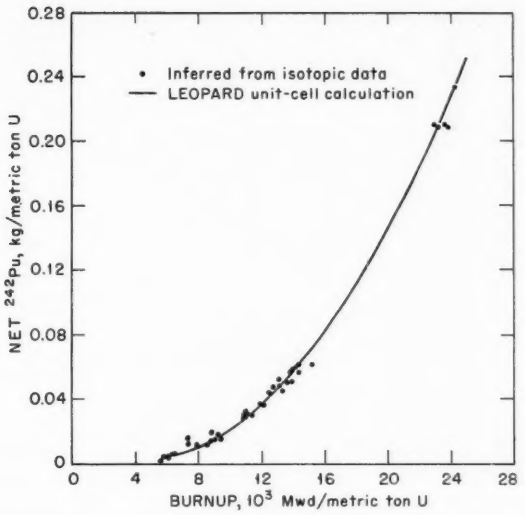

Fig. 4 Specific production of ^{242}Pu vs. burnup in Yankee asymptotic neutron spectrum.[1]

excellent bench mark for testing theoretical tools, it is unfortunate, for reasons to be given later, that the Yankee fuel is not more nearly representative of the fuel specified for PWR's of current design.

VBWR

Although the burnup range was small, measurements were made[4] of the plutonium content of boiling-water-reactor (BWR) fuel from the Vallecitos Boiling Water Reactor (VBWR). The ^{239}Pu/^{238}U atom ratio was determined by a combination of gross alpha counting, alpha-spectroscopic analysis, and mass-spectrometric analysis. Concentrations of ^{240}Pu, ^{241}Pu, and ^{242}Pu were determined by mass-spectrographic analyses. The burnup extended to slightly less than 3000 Mwd/metric ton of uranium, and data are presented in Fig. 5 for the total plutonium atom fraction as a function of burnup.

Calder Hall

Magnox-clad, metallic natural-uranium fuel irradiated in a Calder Hall reactor (CO_2-cooled, graphite-moderated) has been subjected to extensive measurements to determine plutonium content.[5] The burnup in the fuel samples goes as high as about 4500 Mwd/metric ton of uranium, which makes the measured data valuable in correlating theoretical models for these low-design-burnup reactors. Figures 6 to 8

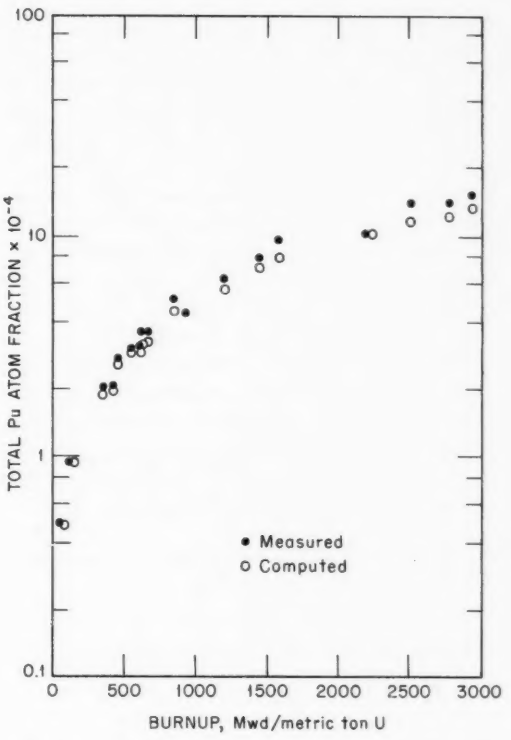

Fig. 5 Total plutonium as a function of burnup for boiling-water-reactor fuel.[4]

summarize the measured Magnox-fuel data and also show the calculated results, which will be discussed later.

NPD

Samples of irradiated natural UO_2 fuel from the Canadian NPD heavy-water reactor have been subjected to measurements to determine plutonium content[6] at a single burnup value of 5600 Mwd/metric ton of uranium. The results of the measurements are given in the "Experiment" column in Table 1; CARIBOU refers to a computer program, which is discussed later in this article.

CVTR

A program that will include measurements of the plutonium content of irradiated UO_2 fuel from the heavy-water Carolinas–Virginia Tube Reactor (CVTR) is reported[7-9] to be in progress. Although results of the work were not available at the time this article was

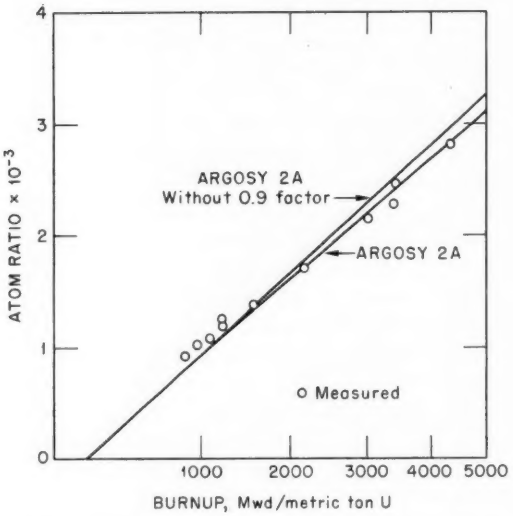

Fig. 6 Plutonium-to-uranium atom ratio as a function of burnup for fuel from a Magnox reactor.[5]

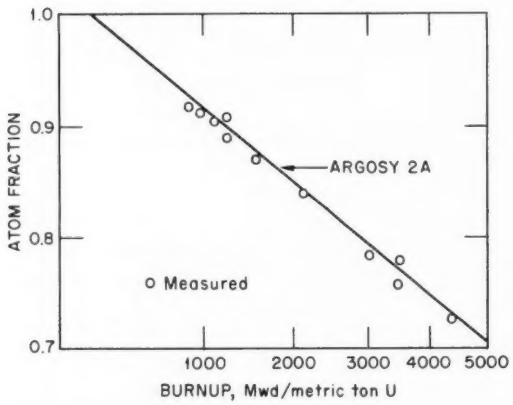

Fig. 7 Atom fraction of ^{239}Pu in total plutonium as a function of burnup for fuel from a Magnox reactor.[5]

written, samples had been sent to laboratories for mass-spectrographic analysis.[9]

Saxton

Measurements made in the Saxton plutonium program are reported for natural UO_2 fuel[10] enriched to 6.6 wt.% PuO_2. The plutonium contained 8.6 wt.% ^{240}Pu. Two types of fuel rods were used in the program; one type had the customary fuel pellets, whereas the other type had vibratory-compacted

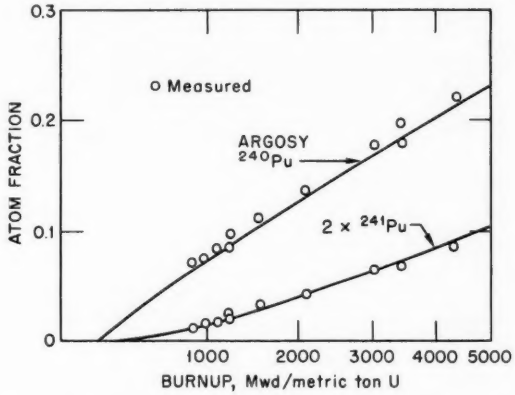

Fig. 8 Atom fraction of ^{240}Pu and ^{241}Pu in total plutonium as a function of burnup for fuel from a Magnox reactor.[5]

(Vipac) fuel. The measured plutonium composition of both types of fuel at burnups of around 5000 to 6000 Mwd/metric ton of uranium is given in Fig. 9. The burnup for these particular samples was measured by using ^{148}Nd. Lines on the figure represent the calculated results, and the results are discussed below.

Measured vs. Calculated Results

Each reactor designer develops his own package of computer programs to describe the behavior of his reactor cores. Theoretical techniques peculiar to each type of reactor are used, but, as would be expected, designers of the same type of reactor have program packages that are very similar. Several computational models are discussed in this section, and results from

Table 1 Comparison of Measured and Calculated* Content[6] of NPD Fuel at 5600 Mwd/Metric Ton of Uranium

	Experiment	CARIBOU	CARIBOU experiment
^{235}U†	0.3905 ± 0.0009	0.3905	
Pu/U (atom ratio)	$3.133 \pm 0.02 \times 10^{-3}$	3.093	0.987
^{239}Pu, at.%	73.34 ± 0.06	73.254	0.999
^{240}Pu, at.%	22.04 ± 0.06	22.093	1.002
^{241}Pu, at.%	3.815 ± 0.1	3.826	1.003
^{242}Pu, at.%	0.812 ± 0.002	0.827	1.018

*Calculations performed with the CARIBOU program.

†$\frac{^{235}\text{U at 5600 Mwd/metric ton of uranium}}{^{235}\text{U at zero burnup}}$

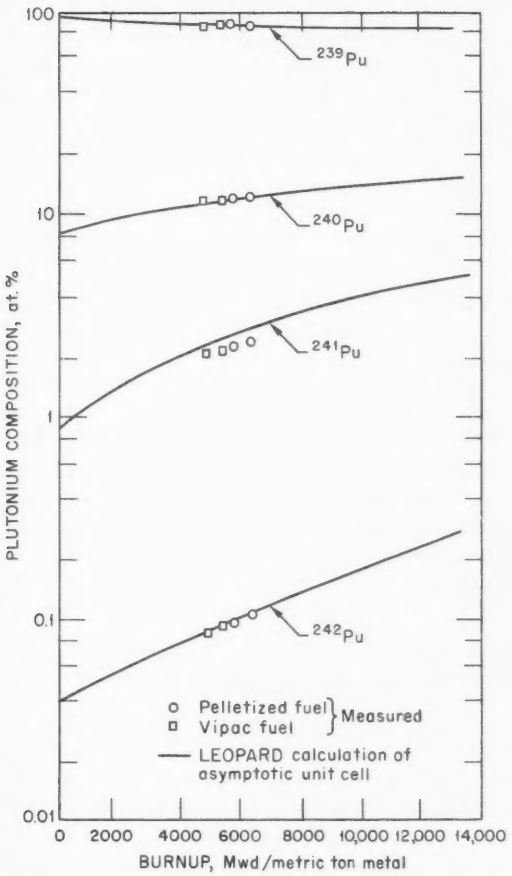

Fig. 9 Variation of plutonium isotopic abundance with fuel burnup for a fuel mixture[10] of natural UO_2 and PuO_2.

these models are compared to the measurements mentioned previously.

Yankee

The LEOPARD[11] computer program, developed by Westinghouse, is designed to calculate the reactor physics of a point within a PWR. Starting with a source neutron, distributed in energy about an appropriate fission spectrum, LEOPARD calculates the absorptions, fissions, and leakage (based on a buckling, B^2) rates as functions of energy from the highest energy in the distribution to zero. In addition to neutron slowing down, the program calculates the effects of fuel lump size (surface-to-volume ratio), scattering per absorber atom, lump temperature, and mutual self-shielding of fuel lumps on the resonance-absorption cross section of ^{238}U. In the range of thermal energies, the program calculates the thermal distribution of neutrons in energy as well as the spatial distribution of these neutrons. From the calculated reaction rates in each of the isotopes comprising the medium, appropriate cross sections are deduced for burnup calculations. The entire neutron spectrum and new cross sections based on the spectrum may be recalculated after each burnup step. Input parameters for the program consist of material specifications, geometry, and temperatures, with all nuclear densities, geometry changes with temperature, etc., being calculated internally.

LEOPARD is an excellent example of the program packages that each light-water-reactor vendor has developed to describe the behavior of fuel within his reactor cores. Since Westinghouse has been the only light-water-reactor vendor to report extensive measurements of the heavy-isotope content of uranium fuel as a function of burnup, it is appropriate to cite their calculations of the plutonium content of irradiated fuel from the Yankee reactor. As can be seen in Figs. 1 to 4, calculated results for net ^{239}Pu, ^{240}Pu, ^{241}Pu, and ^{242}Pu content utilizing LEOPARD for the unit cell are in excellent agreement with measured results.

VBWR

The calculated results (for quite low burnups) for plutonium content of boiling-water-reactor fuel irradiated in the VBWR indicate good agreement with measurements, as seen in Fig. 5. Although no specific computer programs are mentioned in Ref. 4, which describes the calculations, the basic methods are discussed. The Greuling–Goertzel approximation was used for the treatment of heavy isotopes in slowing down, and the hydrogen component of the slowing-down density was calculated directly. The thermal spectrum was based on the Wilkins heavy-gas model, whereas thermal spatial calculations for the unit cell were determined by the P_3 spherical-harmonics approximation to the transport equation. Resonance capture in fertile material was based on a multigroup model in which the capture in individual resonances is determined by the infinite-mass or narrow-resonance approximation. As with most models, the temperature dependence of the ^{238}U resonance absorption is a fit to experimental data.

Calder Hall

The British use a program called ARGOSY to calculate the plutonium content of irradiated Magnox

fuel. The good agreement between ARGOSY calculations and measured data, as shown in Figs. 6 to 8, indicates that the ARGOSY program is adequate. However, as stated in Ref. 5, "The method of calculation used here is the code ARGOSY 2A which contains an arbitrary factor of 0.9 on resonance absorption deduced, in the case of ^{238}U, from a table of resonance integrals." The reference welcomes further checks, since the resonance integrals without the 0.9 factor are consistent with experiment.

NPD

The calculated results in Table 1 compare well with the one measurement made on an NPD bundle irradiated to 5600 Mwd/metric ton of uranium. The basic physics is calculated with the LATREP program, and another program, CARIBOU, uses LATREP spectrum parameters to calculate isotope reaction rates. CARIBOU also integrates the burnup equations and interpolates to get isotopic compositions at specific burnups. Since the design burnup in natural uranium–D_2O systems is not high (when compared with that of light-water reactors), it appears that the LATREP–CARIBOU methods are adequate for predicting plutonium content in the CANDU-type reactors.

Saxton

The LEOPARD program was used to calculate plutonium content of the mixed-oxide fuel irradiated in the Saxton reactor. Results of the LEOPARD calculations are shown in Fig. 9. Note that the fuel initially was 6.6 wt.% plutonium oxide mixed with natural uranium oxide. Although the burnup range for the measured results is limited, the calculations agree well with the measurements over the given range.

There are other comparisons in addition to those given above. For example, the USAEC has sponsored programs to determine the heavy-isotope content of operating fuel elements. The first phase of this work[12] was to investigate the capabilities and limitations of existing computational methods and to express as quantitatively as possible the agreement that might be expected between calculation and experiment. The second phase of the work involved the use of a simplified, three-dimensional program to calculate exposure predictions for a number of operating reactors, and the third phase was the development of a method to check independently the heavy-isotope content of operating fuel elements. The method that was developed (called ISOCHECK) represents a compromise between accuracy of results and simplicity of calculations. When applied to 17 U. S. reactors, ISOCHECK gave results that apparently were good. However, Ref. 13 indicates that, because of design changes to the Yankee (Rowe), Dresden 1, and Humboldt Bay reactors, ISOCHECK is no longer valid. An additional program to determine if and how the method can be modified for application to the much larger reactors now being designed was undertaken.[13]

The comparisons between calculations and measurements indicate that the measured plutonium content in irradiated fuel can be predicted with acceptable accuracy for the reactor systems studied. However, it is important to consider how accurate the calculations will be when extrapolated to reactors whose core characteristics differ significantly from those of the reactors in which the actual fuel irradiations were carried out. In other words, will the calculations that have been correlated with measured data from older reactors apply to reactors of current design?

Measured Yankee Data vs. Calculations for Water Reactors of Current Design

The nuclear designs of modern PWR's are, from the reactor-physics point of view, very similar. The designs specify about the same fuel-rod size, Zircaloy cladding, similar specific powers, moderator and fuel temperatures, fuel densities, enrichments, moderator-to-uranium oxide volume ratios, etc. Because of the similarities in items that influence the reactor physics, the production of plutonium within a unit cell in any of the presently proposed PWR's should be about the same. Although results of the designers' calculations for the point burnup case are not generally available for the current reactors, there are some published data on gross plutonium content, i.e., plutonium content for a whole region of the reactor.

It is interesting to compare the physical properties of a Yankee unit cell, where measured data on plutonium production are available, with the physical properties of a unit cell in a PWR of current design. Such a comparison is given in Table 2. The numbers listed for the "current design" in the table are typical of practically any current PWR. One can see from the table that principal differences between the unit cells lie in lump size, cladding material, moderator-to-fuel ratio, and enrichment. Along with the difference in cladding materials, one of the most important differences as far as the neutron spectrum is concerned is the water-to-fuel-volume ratio, the Yankee lattice being a

Table 2 Infinite-Cell Parameters for Yankee and a PWR of Current Design

Parameter	Yankee	Current design
Enrichment, %	3.4	2.1–2.6–3.2
Pellet OD, in.	0.294	0.3669
Rod OD, in.	0.340	0.4220
Cladding material	Stainless steel	Zircaloy
Cladding thickness, in.	0.021	0.0243
Moderator temp., °F	514.5	573
Average fuel temp., °F	920	1180
Fuel density, g/cm^3	10.2	10.25
Volume moderator/volume UO_2	1.2866	1.68

tighter packed one with smaller fuel rods. Even when all the differences are considered, however, the initial conversion ratios for the two systems are about the same.

References 1 and 14 to 16 give, respectively, the evaluation of mass-spectrometric and radiochemical analyses of Yankee core 1 spent fuel, the results of calculations on a typical PWR considered in a large AEC-sponsored program, a vendor's data on a typical PWR, and a vendor's data on a typical BWR. It is useful to plot the information on fissile plutonium content of irradiated fuel, as given in the references mentioned above, on one graph. The fissile plutonium ($^{239}Pu + ^{241}Pu$) content as a function of burnup is shown in Fig. 10. The large differences between the measured Yankee data and the available calculated data, at burnups typical of design values for current reactors, raise questions that can only be answered by additional experimental measurements. Unfortunately, irradiated fuel from reactors of current design will not be available in the near future. A few of the earlier power reactors, such as Selni, Indian Point 1 core B, and Connecticut Yankee, have water-to-fuel ratios which approach those of the latest reactors and might have spent fuel available. However, as with Yankee, these reactors use small fuel rods clad with stainless steel.

Conclusions

In general, calculations of the plutonium content of irradiated fuel are in good agreement with available measurements. However, different theoretical techniques peculiar to each reactor design must be used. On the basis of the information available on water reactors, it appears that measurements of the fissile plutonium content in the earlier reactors do not agree

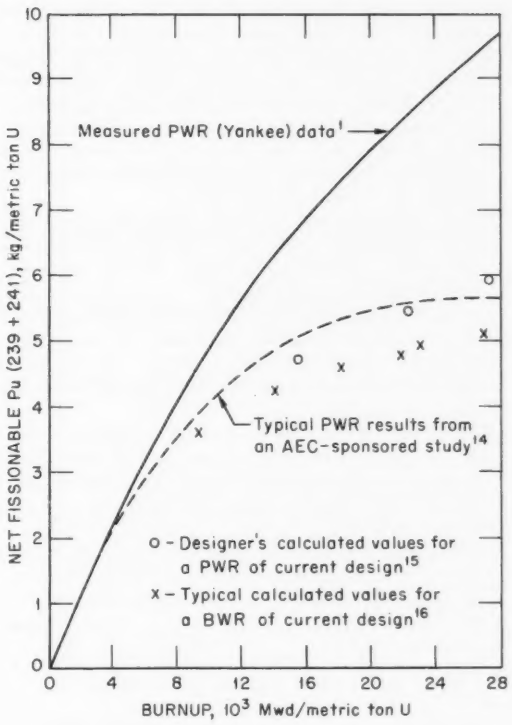

Fig. 10 Fissionable plutonium content of spent UO_2 fuel as a function of exposure.

with reported predictions for the current reactors. These differences may be real because of different physical properties of the designs, but this can be verified only through further measurements on irradiated fuel from the current designs. The reprocessing of fuel from water reactors of current design will provide valuable information, but these batch data will leave much to be desired from the point of view of understanding the reactor physics at a point within the core.

References

1. R. J. Nodvik, Evaluation of Mass Spectrometric and Radiochemical Analyses of Yankee Core I Spent Fuel, USAEC Report WCAP-6068, Westinghouse Electric Corp., Atomic Power Division, March 1966.
2. M. J. O'Boyle (Comp. and Ed.), Yankee Core Evaluation Program Quarterly Progress Report for the Period Ending June 30, 1966, USAEC Report WCAP-6081, Westinghouse Electric Corp., Atomic Power Division, August 1966.
3. M. J. O'Boyle, Yankee Core Evaluation Program Semiannual Progress Report for the Period Ending March 31,

1967, USAEC Report WCAP-6083, Westinghouse Electric Corp., Atomic Power Division, August 1967.
4. M. R. Hackney and C. P. Ruiz, Heavy Element Isotopic Analysis of UO_2 Fuel Irradiated in the VBWR, Report No. 1, USAEC Report GEAP-4107, General Electric Co., Atomic Power Equipment Department, Dec. 28, 1962.
5. C. F. Griggs and R. Richmond, ARGOSY Results for the Long-Term Irradiation Changes in the Calder Hall Reactor, British TRG-Report-917, Jan. 6, 1965.
6. M. J. Halsall, Graphs and Tables of the Isotopic Composition of Plutonium Produced in Canadian D_2O Cooled and Moderated Reactors, Canadian Report AECL-2631 (CRRP-1245), October 1966.
7. M. G. Balfour (Ed.), Postirradiation Examination of CVTR Fuel Assemblies, Quarterly Progress Report for the Period Ending September 30, 1967, USAEC Report WCAP-3850-1, Westinghouse Electric Corp., Atomic Power Division, October 1967.
8. M. G. Balfour (Ed.), Postirradiation Examination of CVTR Fuel Assemblies, Quarterly Progress Report for the Period Ending December 31, 1967, USAEC Report WCAP-3850-2, Westinghouse Electric Corp., Atomic Power Division, March 1968.
9. M. G. Balfour (Ed.), Postirradiation Examination of CVTR Fuel Assemblies, Semiannual Progress Report for Period Ending June 30, 1968, USAEC Report WCAP-3850-3, Westinghouse Electric Corp., Atomic Power Division, August 1968.
10. R. S. Miller and J. B. Roll, Saxton Plutonium Program, Semiannual Progress Report for the Period Ending December 31, 1967, USAEC Report WCAP-3385-14, Westinghouse Electric Corp., Atomic Power Division, March 1968.
11. R. F. Barry, LEOPARD—A Spectrum-Dependent Nonspatial Depletion Code for the IBM-7094, USAEC Report WCAP-3269-26, Westinghouse Electric Corp., Atomic Power Division, September 1963.
12. M. F. Valerino and Z. R. Rosztoczy, Analytical and Experimental Methods of Determining Heavy-Isotope Content of Operating Fuel Elements, USAEC Report CEND-540, Combustion Engineering, Inc., Sept. 30, 1965.
13. G. M. Inman, Research and Development for Safeguards, USAEC Report WASH-1122, Dec. 1, 1968.
14. Z. R. Rosztoczy and R. Kern, Setup of ISOCHECK Method for Determining Heavy-Isotope Content in the Operating Fuel Elements of Connecticut Yankee Core 1, USAEC Report CEND-287, Combustion Engineering, Inc., Dec. 30, 1966.
15. *Nucleonics Week*, Vol. 8, No. 3 (Jan. 19, 1967). (Information used by special permission of *Nucleonics Week*; copyrighted (C) 1967 by McGraw-Hill Publishing Company, Inc., New York, N. Y. 10036.)
16. R. L. Crowther et al., Plutonium Utilization in Boiling-Water-Reactor Power Plants, in Commercial Plutonium Fuels Conference, March 1–2, 1966, Washington, D. C., USAEC Report CONF-660308, p. 229.

Computer Methods for Utility-Reactor Physics Analysis

By E. G. Adensam, J. H. Bell, H. L. McCullough, and M. Raber*

Abstract: *Many computer codes have been developed to assist the reactor physicist in the design of light-water-reactor cores and the analysis of fuel cycles. This paper presents a brief description of the calculation models and computer codes commonly used to obtain cross-section data, reactivity, power distribution, burnup effects, etc. A comparison of computer codes used in each of these areas is made.*

The recent growth of the commercial nuclear power industry has led to widespread interest in the analytical techniques and computer codes for reactor physics analysis. This article gives a brief description of the types of calculations that must be performed to determine and predict the physics behavior of light-water-reactor cores. Some of the major computer codes that have been used to date are described, and the relative merits of different codes developed to perform the same function are discussed.

Most of the codes mentioned were developed by reactor manufacturers, national laboratories, and organizations involved in the Naval Reactors program. The material presented was obtained from reports published by these organizations and others engaged in the analysis of reactor cores. Most organizations involved in the physics analysis of light-water reactors have proprietary versions of some of the codes discussed. These proprietary versions invariably include improvements to the basic calculation model or user convenience features, and no attempt has been made to discuss them in this article.

Description of Physics Calculation Models

Overall Calculation Approach

The objective of nuclear analysis work is to provide the fuel designer or reactor operator with the information needed to make appropriate management decisions concerning the design, operation, safety, and economics of the reactor plant, including:

1. Fuel assembly and core design specifications.
2. Reactor plant operating characteristics.
3. Optimum management programs for fuel and for poison control.
4. Heavy-element isotopic inventory data.
5. Fuel-cycle economics data.

The starting point for these calculations is an actual or postulated set of reactor design characteristics, including material compositions, dimensions, temperatures, and thermal-hydraulic parameters. The overall problem of establishing the distribution of neutrons in three space dimensions, in time, and in neutron energy must be broken down into a number of smaller, related segments, each of which is small enough and simplified enough to be economically solvable with available techniques and computer codes. The knowledge and experience of the reactor analyst is of paramount importance in evaluating the adequacy of the simplifying assumptions on which the calculation model is based.

Figure 1 shows schematically the types of calculations that must be performed to reach the goals listed above and the paths that the calculation effort may take. The first step after defining the reactor design characteristics is the generation of thermal-energy group and nonthermal (fast)-energy-group cross sections. A high degree of separability of spatial and energy effects is usually assumed; and in many cases, cross sections are generated for each core region under the assumption that the neutron-energy spectrum in that region is similar to that in a comparable region of

*Hittman Associates, Inc., Columbia, Md.

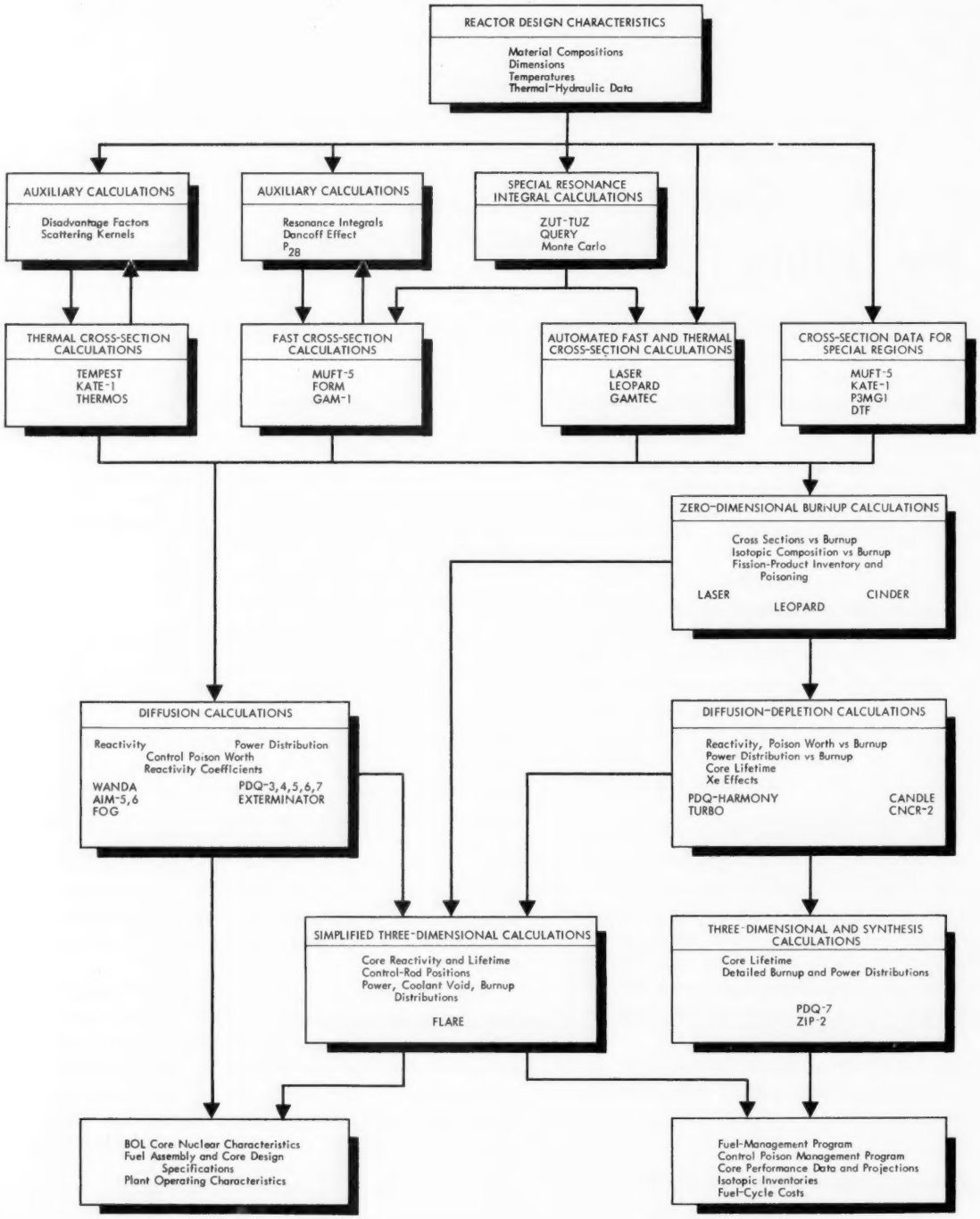

Fig. 1 Flow chart for nuclear analysis calculations.

infinite extent. Cross-section data are usually generated for one thermal group and one to three fast groups of neutrons. These cross sections are then input to a calculation of the spatial distribution of neutrons in each energy group, generally by means of one- and two-dimensional diffusion theory. At this point many of the beginning-of-life core nuclear characteristics may be established.

Fuel-burnup or -depletion calculations must then be performed to establish the variation of these characteristics over core lifetime. Again, a high degree of separability of spatial, energy, and time effects is usually assumed. Zero-dimensional (e.g., point or single fuel rod) burnup calculations may be performed to obtain the variation of neutron-energy spectrum and cross sections with burnup for various fuel regions. These calculations also yield isotopic composition data and estimates of reactivity changes as a function of burnup. One- and two-dimensional diffusion–depletion calculations are then performed to establish spatial effects as a function of burnup. To date, three-dimensional diffusion–depletion calculations have not been common because of their high cost. Instead, a three-dimensional representation of the reactor as a function of life is usually assembled from a series of two-dimensional and one-dimensional calculations using synthesis techniques.

Alternatively, a simplified three-dimensional, modified one-energy-group nodal calculation technique may be used to predict core behavior with burnup. A computer code called FLARE, which is based on this approach, is particularly suitable for boiling-water-reactor analysis because of its treatment of coupled nuclear and thermal-hydraulic effects. The output of the multidimensional burnup calculations consists in a prediction of core performance over lifetime, the information needed to optimize management of fuel and poison-control programs, and the information needed to establish fuel-cycle costs.

Figure 1 also shows the names of some of the computer codes that are used to treat the various segments of the core nuclear analysis problem. These codes, and the calculation models on which they are based, are described in the following subsections.

Generation of Nonthermal-Energy Cross Sections

Several calculational models are available for generating nonthermal-energy cross sections. These models differ in their approaches to slowing-down density calculations, resonance-absorption calculations, age calculations, and fast-fission effects.

The MUFT-type codes[1–3] have proved to be very popular. These codes solve the Fourier transformed (with respect to space) Boltzmann equation expanded in spherical harmonics, using either the P_1 or B_1 approximation, to obtain the first two Legendre coefficients of the neutron flux and the isotropic and anisotropic components of the slowing-down densities owing to a cosine source in space. The energy range from 10 Mev to 0.625 ev is treated in 54 groups. Since neutron mean free paths are long in this energy range, single fuel-rod cells or groups of cells may be homogenized on a volume basis for treatment in MUFT.

The various MUFT codes permit several slowing-down approximations.[4,5] Hydrogen may be treated exactly or in a Selengut–Goertzel approximation. Heavy-element slowing-down contributions may be determined by age or Greuling–Goertzel approximations.[6] Two possible approaches to this heavy-element contribution to slowing down are:

1. MUFT-4: the contributions of all heavy nuclides are lumped together, and coefficients of the heavy-element Greuling–Goertzel slowing-down equations are sums and averages of the coefficients of what would be the individual isotopic equations.
2. MUFT-5: the slowing-down density is calculated separately for each isotope.

Slowing down of neutrons by inelastic scattering is assumed to be isotropic and is determined using inelastic scattering matrices that are included in the MUFT code libraries.[5] No provision is made for explicitly calculating $(n,2n)$ reactions, although some current libraries include modified values of ν to account for this contribution.[8] Absorption resonance integrals are calculated using the narrow resonance infinite-mass approximation with resonance parameters available from the accompanying library tape. Correction for resonance self-shielding, the Dancoff effect, and Doppler broadening is made by the use of an input "L factor." The correct L factor may be determined by running several MUFT cases with different input L factors until an absorption resonance integral or a resonance escape probability for ^{238}U is calculated which corresponds to a correct value that is determined separately. This may be done, for example, by the method of Hellstrand.[9,10] Goldman[11] and Steen and Hanson[12] have developed procedures that could be included in the MUFT resonance calculation to account for Doppler broadening effects and heterogeneity effects. The LASER[13] and LEOPARD[14] codes, which utilize the MUFT method for computing nonthermal cross sections, contain an automatic itera-

tion procedure for the ^{238}U L factor to obtain agreement with the parameter ω (ratio of nonthermal captures in ^{238}U to neutrons thermalized) as calculated using Strawbridge's procedure.[15] The LEOPARD code incorporates a heterogeneity correction to the flux in the first 10 energy groups to improve predictions of the fast-fission reaction rates.

Another model frequently used to generate nonthermal cross sections is that embodied in the GAM-type codes.[16-18] These codes also calculate a neutron-slowing-down spectrum using a P_1 or B_1 approximation to the Fourier transformed Boltzmann equation. The GAM codes treat the energy range from 10 Mev to 0.414 ev in 68 energy groups, each of which has a lethargy width of 0.25. In contrast to MUFT, however, representation of scattering kernels is exact for all isotopes in the GAM codes through the inclusion of a full scattering matrix for both the P_0 and P_1 scattering terms for each isotope. Inelastic scattering and $(n,2n)$ processes are included. A moments age calculation in an infinite homogeneous medium may be included. Resonance absorption is calculated by the method of Adler, Hinman, and Nordheim[19] for any isotope that has resonance parameters in the library, except in GAM-I where only ^{238}U and ^{232}Th are treated by this method. Fast-fission corrections are calculated by an n flight-collision-probability technique in GAMTEC.

In both the MUFT and GAM codes, few-group cross sections are obtained by averaging the multigroup library data over the computed flux spectrum. These few-group cross sections may then be used in diffusion or transport calculations.

Neither the MUFT nor the GAM codes can treat the detailed spatial variation of the neutron slowing-down spectrum and therefore are not always adequate for generating few-group data for core regions such as thin water channels, structure regions, and regions near the core–reflector interface. In these regions, spatial and energy effects are not readily separable, and multigroup spatial calculations may be required to determine the correct neutron spectrum for use in computing few-group cross sections.

The P3MG1 code[20] solves the multienergy transport equation in one dimension using the P_1 or P_3 approximation to compute nonthermal fluxes in slab geometry, and the P_1 or "simplified P_3" approximation to compute these fluxes in spherical or cylindrical geometry. Fifty-four nonthermal groups plus one thermal group are provided. Inelastic scattering and resonance absorption are calculated as in the MUFT-5 code. Slowing-down densities are calculated using the Greuling–Goertzel approximation. The P_3 elastic scattering by hydrogen is treated exactly, but heavy-element slowing down is computed for only the P_0 and P_1 components unless P_2 and P_3 scattering cross sections are input on cards. Fission and inelastic scattering terms are treated as isotropic. The P3MG1 code operates with a microscopic cross-section library similar to that used with the MUFT-5 code.

A spatial model employing GAM-type multigroup cross sections may be obtained using (for example) GAMTEC and DTF. Cross sections are calculated by GAMTEC for up to 33 nonthermal groups plus 1 thermal group and punches these data on cards suitable for input to DTF, a one-dimensional transport code that solves the Boltzmann equation in slab, cylindrical, or spherical geometry using the S_n technique.[21,22] The complete energy-transfer matrices calculated by GAMTEC may be input to DTF.

Generation of Thermal-Energy Cross Sections

In contrast to the nonthermal-energy regime in which neutron–nuclei collisions always result in a loss of kinetic energy by the neutron, a neutron may either gain or lose kinetic energy as a result of a collision in the thermal-energy regime. This thermal-energy regime or "thermal group" of neutrons extends from zero energy to some arbitrarily selected cutoff energy which is chosen to be sufficiently high so that the scattering of neutrons from below the cutoff to energies above the cutoff is a negligible effect. This cutoff energy E_c may be chosen to depend on the medium properties (e.g., four times an effective neutron temperature[23]) or it may be selected as a constant. Typical cutoff energies range between 0.4 and 0.7 ev, although cutoff energies as high as 1.855 ev are used in some calculation models. The cutoff energy for the thermal cross-section calculation must be equal to the lower energy bound of the nonthermal cross-section calculation model selected.

The problem of generating thermal group cross sections involves determining an appropriate neutron-flux spectrum $\Phi(E)$ over the thermal-energy range and averaging cross sections over this flux spectrum to obtain (for a homogeneous system):

$$\bar{\Sigma} = \frac{\int_0^{E_c} \Sigma(E)\,\Phi(E)\,dE}{\int_0^{E_c} \Phi(E)\,dE}$$

A number of reviews are available in the literature[24-26] which describe how $\Phi(E)$ may be determined from the Boltzmann neutron-balance equation

under various assumptions regarding the form of the scattering kernel (probability of scatter between two energies) and scattering isotropy. The following simplified models that apply to the scattering of neutrons by a monatomic gas medium are often used:

1. Maxwell–Boltzmann distribution, which applies to a medium with zero absorption.
2. Wigner–Wilkins model,[27] which applies to a free gas having unit neutron mass and allows for absorption.
3. Wilkins model,[28] which applies to a free gas having effectively infinite mass and which also allows for absorption.

The computer codes SOFOCATE,[29] KATE-1,[30] and TEMPEST[31] were written to compute neutron spectra using one or more of these models. These codes utilize libraries of absorption, fission, and transport cross sections with data tabulated at a fine energy mesh between zero energy and some upper limit (usually 2 ev) to compute the neutron spectrum using the selected model. They then average both macroscopic cross sections for the medium and microscopic cross sections for selected nuclides over this spectrum. Any value of E_c less than the limit of the tabulated data may be called for. The Wigner–Wilkins model is most commonly used for light-water reactors.

Light-water power reactors are generally made up of regular arrays of fuel rods with intermittent regions of water or structural materials. In calculations of the gross spatial distribution of the neutron flux, it is generally impractical to explicitly represent fuel and cladding regions of individual fuel rods. The customary procedure is to define a "unit cell" consisting of a single fuel rod, its cladding, and the water associated with it in the regular portion of the lattice. Cross-section data derived for this appropriately homogenized cell may then be used for relatively large regions of the reactor core. In the thermal-energy regime, the heterogeneity of the cell must be taken into account in deriving the cross sections. The following typical procedure is followed:

1. The cell boundary, which is usually hexagonal or square, is converted into a circle, with material volumes being conserved. The cell is now considered to consist of three or four concentric regions; fuel, optional gas space, cladding, and moderator.
2. A neutron-flux distribution is computed throughout the cell. Since fuel rods are generally strongly absorbing, diffusion theory is inadequate, and one-velocity P_3 or S_4 transport calculations are commonly used. Alternatively, the method of Amouyal, Benoist, and Horowitz (ABH method) may be used.[32] Cross sections for these calculations may be obtained using the method outlined in Ref. 23, Westcott's tabulations,[33] or simple Maxwellian averages. A reflection outer boundary is assumed in the spatial calculations.
3. The cell is converted into an equivalent homogeneous medium by flux- and volume-weighting the atom densities of the actual regions. These homogenized-cell atom densities are then input to the spectrum calculation.

It is generally desirable to iterate between the flux-distribution calculation and the spectrum calculation by using the TEMPEST or KATE output cross sections to compute a new flux distribution, which is then used to compute new homogenized atom densities for input to a second spectrum calculation, etc. This process generally converges rapidly, particularly with low-enriched-uranium systems. Serious errors may sometimes result if this iteration process is not carried out, particularly for plutonium systems.[34] Even with iteration, values of ηf are usually overestimated with this approach.

The above procedure is an attempt to divide the problem of thermal-neutron distribution in a heterogeneous system into separate spatial and energy effects. A more rigorous treatment of space–energy effects may be obtained with the THERMOS code,[35] which solves the integral neutron transport equation in up to 30 energy groups over the thermal-energy range. The THERMOS code can use more exact forms of the monatomic-gas scattering kernel than the Wigner–Wilkins model, or it can use the still more exact Nelkin scattering kernel,[36] which considers in some detail the motions of hydrogen atoms in water. The THERMOS code may be applied to both homogeneous and heterogeneous systems to obtain neutron spectra, spectrum-averaged cross sections, and flux distributions.

The THERMOS code with the Nelkin kernel is probably the most accurate of the methods that may be considered common design tools for the computation of thermal-neutron spectra and cross sections. Significant differences in reactivity have been observed between this model and the simpler model described above based on KATE or TEMPEST, particularly when plutonium is present.[17,37] The LASER code, which is a combination of MUFT and THERMOS, has been designed to take advantage of the capability of THERMOS to accurately treat plutonium systems by careful selection of the group structure to represent the thermal-energy cross-section resonances in the plu-

tonium isotopes in considerable detail. The thermal cutoff is taken to be 1.855 ev to permit treatment of the 1.05-ev resonance in ^{240}Pu within the THERMOS model. The THERMOS calculation is expanded to 35 energy groups in LASER, and provision is made for an isotropic scattering ring around the cell boundary and the use of a transport-corrected scattering kernel. These two items significantly increase the accuracy of computed flux distributions.[26] Comparison of LASER calculations of PuO_2–UO_2 and UO_2 critical experiments indicates that more accurate results are obtained with the Nelkin kernel than with the Wigner–Wilkins free gas kernel. Values of k_{eff} obtained with the free gas kernel tend to be several tenths of a percent higher than those obtained with the Nelkin kernel.[36,38] The chief disadvantages of the THERMOS model are the longer computer times than those required for Wigner–Wilkins model calculations and the need to generate temperature-dependent Nelkin scattering-kernel data separately. These may be conveniently generated by a code called GAKER.[35]

An approximate method of treating space-energy effects by means of multigroup disadvantage factors has also been used[15] and is incorporated into the LEOPARD code. In this approach, disadvantage factors are computed using the ABH method at each of a large number of energies below the chosen cutoff energy. In LEOPARD these calculations are performed at 172 energies between zero and 0.625 ev. Flux- and volume-weighted macroscopic cross sections are then determined at each energy. These energy-dependent macroscopic cross sections are used in a normal spectrum calculation for a homogeneous medium (e.g., SOFOCATE or TEMPEST calculation), and spectrum-averaged cross sections are also computed. This technique lies somewhere between the one-group disadvantage-factor approach and the THERMOS approach in both accuracy and computer time required.

At least one reactor manufacturer utilizes the Mixed Number Density (MND) thermal-activation model.[39] This model corrects for the discontinuity of thermal activations due to a discontinuity in microscopic cross sections at an interface between two media whose cross sections have been determined by separate Wigner–Wilkins model calculations for asymptotic spectra. In effect, the values of D, $\nu\Sigma_f$, and Σ_a used in diffusion calculations are redefined to convert the usual flux-continuity boundary condition in the diffusion calculation to an activation ($\sigma\Phi$)-continuity condition. Also, values of D averaged over a Maxwellian spectrum rather than a Wigner–Wilkins spectrum are used for the reasons described in Ref. 39. The MND model appears to improve predictions of flux peaking near water channels. The KATE-1 and LEOPARD codes are most convenient for generating MND constants.

Reactivity and Power Distributions

The following categories of calculation models are available for the prediction of reactivity and power distributions.[40]

1. Zero dimensional.
2. One dimensional.
3. Two dimensional.
4. Three dimensional.
5. Synthesis techniques.

Zero-dimensional calculations neglect gross spatial effects and are considered useful primarily for survey applications. These calculations treat the reactor as if it were essentially a point reactor by performing neutron-spectrum and reaction-rate calculations on a typical unit fuel-rod cell that is representative of the whole reactor. Since power reactors are somewhat heterogeneous (e.g., they contain regions other than a regular array of fuel-rod cells), a zero-dimensional code greatly oversimplifies the actual physical situation. This model is unable to accurately predict neutron leakage out of the core or between core regions because of the lack of a proper core geometry and composition description and because leakage depends on the flux shape that is not explicitly considered. For this reason, zero-dimensional calculations are particularly difficult to apply to a core containing more than one enrichment zone. However, by properly coupling a geometric buckling with the unit-cell calculations, k_{eff} values can be determined and will indicate reactivity behavioral trends.

Any of the cross-section codes discussed in preceding subsections can be used for zero-dimensional calculations of reactivity. The automated codes that treat both the thermal- and nonthermal-energy regimes are particularly well suited for this purpose. These codes compute a value of k_{eff} based on an input geometric buckling. In addition, LASER will search for the concentration of boron in the moderator that yields criticality for a given input value of buckling. The LEOPARD code can take into account in an approximate manner the effects of portions of the core other than unit fuel-rod cells.

For most design work and almost all work on multiregion cores, a higher order model is desirable. The most commonly used models are based on one-,

two-, or three-dimensional solutions to the few-group (two to four groups) diffusion equations, with input few-group cross-section data generated using the codes described in preceding subsections. The adequacy of these models has been established by numerous checks against critical-experiment data and actual core operating data.[41-44]

In making use of one-dimensional diffusion codes, we assume a high degree of directional separability of spatial effects. If calculations are performed in the radial direction, the core is represented by a set of homogeneous concentric cylindrical regions whose dimensions are derived from actual core-region dimensions on a volume-conservation basis. Since most power-reactor cores are made up of square fuel assemblies and have irregular core boundaries, some geometric distortion is inevitable. A transverse geometric buckling is used to account for axial leakage effects, and the computed radial flux distributions are assumed to be representative of all axial planes. When the gross axial flux pattern is of interest, a one-dimensional calculation is performed in the Z-direction. The $X-Y$ flux variations are then neglected, and radial leakage is approximated by a transverse geometric buckling. Control materials may be treated by placing them as discrete radial zones or as equivalent homogeneously distributed poison. In practice, the more uniform the core, the better the results of a one-dimensional calculation.

WANDA-5,[45] AIM-5,[46] AIM-6,[47] and FOG[48] are typical one-dimensional diffusion codes. Each can be used for slab, cylindrical, or spherical geometry. In the FOG code and in the WANDA series of codes, a maximum of four groups is permitted, but slowing down is allowed only from each group to the next lowest energy group. This is consistent with the type of slowing-down cross sections edited by the MUFT codes but not necessarily consistent with those edited by the GAM codes. The latter codes edit a complete matrix of downscatter cross sections, including cross sections for direct transfer from group 1 to group 3, group 1 to group 4, etc. If a few-group structure having significant group skipping is used, GAM-derived cross sections must be redefined (as described in Ref. 49, for example) for use in WANDA. The boundary conditions in WANDA are limited to zero flux and zero current.

The AIM codes are more flexible than the WANDA codes. Up to 12 energy groups can be specified in AIM-5 and up to 18 energy groups in AIM-6. The complete downscatter matrix is allowed, and thus the convenient use of either MUFT-derived or GAM-derived cross sections is permitted. Input-specified current-to-flux ratio boundary conditions, which are convenient for treating control rods or a vacuum interface condition, are allowed in addition to the zero-flux and zero-current boundary conditions. Macroscopic cross sections must be supplied as input to AIM-5, but the AIM-6 code may be used with a library of microscopic data.

Most one-dimensional codes permit several types of criticality searches, including:

1. Buckling (in particular regions or for the entire reactor).
2. Concentration of homogeneously distributed poison (in particular regions or for the entire reactor).
3. Region or core dimensions.
4. Position of the interface between two regions.

Two-dimensional diffusion calculations greatly reduce the degree of assumed directional separability of spatial effects. Single fuel assemblies, large fractions of a core, or an entire core may be represented in considerable detail, including explicit representation of water slots, control rods, instrument locations, and fuel regions. Calculations may be performed in $X-Y$, $R-Z$, $R-\theta$, or hexagonal geometry, depending on the code selected. The PDQ[50-53] series of codes, which permit calculations with up to four energy groups, is frequently used. The later codes in this series were written for computers of increasingly greater capability and therefore permit the specification of greater numbers of mesh points and material regions than the earlier codes. Improved mathematical techniques in the later codes lead to reduced running time and cost. Zero-flux and zero-current boundary conditions are available in all versions. The PDQ-4 and earlier versions permit a logarithmic-derivative boundary condition that is convenient for treating control rods. A rotational-symmetry boundary condition that is sometimes convenient for partial-core models is available in PDQ-4 and later versions. The PDQ codes permit downscatter to only the next lowest energy group, as discussed above for WANDA. Flux-weighted average values of region-dependent parameters are edited in addition to regionwise and pointwise flux and power distributions.

EXTERMINATOR and EXTERMINATOR-2[54] are multigroup codes that allow downscatter from any of up to 50 groups to any other group. Four different boundary conditions are included as options; zero flux, zero current, periodic, and logarithmic, either along boundaries or internal to the mesh. EXTERMINATOR-2 is the FORTRAN-IV improved version of EXTERMINATOR with added features. For example, eigenvalue problems can be run in which the eigenvalue

can be a nuclide density. The EXTERMINATOR codes are improvements over the slower few-group diffusion code, TWENTY-GRAND.[55]

Codes that provide true three-dimensional solutions of the few-group diffusion equation are available,[56] but their use has been limited because of the very long computer times required and the correspondingly high cost. Synthesis methods,[7,57-59] which involve combining two-dimensional and one-dimensional calculations into a three-dimensional representation of the core have been developed as a more economical substitute for three-dimensional calculations. Three types of synthesis calculations are used: single-channel, multichannel, and variational techniques. These models differ in the degree of assumed separability of radial and axial flux distributions. The fundamental assumption in the simple single-channel synthesis is that of complete regionwise separability of the flux distribution into axial and radial components. Sets of radial calculations are performed with a two-dimensional diffusion code, utilizing transverse geometric-buckling values that are regionwise constant to represent the axial leakage. Flux- and volume-weighted cross sections for each distinct horizontal plane of the core are obtained and input to a single axial calculation that is used to relate the radial calculations to each other. This axial calculation is performed using regionwise constant radial buckling values. The weighted product, regionwise, of the radial and axial solutions, yields an approximation to the true three-dimensional flux.

Multichannel synthesis[7] differs from the single-channel technique in that several flux distributions parallel to the Z-axis are computed simultaneously. Leakage between channels is represented as a linear combination of channel fluxes. The coefficients of combination are determined from detailed flux calculations in $X-Y$ planes. The basic assumption in multichannel synthesis is that local flux variation in several regions is separable with respect to the relative flux levels in these regions (or channels). The number of channels and $X-Y$ zones required depends upon desired accuracy and the degree of flux-separability characteristics of the configuration.

The most recently developed code is PDQ-7,[60] which solves the few-group neutron-diffusion equations in one, two, or three dimensions. Adjoint solutions are available, and two overlapping thermal groups may be used in one- and two-dimensional problems. These may be used to describe a spatially dependent thermal-neutron spectrum as a linear combination of overlapping hard and soft spectra. The geometry may be rectangular, cylindrical, or spherical in one dimension; rectangular, cylindrical, or hexagonal in two dimensions; and rectangular or hexagonal in three dimensions. All geometries provide for variable mesh spacing in all dimensions. Zero-flux, zero-current, and rotational-symmetry boundary conditions are available; and boundary-value problems may be solved by specifying the flux values on one or more boundaries. Only five energy groups can be specified, including the two thermal groups. This code requires a CDC-6600 computer, plus a special input/output package, and should be more economical than earlier three-dimensional codes.

Fuel-Depletion and -Burnup Effects

Calculations of fuel-depletion and -burnup effects fall into the same categories listed in the preceding subsection for reactivity and power-distribution calculations. LEOPARD and LASER are examples of zero-dimensional depletion codes. After computing cross-section and reaction-rate data for a unit fuel-rod cell, these codes solve the uranium-depletion and plutonium-buildup equations to obtain a new fuel composition after a specified burnup (or time) interval. A succession of burnup steps may be calculated automatically. The neutron spectrum, cross sections, and reaction rates are recalculated for each step. LEOPARD assumes a spatially uniform fuel composition at each time step, whereas LASER explicitly considers the spatial variation of isotopic composition within a single fuel rod. These codes are very useful for generating cross sections as a function of depletion for use in few-group diffusion calculations to determine reactivity and power distributions as a function of core life. They yield an indication of the rate of change of reactivity with burnup and also the variation of heavy-element isotopic composition with burnup. In theses codes the poisoning effects of xenon and samarium are treated explicitly, but other fission products are treated as a single aggregate.

More accurate calculations of burnup effects, including reactor lifetime, fuel concentrations as a function of time, and flux and power distributions as a function of time, can be performed with diffusion–depletion codes. These codes perform three types of calculations:

1. Macroscopic cross sections are assembled for each point in the mesh from an input library of microscopic cross sections and self-shielding factors and either input atom densities (first time step) or atom densities computed in the previous time step.

2. The few-group diffusion equations are solved to obtain flux distributions.

3. New isotopic atom densities are calculated at each point in the mesh for a given power–time interval using the computed flux distribution.

The flux is assumed constant at each point during each time interval and is recalculated in each succeeding step. Microscopic cross-section and self-shielding factor data may be computed using any of the cross-section codes described in preceding subsections but are computed most conveniently with LASER or LEOPARD. Most diffusion–depletion codes permit the specification of burnup-dependent values of cross sections and self-shielding factors for at least a limited number of important isotopes.

CANDLE[56] and CNCR-2[61] are one-dimensional diffusion–depletion codes based on the WANDA spatial calculation. The CANDLE code allows up to four energy groups and takes its fast-group microscopic data from a library that may be changed at execution time. Constant self-shielding factors may be specified for the thermal group for most isotopes. Time-dependent self-shielding factors are allowed for ^{235}U in the thermal group and for ^{10}B both in the thermal and in the epithermal groups. A total of 13 time-dependent isotopes is allowed, excluding ^{232}Th, ^{233}U, ^{234}U, and ^{242}Pu. Xenon and samarium are treated individually, whereas the rest of the fission products are grouped into one or two aggregates. Several criticality-control searches are available, including a poison-concentration search, a buckling search, and a movable interface between poisoned and unpoisoned regions.

CNCR-2 is a modified version of CANDLE that can take into account the dependence of the ^{238}U resonance escape probability on spatially varying water density and spatially varying power density. A water-density-dependent poison-control search is also provided. The code is useful for boiling-water-reactor calculations. Variable self-shielding factors are allowed only for ^{235}U and ^{10}B.

For two-dimensional burnup calculations, the TURBO[56] code has been used extensively. This code is based on a two-dimensional PDQ-3 or PDQ-4 diffusion calculation for flux distributions and either library-tape or card-input cross sections. Core parameters such as power level and transverse buckling can be changed at any time step. Different fuel arrangements may be studied by changing number densities at any time step. TURBO*[62] is a modified version of TURBO for the IBM-7090 computer. These codes contain no search options.

The HARMONY[63] code is a model-independent depletion system. It can be used with one-, two-, or three-dimensional few-group diffusion codes. Originally, HARMONY was used with the PDQ-5 and PDQ-6 two-dimensional codes, but its use has been extended to PDQ-7. Any of the cross sections or self-shielding factors used in the spatial or depletion calculations may be represented as time dependent. Isotopic depletion and fission-product chains are specified by the user. The total number of depletable isotopes is limited only by the computer storage requirements. Provision has been made to adjust the thermal flux level at specific times within the basic interval to approximate constant-power operation. Each renormalization interval may be divided into subintervals. The number of subintervals may vary from point to point. Compositions may be replaced at any time in a depletion study to investigate the effects of fuel rearrangements.

The ASSAULT[64] code is a multigroup one- or two-dimensional diffusion–depletion code based on the EXTERMINATOR code for flux-eigenvalue solutions. Most of the features of EXTERMINATOR are included, in addition to user-specified nuclide chains. Interlocked chains and high-energy $(n,2n)$ product chains can be treated. Compositions may be changed as a function of time to facilitate fuel-cycling studies.

Three-dimensional few-group diffusion–depletion codes such as DRACO[56] and PDQ-7 are available, but running times are usually prohibitive. Synthesis techniques for lifetime studies are more common. One of the most widely used synthesis techniques for depletion is the TURBO–ZIP combination. ZIP-2[57] is a one-dimensional few-group diffusion–depletion code based on WANDA which performs a single-channel synthesis as outlined in the previous section. Flux-weighted diffusion constants, macroscopic cross sections, and bucklings derived from TURBO calculations are input to ZIP as a function of the fraction of fuel (^{235}U) not burned. The code computes pointwise axial macroscopic cross-section data and then performs a slab-geometry WANDA calculation. A boundary-search routine to simulate control-rod motion is available. A depletion routine then computes pointwise variable fuel burnup and ^{135}Xe and ^{149}Sm poisoning.

The FLARE Code

The General Electric-developed FLARE code[65] is able to treat a reactor core in three dimensions in order

REACTOR AND FUEL-PROCESSING TECHNOLOGY, Vol. 12, No. 2, Spring 1969

Table 1 Computer Codes for Reactor Physics Analysis

Application	Code	Calculation model	Special features	Advantages	Disadvantages
Nonthermal energy cross sections	MUFT-4	B_1 or P_1 approximation to multigroup Fourier transformed Boltzmann equation; 54 groups			Does not account for resonance self-shielding, Doppler effect, or other heterogeneous effects internally. Edit limited to three groups.
	MUFT-5	Same as MUFT-4	Optional blackness coefficient edit	Heavy element slowing down density is determined separately for each isotope.	Same as MUFT-4
	FORM	Same as MUFT-4	Library may be changed at execution time	Arbitrary few-group output up to 24 groups.	Same as MUFT-4 except for edits.
	GAM-I	Same as MUFT-4; 68 groups. Adler-Hinman-Nordheim resonance treatment		Exact treatment of heavy element slowing down. Calculates multigroup cross section for up to 32 fast groups. Includes n, 2n and inelastic scattering matrices.	Calculates only U-238 and Th-232 resonance integrals. Self-shielding factors must be input for other nuclides.
	HRG	Same as GAM-I	Punches broad group cross sections for input to DTF and other codes	Calculates resonance integrals for any isotope having resonance parameters in the library. Edits data for up to 33 nonthermal groups.	
	GAMTEC-II	Same as GAM-I	Punches cross sections for input to DTF and other codes	Same as HRG. Heterogeneity correction for fast fissions.	
	LASER	Same as MUFT-4 50 groups to 1.855 ev	Critical buckling search	"L-factor" iteration to account for self shielding and Doppler broadening in U-238 resonances. Highly automated.	Limited to single fuel rod cell geometry. Fixed one and two fast group edit structure
	LEOPARD	Same as MUFT-4	Includes portions of core other than fuel rod cells in spectrum calculation. Punches cross section data for input to several codes	Includes "L-factor" iteration for U-238 and heterogeneity correction for fast fissions. Highly automated.	Fixed one and three fast group edit structure.
Nonthermal space-energy effects	P3MG1	One-dimensional multigroup spherical harmonics approximation, 55 energy groups		P_2 and P_3 scattering is allowed. Several boundary conditions are available.	MUFT-5 resonance treatment.
	*GAMTEC-DTF	GAMTEC to determine 34 group constants for input to multigroup, one-dimensional solution of transport equation by S_n method		Handles heavy element slowing down exactly. Higher order transport approximations than P3MG1 are possible.	Codes are not integrated. Fewer energy groups than P3MG1.
Thermal cross sections	SOFOCATE	Maxwellian or Wigner-Wilkins			Requires separate homogenization calculations

	KATE-1	Maxwellian or Wigner-Wilkins	Calculates average cross sections for an extra region or blackness coefficients for a control rod region	Convenient for MND constants.	Requires separate homogenization calculations.
	TEMPEST-II	Maxwellian, Wigner-Wilkins, or Wilkins			Requires separate homogenization calculations.
	THERMOS	Multigroup integral transport	Can use free gas or Nelkin kernel	True space-energy calculation. More accurate, particularly for Pu systems.	Requires more computer time than simpler models.
	LASER	THERMOS	1.855 ev cutoff. Model tailored to handle Pu resonances.	Probably most accurate of automated code models.	Requires more computer time than simpler models.
	LEOPARD	Multigroup ABH disadvantage factors and SOFOCATE		Automated. Convenient for MND constants. Good compromise between accuracy and speed.	
	GAMTEC-II	One group P_3 calculation of disadvantage factors and TEMPEST		Automated. Can handle up to 17 concentric cylindrical regions.	No iteration between disadvantage factor and spectrum calculations.
Reactivity and power distributions	LEOPARD	Zero-dimensional - fuel rod cell plus extra region		Treats extra region outside fuel rod lattice.	No data on power distribution.
	LASER	Zero-dimensional - fuel rod cell only	Critical buckling search. Search for critical boron concentration in moderator.		Restricted geometry. No data on power distribution.
	GAMTEC-II	Zero-dimensional - unit cell with up to 17 concentric cylindrical regions		Relatively flexible geometry.	No data on power distribution.
	WANDA-5	Few group one-dimensional diffusion, three geometries	Criticality searches on buckling, poison concentration, region interface location	Simplified input.	Up to four groups. Input must be macroscopic data. Limited choice of boundary conditions. One group downscatter.
	AIM-6	Multigroup one-dimensional diffusion, three geometries.	Criticality searches on buckling, nuclide concentration, region interface location, region dimensions. Can utilize library of microscopic cross sections. Adjoint calculations.	Up to 18 groups. Complete downscatter matrix. Wide choice of boundary conditions.	
	AIM-5	Same as AIM-6	Same as AIM-6	Up to 12 groups. Complete downscatter matrix.	
	FOG	Few group one-dimensional diffusion, three geometries	Adjoint calculations. Various criticality searches.		Input data must be macroscopic. One group downscatter. Up to four groups.
	PDQ-2	Few group two-dimensional diffusion in X-Y or R-Z geometry. Two to four energy groups	Logarithmic derivative boundary condition.	Up to 6500 mesh points.	Macroscopic input data required. One group downscatter.

*Other GAM-type codes and S_n codes may be used.

(Table continues on the next page.)

Table 1 (Continued)

Application	Code	Calculation model	Special features	Advantages	Disadvantages
	PDQ-3	Same as PDQ-2	Adjoint calculations. Logarithmic derivative boundary condition.	Faster than PDQ-2. More extensive edits. Up to 7500 mesh points.	Same as PDQ-2. X-Y geometry only.
	PDQ-4	Same as PDQ-2, one to four energy groups	180 degree rotational symmetry boundary condition. Logarithmic derivative boundary condition.	Faster. Up to 20,000 mesh points.	Same as PDQ-2.
Reactivity and power distribution	PDQ-5	Same as PDQ-2, one to four energy groups	Rotational symmetry boundary condition. Adjoint calculation.	Extensive edits. Up to 50,000 mesh points.	Same as PDQ-2. No logarithmic derivative boundary condition.
	PDQ-6	Same as PDQ-5, hexagonal geometry only	120 degree rotational symmetry boundary condition. Adjoint calculation.	Same as PDQ-5. Up to 30,000 mesh points. Variable mesh in hexagonal geometry.	Same as PDQ-2.
	EXTERMINATOR-2	Multigroup two-dimensional diffusion in X-Y, R-Z, or R-θ geometry	Adjoint calculation. Logarithmic derivative boundary condition. Nuclide concentration search.	Up to 50 groups. Scattering from any group to any other group. Calculates flux-weighted microscopic cross sections.	
	PDQ-7	Few group diffusion in one, two, and three dimensions	180 degree rotational symmetry boundary condition. Two overlapping thermal groups.	Variable mesh spacing in all dimensions. True three-dimensional calculations.	
Reactivity, burnup, power distribution	FLARE	Three-dimensional, one energy group nodal calculation	Automatic iteration on coolant void distribution for BWR's.	Short running time. Convenient for fuel and control poison management calculations	Simplified model. Not accurate enough for detailed design work.
Fuel burnup effects	LASER	Explicit treatment of one fuel rod cell	Spatial variation of isotopic composition in one fuel rod is treated explicitly. Linear or nonlinear burnup equations may be used. Recalculates neutron spectrum as a function of burnup.		
	LEOPARD	Zero-dimensional. Solves the sets of differential equations for U-238 and Th-232 chains	Recalculates neutron spectrum as a function of burnup.		
	CANDLE	Few group one-dimensional diffusion-depletion, two to four groups	Criticality searches on buckling, poison concentration, region interface location. Treats lumped burnable poison.	Uses library of nonthermal cross sections that may be changed at execution time.	Four-group microscopic data must always be input. One-group downscatter. Limited choice of boundary conditions.

Fuel burnup effects	CNCR-2	Same as CANDLE, two or four groups	Calculates spatial dependence of U-238 resonance escape probability on coolant density and power density. Criticality searches.	Same as CANDLE.	Same as CANDLE.
	TURBO	Few group, two-dimensional diffusion-depletion. PDQ-4 spatial calculation.		Power level, microscopic data, self-shielding factors, transverse buckling, and number densities may be manually changed after each time step.	Fixed system of depletion chains.
	HARMONY	Few group depletion system; can be used with PDQ-5, 6, 7		User-specified depletion chains. Great flexibility in specifying spatial and time dependence of cross sections and self-shielding factors.	
	ASSAULT	One- or two-dimensional multigroup diffusion-depletion. EXTERMINATOR-2 spatial calculation		Poison concentration criticality search. Multigroup. User-specified chains. Interlocked chains and (n, 2n) product chains can be treated.	
Depletion and synthesis	ZIP-2	Few group, one-dimensional diffusion-depletion. Slab geometry	Performs single channel synthesis by stacking X-Y calculations into a three-dimensional representation of core. Region interface location criticality search.	Cheaper than three-dimensional calculation.	Not as accurate as three-dimensional calculation.
Fission product poisoning	CINDER	General solution of time-dependent nuclide concentrations for up to 400 nuclides, 17 nuclides per chain		User can specify any fission product chain or fissile-fertile nuclide chain.	
Resonance Integrals	ZUT	Integral method, narrow resonance, or infinite mass approximation for resolved resonances		Handles a wide variety of temperatures, compositions, and geometries.	
	TUZ	Resonances are defined by an average over a Porter-Thomas distribution of neutron widths		Same as ZUT	
	QUERY	Adler-Hinman-Nordheim method for resolved and unresolved resonances		Handles homogeneous and heterogeneous compositions of metal and oxide fuel.	

to predict reactivity, power and coolant-void distributions, and critical control-rod positions throughout the core lifetime by using very coarse-mesh spacings and by treating only one energy group of neutrons. FLARE permits a maximum of 14 by 14 by 12 nodes in $X-Y-Z$ geometry, with nuclear and thermal-hydraulic properties assumed to be uniform within a single node. These nodes may be used to represent all, one-half, or one-quarter of the core, depending on the prevailing symmetry. FLARE treats reflection at the surface of the core with an albedo, α, and employs transport kernels (which track neutrons for a distance of only one node) to represent the coupling between nodes. A choice of transport kernels is provided in the code so that the specific transport kernel and values for α can be chosen to give the best agreement with experimental data or more precise calculations (usually performed at zero exposure in two-dimensional geometry). FLARE performs calculations at the end of discrete burnup steps assuming that the power distribution during a burnup step is constant. The calculations consist in three levels of iteration: (1) source or power, (2) coolant void, and (3) burnup. In the void calculation the average steam quality at each node is calculated based on the inlet water velocity, inlet enthalpy, and the power distribution integrated from the bottom of the fuel assembly to the given node. Void fraction is then calculated from a numerical fit to a void–quality relation.[65,66]

Much of the input to FLARE consists of coefficients of polynomial expressions that fit the nuclear characteristics k_∞ and M^2 to node-wise values of fuel burnup, coolant-void fraction, and relative power (Doppler effect). Computer codes that may be used to supply data for this polynomial fitting are described in preceding subsections.

Improved, but proprietary, versions of FLARE are known to exist. FLARE has been expanded by United Nuclear Corporation into the code TRILUX.[67] TRILUX is capable of treating larger cores and calculating additional quantities such as burnout heat-flux ratio and nuclear material inventory distributions and uses more complicated forms to fit the dependence of k_∞ on nodal properties and exposure. Neutron model improvement is obtained by tracking neutrons beyond nodes adjacent to the source node. This increases the accuracy of predicted power distributions over that obtained with FLARE, especially in the regions of varying fuel composition and in the vicinity of reflectors.

Severe approximations are inherent in the basic FLARE model. However, comparisons of operating data with the predictions from FLARE and TRILUX indicate that this approach is satisfactory for many purposes. Typical standard deviations between experimental and predicted values of power distributions[40,68] using the FLARE code range between 3 and 9%, whereas agreement between measured values and values predicted by TRILUX are somewhat better.[67,69]

Other Calculations

Fission-Product Poisoning. All fuel-burnup calculations must take into account the poisoning of fission products, either explicitly as in diffusion–depletion calculations or implicitly as in the k_∞ data input to FLARE. In most cases ^{135}Xe and ^{149}Sm are treated individually, but all other fission products are lumped into one to three pseudoelements whose accumulation with burnup characterizes the poisoning effects of the remaining fission-product aggregate. Cross-section and yield data for pseudofission-product elements may be generated with a zero-dimensional burnup code such as CINDER.[70]

CINDER calculates the time-dependent concentrations of nuclides coupled in any linear sequence of radioactive decays and neutron absorptions in a specified neutron-flux spectrum. Chains for heavy isotopes and fission products and all physical data are specified by the user. As many as 99 time steps may be specified, during each of which the flux is held constant. The code handles up to four energy groups and up to 400 total nuclides. The output includes nuclide number densities, activities, macroscopic cross sections and barns/fission cross-section data.

Control-Rod Regions. Special techniques must be utilized to generate cross-section data for highly absorbing control-rod regions. One such technique, called "blackness theory," is described in Ref. 71. Although the computation of blackness coefficients and equivalent values of D and Σ_a for use in diffusion calculations is fairly simple for monoenergetic neutrons, the computation of spectrum-averaged data for the thermal- and epithermal-energy groups can be tedious. The MUFT-5 and KATE-1 codes have a special option for computing spectrum-averaged data for a control rod using the method described in Ref. 71. The spectrum calculated for the medium outside the control rods is used in the averaging process.

Resonance-Integral Calculations. The use of the MUFT-type codes with its input L factor requires some auxiliary method of establishing the resonance integrals

of isotopes in a particular system. Codes such as ZUT and TUZ[72,73] may be used to calculate these resonance integrals. ZUT calculates resonance integrals from resonance-parameter data for the resolved resonances for various geometries, temperatures, and compositions using the integral method, the narrow-resonance approximation, or the infinite-mass approximation for solution.[19] TUZ calculates resonance integrals for the unresolved resonances. QUERY[74] calculates both resolved and unresolved resonances using the method of Adler–Hinman–Nordheim.[19] Either homogeneous systems or heterogeneous metal or oxide systems may be treated.

Computer Codes

Table 1 presents a summary of computer codes that are commonly used in various aspects of light-water-reactor physics analysis. Many of these codes are available from the Argonne Code Center (see Ref. 75), the national laboratories, or independent consultants. Many are also available at commercial computer centers.

With the advent of remote data-transmissions terminals that can utilize telephone lines or leased communications lines, it is possible to select and conveniently use codes that are available at several different computer centers.

References

1. H. Bohl, Jr., M. G. Gelbard, and G. H. Ryan, MUFT-4—Fast Neutron Spectrum Code for the IBM-704, USAEC Report WAPD-TM-72, Westinghouse Electric Corporation, July 1957.
2. H. Bohl, Jr., and A. P. Hemphill, MUFT-5—A Fast Neutron Spectrum Program for the Philco-2000, USAEC Report WAPD-TM-218, Westinghouse Electric Corporation, February 1961.
3. D. J. McGoff, FORM—A Fourier Transform Fast Spectrum Code for the IBM-709, USAEC Report NAA-SR-MEMO-5766, Atomics International, Division of North American Aviation, Sept. 27, 1960.
4. D. H. Roy and R. L. Murray, Introduction to Slowing-Down Approximations in Neutron Transport Theory, Research Bulletin 2, University of North Carolina, June 1962.
5. R. L. Hellens, Neutron Slowing Down in Group Diffusion Theory, USAEC Report WAPD-114, Westinghouse Electric Corporation, May 1956.
6. E. Greuling, F. Clark, and G. Goertzel, A Multigroup Approximation to the Boltzmann Equation for Critical Reactors, USAEC Report NDA 10-96, Nuclear Development Associates, Inc.
7. A. Radkowsky (Ed.), *Naval Reactors Physics Handbook, Vol. I: Selected Basic Techniques*, Superintendent of Documents, U. S. Government Printing Office, Washington, 1964 (TID-7030).
8. M. Raber and E. G. Adensam, Library Manuals for Philco MUFT-5 and KATE-1 Programs, HAI Internal Memorandums, May 1967.
9. E. Hellstrand, Measurements of the Effective Resonance Integral in Uranium Metal and Oxide in Different Geometries, *J. Appl. Phys.*, **28**(12): (December 1957).
10. E. Hellstrand, P. Blomberg, and I. Horner, The Temperature Coefficient of the Resonance Integral for Uranium Metal and Oxide, *Nucl. Sci. Eng.*, **8**: 497-506 (December 1960).
11. D. T. Goldman, Suggested Procedures for Utilizing MUFT Resonance Parameters to Include Doppler Broadening, USAEC Report KAPL-M-6158, Knolls Atomic Power Laboratory, June 1, 1964.
12. N. M. Steen and J. N. Hanson, A Simple Method To Incorporate Heterogeneous and Doppler Broadening Effects in the MUFT-5 Resonance Treatment, LWB–LSBR Development Program, USAEC Report WAPD-TM-675, Bettis Atomic Power Laboratory, July 1967.
13. C. G. Poncelet, LASER—A Depletion Program for Lattice Calculations Based on MUFT and THERMOS, USAEC Report WCAP-6073, Westinghouse Electric Corporation, April 1966.
14. R. F. Barry, LEOPARD—A Spectrum-Dependent Non-Spatial Depletion Code for the IBM-7094, USAEC Report WCAP-3269-26, Westinghouse Electric Corporation, September 1963.
15. L. E. Strawbridge and R. A. Barry, Criticality Calculations for Uniform Water-Moderated Lattices, *Nucl. Sci. Eng.*, **23**: 58-73 (September 1965).
16. G. D. Joanou, E. J. Leshan, and J. L. Dudek, GAM-I—A Consistent P-1 Multigroup Code for the Calculation of the Fast Neutron Spectrum and Multigroup Constants, USAEC Report GA-1850, General Atomic Division, General Dynamics Corp., June 1961.
17. L. L. Carter, C. R. Richey, and C. E. Hughey, GAMTEC-II—A Code for Generating Consistent Multigroup Constants Utilized in Diffusion and Transport Theory Calculations, USAEC Report BNWL-35, Battelle–Northwest, March 1965, and Errata.
18. J. L. Carter, Jr., Computer Code Abstracts, Computer Code-HRG, in Reactor Physics Department Technical Activities Quarterly Report, July–September 1966, USAEC Report BNWL-340, Battelle–Northwest, October 1966.
19. F. T. Adler, G. W. Hinman, and L. W. Nordheim, The Quantitative Evaluation of Resonance Integrals, in *Proceedings of the Second United Nations International Conference on the Peaceful Uses of Atomic Energy, Geneva, 1958*, Vol. 16, pp. 155-170, United Nations, New York, 1958.
20. H. Bohl, Jr., E. M. Gelbard, B. L. Anderson, A. P. Hemphill, and B. P. Peterson, P3MG1—A One-Dimensional Multigroup P-3 Program for the Philco-2000 Computer, USAEC Report WAPD-TM-272, Westinghouse Electric Corporation, September 1963.
21. B. G. Carlson, W. J. Horlton, W. Guber, and M. Shapiro, DTF Users Manual, Report UNC-Phys/Math-3321, Vol. 1, November 1963, Vol. 2, Argonne National Laboratory, May 1964.

22. K. D. Lathrop, DTF-IV—A FORTRAN-IV Program for Solving the Multigroup Transport Equation with Anisotropic Scattering, USAEC Report LA-3373, Los Alamos Scientific Laboratory, July 15, 1965.
23. R. W. Deutsch, Computing Three-Group Constants for Neutron Diffusion, *Nucleonics*, **15**(1): 1957.
24. H. C. Honeck, A Review of the Methods for Computing Thermal Neutron Spectra, USAEC Report BNL-821, Brookhaven National Laboratory, June 1963.
25. C. Ponti and M. G. Tamagnini, A Comparison Between the Codes for the Calculation of Thermal Spectra in Homogeneous Media, in Reactor Physics, Meeting of the Lombarda Physics Society, Milan-Pavia, Italy, Report CONF-469-1, December 1963.
26. H. C. Honeck, The Calculation of the Thermal Utilization and Disadvantage Factor in Uranium/Water Lattices, *Nucl. Sci. Eng.*, **18**: 49-68 (January 1964).
27. E. P. Wigner and J. E. Wilkins, Jr., Effect of the Temperature of the Moderator on the Velocity Distribution of Neutrons with Numerical Calculations for H as Moderator, USAEC Report AECD-2275, 1944.
28. J. E. Wilkins, Jr., Effect of the Temperature of the Moderator on the Velocity Distribution of Neutrons for a Heavy Moderator, Report CP-G-2481, November 1944.
29. H. J. Amster and R. Suarez, The Calculation of Thermal Constants Averaged Over a Wigner–Wilkins Flux Spectrum: Description of the SOFOCATE Code, USAEC Report WAPD-TM-39, Westinghouse Electric Corporation, January 1957.
30. H. J. Amster and J. B. Callaghan, KATE-1—A Program for Calculating Wigner–Wilkins and Maxwellian Averaged Thermal Constants on the Philco-2000, USAEC Report WAPD-TM-232, Westinghouse Electric Corporation, October 1960.
31. R. H. Shudde and J. Dyer, TEMPEST II—A Neutron Thermalization Code, NAA Program Description, USAEC Report TID-18284, Atomics International, Division of North American Aviation, Inc., June 1962.
32. A. Amouyal, P. Benoist, and J. Horowitz, Nouvelle Method de Determination du Facteur d'Utilization Thermique d'une Cellule, *J. Nucl. Energy*, **6**: 79 (1957).
33. C. H. Westcott, Effective Cross-Section Values for Well-Moderated Thermal Reactor Spectra, Report CRRP-960, November 1960.
34. F. G. Dawson, Physics Design Aspects of Plutonium Recycle, in Proceedings of Commercial Plutonium Fuels Conference, Washington, D. C., USAEC Report CONF-660308-3, March 1966.
35. H. C. Honeck, THERMOS—A Thermalization Transport Theory Code for Reactor Lattice Calculations, USAEC Report BNL-5826, Brookhaven National Laboratory, September 1961.
36. M. Nelkin, Scattering of Slow Neutrons by Water, *Phys. Rev.*, **119**(2): (July 1960).
37. R. C. Liikala, A Comparative Study of Unit Cell Homogenization for PuO_2–UO_2–H_2O Lattices, in Physics Research Quarterly Report, July–September 1964, USAEC Report HW-84369, General Electric Company, Hanford Atomic Products Operation, October 1964.
38. Unpublished calculations performed by the authors.
39. R. J. Breen, A One-Group Model for Thermal Activation Calculations, *Nucl. Sci. Eng.*, **9**: 91-93 (January 1961).
40. M. F. Valerino and Z. R. Rosztoczy, Analytical and Experimental Methods of Determining Heavy-Isotope Content of Operating Fuel Elements, USAEC Report CEND-540, Combustion Engineering, Inc., September 1965.
41. D. R. Hostetler, Prediction of Mid-Life Power Distribution in the Indian Point Reactor, Presented at the Annual Meeting of the American Nuclear Society, San Francisco, Calif., December 1964.
42. G. H. Minton and H. W. Graves, Jr., Calculation of Criticality, Power Distribution and Fuel Burnup in Thermal Reactors, in *Proceeding of the Third International Conference on Peaceful Uses of Atomic Energy, Geneva, 1964*, Vol. 3, pp. 372-383, United Nations, New York, 1965.
43. H. W. Graves, Jr., and J. E. Howard, Nuclear Performance of Yankee Core I, in Nuclear Performance of Power-Reactor Cores, American Nuclear Society Topical Meeting, Sept. 26–27, 1963, San Francisco, USAEC Report TID-7672, American Nuclear Society, September 1963.
44. C. G. Poncelet, Analysis of the Reactivity Characteristics of Yankee Core I, USAEC Report WCAP-6050, Westinghouse Electric Corporation, 1962.
45. O. J. Marlowe and M. C. Suggs, WANDA-5—A One-Dimensional Neutron Diffusion Equation Program for the Philco-2000 Computer, USAEC Report WAPD-TM-241, Westinghouse Electric Corporation, November 1960.
46. H. P. Flatt and D. C. Baller, AIM-5—A Multigroup, One-Dimensional Diffusion Equation Code, USAEC Report NAA-SR-4694, Atomics International, Division of North American Aviation, Inc., March 1960.
47. H. P. Flatt and D. C. Baller, AIM-6—A One-Dimensional Diffusion Equation Code, NAA Program Description, January 1961.
48. H. P. Flatt, FOG—One-Dimensional Diffusion Equation Codes, USAEC Report NAA-SR-6104, Atomics International, Division of North American Aviation, Inc., 1961.
49. A. J. Nardi, D. J. Subborough, and J. J. Barth, HELM—A Computer Code To Calculate Macroscopic Cross Sections for the PDQ-4 Computer Code, USAEC Report GEAP-4953, General Electric Company, October 1965.
50. G. G. Bilodeau, W. R. Caldwell, J. P. Dorsey, J. G. Fairey, and R. S. Varga, PDQ—An IBM-704 Code To Solve the Two-Dimensional Few-Group Neutron Diffusion Equations, USAEC Report WAPD-TM-70, Westinghouse Electric Corporation, August 1957.
51. W. R. Cadwell, PDQ-3—A Program for the Solution of the Neutron Diffusion Equations in Two Dimensions on the IBM-704, USAEC Report WAPD-TM-179, Westinghouse Electric Corporation, May 1960.
52. W. R. Cadwell, PDQ-4—A Program for the Solution of the Neutron-Diffusion Equations in Two Dimensions on the Philco-2000, USAEC Report WAPD-TM-230, Westinghouse Electric Corporation, June 1961.
53. W. R. Cadwell, P. F. Buerger, and C. J. Pfeifer, The PDQ-5 and PDQ-6 Programs for the Solution of the Two-Dimensional Neutron Diffusion–Depletion Problem, USAEC Report WAPD-TM-477, Bettis Atomic Power Laboratory, January 1965.
54. T. B. Fowler, M. L. Tobias, and D. R. Vondy, EXTERMINATOR-2—A FORTRAN-IV Code for Solving Multigroup Neutron Diffusion Equations in Two Dimensions, USAEC Report ORNL-4078, Oak Ridge National Laboratory, April 1967.

55. M. L. Tobias and T. B. Fowler, The TWENTY-GRAND Program for the Numerical Solution of Few-Group Neutron Diffusion Equations in Two Dimensions, USAEC Report ORNL-3200, Oak Ridge National Laboratory, February 1962.
56. O. R. Marlowe, Nuclear Reactor Depletion Programs for the Philco-2000 Computer, USAEC Report WAPD-TM-221, Westinghouse Electric Corporation, January 1961.
57. C. J. Pfeifer and F. R. Urbanus, ZIP-2—A One-Dimensional Few-Group Synthesis Nuclear Reactor Depletion Program for the Philco-2000 Computer, USAEC Report WAPD-TM-228, Westinghouse Electric Corporation, November 1961.
58. S. Kaplan, Synthesis Methods in Reactor Analysis, *Advan. Nucl. Sci. Technol.*, **3**: 223 (1966).
59. E. L. Wachspress and M. Becker, Variational Synthesis with Discontinuous Trial Functions, in Proceedings of the Conference on the Application of Computing Methods to Reactor Problems, May 17–19, 1965, USAEC Report ANL-7050, p. 191, Argonne National Laboratory, August 1965.
60. W. R. Cadwell, PDQ-7 Reference Manual, USAEC Report WAPD-TM-678, Bettis Atomic Power Laboratory, January 1967.
61. S. M. Hendley and R. A. Mangan, CNCR-2—A One-Dimensional Few-Group Depletion Code for the IBM-7090, Which Includes the Effects of Water Density Variations on Neutron Moderation, USAEC Report WCAP-6058, Westinghouse Electric Corporation, Atomic Power Division, January 1964.
62. S. Hendley and R. Mangan, TURBO*—A Two-Dimensional Few-Group Depletion Code for the IBM-7090, USAEC Report WCAP-6059, Westinghouse Electric Corporation, March 1964.
63. R. J. Breen, O. J. Marlowe, and C. J. Pfeifer, HARMONY—System for Nuclear Reactor Depletion Computation, USAEC Report WAPD-TM-478, Bettis Atomic Power Laboratory, January 1965.
64. D. R. Vondy, T. B. Fowler, and M. L. Tobias, Reactor Depletion Code ASSAULT (Two-Dimensional, Multi-Neutron-Group, Diffusion), USAEC Report ORNL-TM-1302, Oak Ridge National Laboratory, March 1966.
65. D. L. Delp, D. L. Fischer, J. M. Harriman, and M. J. Stedwell, FLARE—A Three-Dimensional Boiling Water Reactor Simulator, USAEC Report GEAP-4598, General Electric Company, Atomic Power Equipment Department, July 1964.
66. O. H. Gailar, H. Kim, J. D. McGeachy, and A. F. Veras, Computer Programs for Power Reactor Management, in *Proceedings of the American Power Conference, Chicago, Ill., April 23–25, 1968, (Vol. 30)*, Illinois Institute of Technology, Chicago, 1968.
67. L. Goldstein, F. Nakache, and A. Veras, Calculation of Fuel Cycle Burnup and Power Distribution of the Dresden I Reactor with the TRILUX Fuel Management Program, *Trans. Amer. Nucl. Soc.*, **10**(1): 300 (June 1967).
68. A. Ariemma, G. Lesnoni La Parola, M. Paoletti Gualandi, P. Peroni, and B. Zaffiro, Accuracy of Power Distribution Calculation Methods for Uranium and Plutonium Lattices Based on Recent Experiments and ENEL Reactor Operation Data, paper presented at American Nuclear Society International Conference, Washington, November 1968.
69. G. A. Sofer and H. Soodak, Nuclear Fuels for Power Reactors, in *Proceedings of the American Power Conference, Chicago, Ill., April 23–25, 1968 (Vol. 30)*, Illinois Institute of Technology, Chicago, 1968.
70. T. R. England, CINDER—A One-Point Depletion and Fission-Product Program, USAEC Report WAPD-TM-334, Westinghouse Electric Corporation, August 1962 (revised June 1964).
71. A. F. Henry, A Theoretical Method for Determining the Worth of Control Rods, USAEC Report WAPD-218, Westinghouse Electric Corporation, August 1959.
72. G. F. Kuncir, A Program for the Calculation of Resonance Integrals, USAEC Report GA-2525, General Atomic Division, General Dynamics Corporation, Aug. 28, 1961.
73. L. W. Nordheim, A Program of Research and Calculations of Resonance Absorption, USAEC Report GA-2527, General Atomic Division, General Dynamics Corporation, Aug. 28, 1961, and Addendum.
74. An IBM-704 Program for Calculating Effective Resonance Absorption Cross Sections by the Narrow-Resonance or Narrow Resonance–Infinite Mass Approximation in Study of Slightly Enriched Uranium Water Lattices with High Conversion Ratio, Quarterly Progress Report, November 1, 1959–January 31, 1960, USAEC Report CEND-94, Combustion Engineering, Inc.
75. M. K. Butler, N. Hollister, M. Legan, and L. Ranzini, Argonne Code Center: Compilation of Program Abstracts, USAEC Report ANL-7411, January 1968 and USAEC Report ANL-7411 (Suppl. 1), Argonne National Laboratory, October 1968.

AEC SYMPOSIUM SERIES

Available for $3.00 each from the Clearinghouse for Federal Scientific and Technical Information, National Bureau of Standards, U. S. Department of Commerce, Springfield, Virginia 22151

1 **Progress in Medical Radioisotope Scanning (TID-7673),**
Oak Ridge Institute of Nuclear Studies, 1962

2 **Reactor Kinetics and Control (TID-7662),**
The University of Arizona, 1963

3 **Dynamic Clinical Studies with Radioisotopes (TID-7678),**
Oak Ridge Institute of Nuclear Studies, 1963

4 **Noise Analysis in Nuclear Systems (TID-7679),**
University of Florida, 1963

5 **Radioactive Fallout from Nuclear Weapons Tests (CONF-765),**
U. S. Atomic Energy Commission, 1964

6 **Radioactive Pharmaceuticals (CONF-651111),**
Oak Ridge Institute of Nuclear Studies, 1965

7 **Neutron Dynamics and Control (CONF-650413),**
The University of Arizona, 1965

8 **Luminescence Dosimetry (CONF-650637),**
Stanford University, 1965

9 **Neutron Noise, Waves, and Pulse Propagation (CONF-660206),**
University of Florida, 1966

10 **Use of Computers in Analysis of Experimental Data and the Control of Nuclear Facilities (CONF-660527),**
Argonne National Laboratory, 1966

11 **Compartments, Pools, and Spaces in Medical Physiology (CONF-661010),**
Oak Ridge Associated Universities, 1967

12 **Thorium Fuel Cycle (CONF-660524),**
Oak Ridge National Laboratory, 1968

13 **Radioisotopes in Medicine: In Vitro Studies (CONF-671111),**
Oak Ridge Associated Universities, 1968

14 **Abundant Nuclear Energy (CONF-680810)**
Oak Ridge Associated Universities, 1969

Nuclear Science Abstracts

The U. S. Atomic Energy Commission, Division of Technical Information, publishes *Nuclear Science Abstracts (NSA)*, a semimonthly journal containing abstracts of the literature of nuclear science and engineering.

NSA covers (1) research reports of the U. S. Atomic Energy Commission and its contractors; (2) research reports of government agencies, universities, and industrial research organizations on a worldwide basis; and (3) translations, patents, books, and articles appearing in technical and scientific journals.

Complete indexes covering subject, author, source, and report number are included in each issue. These indexes are cumulated and sold separately.

Availability of NSA

SALE *NSA* is available on subscription from the Superintendent of Documents, U. S. Government Printing Office, Washington, D. C. 20402, at $42.00 per year for the semimonthly abstract issues and $38.00 per year for the cumulated-index issues. Subscriptions are postpaid within the United States, Canada, Mexico, and all Central and South American countries, except Argentina, Brazil, Guyana, French Guiana, Surinam, and British Honduras. Subscribers in these Central and South American countries, and in all other countries throughout the world, should remit $52.50 per year for subscriptions to semimonthly abstract issues and $47.50 per year for the cumulated-index issues. The single-copy price for the abstract issues is $1.75 postpaid, with this exception: Add one-fourth of $1.75 for mailing to the countries to which the $52.50 subscription rate applies.

EXCHANGE *NSA* is also available on an exchange basis to universities, research institutions, industrial firms, and publishers of scientific information. Inquiries should be directed to the Division of Technical Information Extension, U. S. Atomic Energy Commission, P. O. Box 62, Oak Ridge, Tennessee 37830.

TECHNICAL PROGRESS REVIEWS may be purchased from Superintendent of Documents, U. S. Government Printing Office, Washington, D. C. 20402. *Nuclear Safety* at $3.50 per year (six issues) for each subscription or $0.60 per issue; each of the other journals at $2.50 per year (four issues) or $0.70 per issue. The use of the order form below will facilitate the handling of your order.

POSTAGE AND REMITTANCE: Postpaid within the United States, Canada, Mexico, and all Central and South American countries except Argentina, Brazil, Guyana, French Guiana, Surinam, and British Honduras. For these Central and South American countries and all other countries: add, for each annual subscription, $1.00 for *Nuclear Safety* and $0.75 for each of the other journals; for single issues, add one-fourth of the single-issue price. Payment should be by check, money order, or document coupons, and MUST accompany order. Remittances from foreign countries should be made by international money order or draft on an American bank payable to the Superintendent of Documents or by UNESCO book coupons.

order form

SUPERINTENDENT OF DOCUMENTS
U. S. GOVERNMENT PRINTING OFFICE
WASHINGTON, D. C. 20402

Please send — 1, 2, or 3 years

- ☐ Isotopes and Radiation Technology ____
- ☐ Nuclear Safety ____
- ☐ Reactor and Fuel-Processing Technology ____
- ☐ Reactor Materials ____

Enclosed: document coupons ☐ check ☐ money order ☐

Charge: Superintendent of Documents No._____

SUPERINTENDENT OF DOCUMENTS
U. S. GOVERNMENT PRINTING OFFICE
WASHINGTON, D. C. 20402

(Print clearly)

_____
Name

_____
Street

_____
City, State, ZIP Code